Proceedings of the 4th International Conference on Transport, Atmosphere and Climate

Bad Kohlgrub, Germany,

June 22nd to 25th, 2015

Edited by

Robert Sausen, Simon Unterstrasser and Anja Blum

DLR

Bayerisches Staatsministerium
für Wirtschaft, Infrastruktur, Verkehr
und Technologie

http://www.pa.op.dlr.de/tac/

Edited by
Robert Sausen, Simon Unterstrasser and Anja Blum

Oberpfaffenhofen, July 2016

Foreword

The "4th International Conference on Transport, Atmosphere and Climate (TAC-4)" held in Bad Kohlgrub (Germany), 2015, was organised with the objective of updating our knowledge on the impacts of transport on the composition of the atmosphere and on climate, three years after the TAC-3 conference in Prien am Chiemsee (Germany).

The TAC-4 conference covered all aspects of the impact of the different modes of transport (aviation, road transport, shipping etc.) on atmospheric chemistry, microphysics, radiation and climate, in particular:

- engine emissions (gaseous and particulate),
- emission scenarios and emission data bases for transport,
- near-field and plume processes, effective emissions,
- transport impact on the chemical composition of the atmosphere,
- transport impact on aerosols,
- contrails, contrail cirrus, ship tracks,
- indirect cloud effects (e.g., aerosol-cloud interaction),
- radiative forcing of transport,
- transport impact on climate,
- metrics for measuring climate change and damage,
- mitigation of transport impacts by technological changes in vehicles and engines (e.g., low NOx engines, alternative fuels, adapted vehicles/aircraft),
- mitigation of transport impacts by operational means (e.g., air traffic management, environmental flight and ship routing).

The conference benefited from substantial financial support by Bayerisches Staatsministerium für Wirtschaft, Infrastruktur, Verkehr und Technologie[1], to whom the organizers are very grateful.

Prof. Dr. Robert Sausen
DLR, Institut für Physik der Atmosphäre
Oberpfaffenhofen
D-82234 Wessling
Germany

Tel.: +49-8153-28-2500
Fax.: +49-8153-28-1841
Email: robert.sausen@dlr.de

[1] Bavarian Ministry of Economic Affairs, Infrastructure, Transport and Technology

Scientific Programme Committee

- Prof. Robert Sausen, DLR, Germany (chair)
- Dr. Daniel Cariolle, CERFACS, France
- Dr David Fahey, NOAA, USA
- Dr. Jan S. Fuglestvedt, Cicero, Norway
- Prof. David S. Lee, MMU, United Kingdom
- Prof. Barbara Lenz, DLR, Germany
- Dr. Richard C. Miake-Lye, Aerodyne Research, USA
- Dr. Olivier Penanhoat, SNECMA, France
- Dr. Peter van Velthoven, KNMI, The Netherlands
- Dr. Bernhard Vogel , KIT, Germany
- Prof. Christos Zerefos, NKUA, Greece

Table of Contents

Presentations

Impact on clouds

Posters

Clouds and cloud processes

Emissions

Impact on climate, metric and mitigation

Interdisciplinary Topicy

TAC-4 AGENDA
ORAL PRESENTATIONS

Monday, 22 June 2015	
Opening ceremony	
Chair: R. Sausen	
09:00	Staatsministerin Ilse Aigner; Bayrisches Staatsministerium für Wirtschaft und Medien, Energie und Technologie: *Opening Address* Prof. Dr.-Ing. R. Henke; Member of the Executive Board of DLR: *Opening Address*
09:30	R. Sausen: *Introduction to the region and technical information*
10:00	D.W. Fahey: *Aviation and Climate: An update (solicited presentation)*
Emissions and near field processes	
Chair: H. Schlager	
11:20	E. Herms: *Aircraft engine emissions - European regulation and certification*
11:40	K. Dogushan, B. Brem, F. Klein, I. El-Haddad, L. Durdina, T. Rindlisbacher, R. Huang, J. Slowik, U. Baltensperger, A. Prevot: *Thrust dependence and engine variability of primary volatile organic compound emissions from commercial aircraft turbine engines*
12:00	J. Peck, Z. Yu, D. Liscinsky, R. Miake-Lye: *A volatile particle microphysical simulation model for the evolution of surrogate organic emissions in an aircraft exhaust plume*
12:20	P.D. Whitefield, P. Lobo, D.E. Hagen, E.A. Black, R.C. Miake-Lye, Z. Yu, L. Durdina, B.T. Brem, J. Wang, G.J. Smallwood, K.A. Thomson, T. Rindlisbacher, F. Siegerist, A.A. Mensah, J.C. Corbin, M. Abegglen, B. Sierau: *Development of a certification method for aircraft engine non-volatile PM emissions: results from the North American reference system deployment in the aviation - Particle Regulatory Instrument Demonstration Experiment (A-PRIDE) 4 Campaign*
12:40	B.E. Anderson, R.H. Moore, A. Brown, H. Schlager: *NASA alternative-fuel effects on contrails and cruise emissions (ACCESS) flight experiments*
Emissions and near field processes	
Chair: R. Miake-Lye	
14:30	M. Abegglen, B. Sierau, B. Brem, J. Wang, T. Rindlisbacher, U. Lohmann: *Chemical characterization of particulate matter aircraft turbine engine exhaust using single particle mass spectrometry*
14:50	B. Brem, L. Durdina, J. Wang, T. Rindlisbacher, F. Siegerist, S. Rocci-Denis, O. Penanhoat: *Sensitivity of aircraft gas turbine non-volatile particulate matter mass and number emissions to fuel aromatic content*
15:10	L. Durdina, B. Brem, J. Wang, T. Rindlisbacher, F. Siegerist, S. Rocci-Denis, O. Penanhoat, G. Andac, J. Zelina: *Spatial variability of PM and gaseous emissions at the exit plane of an in-service commercial aircraft turbine engine*

Emissions and near field processes	
Chair: R. Miake-Lye	
15:30	D. Delhaye, F.-X. Ouf, D. Ferry, D. Gaffie, O. Penanhoat, S. Peillon, F. Salm, X. Vancassel, T. Cottard, C. Focsa, N. Harivel, B. Perez, E. Quinton: *The MERMOSE project: characterization of particulates emissions of a commercial aircraft engine: from morphology to chemical composition*
Chair: P. Whitefield	
16:20	R. Moore, B. Anderson, E. Winstead, L. Thornhill, A. Beyersdorf, C. Hudgins, R. Martin, M. Shook, L. Ziemba, ACCESS Science Team: *In-situ measurements of aircraft engine exhaust measured during the 2013-2014 ACCESS project*
16:40	R. Kurtenbach, P. Wiesen, O. Zaporozhets, K. Synylo: *Measurement of aircraft engine emissions inside the airport area*
17:00	E. Turgut, M. Cavcar, O.D. Yay, E. Yilmaz, O. Usanmaz, K. Armutlu, T. Dogeroglu: *Estimating gaseous emission production of an entire flight of commercial aircraft based on emission measurements and actual flight data records*
17:20	M. Plohr: *Procedures to apply NO_x correlation methods to engine concepts with staged, lean combustor technology*
17:40	C. Loth, Ammergauer Alpen GmbH: *The regions of the Ammergauer Alps*
18:00	End of presentations

Tuesday, 23 June 2015	
Miscellaneous	
Chair: K. Gierens	
09:00	P. Brok, R. Berghof, S. Maertens, M. Hepting: *TEAM_Play for Europe*
09:20	S. Christie, S. Blakey, P. Le Clercq, S. Matthes, H. Schlager, D. Lee, D. Raper, P. Wiesen, N. Zarzalis, T. Panidis, P. Brok: *Research strategies for developing alternative fuels in aviation*
09:40	J. Scheelhaase, R. Sausen, K. Dahlmann, M. Jung, H. Keimel, H. Nieße, M. Schäfer, F. Wolters: *Limiting aviation's full climate impact by market-based measures - Main results of the research project AviClim*

Mitigation of aviation's climate impact	
Chair: M. Gupta	
10:00	V. Grewe: *Eco-efficiency in aviation: From design to routing options for climate mitigation (solicited presentation)*
11:00	P. Lobo, T.W. Chan, P. Canteenwalla, C. Ginestra, B. Dally, D. Hagen, P. Whitefield, G. Hemighaus, J. Bauldreay: *Assessment of non-volatile PM emissions from a turbojet engine with synthesized aromatic kerosene derived jet fuel blends at simulated altitudes*
11:20	F. Linke, V. Grewe, V. Gollnick: *The implications of intermediate stop operations on aviation emissions and climate*
11:40	H. Yamashita, V. Grewe, P. Jöckel, F. Linke, M. Schäfer, D. Sasaki: *Climate impact assessment of routing strategies: Interactive air traffic in a climate model*
12:00	C. Frömming, S. Brinkop, V. Grewe, E. Irvine, A. Søvde, S. Matthes: *Characteristic weather patterns over the North Atlantic and their effect on air traffic climate impact and route optimization*
12:20	S. Matthes, V. Grewe, T. Champougny, C. Frömming, S. Brinkop, E. Irvine, A. Søvde: *Climate-optimized trajectories in the North Atlantic and mitigation potential*
FAA research and poster session	
Chair: R. Sausen	
14:00	M. Gupta: *A brief overview of FAA research on aviation emissions and their environmental impacts*
14:20	2 min presentations by poster authors: *Introduction to posters*
15:00	Posters on display (incl. coffee/tea, selection for Poster Award) *Authors in attendance*

Impact on air quality and climate	
Chair: G. Pitari	
16:30	V. Matthias, A. Aulinger, J. Bieser, M. Quante: *The impact of shipping on air pollution in North Sea coastal areas - situation today and in the future*
16:50	S. Arunachalam, S. Boone, J. Bowden, M. Omary: *Sensitivity analysis approaches for assessing air quality impacts of airport emissions*
17:10	M. Righi, J. Hendricks, R. Sausen: *The global impact of the transport sector on atmospheric aerosol and climate in the representative concentration pathways*
17:30	End of presentations

Wednesday, 24 June 2015	
Impact on air quality and climate	
Chair: S. Matthes	
09:00	G. Pitari, G. Di Genova, N. De Luca, I. Cionni, L. Lim, A. Skowron: *REACT4C: Radiative forcing from aircraft emissions of NO_x: role of H_2O and O_3 stratospheric changes*
09:20	M. Lund, J. Fuglestvedt: *Global and regional climate impacts of aviation and on-road transport*
09:40	J. Hendricks, M. Righi, K. Dahlmann, K.-D. Gottschaldt, V. Grewe, M. Ponater, R. Sausen, D. Heinrichs, C. Winkler, A. Wolfermann, T. Kampffmeyer, R. Friedrich: *Quantifying the climate impact of emissions from land-based transport in Germany*
Impact on clouds	
Chair: U. Schumann	
10:00	C. Voigt, U. Schumann, A. Minikin, T. Jurkat, S. Kaufmann, R. Schlage, D. Fütterer, S. Mertes, S. Molleker, M. Klingebiel, R. Weigel, J. Schneider, S. Borrmann, M. Krämer, C. Rolf, M. Schnaiter, E. Järvinen, M. Wirth, S. Groß, H. Ziereis, K. Graf, L. Bugliaro, M. Zöger: *Detecting contrail cirrus – First results of the HALO mission ML-CIRRUS*
11:00	D. Baumgardner, K. Beswick, M. Gallagher, G. Raga: *Cirrus properties from commercial aircraft measurements and implications for flight operations*
11:20	J.-C. Khou, W. Ghedhaïfi, X. Vancassel, F. Garnier: *Spatial simulation of contrail formation in the near-field of a commercial aircraft*
11:40	S. Unterstraßer, K. Gierens, I. Sölch: *Numerical modeling of natural cirrus and contrail-cirrus. How different are they?*
12:00	R. Paoli, O. Thouron, D. Cariolle: *A numerical study of contrail-to-cirrus transition using 3D large-eddy simulations*
Impact on clouds	
Chair: S. Unterstraßer	
14:00	J. Rosenow, H. Fricke: *Angular dependence of individual condensation trails on the extinction of solar radiation*
14:20	M. Vazquez, L. Bugliaro: *Synergetic study of the evolution of a contrail cluster*
Electro mobility	
Chair: S. Unterstraßer	
14:40	U. Wagner: *Electro mobility: Technological options and contribution to reduction of emissions (solicited presentation)*
15:20	End of presentations

Thursday, 25 June 2015	
Impact on clouds	
Chair: R. Paoli	
09:00	D.P. Duda, T. Chee, S. Bedka, D. Spangenberg, K. Khlopenkov, P. Minnis: *Properties of linear contrails detected in 2012 Northern hemisphere MODIS imagery*
09:20	S. Gruber, B. Vogel, H. Vogel, J. Bechtold: *Simulating contrails with COSMO-ART based on real time flight tracks*
09:40	U. Schumann, K. Graf, C. Voigt: *Contrail-cirrus predictions compared to observations*
10:00	E. Irvine, K. Shine: *The effect of climate change on the potential for contrail formation.*
10:20	S. Unterstraßer: *Technical information concerning your proceedings contribution*
Impact on clouds	
Chair: R. Sausen	
11:10	L. Bock, U. Burkhardt, B. Kärcher: *Modelling of contrail cirrus: microphysical and optical properties*
11:30	A. Bier, U. Burkhardt, L. Bock: *Process-based studies of the life cycle of contrail cirrus in a global climate model*
11:50	S. Barrett, S. Eastham, F. Caiazzo: *Impact of alternative jet fuels on contrails*
12:10	J. Penner, U. Schumann, Y. Chen, C. Zhou, K. Graf: *Simulations of dehydration effects from contrails in a global climate model*
12:30	Summary, conclusions, awards, ...
	End of conference

POSTERS:

A. Clouds and cloud processes	
A.01	D. Cariolle, H. Clark, R. Paoli, O. Thouron, D. Saint Martin, M. Benhamou, A. Schwarzenboeck, D. Hauglustaine, R. Valorso, X. Vancassel: *The TC2 (Traînées de Condensation et Climat) project*
A.02	H. Clark, O. Thouron, R. Paoli, D. Cariolle: *Modelling the chemistry in contrails from the vortex to the diffusion phase using a mesoscale model*
A.03	L. Bock, U. Burkhardt: *Global modelling of contrail cirrus for future scenarios*
A.04	L. Lim, Rodríguez de León, D. Lee, O. Søvde: *Uncertainties with respect to contrail coverage modelling in REACT4C*
A.05	R. Rodríguez de León, L. Lim and D. Lee: *Uncertainties with respect to contrail radiative modelling in REACT4C*
A.06	J. Strandgren, L. Bugliaro, M. Schmidl, M. Rapp: *The life cycle of cirrus clouds from a combination of active and passive satellite sensors*

POSTERS:

B. Emissions	
B.01	K.S. Patel, D. Sahu, B. Blazhev, J. Nicolas, E. Yubero, J. Hoinkis, L. Matini: *Transport pollution in India*
B.02	S. Ramteke, K.S. Patel, D. Sahu, B. Blazhev, E. Yubero, J. Hoinkis: *Contamination assessment of ions in road dust of India*
B.03	Moore, Richard, M. Shook, A. Beyersdorf, C. Corr, S. Herndon, B. Knighton, R. Miake-Lye, L. Thornhill, E. Winstead, Z. Yu, L. Ziemba, B. Anderson: *Influence of jet fuel composition on aircraft engine emissions: a synthesis of aerosol emissions data from the NASA APEX, AAFEX, and ACCESS Missions*
B.04	S. Freeman, D. Lee, L. Lim: *Examining the role of aviation NO_x emissions as a short lived climate forcer*
B.06	G. Pitari, G. Di Genova, N. De Luca: *A modelling study of the impact of land transportation on Arctic black carbon and solar radiation transfer*
B.07	S. Christie, P. Lobo, D. Lee, D. Raper, B. Kandelwal, S. Blakey: *The impact of biofuel blend ratio on gaseous emissions and smoke from an aircraft APU*
C. Impact on climate, metric and mitigation	
C.01	M. Ponater, V. Rieger, S. Dietmüller, R. Sausen: *Towards uncovering the origin of efficacy differences for different radiative forcing contributions related to transport emissions*
C.02	S. Matthes, K. Gierens: *Brief review of the Forum AE workshop on aviation transport impact on climate change – role of NO_x emissions*
C.03	L. Lim, B. Owen, D. Lee: *Aviation impacts on climate: Where are we heading?*
C.04	V. Rieger, V. Grewe: *TransClim: A fast climate-response-model for evaluating new developments in road traffic*
C.05	L. Lim, D. Lee, S. Matthes, U. Burkhardt, S. Dietmüller, D. Iachetti, I. Isaksen, B. Owen, G. Pitari, A. Skowron, O. Søvde: *REACT4C: Simplified mitigation studies*
C.06	V. Grewe, L. Bock, U. Burkhardt, K. Gierens, S. Unterstrasser, T. Reichelt, A. Gangoli Rao, A. Bhat, F. Yin, Y. Levy: *Assessing the climate impact of a multi-fuel blended wing body: Results from the AHEAD EU-project*
C.07	S. Matthes, O. Søvde, L. Lim, S. Dietmüller, A. Skowron, D. Iachetti, G. Pitari: *The global impact of weather-dependent climate-optimal trajectories in the North Atlantic*
D. Miscellaneous	
D.02	S. Seum and the VEU Project Team: *The DLR-Project Transport and the Environment – Building competency for a sustainable mobility future*
D.03	E. Ayalew, Y. Gebre: *A survey of occupational exposure to inhalable wood dust among workers in small- and medium-scale wood-processing enterprises in Ethiopia*

Opening address

Ilse Aigner

Bavarian State Minister
of Economic Affairs and Media, Energy and Technology

Unfortunately, I am unable to be here with you today due to other pressing engagements. However, I didn't want to miss the opportunity to send greetings and share some thoughts with you at this event. You are working on issues affecting the fate of the global community, breaking them down into technological possibilities and economic perspectives in a field of great interest to Bavaria. This endeavour is worthy of attention, indeed.

In an economy with division of labour, mobility and the transportation of people and goods is a prerequisite for prosperity and growth - especially in Bavaria, which is an economic and export powerhouse.

However, we also know that the transport sector accounts for 20% of carbon emissions in Germany. The effects of man-made CO_2 emissions on the climate are beyond dispute - as are the consequences the resulting climate change has on the environment, business and humanity. That is why I would expressly welcome the first globally applicable climate agreement scheduled for the Paris summit at the end of the year. It would be a legally binding commitment among the global community to comply with the two-degree limit. The goal is to stop Earth's temperature from rising more than two degrees by the end of this century. The major industrial nations have already sent an important signal during the G7 Summit at Schloss Elmau on 7/8 June and agreed to ambitious national objectives, thereby assuming a leadership role in containing climate change.

The transportation sector can make an important contribution in meeting the target of two degrees. With a focus on aviation, the 4th TAC Conference is working to advance the transportation sector in an environment-friendly and competitive manner. Given that goal, it was with pleasure that I accepted the patronage for the conference. We must understand the influence that various types of transportation have on the composition of our atmosphere and climate. Based on that understanding, it will be possible to develop climate-friendly concepts for alternative energy, lighter construction models and more efficient power systems. Therefore, it is vital to have ambitious and pro-active policies for innovation. The Bavarian State Government is committed to continuous optimisation in the framework conditions for science and research. One of our focal points to that end is smooth technology transfer.

Promoting aerospace technology is a prime example in this respect. We have a clear objective: we want Bavaria to be one of the world's leading aviation & aerospace sites in the future as well. Our new "Aviation Strategy 2030" is bundling Bavaria's activities. We want Bavaria to remain a step ahead of the growing global competition, which we will only accomplish with strength in research. Today, we already have broad positioning in the aviation & aerospace industries. There are around thirty specialised universities, research organisations and institutes active in Bavaria.

We want to assume a technology leadership role when it comes to environment-friendly air transportation systems, for the future of aviation is largely dependent upon environmental compatibility and resource conservation.

To that end, we'll need innovative technologies that reduce noise and hazardous emissions. The goal is to include the entire production cycle when making evaluations based on the principle of ecological balance, with the relevant factors including noise, carbon emissions and resource consumption - in manufacturing, maintenance and disposal processes alike.

The think tank Bauhaus Luftfahrt, sponsored by the Bavarian government, uses precisely that approach to research sustainable and energy-preserving power systems in aviation. The Ludwig Bölkow Campus for Aerospace and Security in Ottobrunn represents a platform for innovation in science and business. The Cluster BavAIRia, also sponsored by the Bavarian government, is advancing extremely well. It already has more than 200 member companies from all sectors in aviation, aerospace and space applications. BavAIRia's primary objective is to attain even tighter integration in the key fields of satellite navigation and geo information.

Satellite navigation and earth observation have particularly been in the focus of our research funding over the past years due to their increasing importance. Satellite-based monitoring of the atmosphere provides important contributions in researching the effect emissions have on the climate. That is why we have provided 8.5 million euros in funding for the DLR Earth Observation Centre, which helps to establish the preconditions for a Copernicus Satellite Data Archive in Bayern.

This brief overview illustrates: we are conscious of the importance of aviation & aerospace engineering as drivers of innovation. That is why we, too, are taking on the challenges being faced in those industries. We want to pave the way for outstanding research and foster economical, environment-friendly implementation into practice.

I wish the conference and all attendees a successful event, new insights, fruitful discussions, interesting contacts and all the best for the future.

Opening address

Prof. Rolf Henke

Member of the Executive Board
German Aerospace Center
Aeronautics Programme

Dear All,

Not being here does not mean not being with you. Despite my physical absence, I do follow your work by all means; the topic of your conference is for utmost importance for the whole aviation system worldwide.

This is why climate research is also reflected in the DLR research agenda. A large part of our programmatic work is dedicated to research for a better understanding of climate impact due to aviation and how to reduce it. In addition we work in consortia such as the one operating the German Atmospheric Research Aircraft HALO, and we contribute to international groups such as EUFAR. The core of most of these activities lies at our Institute of Atmospheric Physics, one of the leading institutions worldwide, a well reputed partner in many international programs, and the host of this conference, which makes me proud again of our colleagues here.

Let me give you a few examples of our institutional research work in your fields of activity:

- We address the issue of alternative fuels and their impact on weather and climate by internal projects and also in cooperation with other international institutions. One success-story is the project ACCESS II in cooperation with NASA, in which the DLR Falcon flew behind the NASA DC-8 to measure the composition of the exhaust gas at several distances. The internal follow-on project at DLR is the project ECLIF with the research focus on various types of alternative fuels and the investigation of both the combustion in the engine and the resulting emissions. Of course, DLR also cooperates with airlines such as Lufthansa, for example during their regular flight campaign between Hamburg and Frankfurt operating a B 737 with biofuel. And we are founding member and hold a presidency of AIREG, the Aviation Initiative for Renewable Energy in Germany, me personally being in the AIREG Advisory Council.

- Addressing climate directly, DLR has also investigated impact functions in order to derive aircraft design requirements from ecological impact parameters, finally applying these functions in internal as well as in European projects in order to find aviation routes with minimum climate impact.

- An important factor for the future of aviation is the resilience of the system. We have gained much experience from flight measurements as well as satellite image evaluations during the two volcano eruptions in Iceland. This has led to an internal project called VolCats, where we look for the quantitative identification of ash cloud properties from space as well as on the actual impact of that ash on an aircraft in order to define limit values.

DLR is by far the leading aerospace research organization in Europe. Apart from being proud, which is what I am, this goes along with accepting responsibility including leadership in certain areas. For example, DLR was the only research organization involved in the establishment of the European aviation vision “Flight Path 2050”. At the end of my introduction, let me cite a few statements out of this very important document for aviation research:

At first, an analysis is made on the impact of aviation:

- "Europe is entering a new age where it faces many challenges such as globalisation, a financial system in need of reform, climate change and an increasing scarcity of resources."

- And more specific: "Aviation also contributes to society in other critical, nontransport areas such as emergency services, search and rescue, disaster relief and climate monitoring."

Out of this, challenges or better objectives have been identified which could also be the guideline for your conference when it comes to aviation:

- "In 2050, the effect of aviation on the atmosphere is fully understood." This is easily written down, but is asking for much coordinated research!

- And finally, the one I like most: "Europe is at the forefront of atmospheric research and takes the lead in the formulation of a prioritised environmental action plan and establishment of global environmental standards."

Now please go ahead, talk about these issues and finally work on it, for the sake of society. All the best for this conference, I wish you inspiring presentations in the sessions as well as good talks during the breaks, but also fun in being together the rest of the time.

EASA's Work to Support the Regulation of Aircraft Engine Emissions

Erika Herms*
EASA, Certification Directorate, Environment

Keywords: European Commission, European Aviation Safety Agency, regulation, certification, International Civil Aviation Organisation, smoke, unburned hydrocarbon, carbon monoxide, dioxide of nitrogen, non-volatile particulate matter, EASA SAMPLE studies, carbon dioxide.

ABSTRACT: EASA certifies civil aeronautical products to ensure a high uniform level of safety and environmental protection in Europe. The certification process concerning aircraft noise and aircraft engine emissions is based on Annex 16 to the ICAO Chicago Convention. The regulated species for aircraft engines are smoke, HC, CO and NO_x. The standards apply to all turbojet and turbofan engines in the case of smoke, and to those engines with a thrust greater than 26.7kN for gaseous emissions. The regulatory NO_x limits have been periodically updated to increase their stringency. The ICAO Committee on Aviation Environmental Protection meets in February 2016. It is expected that a new non-volatile particulate matter (nvPM) standard for engines, and a new CO_2 (fuel efficiency) standard for aeroplanes, will be proposed for adoption and future implementation in the European Regulation. EASA is supporting research work to establish the technical requirements for a nvPM measurement method (SAMPLE programme), and studies to support the development of the CO_2 certification requirements and regulatory limits. The EU is funding studies related to engine testing and the acquisition of nvPM data for the improvement of the nvPM standard and modelling of cruise nvPM.

1 EASA: ACTIVITY OVERVIEW AND MAIN RULES

The European Aviation Safety Agency (Ref. 1) was established in 2003 and has its headquarters in Cologne, Germany. EASA is an agency of the European Union, which provides technical expertise to the European Commission including the provision of assistance in the drafting of rules for aviation safety and environment. In addition, the Agency has been given powers to carry out certain executive tasks related to aviation safety and environment, such as the certification of aeronautical products and organisations involved in product design, production and maintenance. These certification activities ensure compliance with airworthiness and environmental protection standards.

EASA is obliged to ensure a common and uniform level of safety and environmental protection within the EU to avoid duplication in the regulatory and certification processes among Member States.

The two legally binding rules are:

- common rules in the field of civil aviation and the establishment of a European Aviation Safety Agency laid down in the Basic Regulation (Regulation (EC) No 216/2008) (Ref. 2); and
- related Implementing Rules laid down in Regulation (EU) No 748/2012 (Ref. 3) for the airworthiness and environmental certification of aircraft products, parts and appliances, as well as for the approval of design and production organisations.

Non-binding rules, the Certification Specifications, can be directly adopted by EASA along with guidance material and acceptable means of compliance for certification.

* *Corresponding author:* Erika Herms, European Aviation Safety Agency, Postfach 10 12 53, D-50452 Köln, Germany, Email: erika.herms@easa.europa.eu

2 EASA ENVIRONMENTAL PROTECTION REGULATION

EASA certifies aircraft for noise and aircraft engines for emissions according to standards which by direct reference from the Basic Regulation are the chapters of Annex 16 to the Chicago Convention on International Civil Aviation. Annex 16 provides International standards and recommended practices in the fields of aircraft noise (Volume I) and aircraft engine emissions (Volume II). EASA is fully engaged in the work of the various ICAO/CAEP technical groups that maintain Annex 16 on behalf of the Committee on Aviation Environmental Protection (CAEP) of the International Civil Aviation Organisation (ICAO) (Ref. 4).

In certain domains the ICAO CAEP standards rely on technical specifications developed by SAE International (Ref. 5). In the area of engine emissions the SAE E-31 Committee works on technical standards that support Annex 16 Volume II. EASA contributes directly to the work of SAE E-31. For example EASA funds work such as the SAMPLE studies (Studying, sAmpling and measuring of aircraft ParticuLate Emissions) (Ref. 6).

In summary the certification of aircraft engine emissions EASA relies on the Basic Regulation, the Implementing Rules and CS-34 (Ref. 7). The latter provides the certification specifications and the acceptable means of compliance for aircraft engine emissions and fuel venting.

3 REGULATED AIRCRAFT ENGINE EMISSIONS

The first edition of ICAO Annex 16 Volume II was published in 1981. It contained standards for the control of emissions species that are still regulated today, smoke, unburned hydrocarbons, carbon monoxide and oxides of nitrogen. Smoke is measured as a smoke number that samples soot to determine the visibility of exhausted smoke. The emissions of gaseous species are regulated at an altitude that is assumed to represent the boundary layer (below three thousand feet). To this end a landing-take-off cycle was defined to simulate local aircraft operations.

The standard applies to all turbojet and turbofan engines intended for propulsion at subsonic speeds in the case of smoke, and those engines with a thrust greater than 26.7kN in the case of gaseous emissions. Since the publication of the Annex 16 Volume II the regulatory limits for smoke, HC and CO have not changed. They are still considered to be sufficient for the control of local emissions. The priority for increasing the stringency of the regulatory limits has been NO_x emissions. Four successive reductions have been adopted at the CAEP/2, CAEP/4, CAEP/6 and CAEP/8 meetings.

Figure 1 illustrates the effect of the increase in stringency for NO_x emissions from engines with thrusts greater than 89kN and an overall pressure ratio (OPR, pressure at the exit of the compressor/pressure at the engine inlet) of around 30. This example shows a decrease in NO_x emissions that is related to the improvement in engine technology.

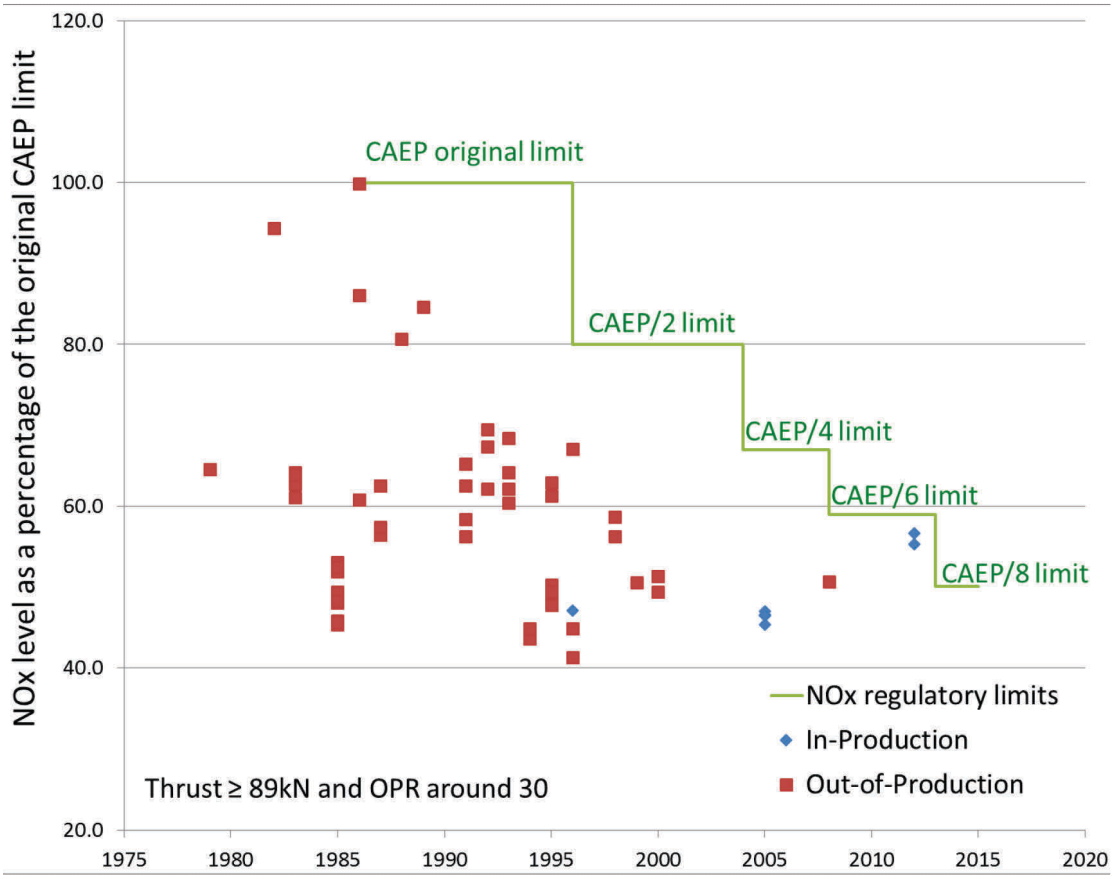

Figure 1: illustration on the effect of the decrease in stringency for NO_x

Certified emissions data are published in the ICAO Engine Emissions Data Bank (Ref. 8) that is hosted by EASA. This databank can support the modelling of emission inventories.

4 NEW STANDARDS

CAEP is working on establishing two new standards concerning:

- non-volatile particulate matter (nvPM) mass and number for aircraft engines (to be added to Annex 16 Volume II); and
- CO_2 emissions standard for aeroplanes to be published in a new Volume III of Annex 16.

In the 1980's the smoke number was considered to be an effective parameter to quantify the visual effect of aircraft engine emissions. It is though inappropriate for the assessment of their impact on health and climate change. CAEP first considered the development of a standard for nvPM in 2009 and since then considerable effort has been spent to support this activity. EASA has funded the SAMPLE studies, the outcome of which has been fed into the CAEP and SAE technical work.

The procedure for the continuous sampling and measurement of non-volatile particle emissions from aircraft turbine engines has been developed by the SAE E-31 Committee and is published in the Aerospace Information Report AIR6241. It has served as a basis for the drafting of the related certification requirements that will be added to Annex 16 Volume II.

In addition to the technical specifications, CAEP has worked on the establishment of a regulatory limit. For the CAEP/10 meeting in February 2016, a limit to control the maximum nvPM mass concentrations at engine exhaust will be proposed for adoption. During the next three years more emissions data will be gathered. It is expected regulatory limits for nvPM mass and number will be proposed at the CAEP/11 meeting in 2019.

Among the measures being considered by ICAO to reduce the impact of aviation on the climate, CAEP has a remit to work on an aeroplane CO_2 (fuel efficiency) standard. EASA has very significantly contributed to this effort by funding experts to support the process. At CAEP/10 a new Volume III of the Annex 16 containing a standard on aeroplane CO_2 emissions will be proposed for adoption.

When the two new standards are adopted by ICAO, EASA will start the process to implement them in its regulations for the additional certification of nvPM for engines and of CO_2 for aeroplanes.

5 RESEARCH STUDIES

The European Commission is funding a two-year study for the development of a public European environmental model suite for aviation. This study began in May 2015 and includes the collection of data on aircraft engine nvPM emissions. To that end measurements will be made at the exhaust of two modern engines, each having a thrust greater than 26,7kN. The data will contribute to the establishment of the nvPM mass and number emissions standard.

6 CONCLUSION

The main pollutants emitted by aircraft engines due to the combustion of kerosene are regulated and certified by EASA. The Agency is also involved in efforts to maintain and update the relevant regulations, including the possible expansion of the list of regulated species. EASA has expended considerable resources and funded studies to hasten the development of a robust nvPM and CO_2 standard. The greatest difficulty facing the development of an nvPM standard has been how to define technically acceptable sampling and measurement methods considering the complexity of measuring the very small particles emitted by aircraft engines. The CO_2 regulatory work has also been technically and commercially challenging given the politically urgency of climate change.

REFERENCES

1. EASA website: http://easa.europa.eu
2. Regulation (EC) No 216/200: http://easa.europa.eu/regulations
3. Regulation (EU) No 748/2012: http://easa.europa.eu/regulations
4. ICAO website: http://www.icao.int/
5. SAE International website: https://www.sae.org/
6. SAMPLE studies (SAMPLE I, SAMPLE II and SAMPLE III): http://easa.europa.eu/document-library/research-projects/easa2008op13
7. CS-34: http://easa.europa.eu/regulations
8. Engine Emissions Data Bank: http://easa.europa.eu/document-library/icao-aircraft-engine-emissions-databank

A Volatile Particle Microphysical Simulation Model for the Evolution of Surrogate Organic Emissions in an Aircraft Exhaust Plume

Jay Peck*, Zhenhong Yu, and Richard C. Miake-Lye
Aerodyne Research, Inc. Billerica, MA, USA

David S. Liscinsky
United Technologies Research Center, East Hartford, CT, USA

ABSTRACT: A microphysics model is presented that numerically simulates the evolution of volatile sulfate and organic particulate matter (PM) in the near-field aircraft plume. Six surrogate organic compounds, pentanoic acid ($C_5H_{10}O_2$), naphthalene ($C_{10}H_8$), anthracene ($C_{14}H_{10}$), pyrene ($C_{16}H_{10}$), perylene ($C_{20}H_{12}$), and anthanthrene ($C_{22}H_{12}$), were selected to represent the range of organics present in the exhaust based on saturation vapor concentration, and their dry mass accommodation coefficients were derived from a correlation to the species water solubility. The 6-species surrogate model was validated against two field measurements, and showed that it can reproduce the experimental results and simulate the evolution of the volatile aircraft emissions both qualitatively and quantitatively. First, through a sector combustor rig test at United Technologies Research Center (UTRC), the model was able to predict the amount of organic and sulfate coatings on the combustion soot particles. It also explained why there is more organic soot coating at higher soot loading condition although the initial vapor concentration of volatile organic species was lower. Second, an Allison T63 turboshaft engine with artificially sulfur-doped fuel was used to investigate the relative compositions among the nucleation/coagulation and soot coating modes. The model reproduced the experimental observation that the nucleation/coagulation mode is dominated by organics and the soot coating mode by sulfates. The model provides an explanation why the nucleation/coagulation mode eventually becomes organics-rich even though the nucleation process is initiated by sulfates. Through this work, the microphysics model demonstrated that it can serve as a working engineering model to simulate the volatile PM emissions from aircraft engines.

1 INTRODUCTION

Aircraft engine exhaust evolves as it is cooled and diluted by ambient air. The particulate matter (PM) emission is dominated by non-volatile black carbon particles at the engine exit plane, but volatile sulfate and organic species form new particles and/or add mass to existing ones. While non-volatile PM is relatively well-understood, and can be measured with good accuracy and precision, the volatile PM poses many more challenges. Volatile PM is a moving target, evolving and aging according to the dilution conditions, and they are typically much smaller in size, making it extremely difficult to measure with any instrument. To improve our understanding of aviation PM emissions, a reliable modeling tool is highly desired.

2 MICROPHYSICAL SIMULATION MODEL

To understand the volatile PM microphysics, Wong et al. (Wong, et al., 2008) wrote a numerical simulation code with a 1-D time-tracing. The model takes the engine exit conditions such as temperature, pressure, velocity, and soot loading, as well as the dilution profile, as user inputs, and evaluates nucleation and coagulation based on a quasi-unary nucleation model by Yu (Yu, 2007). It assumes that sulfuric acid can form nucleation clusters as unary nucleation, and water is immediately drawn to the cluster to establish a thermodynamic equilibrium. For soot coating, the simulation model uses a 2-step mechanism; the initially hydrophobic soot surface must be first activated by

* *Corresponding author:* Jay Peck, Aerodyne Research, Inc., 45 Manning Rd, Billerica, MA 01821 USA. Email: jpeck@aerodyne.com

sulfuric acid, and only when a portion of the soot surface is activated, more sulfuric acid can condense on the activated spots.

The original model only had the sulfuric acid mechanisms, but Jun and co-workers included the organics mechanism in the code (Jun, 2011), (Wong, et al., 2014), (Wong, et al., 2015). And through the present work, we improve the organic PM mechanism by using a six-species surrogate representation of organic PM precursors. As shown in Figure 1, we chose six organic and hydrocarbon species (pentanoic acid ($C_5H_{10}O_2$), naphthalene ($C_{10}H_8$), anthracene ($C_{14}H_{10}$), pyrene ($C_{16}H_{10}$), perylene ($C_{20}H_{12}$), and anthanthrene ($C_{22}H_{12}$)) to cover a relevant range of saturation vapor pressure, and assumed that the relative composition between these six-species follow a normal distribution with regard to the saturation vapor pressure. Similar method has been used by Robinson (Robinson, et al., 2007) to represent diesel exhaust.

In addition, after experimentally measuring the mass uptake by soot for several different species, Yu and co-workers found that the uptake coefficient or mass accommodation coefficient can be correlated with the species water solubility, which is much more readily available in the literature (Yu, et al., 2014).

Highly oxidized organic species are typically not found in the aircraft engine exhaust because it takes a longer time-scale and usually requires a photo-chemistry outside the engine to form further oxidized organic compounds. Thus, we included only one organic acid (pentanoic acid) in the most volatile bin.

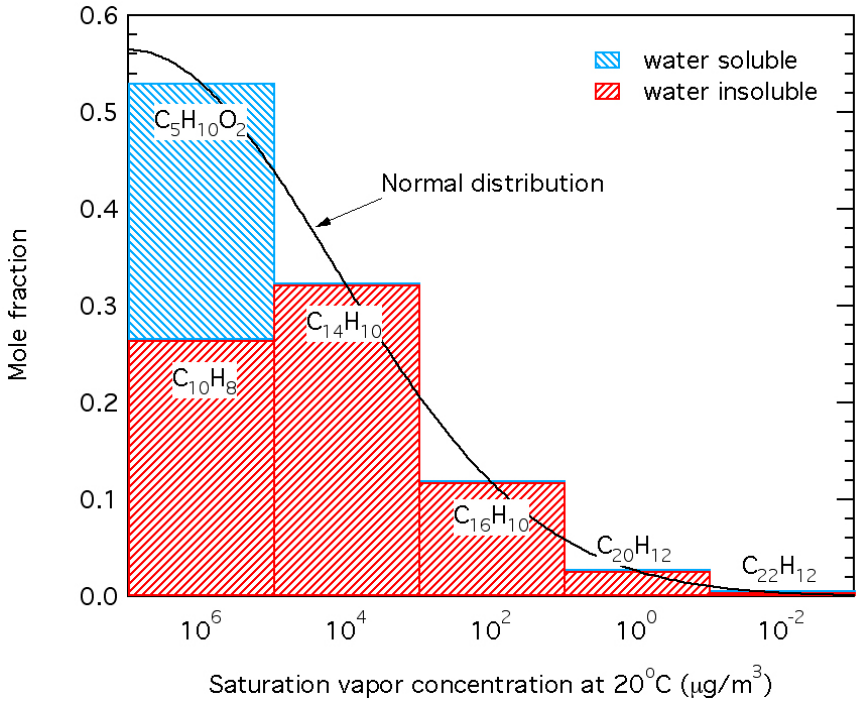

Figure 1: Relative composition of the six surrogate species used in the simulation

3 EXPERIMENTAL VALIDATION

Using this six-species surrogate representation of organic PM precursors, we validated the model with two different experiments. First, we tested a Pratt & Whitney Rich burn – Quick quench – Lean burn (RQL) combustor sector rig at United Technologies Research Center (UTRC), which generates emissions with similar characteristics as real engines. In this experiment, we made an observation that at high power setting where the initial organic species concentration is lower, higher organic PM loading is detected with an Aerosol Mass Spectrometer (AMS) than low power settings where the initial hydrocarbon concentration was higher (Peck, et al., 2014). It seemed somewhat counter-intuitive at first, but using the microphysical simulation model with proper soot loading and initial hydrocarbon concentrations, we were able to demonstrate that the simulation can capture the organics behavior well; more organic PM was formed at high power even though the initial precursor concentration was lower. The comparison between the model and the experiments is shown in

Figure 2. Through the simulation, it was found that the condensation of organic species is slow and is limited by the availability of the soot surfaces, not by the initial vapor phase concentration, and therefore, more organic PM can condense on the soot surfaces as more surface area is available at high power due to higher soot production. On the contrary, due to faster condensation, almost all sulfates are already condensed even for the low soot condition, and more surface area does not necessarily promote more sulfate PM.

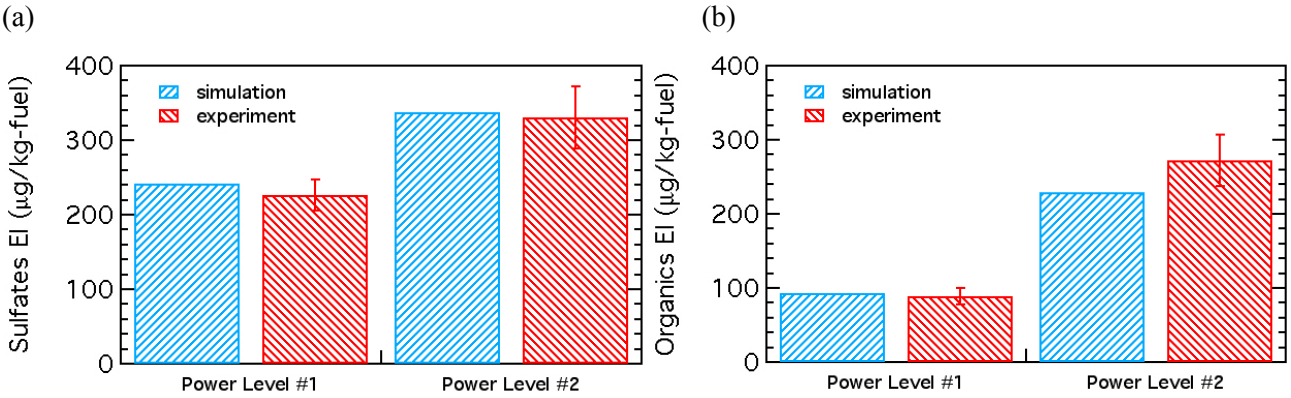

Figure 2: Comparison between the microphysical simulation and experiments for (a) sulfates and (b) organics

The second validation was with a T63 turboshaft engine at Wright-Patterson Air Force Base. Figure 3 shows an interesting experimental result using a sulfur-doped JP8 fuel at idle power. In this case, the sulfur compounds were added to the fuel to the specification maximum of 3000 ppm. In this sulfur-doped fuel experiment, we found that the nucleation/coagulation mode is dominated by organics whereas the soot coating mode is dominated by sulfates. This seemed counter-intuitive because it has been known that the nucleation process is initiate by sulfates, and the nucleation mode was expected to have more sulfates. The soot surfaces are initially hydrophobic, so it was expected that more water-insoluble hydrocarbons are present in the soot mode.

(a)

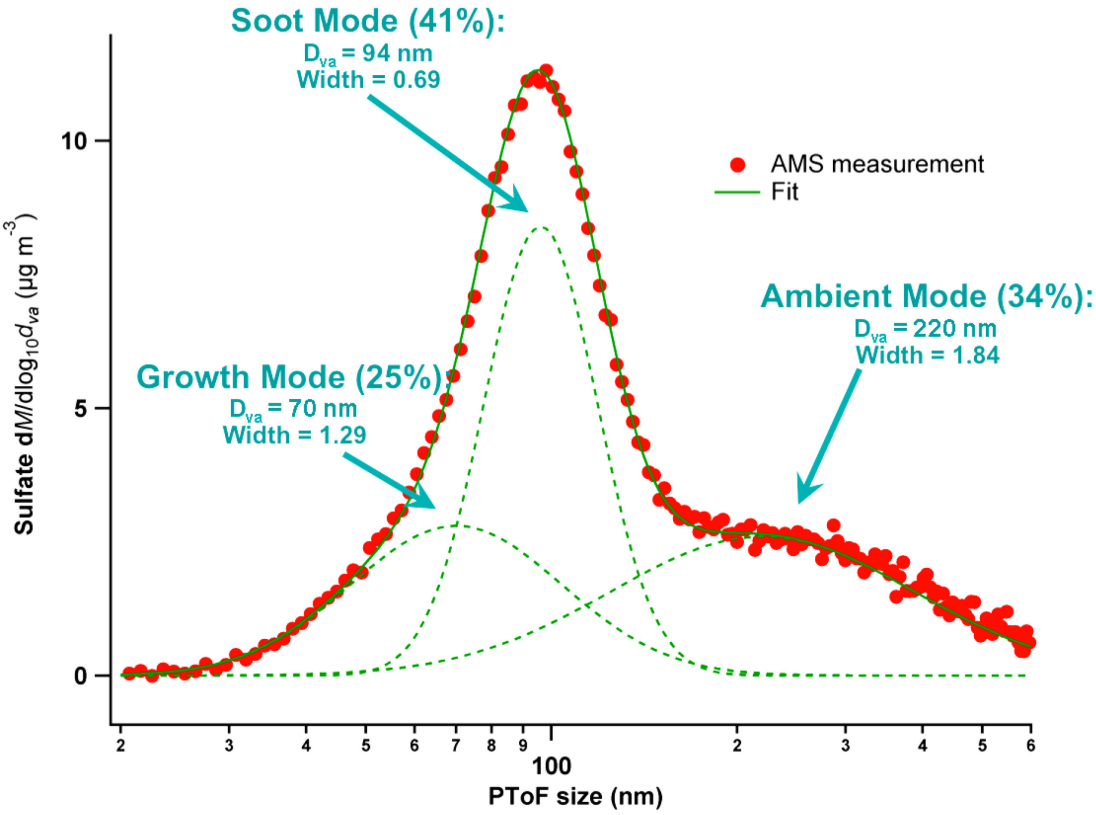

(b)

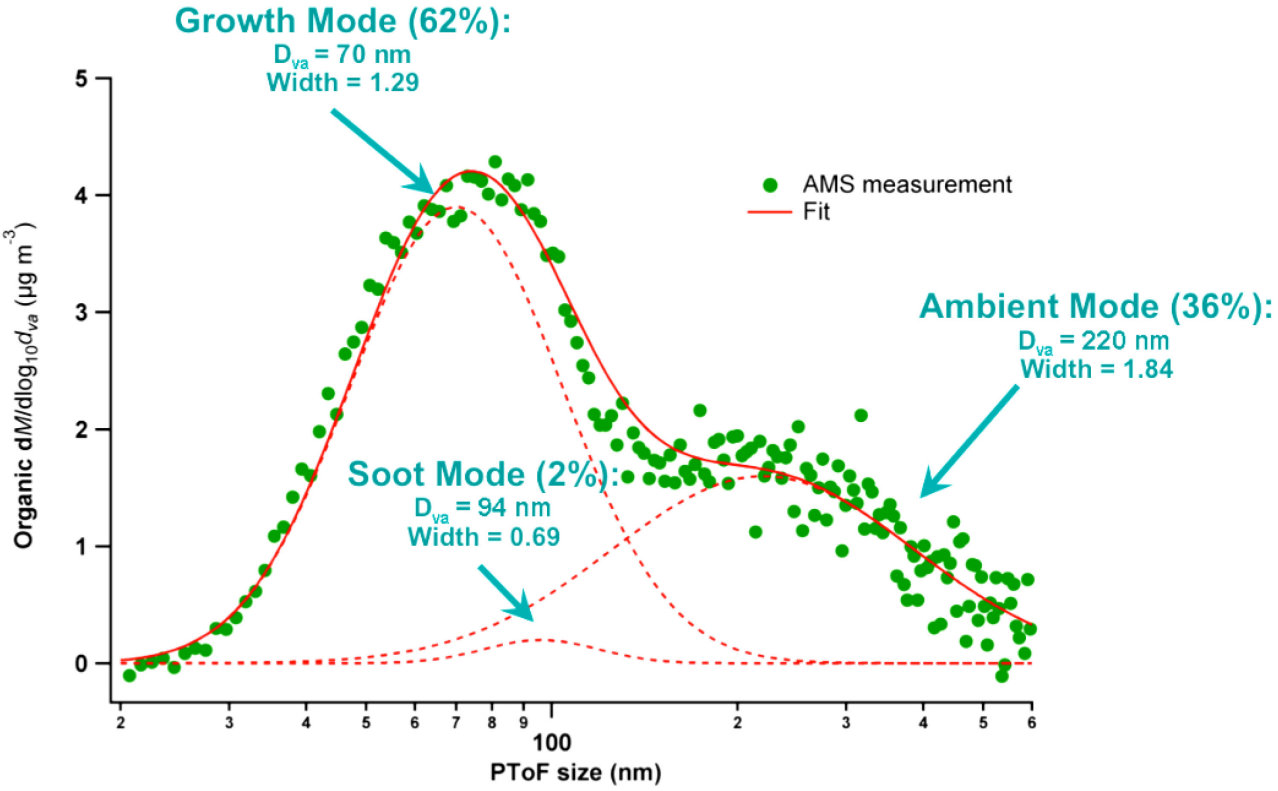

Figure 3: PM mode breakdown for (a) sulfates and (b) organics

To investigate this experimental observation, we ran the microphysical simulation model, and achieved results that agree with the experiments; sulfates primarily went to the soot coating mode, and organics existed in the liquid droplet mode. Figure 4(a) shows the sulfuric acid mass fraction in each mode as a function of time. It shows that more than 90% of sulfuric acid goes to the soot coat-

ing mode, and Figure 4(b) indicates that some hydrocarbons go to the liquid droplet mode, and the soot coating mode has almost no organic composition.

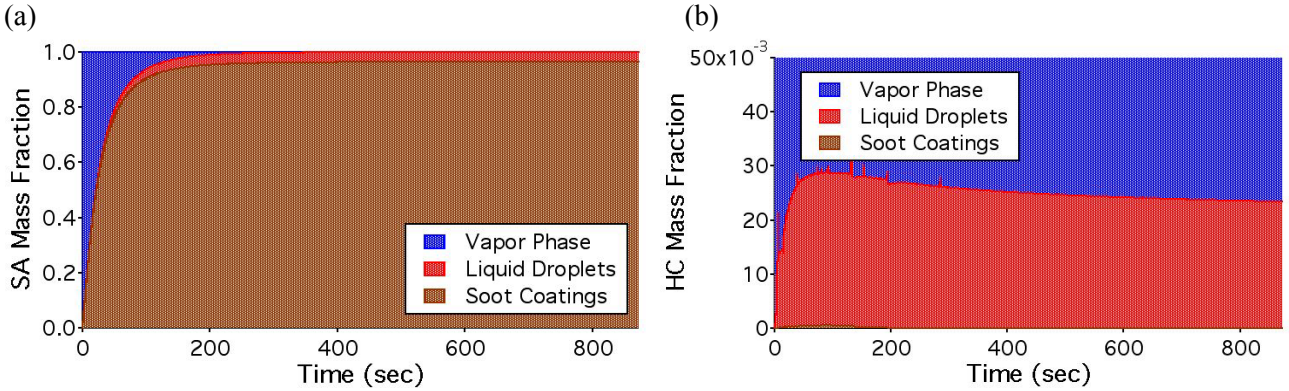

Figure 4: Mass split of (a) sulfates and (b) organics for the liquid droplet mode and the soot coating mode

We attribute this difference in the mode split to different surface uptake mechanisms between the liquid droplets and soot particles. Through the simulation, we found that because of surface tension, the soot particles can accommodate both water-insoluble and water-soluble species on the surface, and can still grow significant water-soluble coatings. However, on the liquid droplets, although the initial core is formed by water-soluble sulfuric acid, as some water-insoluble hydrocarbons start to come to the surface, it forms a thin-film of water-insoluble layer, and prevent water-soluble sulfuric acid to condense any more. At this point, only water-insoluble hydrocarbons can condense on liquid droplets. Figure 5 illustrate the difference of uptake mechanisms.

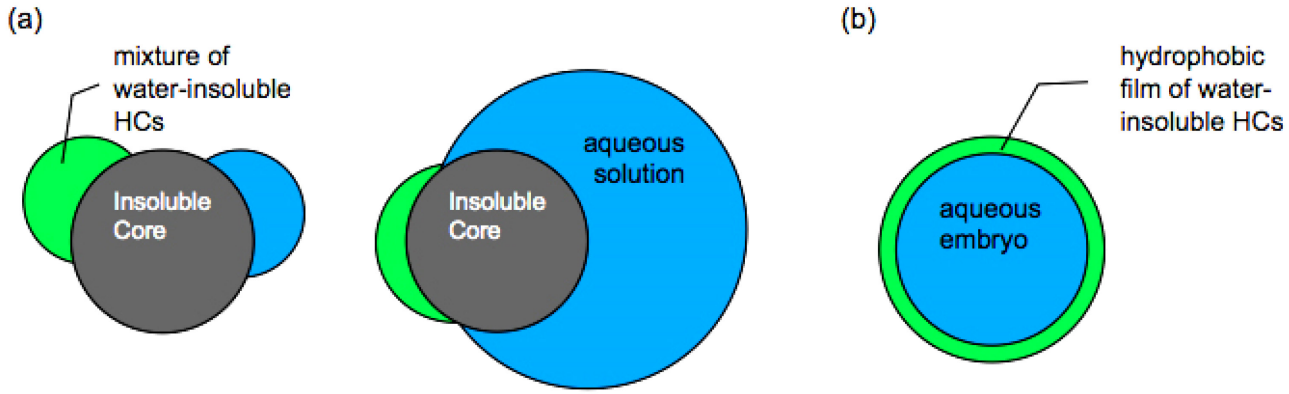

Figure 5: Different uptake mechanisms by (a) solid soot core and (b) liquid sulfuric acid core

4 CONCLUSION

We developed a microphysical simulation model to include organic PM mechanisms. By adopting a six-species surrogate organic species, we could explain the organic PM behavior obtained from two different experimental measurements both qualitatively and quantitatively. This microphysical model with surrogate organics species will be able to contribute to understanding of the full aspects of volatile PM in the aircraft engine exhaust.

REFERENCES

Jun, M., 2011. Microphysical Modeling of Ultrafine Hydrocarbon-containing Aerosols in Aircraft Emissions, s.l.: PhD thesis, Department of Aeronautics and Astronautics, Massachusetts Institute of Technology.

Peck, J. et al., 2014. Experimental and Numerical Studies of Sulfate and Organic Condensation on Aircraft Engine Soot. Proceedings of ASME Turbo Expo 2014.

Robinson, A. et al., 2007. Rethinking Organic Aerosols: Semivolatile Emissions and Photochemical Aging. Science, Volume 315.

Wong, H.-W.et al., 2014. Detailed Micrphysical Modeling of the Formation of Organic and Sufuric Acid Coatings on Aircraft Emitted Soot Particles in the Near Field. Aerosol Science & Technology, Volume 48, pp. 981-995.

Wong, H.-W.et al., 2015. Roles of Organic Emissions in the Formation of Near Field Aircraft-Emitted Volatile Particulate Matter: A Kinetic Microphysical Modeling Study. Journal of Engineering for Gas Turbines and Power, Volume 137, p. 072606.

Wong, H.-W.et al., 2008. Microphysical Modeling of Ground-Level Aircraft-Emitted Aerosol Formation: Roles of Sulfur-Containing Species. Journal of Propulsion and Power, Volume 24, pp. 590-602.

Yu, F., 2007. Improved Quasi-Unary Nucleation Model for Binary H2SO4-H2O Homogeneous Nucleation. Journal of Chemical Physics, Volume 127.

Yu, Z. et al., 2014. Uptake Coefficiencts of Some Volatile Organic Compounds by Soot and Their Application in Understanding Particulate Matter Evolution in Aircraft Engine Exhaust Plumes. Journal of Engineering for Gas Turbines and Power, Volume 136, p. 121501.

Development of a Certification Method for Aircraft Engine Non-volatile PM Emissions: Results from the North American Reference System Deployment in the Aviation-Particle Regulatory Instrument Demonstration Experiment (A-PRIDE) 4 Campaign

Philip D. Whitefield*, Prem Lobo, Donald E. Hagen, Elizabeth A. Black
Center of Excellence for Aerospace Particulate Emissions Reduction, Research, Missouri University of Science and Technology, Rolla, Missouri, USA

Richard C. Miake-Lye, Zhenhong Yu
Aerodyne Research Inc., Billerica, MA, USA

Lukas Durdina, Benjamin T. Brem, Jing Wang
Empa, Swiss Federal Laboratories for Materials Science and Technology, Dübendorf, Switzerland

Gregory J. Smallwood, Kevin A. Thomson
National Research Council Canada, Ottawa, Canada

Theodor Rindlisbacher
Federal Office of Civil Aviation, Bern, Switzerland

Frithjof Siegerist
SR Technics, Zürich Airport, Switzerland

Amewu A. Mensah, Joel C. Corbin, Manuel Abegglen, Berko Sierau,
Institute for Atmospheric and Climate Science, ETH Zürich, Zürich, Switzerland

THE RESULTS ARE PUBLISHED IN THE PAPER

Measurement of Aircraft Engine Non-Volatile PM Emissions: Results of the Aviation-Particle Regulatory Instrumentation Demonstration Experiment (APRIDE) 4 Campaign

Prem Lobo,[1,2] Lukas Durdina,[3,4] Gregory J. Smallwood,[5] Theodor Rindlisbacher,[6]
Frithjof Siegerist,[7] Elizabeth A. Black,[1] Zhenhong Yu,[8] Amewu A. Mensah,[9] Donald E. Hagen,[1]
Richard C. Miake-Lye,[8] Kevin A. Thomson,[5] Benjamin T. Brem,[3,4] Joel C. Corbin,[9,*]
Manuel Abegglen,[9] Berko Sierau,[9] Philip D. Whitefield,[1] and Jing Wang[3,4]

1 *Center of Excellence for Aerospace Particulate Emissions Reduction Research, Missouri University of Science and Technology, Rolla, Missouri, USA*
2 *Centre for Aviation Transport and the Environment, Manchester Metropolitan University, Manchester, UK*
3 *Empa, Swiss Federal Laboratories for Materials Science and Technology, Dübendorf, Switzerland*
4 *Institute of Environmental Engineering, ETH Zürich, Zürich, Switzerland*
5 *Measurement Science and Standards, National Research Council Canada, Ottawa, Canada*
6 *Federal Office of Civil Aviation, Bern, Switzerland*
7 *SR Technics, Zürich Airport, Zürich, Switzerland*
8 *Aerodyne Research Inc., Billerica, Massachusetts, USA*
9 *Institute for Atmospheric and Climate Science, ETH Zürich, Zürich, Switzerland*

Aerosol Science and Technology, volume 49, issue 7, pp 472-484

http://dx.doi.org/10.1080/02786826.2015.1047012

* *Corresponding author:* Philip D. Whitefield, Center of Excellence for Aerospace Particulate Emissions Reduction, Research, Missouri University of Science and Technology, Rolla, MO 65409, USA, Email: pwhite@mst.edu

Measurement of aircraft engine emissions inside the airport area

Ralf Kurtenbach*, Peter Wiesen,
University of Wuppertal, Inst. Atmos. & Environ. Res., 42097 Wuppertal, Germany

Oleksandr Zaporozhets, Kateryna Synylo
National Aviation University, Kosmonavta Komarova 1, 03058 Kyiv, Ukraine

Keywords: airport air pollution, aircraft engine emissions, exhaust gases jet, plume, concentration, emission, index, real operation conditions

Abstract: Deterioration of air quality near the busiest airport and adverse consequences for public health is a crucial problem, especially in relation to the breach of limit and target values for many air pollutants, mainly nitrogen oxides and particulate matter. Analysis of inventory emission results at major European airports highlighted, that aircraft is the dominant source of air pollution in most cases under consideration. Aircraft is a special source of air pollution due to some features. The most important feature of the source of emission is a presence of exhaust gases jet, which contains significant momentum and thermal buoyancy and in accordance may transport contaminant on rather large distances. The value of such a distance is defined by engine power setting and installation parameters, mode of an airplane movement, meteorological parameters. Of course aircraft is a moving source of pollution and with varied emission factor during the LTO and ground running procedures. In addition, despite designed LTO cycles, operational procedures of aircraft are sometimes not well adapted to engine settings (thrust), which are specified under ICAO engine emission certification procedure. This study was devoted to measure the concentrations of NO_x and CO_2 in jet and plume modes under real operation conditions (when aircraft is taxing, accelerating on the runway and take-offs) at the airport area with aim to provide input data (emission index and maximum concentration) for improvement and validation tasks of complex model PolEmiCa. Combined approach of modeling and measurement methods provides a more accurate representation of aircraft emission contribution to total air pollution (local pollution) in airport area. Such an approach has been proven to be successful at International Boryspol Airport.

1 INTRODUCTION

During the last decade several studies were focused on the effects of aircraft emissions at ground level because they contribute significantly to air pollution at airports and nearby residential areas [Heland et al., 1998; Popp et al., 1999; Schäfer et al., 2003; Herndon et al., 2004; Celikel et al., 2005; Schäfer et al., 2007; Johnson et al., 2008; Bossioli E. et al., 2013].

Aircraft are a special source of air pollution due to some features. Most important is the presence of a jet of exhaust gases, which can transport pollutants over rather large distances because of high exhaust velocities and temperatures. Such a distance is determined by the engine power setting and installation parameters, mode of airplane movement and meteorological parameters. The results of jet model calculations show that, depending on initial data, the jet plumes from aircraft engines range from 20 to 1000 m and sometimes even more [Zaporozhets and Synylo, 2005]. Of course aircraft is a moving source of pollution and with varied emission factor during the LTO and ground running procedures. In addition, despite designed LTO cycles, operational procedures of aircraft are sometimes not well adapted to engine settings (thrust), which are specified under ICAO engine emission certification procedure [Hüttig et al., 1999; Masiol et al., 2014].

Local and regional air pollution produced by aircraft emissions is assessed by measurements, which provide initial information on pollutant concentrations from which corresponding emission

* *Corresponding author:* Ralf Kurtenbach, University of Wuppertal, Inst. Atmos. & Environ. Res., 42097 Wuppertal, Germany. Email: kurtenba@uni-wuppertal.de

indices (EI) are derived. These data are then used in specific models to describe airport air quality. The model output e.g. PolEmiCa may be used for the development of certain measures to improve air quality around airports.

In the present study air pollutant emissions, e.g. nitrogen oxides ($NO_x = NO + NO_2$), were measured from passenger aircraft at Boryspol airport (Kiev) or existing emission data from Athens International Airport (AIA) were used for the improvement of the model PolEmiCa. Investigation of aircraft emissions under real conditions (take-off, landing and ground taxi) in the plume (jet- and dispersion-regime) to determinate of aircraft emission indices under real operation conditions and comparison to ICAO databank. At least measurement data will use to validate complex model PolEmiCa for different operational and meteorological conditions.

2 RESULTS AND DISCUSSIONS

2.1 *Experimental investigation inside the airport area*

Existing emission data from Athens International Airport (AIA) campaign were used for the evaluation and the first comparison with the PolEmiCa. In table 1 the comparison between PolEmiCa model output (1) and the measured (2) NO_x concentration in the dispersion-regime is shown.

Table 1: Comparison between PolEmiCa model output (1) and the measured (2) NO_x concentration in the dispersion-regime

aircraft	engine	$C_{NOx}[\mu/m^3]$ (1)	$C_{NOx}[\mu/m^3]$ (2)
B737-3YO	CFM56-3	26±3	33±3
B737-3Q8	CFM56-3	27±3	33±3
B737-45S	CFM56-3B-2	25±3	31±3
B737-4Q8	CFM56-3B-2	28±3	63±6
A310	CF6-80C	73±7	90±9
319	CFM56-5B5	30±3	46±5
B747-230	JT9D-7R4G	95±10	90±9
A321-211	CFM56-5B-3	40±4	52±5
A320-214	CFM56-5B4	20±2	23±2
B737-33A	CFM56-3	25±3	18±2

Good agreement between model results (1) and measurements (2) were found, but in some cases large differences were observed, which can been explained by following reasons:

Averaging period of measured concentration (1 minute) is quite difficult to detect maximum concentration in plume due to quite big transport distance between aircraft engine and monitoring station (1000±500 m); the investigation of the dispersion-regime was only implemented under campaign.

Experimental studies at International Boryspol Airport (IBA) were focused on measurement of NO_x concentrations in the plume, both the jet- and dispersion-regime of aircraft engines under real operating conditions (taxi, accelerating on the runway and take-off). Measurements were carried out at two measurement sites. A stationary station A (jet-regime) close-by the runway (30 m) with a measuring height of 3.0 m. A mobile station B (dispersion-regime) at varying distances and locations from the runway due to prevailing wind direction and with a measuring height 3.6 and 5.7 m. Figure 1 shows as an example the measurement location set up 2 at A and B.

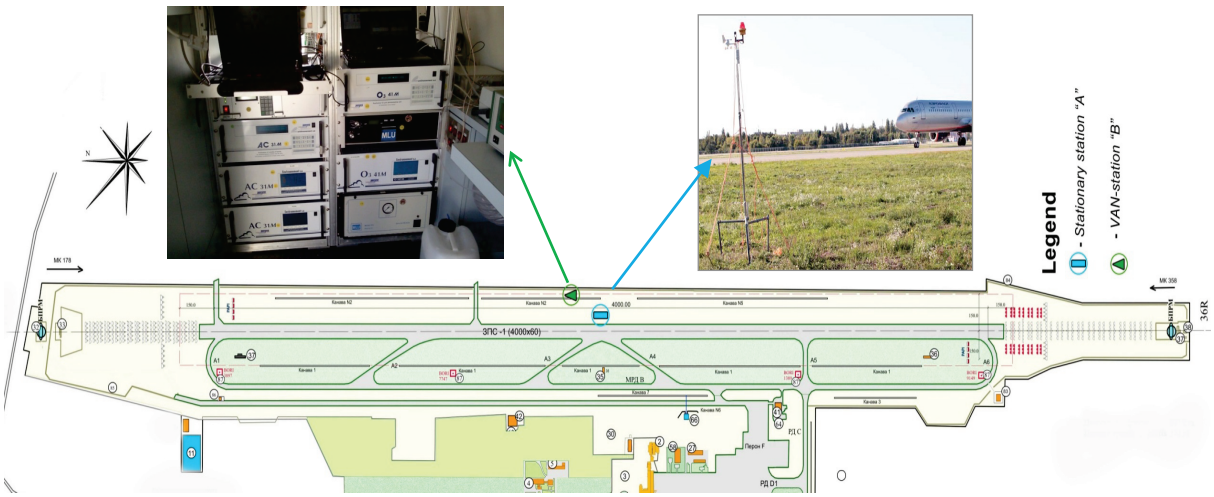

Figure 1: Location set up 2: Stationary station A and mobile Station B (Van), both downwind. Investigation of aircraft movement at landing and take-off

It was guaranteed, that largest part of the aircraft exhaust was scanned by NO_x measurement systems. Analysis of the data exhibited that concentration peaks for NO_x and CO_2 are unambiguously correlated with aircraft plumes. Figure 2 shows the background and plume concentration for NO, NO_x and CO_2 at 3.6 m sampling height for different aircraft at take-off (T/O) and ground taxi (TX) conditions.

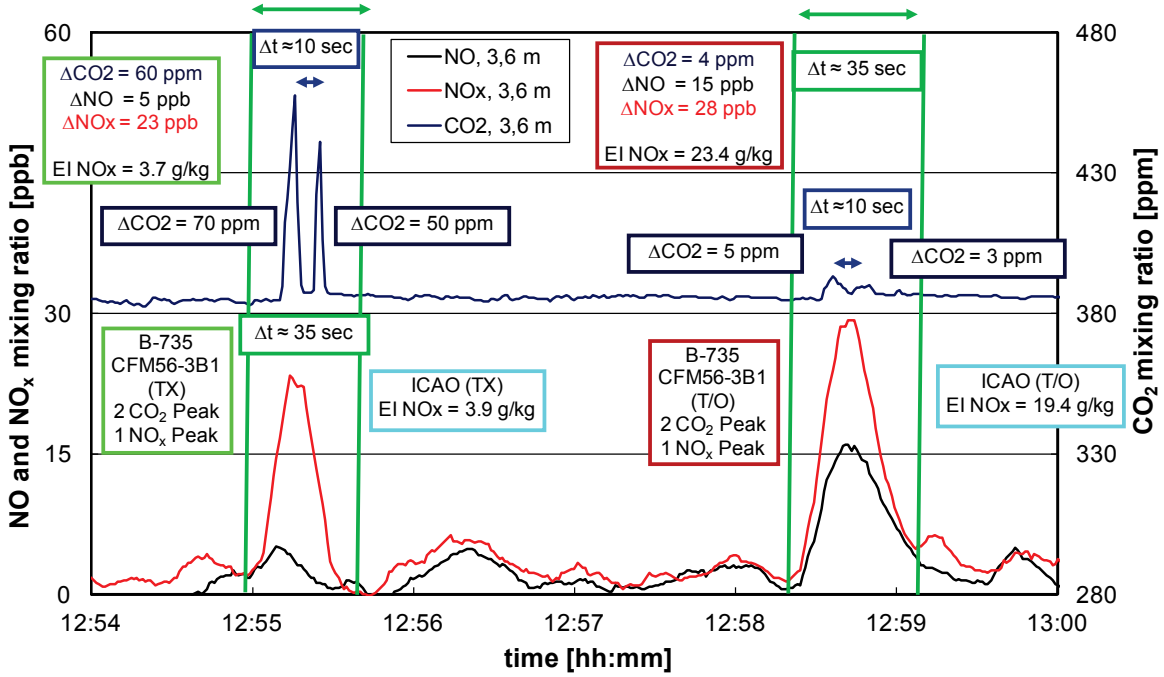

Figure 2: Location set up 1: Background and plume concentration for NO, NO_x and CO_2 at mobile station B at take-off (T/O) and ground taxi (TX)

Thus, the maximum operation mode of an aircraft engine is characterized by the highest NO_x emission, while the taxi mode – by a much lower NO_x value. Clear separated emissions from both engines, delay time ≥ 10 sec (peak to peak); e.g. Boeing B735 with two CFM56-3B1 engines were detectable for TX and T/O conditions (see figure 2). This indicate a jet -regime.

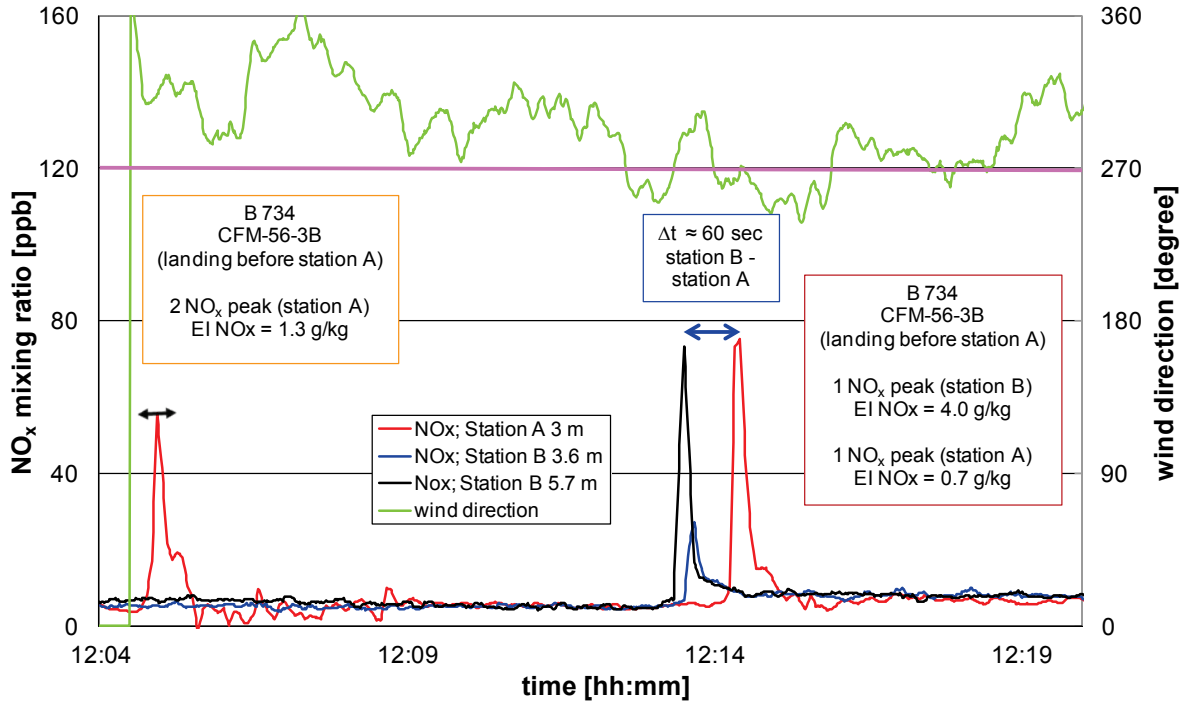

Figure 3: Location set up 2: Background and plume concentration for NO_x at station A and B at landing (L) and the prevailing wind direction

Figure 3 shows the background and plume concentration for NO_x at station A and B at landing (L) and the prevailing wind direction. Overlap emissions from both engines, delay time ≤ 10 sec (peak to peak); e.g. B 734 with two CFM-56-3B engines, were detectable for T/O conditions. Indication of a dispersion-regime.

At 12:14 the emission peak of NO_x is measured at both stations, because this wind direction guarantees, that the maximum concentration in jet will be detected first at station B and 60 sec later at station A. In case of north-west wind direction e.g. at 12:05 only a emission peak of NO_x can be detected at station A.

General measured delay time, peak to peak at one station and peak station A to peak station B e.g. 60 sec for B734 and in addition the prevailing wind direction are important parameter for model validation! From the measured emission data at least emission indices were calculated for TX , L and T/O conditions.

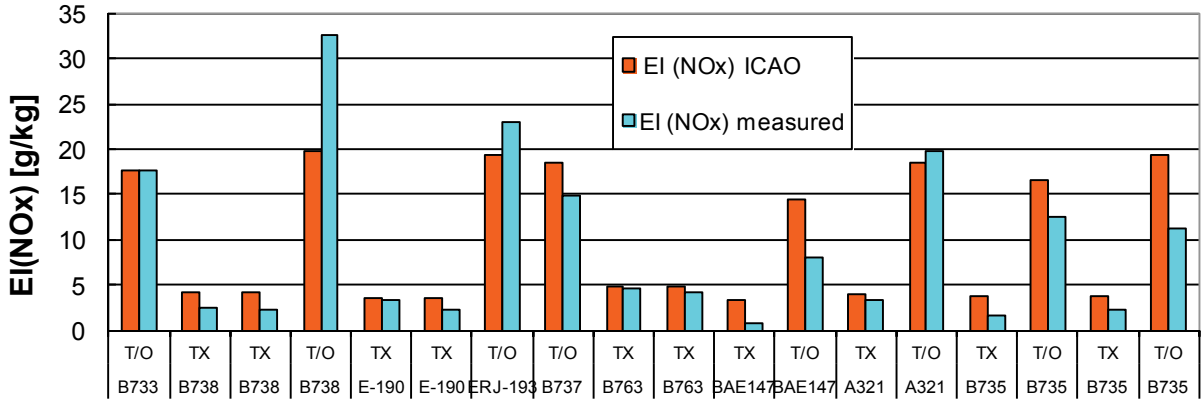

Figure 4: Calculated emission indices e.g. for T/O and TX in comparison with ICAO data

Figure 4 shows the comparison between calculated emission indices e.g. for T/O and TX and ICAO data. Differences between measurements and ICAO data for EI_{NOx} at T/O and in particular for EI_{NOx} at TX were found, because real operation conditions are not corresponding to certification one. For further calculations and in particular model validation real measured EI_{NOx} were used.

2.2 *Validation of complex model PolEmiCa*

A complex model PolEmiCa (Pollution and Emission Calculation) for the assessment of air pollution produced inside the airport and emission inventory analyses, has been developed at the National Aviation University (Kyiv, Ukraine) [Zaporozhets and Synylo, 2005]:

1. engine emission model – emission assessment for aircraft engines, including the influence of operational factors;
2. jet transport model – transportation of the pollutants by the jet from the aircraft engine exhaust nozzle;
3. dispersion model – dispersion of the pollutants in the atmosphere due to turbulent diffusion and wind transfer.

At an airport the biggest part of the LTO cycle is devoted to aircraft maneuvering on the ground (engine run-ups, taxing, accelerating on the runway). It is subjected to a fluid flow that can create a strong vortex between the ground and engine nozzle, which has essential influence on the structure and basic mechanisms (Coanda and buoyancy effects) of the jet of exhaust gases. The complex model PolEmiCa has been improved in the jet/plume transportation modeling regime by a CFD code (Fluent 6.3). Using CFD codes allow investigating structures, properties, and fluid mechanisms of the jet and also to obtain a deep understanding of pollutant transportation and dilution by the jet from an aircraft engine also taking into account interplay with the ground surface.

As shown from table 2 and figure 5, the modeling results for each engine are in good agreement with the results of NO_x measurements due to taking into account the jet- and dipersion-regime during experimental investigation at Boryspol airport. Also using CFD-code (Fluent 6.3) allow to improve results on 30% (coefficient of correlation, r = 0.76) due to taking into account the lateral wind and ground impact on jet parameters (buoyancy effect height, lateral and vertical deviation) and correspondingly on concentration distribution in plume.

Table 2: Comparison measured and calculated concentration of NO_x produced by aircraft engine emissions at accelerating stage on the runway

Aircraft	Aircraft Engine	NO_xmeasured			PolEmiCa CFD (Fluent 6.3)		PolEmiCa	
		Back ground NO_x	3 м NO_x	6 м NO_x	1 engine NO_x	All engines NO_x	1 engine NO_x	All engines NO_x
BAE147	LY LF507-1H	1,70	22,067	33,9	35,1	70,46	48,9	202,3
A321	CFM56-5B3/P	0,72	44,00	54,2	90,85	182,90	184,2	371,2
B735	CFM-563C1	0,77	94,095	76,57	60,03	120,91	35,3	71,10
B735	CFM56-3B1	1,74	29,20	23,4	42,34	85,30	33,7	67,76

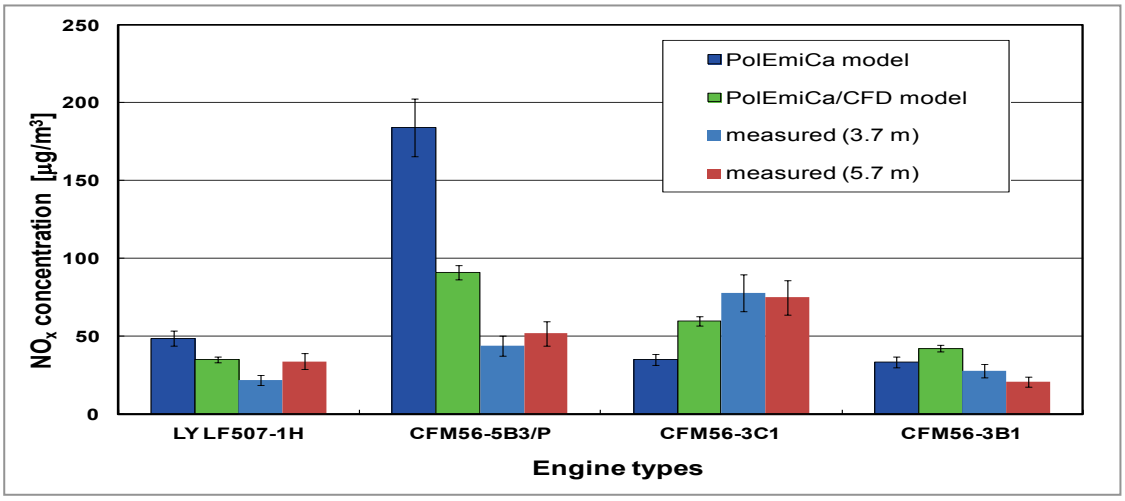

Figure 5: Comparison of the PolEmiCa and PolEmiCa/CFD model results with the measured NO_x concentration at different height for selected aircraft engines under maximum operation mode

The combined approach of modeling and measurement methods provides a more accurate representation of aircraft emissions to total air pollution (local pollution) at an airport. Modeling gives the scientific grounding for the measurement campaign of aircraft engine emissions, particularly, a

scheme for the positioning of monitoring stations with aim to detect maximum concentration in plume from aircraft engines. The model allows to predict the sample height of the exhaust gas jet with taking into account buoyancy effects and the interplay with the ground surface.

3 CONCLUSIONS:

- Aircraft emissions of nitrogen oxides (NO_x = NO+NO_2) were measured under real conditions (take-off, landing and ground taxi) in the plume (jet- and dispersion-regime) to determinate NO_x emission indices (EI_{NOx})and to compare this with ICAO databank.
- Differences between measurements and ICAO data for EI_{NOx} at T/O and in particular for EI_{NOx} at TX were found, because real operation conditions are not corresponding to certification one. For further calculations and in particular model validation real measured EI_{NOx} were used.
- The results of measurement campaign provide the validation and improvement of complex model PolEmiCa.
- The modeling results for each engine are in good agreement with the results of NO_x measurements due to taking into account the jet- and dipersion-regime during experimental investigation at Boryspol airport. Using CFD-code (Fluent 6.3) allow to improve results on 30% due to taking into account the lateral wind and ground impact on jet parameters (buoyancy effect height, lateral and vertical deviation) and correspondingly on concentration distribution in plume.

REFERENCES:

Ayres E., 2001, Airports and cities: can they coexist? World Watch Institute.V.14. N°4.

Bossioli E., Tombrou M, Helmis C, Kurtenbach R, Wiesen P, Schäfer K, et al., 2013, Issues related to aircraft take-off plumes in a mesoscale photochemical model. Science of the Total Environment: 456-457.

Celikel A, Duchene N, Fuller I, Peters S., 2005, Airport local air quality studies: concept document. EUROCONTROL Experimental Centre EEC/SEE/2005/003.

Heland, J.; Schäfer, K., 1998, Determination of major combustion products in aircraft exhausts by FTIR emission spectroscopy. Atmospheric Environment 32: 3067-3072.

Herndon, S C.., Shorter, J.H., Zahniser, M.S., Nelson, D.D., Jayne, j., Brown, R.C., Miake-Lye, R.C., Waitz, I., Silva, P., Lanni, Th., Demerjian, K. and Kolb, C.E., 2004, NO and NO_2 Emission Ratios Measured from In-Use Commercial Aircraft during Taxi and Takeoff. Environmental Science & Technology 38: 6078-6084.

Hüttig G, Bleschmidt F, Hotes A., 1999 Entwicklung und Erprobung einer Methode zur Bewertung der Schadstoffimmissionen in der Umgebung von Flugplätzen, Band I: Ermittlung der Emissionen, Forschungbericht.

Johnson, G.R., Mazaheri, M., Ristovski, Z.D., Morawska, L.A., 2008. Plume capture technique for the remote characterization of aircraft engine emissions. Environmental Science & Technology 42: 4850-4856.

Masiol M., Harrison R., 2014, Aircraft engine exhaust and other airport-related contribution to ambient air pollution: a review. Atmospheric Environment 95: 409-455.

Schafer, K.; Jahn, C.; Sturm, P.; Lechner, B.; Bacher, M., 2003, Aircraft emission measurements by remote sensing methodologies at airports. Atmos. Environ. 37: 5261-5271.

Schürmann G., Schäfer K. et.al., 2007, The impact of NO_x, CO and VOC emissions on the air quality of Zurich airport. Atmospheric Environment 41: 103-118.

Zaporozhets O., Synylo K., 2005, POLEMICA – tool for air pollution and aircraft engine emission assessment in airport, The Second World Congress “Aviation in the XXI-st century”, Kyiv: National Aviation University, 2005: 4.22–4.28.

Estimating Gaseous Emissions Production of an Entire Flight of a Commercial Aircraft Based on Emission Measurements and Actual Flight Data Records

Enis T. TURGUT*,
Anadolu University, Aircraft Airframe and Powerplant Dept., Eskisehir, Turkey

Mustafa CAVCAR
Anadolu University, Dept. of Flight Training, Eskisehir, Turkey

Ozan D. YAY
Anadolu University, Dept. of Environmental Engineering, Eskisehir, Turkey

Mehmet UCARSU
Turkish Technic, Inc., Istanbul, Turkey

Elif YILMAZ
Anadolu University, Dept. of Environmental Engineering, Eskisehir, Turkey

Oznur USANMAZ
Anadolu University, Dept. of Air Traffic Control, Eskisehir, Turkey

Kadir ARMUTLU
Anadolu University, Aircraft Maintenance Center, Eskisehir, Turkey

Tuncay DOGEROGLU
Anadolu University, Dept. of Environmental Engineering, Eskisehir, Turkey

ABSTRACT: In this study, engine emissions measurement results and actual flight data records are used to obtain an emissions production profile of gate-to-gate flight activity. The platform and powerplant selected are B737-800 and CFM56-7B26, while the emissions measured are carbon monoxide (CO) and nitrogen oxides (NO_x). By installing a sample probe inside the engine, the emissions are measured during a test matrix between idle and the highest power of an engine, in a test-cell environment. By establishing empirical relationships between the engine power and the amount of certain regular emissions species, emissions are not only identified for a landing and takeoff (LTO) envelope, but also for climb, descent and cruise flights, which take place above 3000 ft, the theoretical mixing height altitude. According to the analyses, the total CO emissions of 52 minute flight was found to be 28.1 kg, with 37.1% of this value being produced during the LTO activity, below an altitude of 3000 ft. The total NO_x emissions were found to be 27.4 kg, with the LTO activity emissions constituting 21.2% of the total NO_x emissions of the entire flight. In addition, since CO emissions are strong functions of fuel flow at low power settings, in real world operating conditions, the CO emissions during a taxi run may be considerably different from the standard values, due to variation in engine power based on a number of factors, such as, ambient air temperature, bleed air utilization or engine state.

1 INTRODUCTION

To understand the environmental impact of aviation, emissions research involving aircraft has been of great importance during the last decade. In addition to comprehensive emission testing by the International Civil Aviation Organization (ICAO), a number of field campaigns were dedicated to understanding emissions production of aircraft engines, particularly at ground or near ground operations and, together with other segments of flight, have yet to be fully understood (Anderson et al., 2006; Corporan et al., 2008; Presto et al., 2011).

* *Corresponding author: Enis T. Turgut, Anadolu University, Faculty of Aeronautics and Astronautics, Aircraft Airframe and Powerplant Dept., TR26470, Eskisehir, TURKEY, Email: etturgut@anadolu.edu.tr*

Since there are a great many difficulties related to actual emissions measurement of an aircraft engine, obtaining a full emissions profile for a complete flight activity, or validation of the results of different research groups, requires significant effort and close collaboration.

One of the main obstacles to a precise identification of the total emissions production of a complete flight is difficulties of obtaining actual emissions index. Existing emissions indices, obtained through actual measurements, have certain limitations. These include explaining limited areas of a flight (i.e., only the LTO cycle), determination for only specific fuel flow rates and power settings, not considering the effects of engine age or maintenance history, ambient conditions, and so on. Although there have been certain studies on modelling emissions on engine parameters (Tsague et al., 2007; Chandrasekaran and Guha, 2012), it is difficult to obtain particular information, such as the total emissions production of a flight, or the emissions footprint (not only CO_2) of each flight, or even of each seat. Furthermore, this uncertainty creates unfair treatment of airlines, via overestimated or underestimated emissions charges, based on highly generalized standard data (e.g., the emissions index or time in mode).

In this study, the emissions production mechanism of a B737-800 aircraft powered by a CFM56-7B26 series engine is modelled using the results of two consecutive actual test cell emissions measurements and actual flight data records of a single short-ranged domestic flight of the same aircraft. The measurements were conducted at the overhaul engine test cell facility of Turkish Technique Inc. in Istanbul, with flight data obtained from the national flag carrier airline of Turkey, Turkish Airlines, in a framework as part of a national project.

2 BACKGROUND

In the following sections, all of the engine emissions results are based on two consecutive measurements. During the tests, the engine is run for relatively longer durations (e.g., more than five minutes) at certain stable power settings. Since the same observations at these stable power settings may affect the empirical equations and lead to a higher root-mean square error (RMSE), only observations during the acceleration and deceleration are considered. Although not considering the data points at stable power settings greatly decreases the size of the dataset, the remaining data points (i.e., 671 for Test1 and 412 for Test2) are still comfortably sufficient for a statistical empirical analysis. Unless otherwise stated, the dataset represents the data points of both tests.

2.1 *Test Procedure and Measurement System Overview*

A Teledyne 7500 model non-dispersive infrared (NDIR) instrument was used to measure CO and CO_2 emissions as is required in ICAO procedures. The method depends on the fact that CO and CO_2 absorb infrared radiation. A Teledyne 9110 TH model gas analyzer was used for the measurement of NO, NO_2 and NO_x concentrations. The temperature of the heated line before the NO_x analyzer was approximately 65±15ºC. Water vapor was removed from the sample line and an NO_x measurement was made on a dry basis in order to minimize any quenching effect. Lastly, a Teledyne 4030 model THC analyzer was used for the measurement of total hydrocarbons equivalent to CH_4 in the sample gas. The analyzer measures THC with a flame ionization detector. The measurement system is mostly in accordance with ICAO gas turbine engine gaseous emission measurement recommendations.

2.2 *Empirical Model*

Observations plotted with fuel flow and fit curves are shown in Fig. 1. In order to increase accuracy, a number of the outliers, depicted by red crosses, have not been accounted into empirical models. Note that a proportion of outliers is observed due to engine warm-up effects, whereas others are caused by log error of the analyzers.

As can be seen from Fig. 1, at low fuel flow rates, CO concentrations appear to be a strong function of fuel flow, where even a slight variation in fuel flow at low power settings results in a dramatic variation in CO concentrations. Being strongly dependent on fuel flow at low engine power settings, and considering that the idle power of an aircraft engine can be affected by a number of external factors, the trend shown in Fig. 1 reveals that inventory studies of typical airport traffic may involve large variability in CO concentrations during the LTO cycle. It is also found that a best fit

curve for NO_x concentrations and fuel flow rates can be established with a second degree polynomial function.

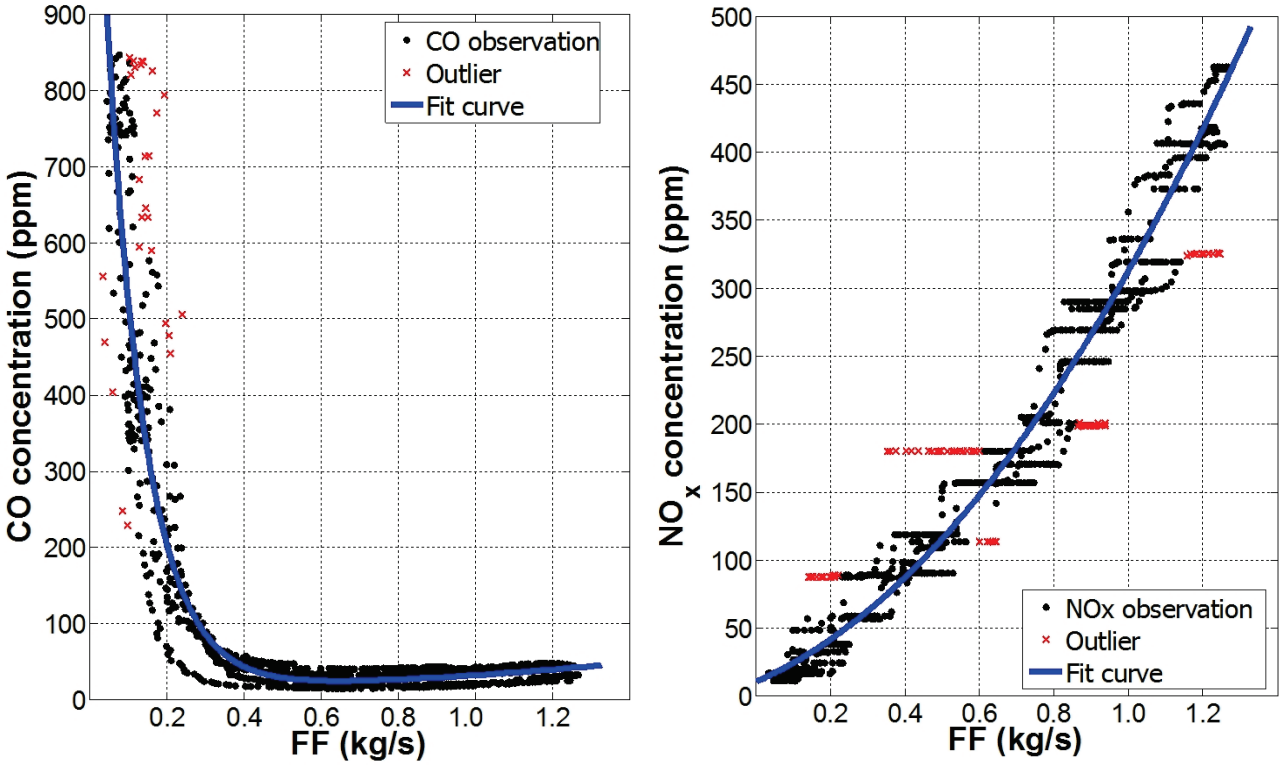

Fig. 1 CO (left) and NO_x concentrations as a function of fuel flow (Tests 1 and 2)

The coefficients and key statistical parameters of each empirical model are shown in Table 1. Even though the statistical parameters can be improved when each test is considered separately, the results of the dataset of two tests appear to be statistically highly significant.

Table 1 Coefficients of empirical equations (ff represents fuel flow)

Species	Empirical equation	Adjusted R^2	RMSE
CO	$1381 \times e^{-9.904 \times ff} + 11.37 \times e^{1.038 \times ff}$	0.897	55.71
NO_x	$184.1 \times ff^2 + 118.2 \times ff + 10.36$	0.978	21.06

3 RESULTS AND DISCUSSION

Once the concentrations of CO and NO_x as a function of fuel flow (at sea level) are obtained, sea level emission indices can be calculated using (Johnson et al., 2008; Timko et al., 2010),

$$EI_X\left(\frac{g}{kg\ of\ fuel}\right) = \frac{X\ (ppm)}{CO_2\ (ppm)} \times \left(\frac{MW_x}{MW_{CO_2}}\right) \times 3160\left(\frac{g}{kg\ of\ fuel}\right) \quad (1)$$

where, X and EI_X denote the pollutant and the gram mass of pollutant per kilogram of fuel. MW_x and MW_{CO2} represent the molecular weight of the pollutant and carbon dioxide, respectively.

The variation of CO and NO_x concentrations and emissions indices with fuel flow can be seen in Fig. 2. Whilst the patterns of the emissions index and the concentrations of CO are similar, this is not true for the NO_x concentration and emissions index. The CO patterns of the empirical model are as for the pattern of raw data between the fuel flow and the measured CO concentrations during the emissions measurements. Regarding the case of NO_x, a different pattern is observed for the emissions index. It can be seen from Fig. 2 that the relationship between the fuel flow and the NO_x emissions index can be also explained as a linear function.

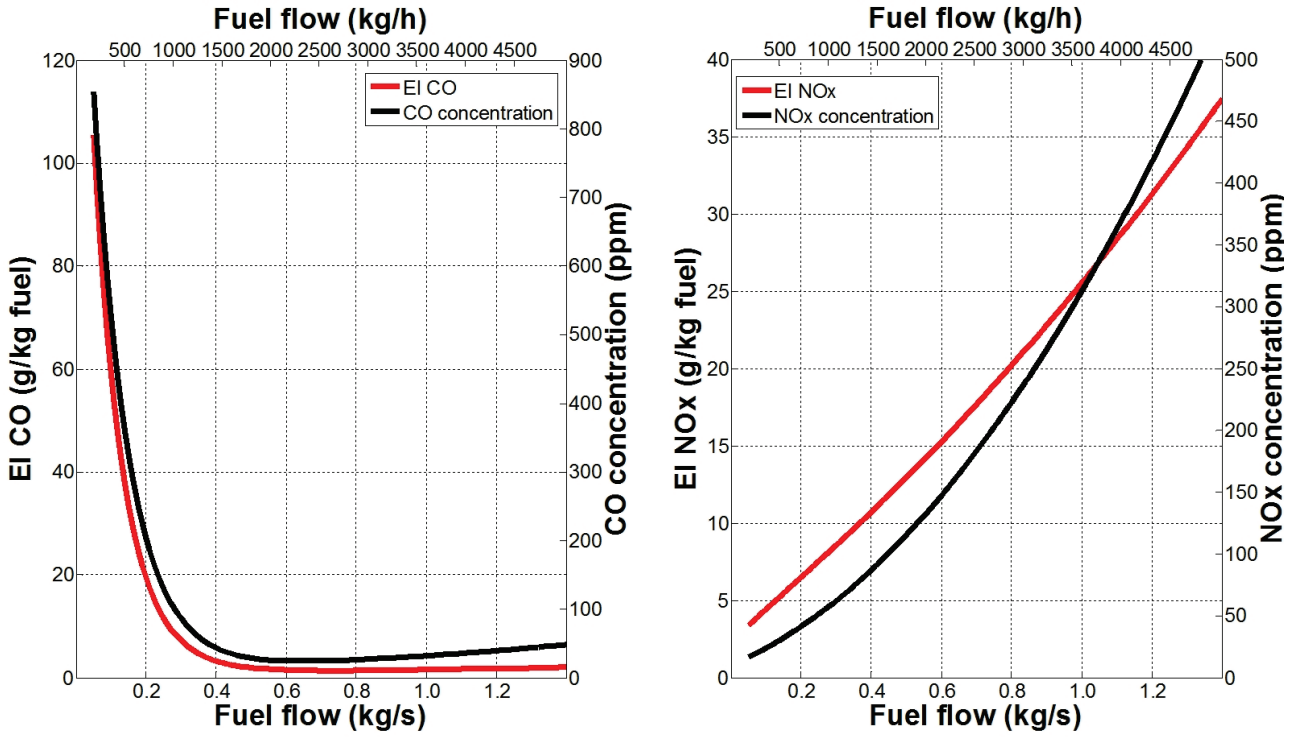

Fig. 2 Variation of emissions indices and concentrations with fuel flow based on empirical models

3.1 *Altitude Calibration*

Using Eq. (1), sea level emissions indices are determined, and enabling the calculation of corresponding emissions at ground level, up to a point where the ambient conditions and flight Mach number are still negligibly different from ground operation conditions. However, to calculate altitude emissions, the sea level emissions indices need to be calibrated. To do this, in this study, the Boeing Fuel Flow Method 2 (DuBois and Paynter, 2006) is applied as follows:

$$EICO_{Alt} = EICO_{SL}\left(\frac{\theta_{amb}^{3.3}}{\delta_{amb}^{1.02}}\right)^{x} \tag{2}$$

$$EINO_{x_{Alt}} = EINO_{x_{SL}}\left(\frac{\delta_{amb}^{1.02}}{\theta_{amb}^{3.3}}\right)^{y} e^{H} \tag{3}$$

where θ_{amb} is $T_{amb}/288$ and δ_{amb} is $P_{amb}/14.696$. The denominators are standard sea level temperature and pressure, respectively. The exponents of x and y are assumed to be 1 and 0.5, respectively. The last term of eq. (3) represents the humidity correction (H) and can be calculated from:

$$T_{ambc} = (T_{amb}/1.8) - 273.15 \tag{4}$$

$$P_{sat} = 6.107 \times 10^{((7.5\times T_{ambc})/(237.3-T_{ambc}))} \tag{5}$$

$$\omega = \frac{(0.62197058\times RH\times P_{sat})}{(P_{amb}\times 68.9473)\times(RH\times P_{sat})} \tag{6}$$

$$H = -19 \times (\omega - 0.00634) \tag{7}$$

where ω is humidity ratio, T_{ambc} is ambient temperature in °C and P_{sat} is saturation pressure at the corresponding ambient in *psi*, and *RH* is relative humidity at 60%.

Lastly, to consider the variation in air mass flow and compressibility effects, the fuel flow rate at a given altitude must be corrected to sea level fuel flow rates as follows:

$$W_{f_{SL}} = W_{f_{Alt}} \frac{\theta_{amb}^{3.8}}{\delta_{amb}} e^{0.2M^2} \tag{8}$$

where *M* denotes Mach number of flight. Once the altitude fuel flow is corrected to sea level fuel flow rates, the emissions indices at sea level for the corrected fuel flow can be easily found from empirical concentration models and Eq.(1) given above.

3.2 *Case Study*

In order to identify the amount of emissions for an entire flight, a case study is carried out in this section. For this purpose, actual flight data records of a domestic flight, with a range of 232 NM, are considered. The aircraft type selected is a B737-800, powered by a CFM56-7B26 series engine; the same engine model on which the emissions models are developed in the present study. Although the dataset of the FDR is composed of up to 50 parameters, the altitude, fuel flow, true air speed (TAS), Mach number, ambient temperature, ambient pressure and ground logic are used, as they are relevant to the current analysis.

The cumulative CO and NO_x emissions, as a function of the flight phase and the flight altitude, are shown in Fig. 3. According to the analyses, the total calibrated CO emissions of a 52 minute flight is found to be 28.1 kg, with 37.1% of this total amount being produced during LTO activity, below an altitude of 3000 ft. Given that the emissions index of CO is higher at lower power settings, such as at idle, it is also observed that almost one quarter of the total CO emissions is produced at taxi-out. Considering the taxi-out time in mode of this case study is well below ICAO standards, higher taxi-out times at busy airports may lead to an increase in this percentage. From these results, it can be seen that, for about 9.5 minutes of taxi-out, almost 6.6 kg of CO is emitted.

As expected, the CO emissions of the takeoff phase are found to be negligible. Of the other flight phases, the highest emissions production of 6.5 kg is observed during descent. One factor leading to high CO production at this phase is most likely continuous descent at relatively low power. This approach procedure could be used for less fuel consumption, using a balance between the potential and kinetic energy of the aircraft and with lower power utilization. Continuous descent approaches might lead to less fuel consumption, however, from the emissions point of view, the result might not be as straightforward as it is for fuel. Lastly, in the taxi-in phase, since traffic at the arrival airport is less than that at the departure airport, and the taxi-in time in modes are generally lower compared to taxi-out, the CO emissions are observed as only 2.4 kg.

As regards NO_x emissions, the total calibrated NO_x emissions are calculated as 27.4 kg, with an opposite pattern compared to that of CO. First, the total NO_x emissions during LTO activity constitutes 21.2% of the NO_x emissions for the entire flight. It is interesting to note that, during ground operations, the contribution of the taxi phases (both out and in) is at a relatively low level. It is calculated that during taxi-out and taxi-in, only 0.6 kg of NO_x is emitted, while during takeoff the NO_x emissions are found to be 1.2 kg. From these results, and considering takeoff time in modes do not differ greatly, the effect of longer taxi time in modes on NO_x emissions can be negligible for even lengthy time-in-mode ranges.

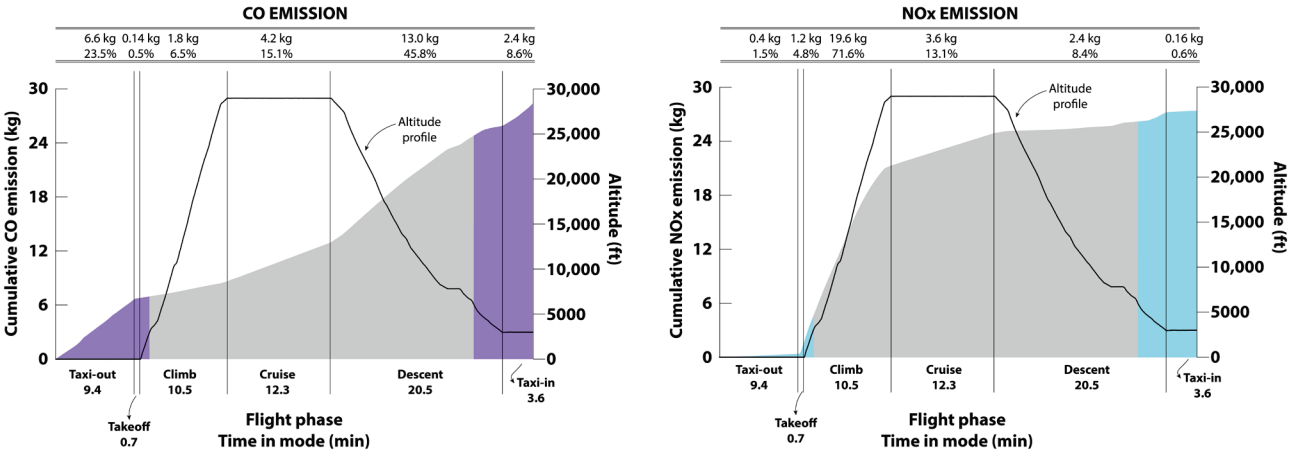

Fig. 3 CO and NO_x emissions production patterns for a typical domestic flight of 232 NM with B737-800 powered by two CFM56-7B26 turbofan engines

Regarding airborne flight activity, the climb phase becomes a flight phase, where the highest NO_x emissions are observed. The calculation reveals that almost 20 kg of NO_x emissions are emitted during 10.5 minutes of climb to an altitude of 28,000 ft. However, cruise and descent NO_x emis-

sions appear to be relatively lower than those during the climb phase, despite having a longer time in modes. During descent, there is a short low level flight at an altitude of around 7800 ft. Although it only takes a short time, this duration is sufficient for the relevant parameters to become stabilized.

Considering a typical 70% load factor, the total CO and NO_x emissions per passenger may be calculated as 250 g and 242 g, respectively. This calculation can be extended to a unit nautical mile basis, as 1.1 g CO/Pax-NM and 1.0 g NO_x/Pax-NM. It is also found that cruise distance has a significant influence on these results, because the mean cruise emissions rates are lower than the total mean of the emissions rates, depending on the flight distance and, as the cruise distance increases, both emissions per Pax-NM tend to decrease. However, since this study involves only a single case with a single flight distance, justification for this argument cannot currently be made.

If ICAO standard emissions indices, fuel flows and the time-in-modes had been used, the total CO and NO_x LTO emissions would have been calculated as 3.5 kg and 6.2 kg, respectively. According to these results, it can be concluded that the results of the actual LTO CO and NO_x emissions are found to be 48% higher and 53% lower, respectively.

Furthermore, according to ICAO standards, 94% of total LTO CO emissions and 14% of total LTO NO_x emissions would have been produced during taxi activity. However, the ratios of actual CO and NO_x emissions of the taxi activity to the total actual LTO emissions are found to be 86% and 10%, respectively.

Even though the amount of emissions is found to be significantly different than those given by the ICAO standard LTO emissions, in particular being dependent on the different time in modes, the percentages of emissions per LTO phase of the ICAO measurements and the actual measurements are found to be relatively close.

4 CONCLUSION

In this study, an emission profile of a full flight is developed using both actual emissions measurement results and actual flight data. A case study of a B737-800 flight over a 232 NM distance reveals 28.1 kg of CO and 27.4 kg of NO_x emissions, while the relative quantity of the emissions of LTO activities alone are found to be 37.1% and 21.2%, respectively. The flight phases, where the highest CO and NO_x emissions produced, are determined. Considering a conservative load factor, emissions per passenger are also calculated as 250 g CO and 242 g NO_x. The results of the study emphasize the importance of using actual data for emissions calculations.

ACKNOWLEDGMENTS

This study was supported by the Scientific and Technological Research Council (TUBITAK) (Project No. 111Y048) and Anadolu University Scientific Research Project Commissions (Project No. 1205F091) of Turkey, in partnership with Turkish Airlines and Turkish Technic. The authors thank lead engineer Mr. Mehmet Gungor, operational fuel manager Mr. Resat Gunduz, and the staff of the test cell, Mr. Cemil Ovacik, Mr. Cetin Nogan, Mr. Ersin Gokdemir, Mr. I. Volkan Kadioglu and Mr. Sevdar Ozkan, for providing the necessary installations and many useful discussions.

REFERENCES

Anderson, B. E., Chen, G., & Blake, D. R. (2006). Hydrocarbon emissions from a modern commercial airliner. Atmospheric Environment, 40(19), 3601–3612.

DuBois, D., & Paynter, G. C. (2006). Fuel flow method 2 for estimating aircraft emissions (No. 2006-01-1987). SAE International.

Chandrasekaran, N., & Guha, A. (2012). Study of prediction methods for NO_x emission from turbofan engines. Journal of Propulsion and Power, 28(1), 170–180.

Corporan, E., Quick, A., & DeWitt, M. (2008). Characterization of Particulate Matter and Gaseous Emissions of a C-130H Aircraft. Journal of the Air & Waste Management Association, 58(4), 474–483.

Johnson, G. R., Mazaheri, M., Ristovski, Z. D., & Morawska, L. (2008). A plume capture technique for the remote characterization of aircraft engine emissions. Environmental Science and Technology, 42(13), 4850–4856. doi:10.1021/es702581m

Presto, A. A., Nguyen, N. T., Ranjan, M., Reeder, A. J., Lipsky, E. M., Hennigan, C. J., … Robinson, A. L. (2011). Fine particle and organic vapor emissions from staged tests of an in-use aircraft engine. Atmospheric Environment, 45(21), 3603–3612.

Timko, M. T., Herndon, S. C., Wood, E. C., Onasch, T. B., Northway, M. J., Jayne, J. T., … Knighton, W. B. (2010). Gas turbine engine emissions—Part I: Volatile organic compounds and nitrogen oxides. Journal of Engineering for Gas Turbines and Power, 132(6), 061504. doi:10.1115/1.4000131

Tsague, L., Tatietse, T. T., Ngundam, J., & Tsogo, J. (2007). Prediction of emissions in turbojet engines exhausts: relationship between nitrogen oxides emission index (EINOx) and the operational parameters. Aerospace Science and Technology, 11(6), 459–463.

Turgut, E. T., Usanmaz, O., & Rosen, M. A. (2013). Empirical model assessment of commercial aircraft emissions according to flight phases. International Journal of Energy and Environmental Engineering, 4(1), 15.

Procedures to apply NO_X correlation methods to engine concepts with staged, lean combustor technology

M. Plohr*
DLR, Institute of Propulsion Technology, Köln, Germany

Keywords: Transport and environment, aircraft emissions, emissions modelling, NO_X, low NO_X, lean combustion, staged combustor, correlation method, fuel flow method

ABSTRACT: Reduction of NO_X emissions has been an important goal in combustor technology development for many years. RQL technology has been able to control NO_X emissions even with increasing cycle pressure and temperature which are needed to improve engine efficiency and reduce CO_2 emissions. To be able to provide input data for local air quality as well as atmospheric and climate modelling, correlation methods have been developed, which allow for estimating the emissions of the global fleet on the basis of publically available data only. Only recently new engine types with advanced low NO_X combustion technology have been certified and similar types from other manufacturers are expected to follow. These engines make use of lean combustion technology and usually feature some sort of fuel staging to provide the combustion stability required for aircraft engines. As a result, standard application procedures of correlation methods cannot be applied for modelling emissions of these types of engines. Therefore new, alternative procedures have been developed and analyzed, which take into account the specific properties and parameters that influence NO_X production in staged, lean burn combustion systems.

1 INTRODUCTION

As an input into atmospheric and climate modelling, aircraft engine emissions data under actual flight conditions are required. Up to date the only practical way to create these inventories is by applying so-called relative emission correlation methods. These methods calculate the emissions of a particular aircraft engine in flight on the basis of measured data from sea level static tests of the same engine type. The applicability of these correlation methods has been verified well for conventional combustion technology, which is based on the Rich-Quench-Lean (RQL) principle.

Recently, engines with new technology combustors have entered into service. These combustors operate fully lean during medium and high power operation, but still use a rich burning zone for ignition and low power operation. Due to this change of the combustion mode, depending on the engine operating condition, this technology is called staged lean combustion. Since there are no regions of stoichiometric mixture present in the lean burn mode, it has the potential for very low NO_X emissions. However, to stay within the narrower stability limits of lean combustion, good control of the Fuel to Air Ratio (FAR) is needed and that might require additional fuel staging in the lean burn mode. The fuel staging must be taken into account as an additional impact on NO_X formation and might result in discontinuities in the NO_X emission characteristic. Moreover, for lean burn technology the impact of the thermodynamic parameters driving the NO_X production rate is changed (Lefebvre et al., 2010). In particular the effect of combustor pressure (p3) is reduced, while there is an additional impact of the FAR, which is not observed in conventional combustors. Therefore, to account for these additional impacts, new procedures are needed to apply the established NO_X correlation methods to aircraft engines with staged, lean combustion technology.

2 APPROACH

To develop procedures that allow for the application of the established emission correlation methods to engines with advanced, staged and/or lean burn combustors, the following approach has been

* *Corresponding author:* Martin Plohr, DLR, Institute of Propulsion Technology, D-51147Köln, Germany. Email: martin.plohr@dlr.de

taken: As a first step, publically available emissions data of lean combustion concepts have been aggregated and analyzed. With help of further information on such combustor concepts and general physics of lean combustion, a reference emission model of a staged, lean aircraft engine combustor has been created. This model is needed to create cruise NO_X emissions data to compare with the results of the relative NO_X correlation methods, which are applied on the basis of sea level static emissions data only as a matter of principle. Part of this model is the fuel staging schedule, which describes the distribution of the fuel to the different combustion stages or zones with varying engine power setting. Subsequently, established NO_X correlation methods have been applied with the sea level static emissions data. For this step, different application procedures have been proposed and analyzed, to select procedures which account for the specific properties of staged, lean burn combustion systems to the extent possible with the amount of available supplementary data. From these analyses finally recommendations were developed, which procedures would be suitable for certain applications of NO_X emissions modelling techniques. This paper focuses on procedures suitable for inventory purposes, the complete analysis may be found in (Plohr, 2015).

3 REFERENCE EMISSION MODEL

The reference emission model was based on emissions data of the General Electric GEnx-1B70 engine from the ICAO engine emissions database (ICAO, 2013), certification data sheets (EASA, 2011) and information from GE presentations (Dodds, 2005), (Mongia, 2008), (Foust et al., 2012), (GE, 2014). Additionally, information from NASA publications on experimental lean combustion systems (Tacina et al., 2002), (Tacina et al., 2008) was used. The combustor of the GE engine is labeled TAPS, which stands for Twin Annular Premixing Swirler. From the available information it was concluded that the fuel is injected into the TAPS combustor by Pilot and Main fuel injector stages. During medium and high engine power operation, both Pilot and Main stages are operating under fully lean conditions. For low engine power operation, only the Pilot stage is fueled and then operating with a rich primary zone, similar to a conventional RQL concept.

To model the NO_X emission behavior of the lean burn mode as a function of thermodynamic engine parameters, absolute correlation methods have been taken from (Tacina et al., 2002) and (Tacina et al. 2008) and the coefficients of these correlations have been carefully adjusted to fit the available SLS measurement data. These data was taken from all thrust variants of the GEnx-1B engine in the ICAO database (54000lbf up to 75000lbf). The same procedure was used to model the emission characteristic of the rich burn Pilot only mode with an absolute correlation given in (Prather et al., 1992).

As a next step, a fuel distribution schedule has been created in a way that the combined NO_X emissions of the (individually modelled) Pilot and Main stages match the total SLS emissions data of the GEnx engine. The result of this procedure is shown in figure 1, where the NO_X emission characteristic of the reference emission model in Sea Level Static operation is indicated by triangles. For comparison, data points of GEnx-1B engines with different thrust ratings from the ICAO database are plotted as crosses. The dark grey lines in the diagram indicate data taken from the GE presentations on the TAPS combustor concept mentioned above. Obviously, the reference emission model shows good agreement with both datasets.

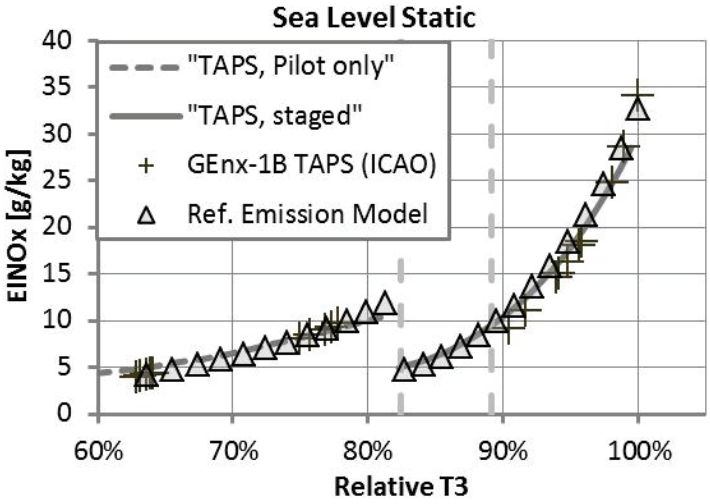

Figure 1: Sea Level Static $EINO_X$ characteristic of the Reference Emission Model, compared with data from different sources

In this figure the different operating regimes of the combustor can easily be distinguished. At high engine power (high relative T3), both Pilot and Main combustion zones are operating with lean fuel air mixture. With reducing T3 the mixture becomes leaner, and would approach the stability limit at a certain point. Therefore it is assumed that, starting from the dashed light grey line slightly below 90% relative T3, the reduction of the fuel flow is realized through the Main stage only, keeping the Pilot flame at higher temperature to stabilize the overall combustion. With further reduced engine power, fuel supply to the Main stage is cut off completely (at the second dashed line in the figure) and the Pilot stage switches to a rich burn mode which is similar to a conventional RQL system.

Figure 2 shows the emission characteristic in cruise conditions (Flight altitude 35000ft, Mach 0,80), resulting from these modes of operation. For comparison the (modelled) emission characteristic of a modern engine with optimized RQL combustor is shown by the solid line. It becomes obvious that in the cruise thrust range, the TAPS combustor is always operating in staged mode, producing very low NO_X emissions, approx. 60% below the optimized RQL system. This is consistent with information published by the engine manufacturer.

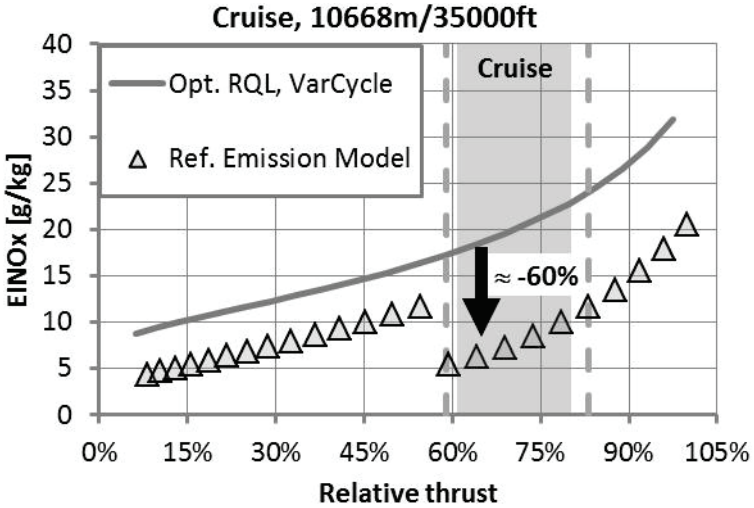

Figure 2: Cruise $EINO_X$ characteristic of the Reference Emission Model, compared with results of a modelled conventional (optimized RQL) combustion system

When applying relative correlation methods to calculate cruise NO_X emissions of such types of engines, the specific mode of operation must be taken into account. To realize this, new application procedures are required. The following chapter describes the basic application procedure of these methods, from which the new procedures are derived in the subsequent step.

4 RELATIVE EMISSION CORRELATION METHODS

All relative correlation methods are based on the assumption, that the emission characteristic of a given gas turbine engine can be modelled by an empirical function of a reduced set of characteristic thermodynamic parameters, which is determined on the basis of a given dataset for one single operating condition. Usually this operating condition is Sea Level Static, because in the ICAO aircraft engine emissions database, Emission Indices (EIs) of Nitrous Oxides (NO_X) and fuel flow data are given for any turbofan engine with more than 26.7kN rated thrust for four thrust settings under Sea Level Static conditions.

4.1 *Standard Application Procedure*

The first step of the standard procedure to apply an emission correlation method is to plot the EI values of the four data points from the ICAO database against a characteristic thermodynamic engine parameter. Then a curve is fitted to these four data points, which is denoted as the reference function of the correlation method. The characteristic parameter must be selected in a way that for any operating condition the $EINO_X$, corrected to SLS conditions, can be read from this curve. The most common relative correlation methods use combustor inlet temperature T3, or a corrected Fuel Flow wF,corr. Finally, depending on the characteristic parameter, subsequent corrections for pressure and FAR, or for ambient conditions are applied to calculate the actual $EINO_X$ value of the operating condition in question.

4.2 *Application Procedure for staged lean combustion systems*

Figure 3 shows $EINO_X$ data points for engines with a staged lean and a conventional combustion system. On the first view it is obvious that the standard application procedure of the relative correlation methods cannot be applied to the staged lean dataset. A suitable application procedure for this technology must account for the staging points and potentially different curve shapes of the diverse operating regimes. Figure 3 shows a sketch of the principle of a procedure that meets these requirements:

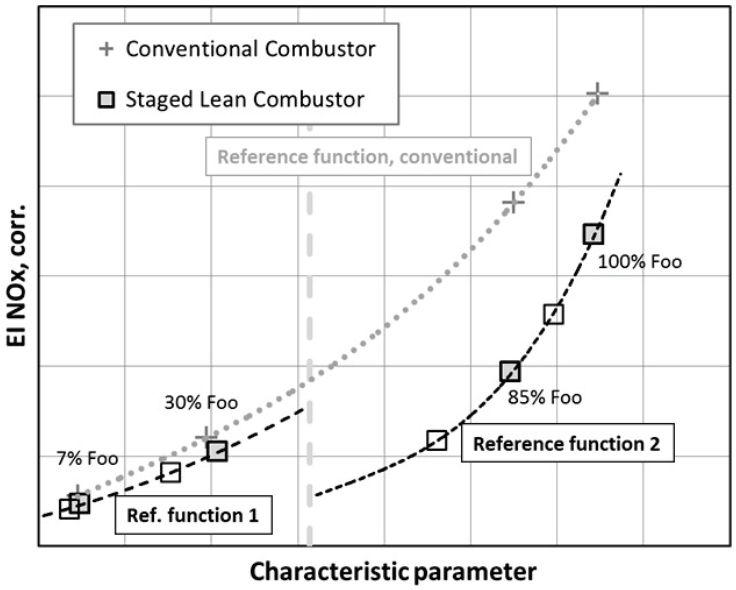

Figure 3: Proposed application procedure of relative correlation methods for staged lean combustion systems

As the first step of this alternative application procedure, the staging point(s) need to be defined as a function of the correlation method's characteristic parameter (light grey dashed line). Then individual reference functions are defined for all operating regimes that are separated by the staging point(s). Since there might be only few data points left between staging points to fit a reference function to, additional information should be used in this step, for example data points of engine variants with different thrust ratings (open symbols), or general information on the curve shapes of (here: lean burn) emission characteristics. Finally the corrections need to be adjusted, ideally guided by information on the cruise emission level or general information on the influence of ambient conditions on the emission formation processes. In this analysis, data from the Reference Emission Model were used to adjust the correction factors.

5 APPLICATION EXAMPLES

The general procedure as described in the previous chapter has been used to apply the most common relative NO_X correlation methods for verification and accuracy check. These are the methods recommended by ICAO for emission inventory purposes (ICAO, 2011): The so called p3-T3 method (Madden et al., 2003) and the fuel flow methods developed by Boeing (Dubois et al., 2007) and DLR (Döpelheuer et al., 1999). The p3-T3 method was developed by engine manufacturers and uses the combustor inlet temperature T3 as characteristic parameter and corrections for combustor pressure p3 and fuel to air ratio (FAR). This method has the potential to provide the best accuracy of all relative correlation methods; however the required base data are usually not publically available. The so-called fuel flow methods can be applied with publically available data only, since these methods use a corrected fuel flow as characteristic parameter and corrections for ambient conditions. Two methods have been proposed, one by DLR and another one by Boeing. While the DLR method uses the standard definition for the corrected fuel flow, based on ambient total pressure and temperature, the Boeing method applies a different definition which is based on static ambient conditions and Mach number.

The p3-T3 method includes the most NO_X-relevant parameters T3, p3 and FAR, so their impact is easily adjustable by their individual exponents in the correlation formula. In the fuel flow correlations the NO_X-relevant parameters are only implicitly included. The pressure impact is represented by an ambient pressure correction and partly by the corrected fuel flow, which is a power parameter of the engine, representing the actual operating condition. A FAR correction is not provided in the fuel flow correlations, therefore to account for the FAR impact on the NO_X production of lean burn operating modes an extension of these methods is required, similar to the FAR correction of the p3-T3 method. For this study, the reference emission model has been used to provide all information needed to apply these correlation methods with the procedures described earlier. In addition, the methods have been applied on the basis of only a minimum dataset that is more typical for common inventory applications.

5.1 *Application of the p3-T3 method*

Figure 4 shows the calculated NO_X emission characteristic of a cruise operating line as result of the staged application of the p3-T3 method, based on a minimum dataset (a single ICAO database entry). The required thermodynamic engine data have been generated by an engine performance model.

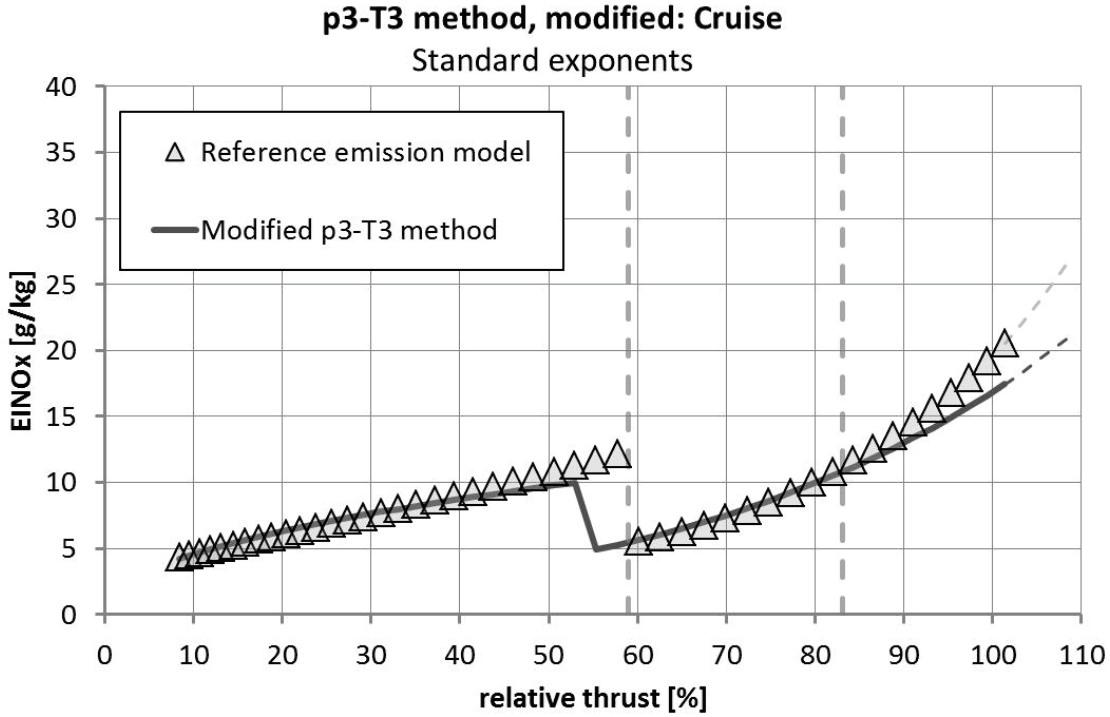

Figure 4: Results of modified p3-T3 method: Application with staged reference function, based on a minimum dataset, compared to the reference emission model

In this case the first staging point was set just above the 30% SLS thrust point. The second staging point was ignored as it is not obvious in the ICAO dataset. Separate reference functions have been defined on the basis of the Sea Level Static emissions data above and below this staging point. The exponents of the correction factors have not been adjusted, because the required data would usually not be available. However, even with this reduced data set the staged application of the p3-T3 method with two reference function gives satisfactory results, compared with the reference emissions model, particularly in the cruise thrust range.

The most obvious improvement potential of this very basic application of the correlation method is on the slope of the emission characteristic at high relative thrust (above approx. 85%) and the position of the staging point. Furthermore, the shape of the emission characteristic of the Pilot only mode (below the staging point) is not well met.

With emissions data of engine variants with different thrust ratings available, it is possible to improve the shapes of the reference functions and to set the position of the staging point more accurately. If furthermore either the cruise NO_X level or the pressure and FAR exponents are given for this engine type, the results of the staged application of the p3-T3 method can be significantly improved, as shown in figure 5:

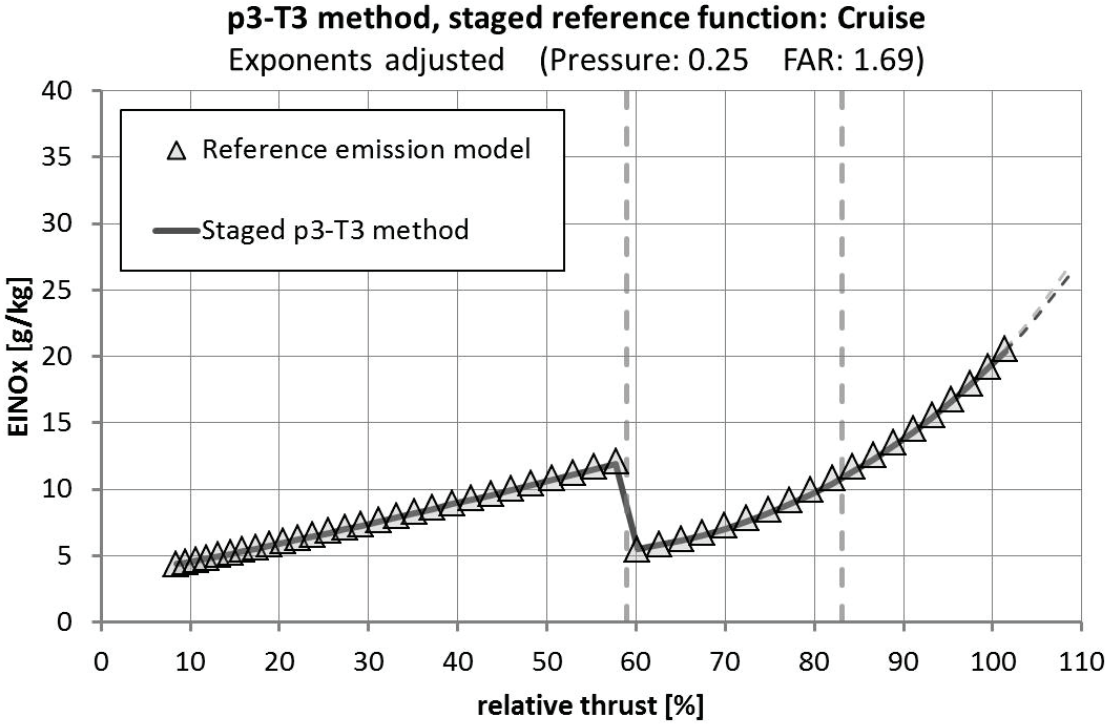

Figure 5: Results of the staged application of the p3-T3 method, based on an optimum dataset, in comparison with the reference emission model

Obviously, with this optimum set of input data, the method allows for a very accurate modelling of the cruise NO_X emission characteristic of the staged lean burn combustor model.

5.2 *Application of the DLR fuel flow method*

Again as a first step this method has been applied on the basis of a minimum dataset. However in this case satisfactory results could only be achieved when the pressure exponent of the correlation method was adjusted. With standard exponents the method would overestimate the cruise NO_X production in the staged, lean burn mode. Figure 6 shows the results of this application procedure of the DLR fuel flow method:

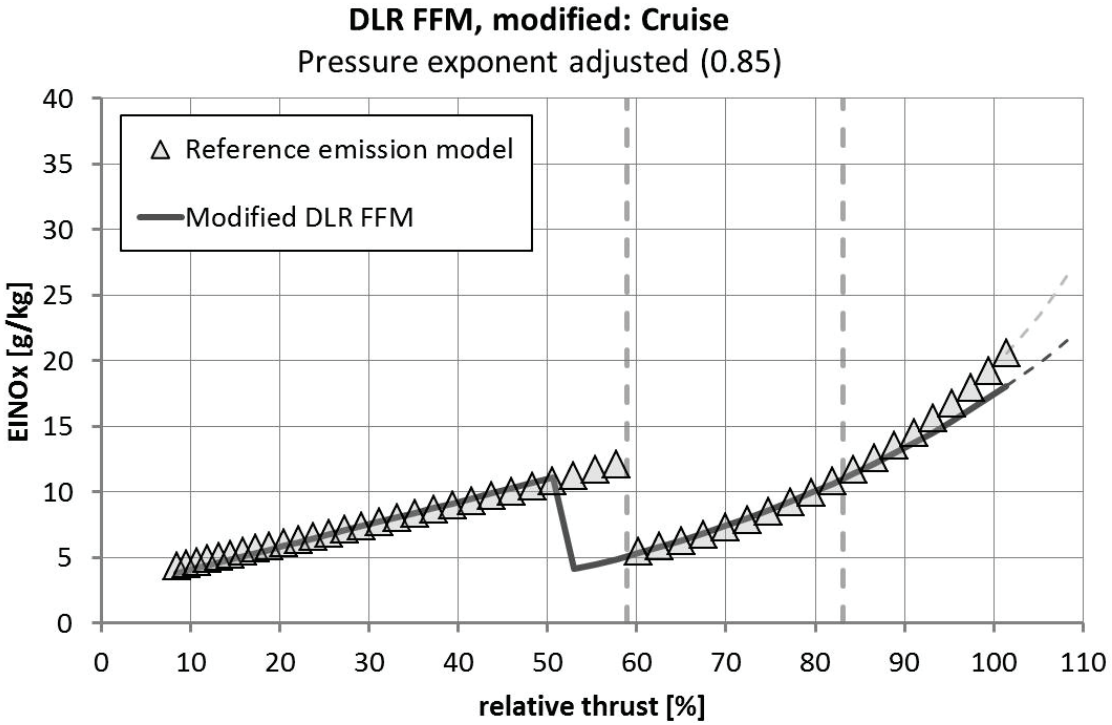

Figure 6: Results of modified DLR fuel flow method: Application with staged reference function, based on a minimum dataset, compared to the reference emission model

Although the method gives quite a good representation of the cruise NO_X emission characteristic, some potential for improvement is still obvious in the high thrust range (slope of the curve) and concerning the position of the staging point. Again emissions data of engine variants with different thrust ratings have been used to optimize the shape of the reference function for the staged, lean burn operating regime. Furthermore an additional FAR correction has been added for this operating regime and the pressure exponent has been adjusted again. The results of this improved method are shown in figure 7:

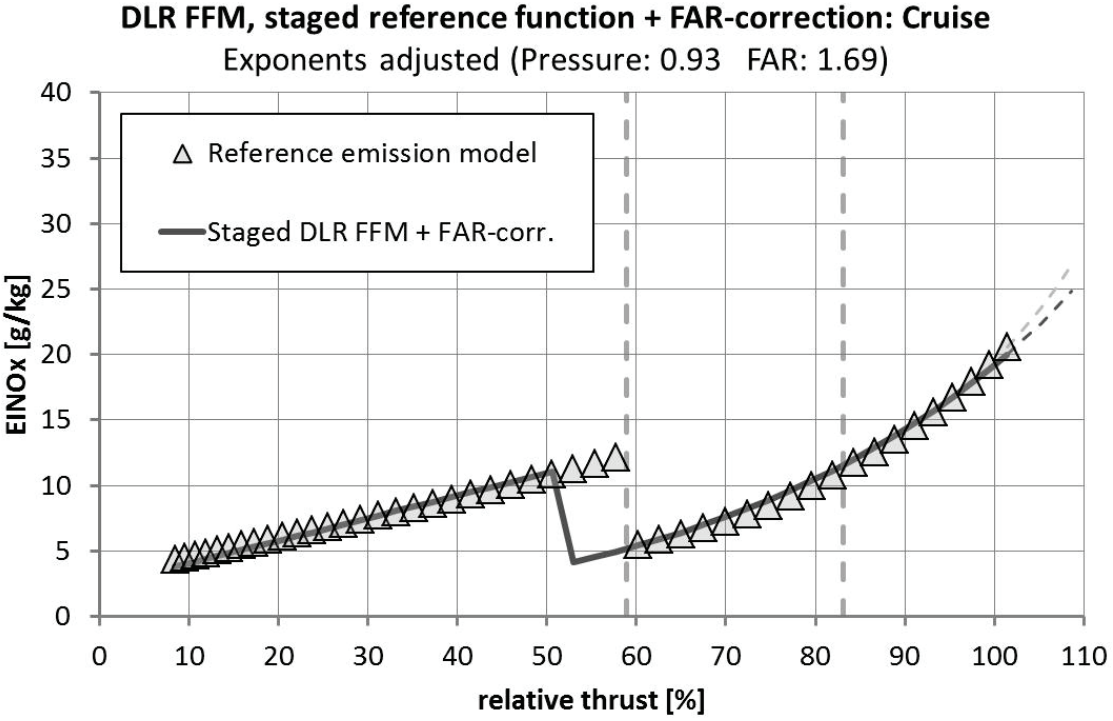

Figure 7: Results of the staged application of the DLR fuel flow method, based on an optimum dataset, in comparison with the reference emission model

The figure shows that, with optimum data availability, the DLR fuel flow method gives only slightly less accurate results than the p3-T3 method (figure 5, both in staged application). The small in-

accuracies are caused by the fact that the impact of the combustor pressure is only implicitly included in the fuel flow methods. Additionally, the position of the staging point is not reproduced exactly in cruise operating conditions, if defined by the corrected fuel flow. However since the staging point remains below the thrust range for typical aircraft cruise conditions, this is not relevant for inventory applications of the correlation method.

5.3 *Application of the Boeing fuel flow method*

The application procedures of the Boeing fuel flow method with minimum and optimum datasets are completely analog to those of the DLR fuel flow method. The results of these procedures for the cruise working line achieve very similar accuracy and therefore are not displayed separately here.

6 RESULTS FOR A SIMULATED FLIGHT MISSION

Finally, the application procedures of the correlation methods as described in the previous chapters have been used in the frame of a flight mission calculation, to verify their applicability for inventory purposes. The flight mission calculation was performed with DLR's generic model of a Boeing B787-8 type aircraft, powered by a GEnx-1B70 engine. Flight mission distance was 5500nm with a cruise Mach number of 0.85. Initial cruise altitude was 35000ft and a step climb was performed to reach the final cruise altitude of 39000ft. Figure 8 shows the NO_X emission per flight phase, calculated by the different NO_X correlation methods and application procedures as described before.

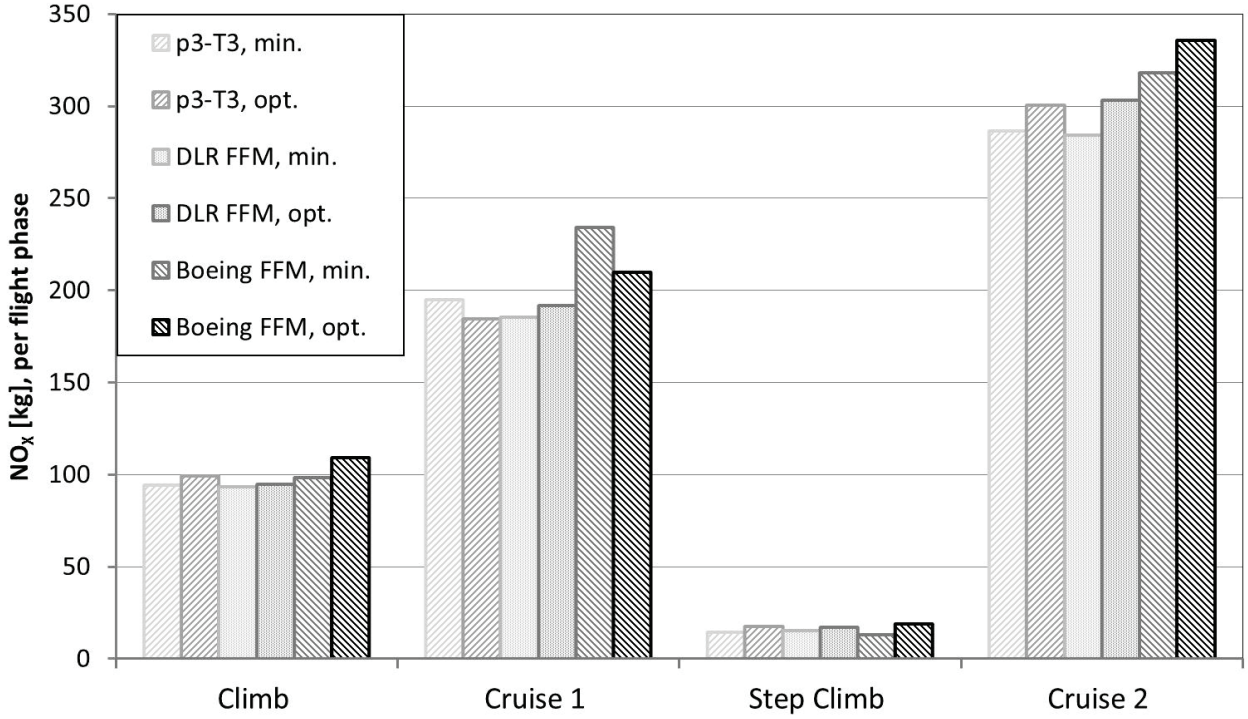

Figure 8: NO_X emission per flight phase, calculated by different NO_X correlation methods and application procedures

While the results of the p3-T3 and the DLR method appear quite similar, the Boeing method shows larger deviations, which have not been observed in the results for the cruise working line. The only difference between the cruise conditions of the working line analyses and the initial flight mission cruise phase was the Mach number. Therefore it was assumed that the observed deviation is most probably caused by Mach number effects, which can occur with this method when the exponents are changed. Potentially this Mach number effect could be eliminated, if a larger amount of measured data for different cruise Mach numbers would be available to adjust the exponents for application to lean combustion concepts. However, at this point in time such data are not publically available.

From the flight mission results it becomes obvious that the NO_X production of the staged lean combustor is reduced in all phases of the flight, compared with the optimized RQL combustor. The

largest reduction is achieved in the cruise phases, where the engine is operating most of the time on medium and long range flight missions. The calculated NO_X emission reduction in these cruise phases is approximately 60%.

7 SUMMARY AND CONCLUSIONS

For this study, publically available information and data on operation and emission production of lean burn combustors for aircraft engines have been collected and analyzed. Based on this analysis, a reference NO_X emission model of a staged, lean combustor has been developed using absolute correlation methods from the literature. The required thermodynamic engine data has been taken from a performance model. Subsequently, the most common relative NO_X correlation methods have been applied with their standard and potential new application procedures; and the results compared to those of the reference emission model for a cruise working line of the engine. These comparisons verified that the newly developed procedures are suitable to apply the established NO_X correlation methods to new, staged lean burn combustor concepts.

Finally, the new procedures have been applied to calculate the NO_X emissions of a full flight mission of an aircraft, powered by engines with staged lean burn combustors, to demonstrate their applicability within the scope of flight mission calculations (and subsequent inventory generation). This demonstration was successful for two of the three methods presented herein. Therefore it is recommended to use the p3-T3 method or the DLR fuel flow method with the application procedures developed and presented in this study to model NO_X emissions of aircraft engines with staged, lean combustors for the purpose of inventory creation.

For the future it is planned to expand these application procedures to other emissions modelling techniques, particular such for aircraft PM emissions.

REFERENCES

Dodds, W., 2005: Twin Annular Premixing Swirler (TAPS) Combustor, „The Roaring 20th“ Aviation Noise & Air Quality Symposium, University of California, Berkeley, USA

Döpelheuer, A., Lecht, M., 1999: Influence of Engine Performance on Emission Characteristics, Paper No. 20 in „Gas Turbine Engine Combustion, Emissions and Alternative Fuels“, RTO-MP-14, ISBN 92-837-0009-0, Lisbon, Portugal

Dubois D., Paynter, G. C., 2007: „Fuel Flow Method 2“ for Estimating Aircraft Engine Emissions, SAE Technical Paper 2006-01-1987, SAE international, Warrendale, PA, USA

EASA, 2011: Type-Certificate Data Sheet GEnx Series Engines, TCDS IM.E.102, Issue 02, EASA, Köln, Germany

Foust, M. J., Thomsen, D., Stickles, R., Cooper, C., Dodds, W., 2012: Development of the GE Aviation Low Emissions TAPS Combustor for Next Generation Aircraft Engines, AIAA 2012 0936, AIAA, USA

GE Aviation, 2014: The GEnx Engine Family, Website http://www.geaviation.com/engines/commercial/genx/, as of May 2014

ICAO, 2011: Airport Air Quality Manual, ICAO Doc. 9889, Attachment D to Appendix 1, ISBN 978 92 9231 862 8, ICAO, Montréal, Canada

ICAO, 2013: Aircraft Engine Emissions Data Bank, Version 19, Document online under http://easa.europa.eu/document-library/icao-aircraft-engine-emissions-databank

Lefebvre, A. H., Ballal, D. R., 2010: Gas Turbine Combustion, 3rd Edition, ISBN 978-1-4200-8605-8, CRC Press, Boca Raton, FL, USA

Madden, P., Park, K., 2003: Methodology for Predicting NO_X Emissions at Altitude Conditions from Ground Level Engine Emissions and Performance Test Information, Rolls Royce Technical Report No DNS 90713, Rolls-Royce plc., Derby, UK

Mongia, H. C., 2008: GE Aviation Low Emissions Combustion Technology Evolution, Presentation on AIAA-IITK

Plohr, M., 2015: Anwendungsorientierte Methoden zur Analyse und Modellierung des Emissionsverhaltens moderner Triebwerke mit gestuften, mageren Brennkammersystemen auf Basis thermodynamischer Triebwerksmodelle, internal report, DLR Institute of Propulsion Technology, Köln, Germany, in press

Prather, M. J., Wesoky, H. L., 1992: The Atmospheric Effect of Stratospheric Aircraft: A First Program Report, NASA Reference Publication 1272, NASA

Tacina, K. M., Lee, C., Wey, C., 2008: NASA Glenn High Pressure Low NO_X Emissions Research, NASA/TM-2008-214974, NASA

Tacina, R., Wey, C., Laing, P., Mansour, A., 2002: A Low NO_X Lean-Direct Injection, Multipoint Integrated Module Combustor Concept for Advanced Aircraft Gas Turbines, NASA/TM-2002-211347, NASA

TEAM_Play for Europe

P.H.H. Brok*,
NLR – Air Transport Division, Amsterdam, Netherlands

R. Berghof, S. Maertens, M. Hepting
DLR – Institute of Air Transport and Airport Research, Cologne, Germany

Keywords: Aviation & environment, economics, interdependencies, data warehouse, modelling tool suite, scenario analysis, and policy decision support

ABSTRACT: TEAM_Play-Tool Suite for Environmental and Economic Aviation Modelling for Policy Analysis – offers a range of European capabilities for the modelling of aviation noise, local air quality, greenhouse gas emissions, climate response, technology and economic impacts, and respective interdependencies. These useful capabilities for historic, current and future year impact assessments are combined in a unique single tool suite, and thus to be operated in a common environment. The further use of a single input data source (i.e., data warehouse and exchange platform) is an enabler for consistent and more accurate aviation economic and environmental trade-off studies and policy impact assessments.

The collaborative project TEAM_Play, co-funded by the European Commission (EC) as part of the 7th Research Framework Programme (FP7) of the European Union (EU), ended in 2013. Progress on aviation environmental modelling and capability management in Europe has been slow since (or concentrated within specific activities as, for instance, in ICAO-CAEP, Clean Sky and SESAR). In order to collaboratively move on, and supporting and strengthening the European position in the international policy arena, the European aviation environmental modelling strategy needs further implementation and momentum.

In this context, the paper addresses TEAM_Play for Europe.

1 INTRODUCTION

Aviation environmental impact assessment and modelling activities give support to policy decision making in Europe and other regions of the world. This is especially true for the complex assessment of interdependencies which involves the combined analysis of emissions, noise, economics and other relevant parameters linked to commercial aviation. Assessments and policies (national, regional as well as those negotiated internationally such as in ICAO-CAEP) concern impacts such as community noise, air quality and climate change.

The collaborative project TEAM_Play (Tool Suite for Environmental and Economic Aviation Modelling for Policy Analysis; www.teamplay-project.eu) substantially enhanced the capabilities of the European modelling community to estimate air traffic developments and to assess the impact of specific aviation-related policy measures. Eighteen partners[1] participated and contributed to TEAM_Play which was a project co-funded by the European Commission (EC) as part of the 7th Research Framework Programme (FP7) of the European Union (EU) for approximately 3.8 million €, and which took place from December 2010 until March 2013.

Progress in Europe has been slow since on aviation environmental modelling and capability management or has been concentrated within specific activities, for instance in ICAO-CAEP, Clean Sky and SESAR. In order to collaboratively move on, and supporting and strengthening the European position in the international policy arena, the European aviation environmental modelling strategy needs further implementation and momentum.

The current paper presents TEAM_Play's products and results. Its main message is that TEAM_Play capabilities, expertise and the community are still out there and available to further contribute and strengthen Europe's capabilities and activities on modelling and impact assessment

* *Corresponding author:* Paul Brok, NLR – Air Transport Division, Anthony Fokkerweg 2, 1059 CM Amsterdam, Netherlands. Email: Paul.Brok@nlr.nl

[1] TEAM_Play consortium partners: see page 55

of aviation trends and environmental policies (technology, operations, market-based measures, et-cetera).

2 TEAM_PLAY PROJECT AIMS, PRODUCTS, TEST RUNS AND OUTREACH

2.1 *TEAM_Play project aims*

Prior to TEAM_Play, numerous individual models existed in Europe, addressing different aspects of air transport and related impact modelling (noise, local / greenhouse gases emissions, but also climate change and economic impacts). The main focus of TEAM_Play was on creating a modelling framework in which existing European modelling capabilities could be combined in order to support and strengthen the European perspective in the international policy arena.

The development of the TEAM_Play tool suite was also aimed at broadening the scope of potential impact assessments, in order to improve insight and awareness of additional effects which are crucial for aviation developments but were not yet fully covered in other modelling systems. Examples are impact monetisation, third party risk, airport capacity constraints, extended forecast horizon, and alignment of local, regional and global assessments.

2.2 *TEAM_Play products*

TEAM_Play's main products are the Data Warehouse & Data Exchange Platform and the Tool Suite.

The developed and populated Data Warehouse & Data Exchange Platform (DW/DEP; based on the most used open source content management system Alfresco) allow consistent provision of data and structured transfer of input and output data between the models in the TEAM_Play Tool Suite. In addition, a document with TEAM_Play Data Format Guidelines was prepared and released for common use within the aviation modelling community. This set of guidelines was the basis for harmonisation of input and output data to be exchanged and stored in the data warehouse.

The TEAM_Play Tool Suite was established through development of the necessary model interfaces combining -in a single environment- European tools (either existing, updated or new) for modelling future air transport (technology), local airport and greenhouse gas emissions, aviation noise, economics and environmental impacts. The tool suite consists of a Basic Modelling System (BMS) working in high granularity, and a Responsive Modelling System (RMS) allowing for feedback loops; central tool in the RMS is the enhanced AERO modelling system owned by EASA. Policy decision support tools are developed including a macro-economic impact model and an energy module putting employment numbers respectively energy consumption linked to aviation in a global perspective.

Figure 1 outlines the complete TEAM_Play system including the DW/DEP, BMS and RMS. TEAM_Play's website (www.teamplay-project.eu) offers further elaborated descriptions of the Data Warehouse & Data Exchange Platform, Tool Suite and individual tools.

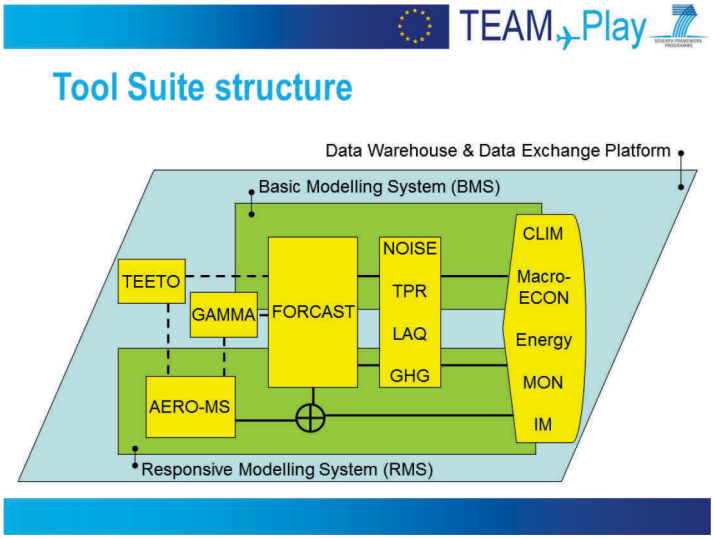

Figure 1: Outline of the complete TEAM_Play system

2.3 *TEAM_Play test runs*

System runs for selected baseline, business as usual and policy scenarios were carried out to test the functioning of the complete TEAM_Play system, i.e. Data Warehouse & Data Exchange Platform and Tool Suite. Prior to this, substantial work was performed to harmonise and update default databases which are in use by many modelling tools (such as sets of aircraft, engines and emissions data). Moreover, scenario-specific air traffic files for local and global modelling studies were prepared and provided to modellers via the data warehouse and data exchange platform.

All TEAM_Play tools were applied in at least one scenario run and modelling system. Both modelling systems (i.e., BMS and RMS) were tested with a baseline 2006 and a 2026/2050 "business as usual" scenario (BaU; in our case the CONSAVE "unlimited skies" scenario). The reference scenario run results were compared to the results of 2026/2050 BaU scenario runs in which additional environmental policies and or measures were applied. The basic modelling system (BMS) was also tested with a 2006/2026 ICAO-CAEP dataset.

The following set of environmental policies and measures were applied, also reflecting TEAM_Play's (cap)ability of assessing the economic and environmental impact of potential policy measures for civil aviation:

- BMS: CO_2 Standard, Open Rotor, Biofuel
- RMS: Ticket Tax, CO_2 Standard, Long-term emission trading system (ETS), Biofuel, and Eco-routing.

The tests demonstrated the applicability of the TEAM_Play modelling systems to multiple realistic air traffic scenarios and policy use cases. Chosen air traffic scenarios remained as close as possible to scenarios envisaged within, for instance, ICAO-CAEP so that any improvements and shortcomings of the TEAM_Play system could clearly be assessed.

Figure 2 shows an example of test run results combined in a so-called radar plot suitable for interdependency analysis. NB: Current scenario studies were aimed at capability demonstration and sometimes based on simplified assumptions only. Results from scenario runs are therefore only for demonstration purposes (not yet for policy decision making).

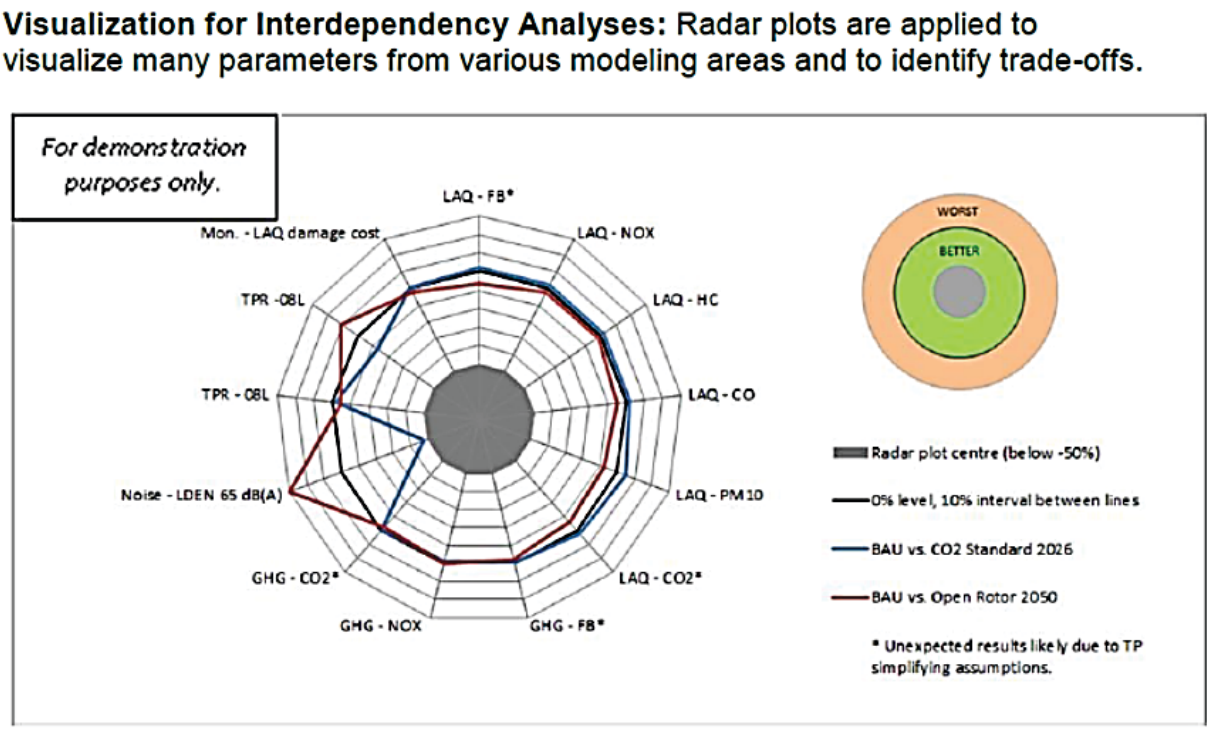

Figure 2: Example of TEAM_Play test run results

2.4 *TEAM_Play dissemination & outreach*

The TEAM_Play results were first presented in Advisory Committee and User Group meetings. In addition, a public website (www.teamplay-project.eu; Figure 3 shows the home page) was setup and now offers a lot of information and material concerning TEAM_Play. Printed material and presentations are also provided at different events such as ANERS and TAC.

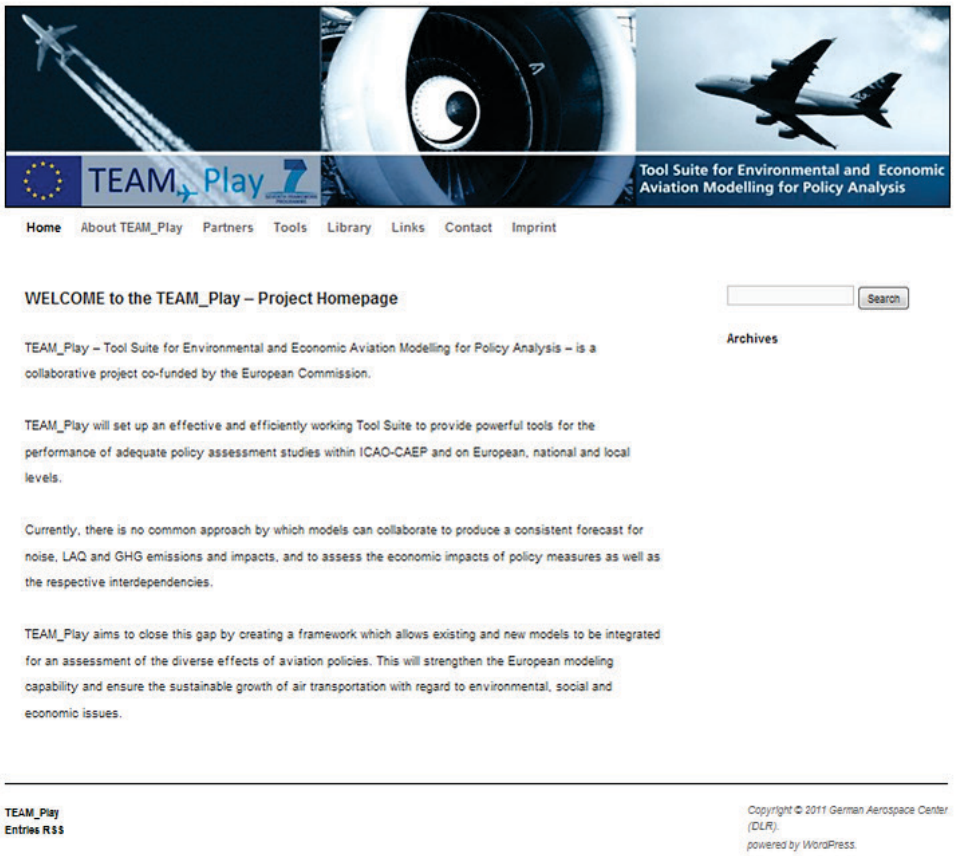

Figure 3: TEAM_Play project website home page

With respect to the future and a durable implementation, a number of reports were prepared and discussed within the TEAM_Play community, including Advisory Committee and User Group, and also outside in the ECAC-ANCAT Modelling Interdependencies Task Group (MITG) and European networks like ECATS and X-NOISE. Relevant reports are:

- Design of durable structures for future operational management and coordination of use, maintenance and enhancement of the TEAM_Play Tool Suite capabilities
- Management and updating of provisions on use, access, intellectual property and ownership of the TEAM_Play Tool Suite
- Development of business plan for sound applications of the toolset in the future.

3 TEAM_PLAY FOR EUROPE

TEAM_Play offers a unique system to Europe connecting individual tools and providing tested work flows for aviation environmental and economic modelling for policy analysis and impact assessments. The current capabilities of the TEAM_Play tool suite are:

- Quantification of current and future aviation impacts, addressing ecology, economy, trends, technologies, operations and policies
- Goal assessment (e.g., ACARE/Flightpath 2050, Clean Sky and SESAR) quantifying success level based on user-defined scenarios
- Normative modelling (identifying requirements to reach the goals)

– Quantified scenarios on long-term developments, providing know-how depending on various aviation internal and external trends
– Analysis from global and European level down to local airport level
– A populated data warehouse and operational data exchange platform.

The TEAM_Play Tool Suite and expertise is ready for use and available for Europe to be exploited in any relevant ongoing and or future activity.

The European aviation environmental assessment structure and modelling strategy (see Figure 4) eventually adopted in December 2013 at the ECAC Directors General of Civil Aviation meeting in Paris (FR) is the best way forward. TEAM_Play expertise fits well in the Pool of Excellence and the Advisory Group. The strategy needs however further implementation and momentum mainly through the ECAC-ANCAT-MITG task group. In this respect, the current initiative of the European Commission (DG-MOVE; in close cooperation with EASA and EUROCONTROL) is appreciated; it will develop a publicly available helicopter noise model and make progress on aircraft engine nvPM emission measurement and modelling; in this way it will contribute to the further establishment of a public European environmental model suite for aviation.

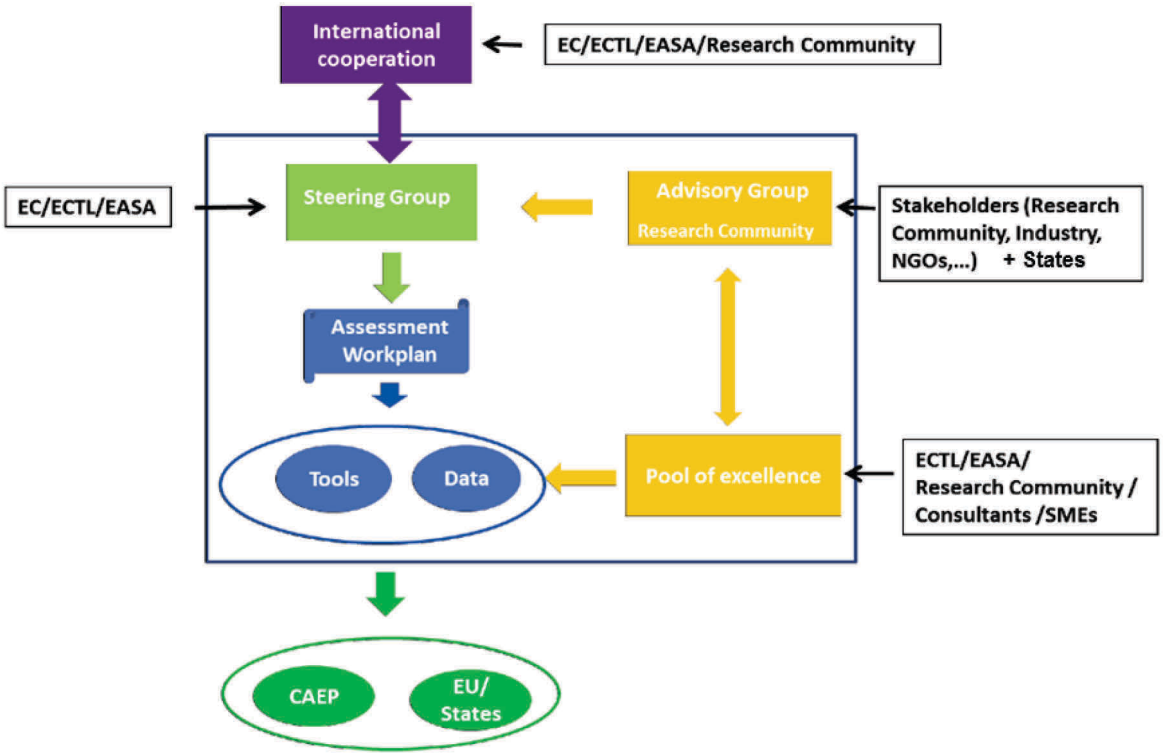

Figure 4: The European aviation environmental assessment structure and modelling strategy

REFERENCE LIST

TEAM_Play website: www.teamplay-project.eu.

TEAM_Play consortium partners: DLR (coordinator), NLR, ENVISA, FOI, MMU, Ricardo AEA, ANOTEC, Janicke Consulting, CERC, COMOTI, Snecma, Airbus, Rolls-Royce, University of Cambridge, ENAC, TAKS, National Aviation University, and LimitedSkies.

Limiting aviation's full climate impact by market-based measures: Results of the research project AviClim

K. Dahlmann*, R. Sausen
Deutsches Zentrum für Luft- und Raumfahrt (DLR), Institut für Physik der Atmosphäre, Oberpfaffenhofen, Germany

J. D. Scheelhaase, M. Jung, H. Nieße, H. Keimel
Deutsches Zentrum für Luft- und Raumfahrt (DLR), Institut für Flughafenwesen und Luftverkehr, Köln, Germany

Martin Schaefer, Florian Wolters
Deutsches Zentrum für Luft- und Raumfahrt (DLR), Institut für Antriebstechnik, Köln, Germany

Keywords: Aviation, Emission Trading

ABSTRACT: Aviation contributes to climate change by both long-lived CO_2 and short-lived non-CO_2 effects, such as NO_x or contrail cirrus. According to Lee et al. (2009), aircraft-induced CO_2 contributed 1.6% to the total anthropogenic radiative forcing in the year 2005. If both CO_2 and non-CO_2 effects are considered, aviation contributed 4.9% to the total radiative forcing in 2005. The interdisciplinary research project AviClim has explored the feasibility for including aviation's full climate impact in international protocols for climate protection and has investigated the economic impacts. The present paper provides results of this research project. In AviClim four reduction scenarios have been designed which differ concerning the level of international support for climate protecting measures. These scenarios have been combined alternatively with an emissions trading for all climate relevant species, a climate tax and a NO_x emission charge combined with operational measures. Also, two different metrics for quantifying aviation's full climate impact have been assumed alternatively: Average Temperature Response 'atr 20' and 'atr 50'. All in all, a global emissions trading scheme for both CO_2 and non-CO_2 emissions would be the best solution.

1 INTRODUCTION

Aviation contributes to climate change by several components: CO_2 with an atmospheric lifetime up to thousands of years and H_2O with a lifetime between hours and months contribute to a positive RF. The NO_x emissions have several effects: Ozone (O_3) is formed (warming effect) with a life-time from weeks to months. As a secondary effect, methane (CH_4) is destroyed (cooling effect) with a life-time of about a decade. Finally, from the reduced methane a secondary reduction of the ozone concentration results (cooling effect), which has the same life-time as methane. Contrail induced cloudiness (CiC, individual contrails and the associated contrail cirrus) result in a positive RF, which is of a similar magnitude than the RF from CO_2 on global and annual average (e.g., Lee et al., 2009, Burkhardt and Kärcher, 2011).

While the climate impact of CO_2 emissions is independent from the emission location and time, aviation's non-CO_2 effects depend on flight altitude, geographical location and partly day time, weather situation, etc. (e.g., Fichter et al., 2005; Mannstein et al., 2005; Fichter, 2009, Frömming et al., 2012). Due to the different life-times and due to the spatially dependent impacts, the climate change induced by the aviation non-CO_2 effects is not directly proportional neither to the CO_2 emissions nor to the amount of non-CO_2 emissions. Therefore simply applying a factor to the CO_2 emissions to account for aviation's non-CO_2 effects, as suggested by, e.g., the European Parliament, is not appropriate as it would provide incorrect incentives (e.g. Forster et al., 2006).

Overall, the global framework for limiting the climate relevant emissions of aviation is diverse. Whilst international aviation carbon dioxide emissions have been regulated in several countries in the recent years, this is not the case for most of the non-CO_2 climate effects. Until now, the non-

* *Corresponding author:* Katrin Dahlmann, DLR-Institut für Physik der Atmosphäre, Oberpfaffenhofen, D-82234 Wessling, Germany. Email: Katrin.Dahlmann@dlr.de

CO_2 species have only been addressed scarcely both on ICAO and on a national level. Nevertheless it is important to include the non-CO_2 effects as the total climate impact of aviation (in terms of RF) was 4.9% (in 2005) while the aircraft-induced CO_2 contribution to total anthropogenic radiative forcing was only 1.6% (Lee et al., 2009). Due to urgent environmental needs, the political regulation of the full climate impact of aviation is strongly recommended in the foreseeable future.

Therefore the research project AviClim (Including Aviation in International Protocols for Climate Protection), funded by the German Bundesministerium für Bildung und Forschung (BMBF), focussed on the question: How can international aviation be best included in international protocols for climate protection from an economic point of view? For details see Scheelhaase et al. (2015).

2 METHOD

In the present study four geopolitical scenarios have been defined, which differ concerning the level of international support for climate protecting measures in aviation: "Greater EU" with EU, Norway, Iceland and Liechtenstein, "Great Aviation Countries" with the main players in international and national aviation, "Annex-I Countries" with "Annex-I Countries" plus the BRIC countries (Brazil, Russia, India and China) and "World" with global support. Within AviClim it has been generally assumed that all flights to, from and within the countries belonging to the respective geopolitical scenario will be regulated.

The four geopolitical scenarios have been combined with three selected market-based measures to reduce aviation's climate relevant emissions, which have been chosen in respect to economic efficiency, potential environmental benefits and practicability: (1) Emissions trading scheme for all climate relevant emissions, (2) climate tax and (3) NO_x emission charge combined with a CO_2 trading scheme and operational measures, which assume that 50% of flights operated between 30°N and 60°N and on an altitude between 28-38 kft (about 9 and 12 km) will be flying 2 kft (about 630 m) lower to reduce contrail cirrus. The combination of NO_x emission charge, CO_2 trading scheme and operational measure will be called "NO_x charge" afterwards.

The airlines under the respective scheme have increasing costs due to the regulatory measures. These additional costs depend on the future development of prices for CO_2 equivalents, which is difficult to foresee. Therefore we have assumed three different price development paths: For 2010 we assume a price of 10 USD per ton CO_2 for all price development paths and for 2030 80 USD per ton for the 'High Price Path' and 30 USD for the 'Low Price Path. Additionally we assume a 'Mixed Price Path' with low CO_2 equivalent prices for both trading schemes and high prices for the climate tax and the NO_x charge. For both trading schemes a free allocation of 85% of 2010 emissions has been assumed. For any emissions exceeding 2010 emissions, emissions permits have to be purchased by the airlines on the permits market.

Under the assumption that the airlines will try to pass-on the full cost increase to their customers, prices for air services will become more expensive. We assume three cases of price elasticities: (Case 1) The quantitative demand for air services remains unchanged. (Case 2) The quantitative demand reaction is under proportionate to the price increase by the airlines; a price increase of 1% leads to a demand reduction of 0.8%. (Case 3) The quantitative demand reaction is disproportionate to the price increase by the airlines; a price increase of 1% leads to a demand reduction of 2.1%.

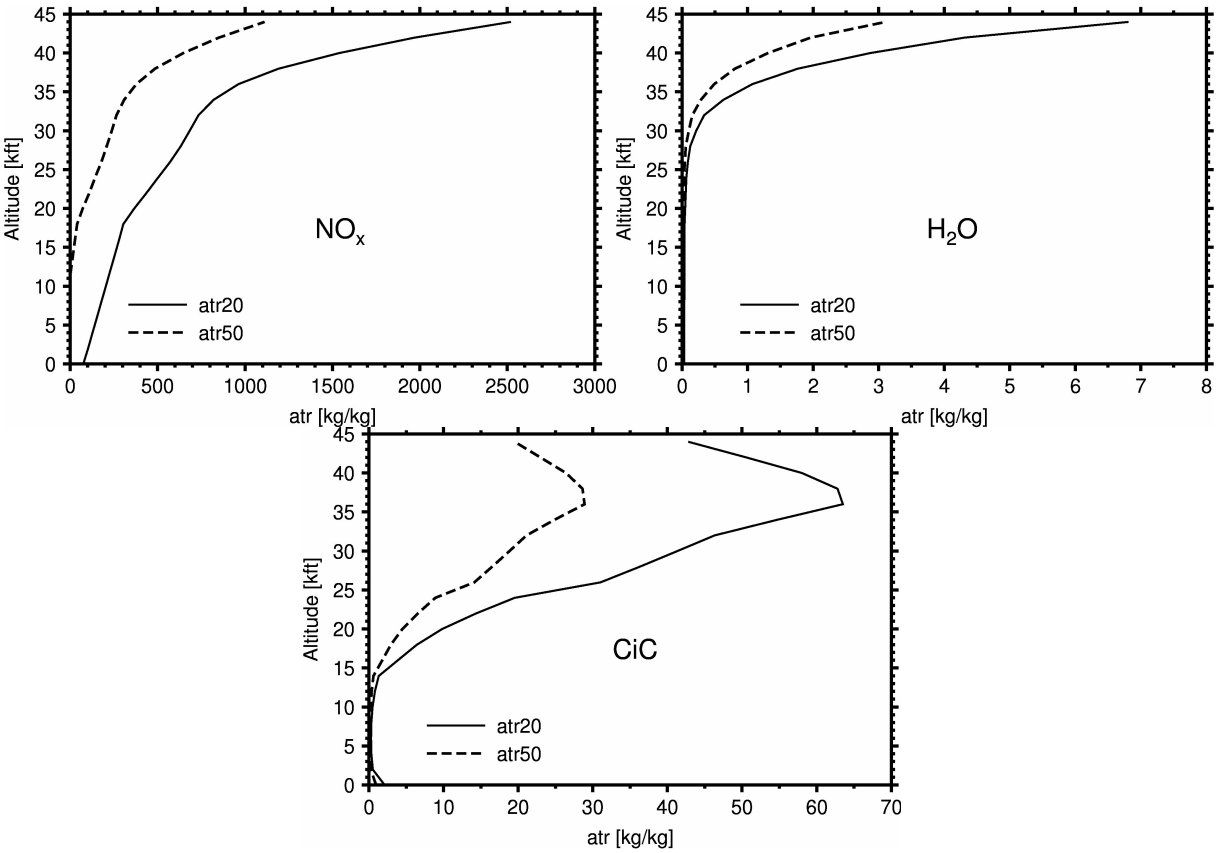

Figure 1: CO_2 equivalence factors (in kg(CO_2equi) per kg emission or flown km) in dependency of flight altitude for NO_x, H_2O and CiC using atr_20 and atr_50 as metric, respectively.

For the present study, the Average Temperature Response (ATR), which is the mean temperature change over a time horizon of 20 and 50 years (atr_20 and atr_50) respectively, was used as metric to tranfer non-CO_2 effects into CO_2 equivalents. To find a reasonable compromise between calculation effort and accuracy of the results we decided to use only an altitude dependency of the climate impact. Therefore we calculated the impact of nowadays air traffic for each flight level separately with the response model AirClim (Grewe and Stenke, 2008; Grewe and Dahlmann, 2012; Dahlmann et al., 2015) which calculates the climate impact of different climate agents (CO_2, H_2O, NO_x (O_3+CH_4+O_3pm) and CiC) as functions of the emission location. Then we got the CO_2 equivalents by calculating the climate impact of each species per kg emission or flown distances relative to the impact of one kg CO_2. The CO_2 equivalence factors, which in particular depend on flight altitude, are shown in Figure 1 for atr_20 and atr_50, respectively. An emission of 1 kg NO_x in an altitude of 35 kft, for example, has the same impact on climate over 20 years as about 1000 kg CO_2.

In brief, the modelling of the climate effects of the market-based measures has been analysed by the following steps (Figure 2, for details see Scheelhaase et al., 2015): VarMission (Schaefer, 2012; Schaefer et al., 2010) and 4D-Race (4 Dimensional distRibution of AirCraft Emissions) calculate the absolute amount as well as three-dimensional distributions of the CO_2 and non-CO_2 emissions of aviation in the timeframe 2010-2030 differentiated by the different geopolitical scenarios, which is the forecast emission inventory. The forecast emission inventory was combined with the CO_2 equivalence factors (Figure 1) to calculate the associated amounts of CO_2 equivalents of all climate relevant species for each flight. These amounts of CO_2 equivalents were used to calculate additional cost as well as demand effects, which influence the development of revenues of the airlines addressed by the climate protecting measure. This will lead to a decrease in air traffic and a loss of employment in the aviation sector. This also leads to a reduction in fuel burn as well as other climate relevant emissions, which has been estimated by VarMission on a flight-by-flight-basis. For both trading schemes (trading scheme for all climate relevant emissions and CO_2 trading scheme, respectively), additional CO_2 savings can be derived from the CO_2 purchases from other emitting sectors (e. g. stationary sources). These purchases are necessary to comply with the trading schemes. The change in climate impact due to emission reduction of air traffic and in other sectors due to emission trading was again analysed by AirClim.

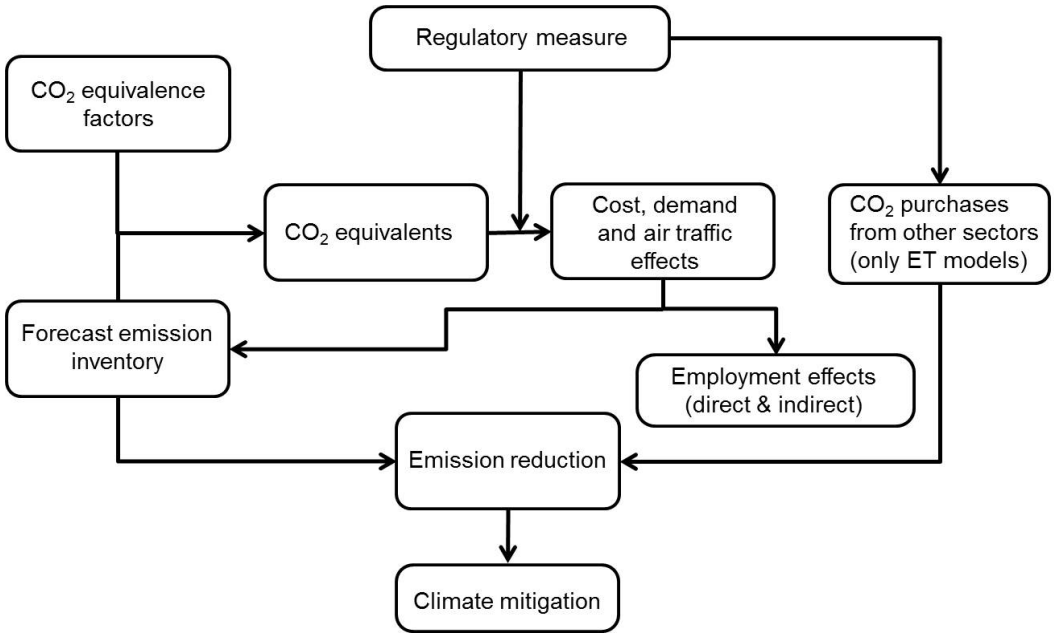

Figure 2: Schematic of the AviClim modelling approach.

3 RESULTS

Here we only present results for the scenario "World" with the assumption of "Low Price Path" and atr_50 as climate metric. More results can be found at Scheelhaase et al., 2015. The cost impacts of the market-based measures are presented in Figure 3a as total. Total costs will be the highest for a climate tax (solid line). Both, an emissions trading scheme (dashed line) and a NO_x charge (dotted line) will lead to much lower overall costs. This can be explained by the specific assumptions that for the trading schemes a free allocation of 85% of 2010 emissions has been assumed.

Under the assumption that the airlines pass on all additional costs, prices for air services will increase. Modelling results show that under the assumption of a price elasticity of demand of -0.8 (case 2), revenues will decrease by 3 to 7% in the period 2010-2030 (Figure 3b). Again, effects of the climate tax are the largest while the impacts of the emissions trading scheme and the effects of the NO_x charge are far lower.

The reduction in air traffic leads to a reduction of climate impact from aviation since less fuel will be burned and also the non-CO_2 climate effects such as contrails are reduced. For the two market-based measures including emissions trading, additional environmental benefits are derived from the necessary purchase of CO_2 allowances from other sectors to comply with the regulation scheme.

The temporal development of climate impact in terms of temperature change is presented in Figure 4. For the emissions after 2030 we assume constant emissions as the future development is difficult to foresee. Without the possibility to buy permits from other sectors, only small impacts on the temperature change can be realized (3% to 8%). If purchases of permits are taken into consideration, the temperature change in the year 2100 will be reduced by up to 65%. Due to the fact that for emissions trading the amount of purchases from other sectors is larger than the CO_2 emission from aviation, the temperature change decreases after 2040 despite constant aviation emission after 2030.

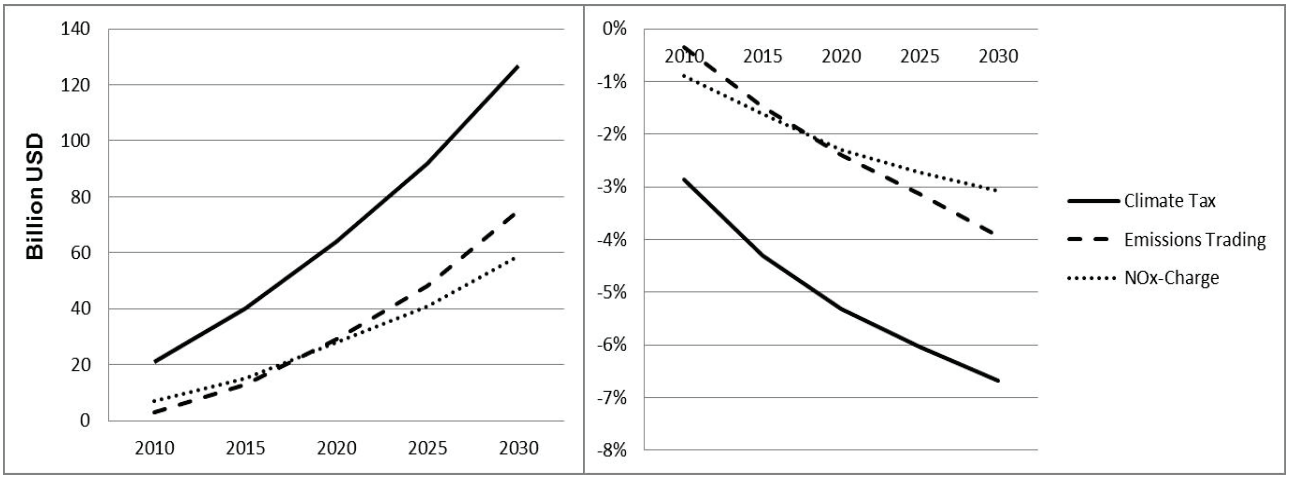

Figure 3 Costs of different market-based measures (left) and changes of demand relative to Business-as-usual for a price elasticity of demand of -0.8 (case 2, right) analysed in Scenario "World", assuming the 'Low Price Path' and the metric atr_50.

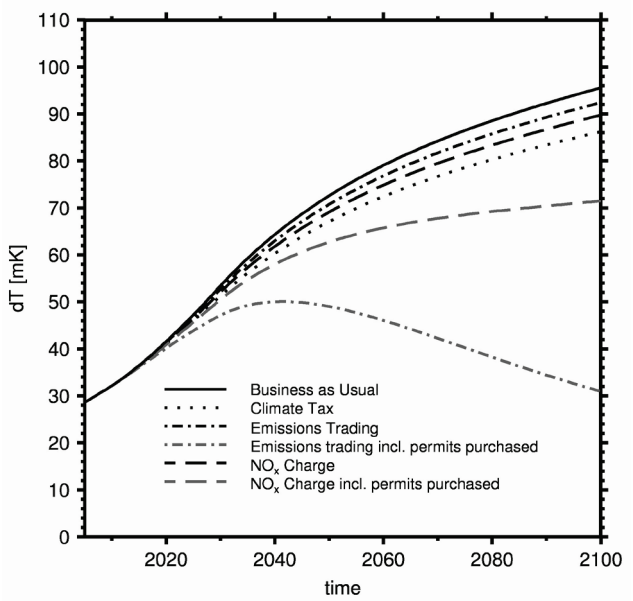

Figure 4: Temporal development of temperature change for the scenario "World" with the 'Low Price Path' and the metric atr_50.

The increasing temperature change after 2030 for all other scenarios is due to the thermal inertia of the atmosphere and the very long lifetime of CO_2, which leads to an accumulation in the atmosphere. Overall, AviClim results show that environmental benefits are the greatest for the emissions trading scheme for all climate relevant emissions from aviation.

4 FINAL REMARKS

Her we only have presented the results for atr_50. The AviClim project indicates that the choice of the metric has a great influence on both the economic and the environmental effects of the market-based measure analysed. For simplification reasons modal switching has not been considered in the present study. This will be subject to further research. Therefore, environmental benefits calculated are at the upper end and may be smaller in reality.

REFERENCES

Burkhardt, U., Kärcher, B., 2011. Global radiative forcing from contrail cirrus. Nature Climate Change 1, 54–58.

Dahlmann, K., Grewe, V., Frömming, C. and Burkhardt, U., 2015. Can we reliably assess climate mitigation options for air traffic scenarios despite large uncertainties in atmospheric processes? Transportation Research Part D: Transport and Environment, in prep.

Fichter, C., S. Marquart, R. Sausen and D.S. Lee, 2005. The impact of cruise altitude on contrails and related radiative forcing. Meteorologische Zeitschrift 14, 563-572.

Fichter, C., 2009. Climate impact of air traffic emissions in dependency of the emission location and altitude. DLR-Forschungsbericht. DLR-FB 2009-22.

Forster, P.M., K.P. Shine and N. Stuber, 2006. It is premature to include non-CO_2 effects of aviation in emission trading schemes. Atmospheric Environment 40, 1117–1121, doi:10.1016/j.atmosenv.2005.11.005.

Frömming, C., M. Ponater, K. Dahlmann, V. Grewe, D.S. Lee and R. Sausen, 2012. Aviation-induced radiative forcing and surface temperature change in dependency of the emission altitude. Journal of Geophysical Research, Vol. 1 (D19104). DOI: 10.1029/2012JD018204. ISSN 0148-0227.

Grewe, V., Stenke, A., 2008. AirClim: an efficient climate impact assessment tool. Atmospheric Chemistry and Physics 8, 4621–4639.

Grewe, V., Dahlmann, K., 2012. Evaluating climate-chemistry response and mitigation options with Airclim, in: Schumann, U. (Ed.), Atmospheric Physics: Background - Methods - Trends. Springer Verlag Berlin Heidelberg, pp. 591–606.

Lee, D.S., D.W. Fahey, P.M. Forster, P.J. Newton, R.C.N. Wit, L.L. Lim, B. Owen, and R. Sausen, 2009. Aviation and global climate change in the 21st century. Atmospheric Environment 43, 3520–3537.

Mannstein, H, P. Spichtinger, and K. Gierens, 2005. A note on how to avoid contrail cirrus. Transportation Research Part D 10, 421-426.

Schaefer, M., 2012. Development of a Forecast Model for Global Air Traffic Emissions, DLR Forschungsbericht 2012-08, Cologne.

Schaefer, M., Scheelhaase, J., Grimme, W., Maertens, S., 2010. The economic impact of the upcoming EU emissions trading system on airlines and EU Member States – an empirical estimation. European Transport Research Review 2, 189-200.

Scheelhaase, J. D., Dahlmann, K., Jung, M., Keimel, H., Nieße, N., Sausen, R., Schaefer, M., and Wolters, F., 2015. How to best address aviation's full climate impact from an economic point of view? – Main results from AviClim research project. Transportation Research Part D: Transport and Environment, in press.

The Implications of Intermediate Stop Operations on Aviation Emissions and Climate

F. Linke, V. Gollnick*
DLR Air Transportation Systems, Hamburg, Germany

V. Grewe
DLR Institute of Atmospheric Physics, Oberpfaffenhofen, Germany

Keywords: Intermediate Stop Operations, staging, emission inventory, climate assessment, operational concept, mitigation strategies, system-wide analysis

ABSTRACT: Among the various transport modes aviation's impact on climate change deserves special attention. Due to typical flight altitudes in the upper troposphere and above the effect of aircraft engine emissions like carbon dioxide, water vapour, nitrogen oxides and aerosols on radiative forcing agents is substantial. The projected duplication of aircraft movements in the next 15 years will lead to an increase of aviation's impact on climate and requires immediate mitigation options. Besides technological measures also new operational strategies are widely discussed; one of these concepts which has been subject of several studies in the past is Intermediate Stop Operations (ISO). It is based on the idea to reduce the stage length of flights by performing one or more intermediate landings during a mission. Due to shorter flight distances the amount of fuel burnt over the mission can be reduced, as the amount of fuel necessary to transport a certain percentage of the fuel for a long distance can be omitted. Besides fuel cost saving implications, many previous studies anticipate a strong reduction of the environmental impact compared to direct flight operations. So far, none of them has actually quantified this impact in a realistic scenario. While for the amount of emitted species which are produced proportional to fuel burn, a reduction is straightforward, this is not the case for other species. Moreover, the geographic location and altitude of the emissions have to be taken into account for a sound climate impact assessment.

The paper presents results of the ecological analysis of the ISO concept for today's worldwide aircraft fleet, including its influence on global emissions distributions as well as the impact on climate change. A method is described that comprises of different models for a realistic traffic simulation taking into account operational constraints and ambient conditions, like e.g. wind, the calculation of engine emissions and the integration of a climate response model.

1 INTRODUCTION

As aircraft most of the time cruise at high altitudes in the upper troposphere and lower stratosphere the effect of gaseous emissions from aviation on radiative forcing agents is substantial. Given the projected duplication of aircraft movements in the next 15 years aviation's impact on climate therefore deserves special attention and immediate mitigation options are required. Besides technological measures like e.g. new combustion technologies also new operational strategies are widely discussed; one of these concepts is Intermediate Stop Operations (ISO). It is based on the idea to reduce the stage length of flights by performing one or more intermediate landings during a mission. Due to shorter flight distances the amount of fuel burnt over the mission can be reduced, as the amount of fuel necessary to transport a certain percentage of the fuel for a long distance can be omitted.

The ISO concept has been subject of numerous studies in the past, ranging from generic analyses of single missions based on aircraft design methods to investigations on fleet as well as global level. The focus of these studies was mainly to evaluate the potential fuel savings that can be gained by the concept but partly the authors also looked into the effects on block times, costs (both single flight operating costs and lifecycle costs) and safety. From payload-range efficiency considerations derived from aircraft design relationships it was found that fuel savings are in the order of 13%-

* *Corresponding author:* Florian Linke, DLR Air Transportation Systems, Blohmstr. 20, 21079 Hamburg, Germany. Email: florian.linke@dlr.de

23% for missions with a single stopover if aircraft are used that are optimized for shorter ranges (Martinez-Val et al., 2014; Lammering et al., 2011; Langhans et al., 2010; Creemers and Slingerland, 2007). But also with existing aircraft 5%-15% fuel can be saved depending on the aircraft type and mission length (Poll, 2011; Lammering et al., 2011; Langhans et al., 2010; Creemers and Slingerland, 2007). Fleet and global level assessments have been conducted by Poll (2011), Langhans et al. (2010), Green (2005) and Linke et al. (2011). Assuming a real geographical distribution of possible intermediate airports for flights operated by Boeing 777 or Airbus A330 Langhans et al. (2010) and Linke et al. (2011) found 10%-11% fuel savings globally if the aircraft is redesigned for 3000 NM.

In addition to the positive implications of the ISO concept on fuel consumption and operating costs many authors infer that the concept may consequently reduce the environmental impact of aviation. With regard to the CO_2 footprint this conclusion is valid without further ado, for a sound understanding of the impact of the concept's non-CO_2 emissions on the climate, however, a detailed analysis of the changes of quantities and distribution of individual pollutant species is necessary. Creemers and Slingerland (2007) have estimated a global warming potential reduction of 13% by ISO with optimized aircraft using a simplified method. For these findings it was assumed that flight altitudes of the redesigned aircraft will slightly increase and that the impact of CO_2, NO_x and H_2O emissions of one kilogram fuel can be modeled as a function of altitude.

As stated above, system-wide studies taking real-world air traffic and route networks into account have been performed with a focus on the global fuel saving potential only. A comprehensive study of the global impact of ISO on the environment, i.e. emissions and climate, has not been done so far. This paper presents a system-wide analysis of the short-term environmental impact of Intermediate Stop Operations. Due to the global character of the study small-scale effects like changes of the local air quality at airports are not considered. The environmental impact is quantified by the amount and the distribution of gaseous engine emissions as well as their effect on climate given as Average Temperature Response (ATR) metrics. It is assumed that ISO are carried out with the current world-wide aircraft fleet in a real flight and airport network and all aircraft types that potentially benefit from ISO are considered and realistic operational influences, including wind, are taken into account.

2 METHODOLOGY

A modeling system was developed that allows for the assessment of operational concepts, like e.g. ISO, with respect to their impact on global emissions and climate. As depicted in figure 1 this system comprises of different models. Flight movements are simulated using DLR's Trajectory Calculation Module (Lührs, 2013), which computes aircraft trajectories from lift-off to touch-down applying a kinetic mass-point model that provides simplified equations of motion known as Total Energy Model. One of the key features implemented in the TCM for the purpose of this research is the use of the advanced aircraft performance model BADA (Base of Aircraft Data) family 4, which allows for modeling typical flight operations more realistically than other models. The BADA 4 models cover the whole flight envelope, capture the flight physics more accurately and thus can be used to determine e.g. optimized vertical profiles, i.e. optimum altitudes and speeds (Mouillet, 2013). Using this capability airline-preferred cruise profiles can be estimated including the location of step climbs depending on the selected step climb strategy and the heading-dependent available flight levels.

Regarding meteorological data the TCM can either be used with International Standard Atmosphere (ISA) conditions or with real atmospheric data in NetCDF or GRIB format that can e.g. be obtained from the European Center for Medium-range Weather Forecasts (ECMWF). In order to account for the effect of wind a new and highly efficient method has been developed which is able to process daily wind data and statistically analyze it resulting in a data set of local wind distributions. This data is used to determine characteristic mean still air distances for any given flight route that serve as a basis for system-wide analyses for longer periods of time, e.g. one year (Swaid, 2013).

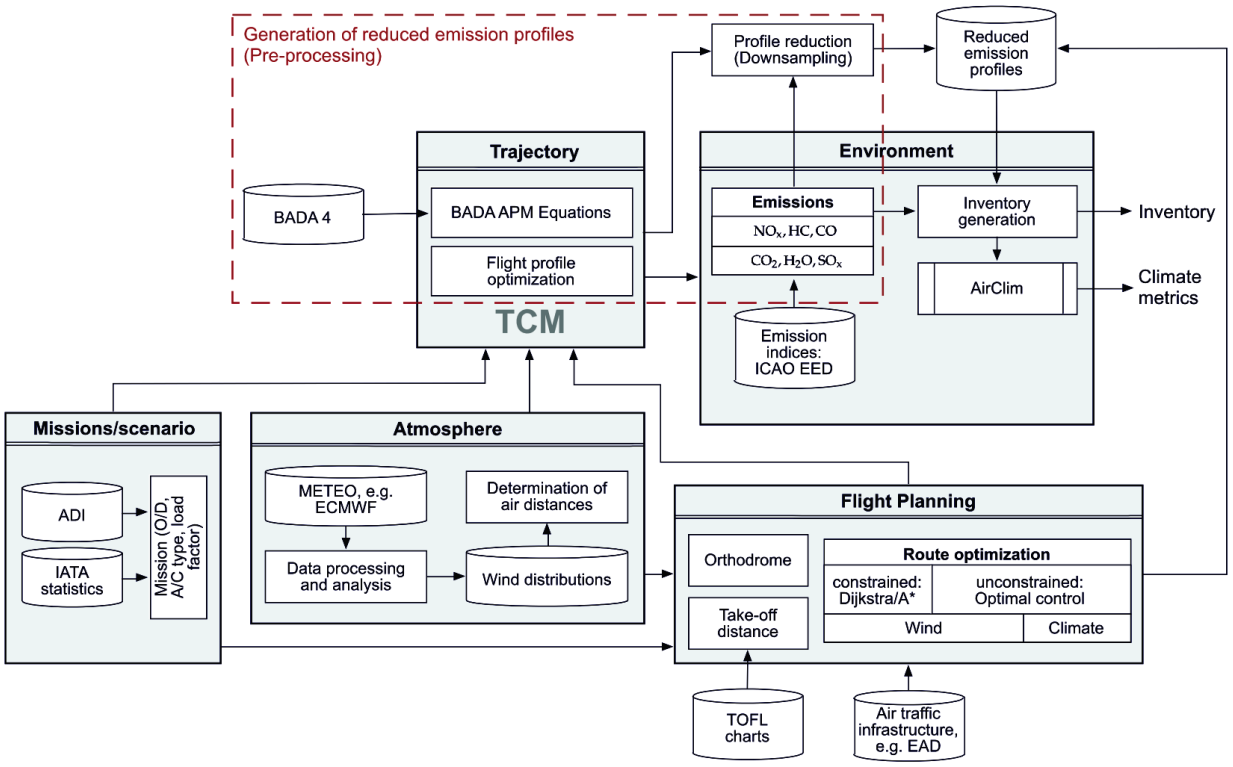

Figure 1: Schematic diagram of the developed modeling system

For the environmental analysis the modeling system comprises of an emission model that determines the gaseous emissions along resulting trajectories from TCM. Here, both emission species that are produced proportionally to fuel burn, i.e. CO_2, H_2O, as well as species that develop in a non-proportional way, i.e. NO_x, HC and CO, are determined. For the latter the state-of-the-art fuel flow correlation method Boeing Fuel Flow Method 2 (DuBois and Paynter, 2006) is applied in combination with Emission Indices for sea level conditions taken from ICAO Engine Emission Databank. With a gridding algorithm these emission distributions are mapped into a geographical grid, which allows for the generation of emission inventories by superposing the emissions of a large number of flights. These inventories are then used by the climate-chemistry response model AirClim (Grewe and Stenke, 2008; Fichter, 2009; Dahlmann, 2011) to determine the climate impact resulting from the emissions. The basis of this method constitute pre-calculated changes of the atmospheric concentrations of radiative forcing agents to unit emissions with the complex climate chemistry model ECHAM4.L39(DLR)/CHEM (Hein et al., 2001) as a function of latitude and altitude as well as the corresponding radiative forcing. Further modules include flight planning capabilities used for horizontal route optimization.

In order to reduce the necessary number of trajectory simulations in the course of a global analysis with a large number of flights the developed modeling system makes use of a method that is commonly used to reduce the complexity during the generation of emission inventories. So-called reduced emission profiles are used that were derived from pre-calculated trajectories and emission distributions. During the inventory generating process for every flight the appropriate profile is taken from a database, adjusted to the actual air distance of the particular flight and mapped into the geographical grid by scaling it to the respective ground distance and aligning it to the flight path. Thereby, this method can also account for the effect of wind and potential horizontal flight inefficiencies.

Through the above mentioned combination of trajectory computation, flight planning and environmental analysis capabilities the modeling system can be used to evaluate the environmental effects resulting from changes of flight and fleet operations.

3 STUDY SET-UP

In this study the modeling system was applied to analyze the implications Intermediate Stop Operations have on global aviation emissions and climate. For this purpose, emission inventories were generated for two scenarios which were then compared to each other: The reference case is made up of a large-scale traffic scenario in which every mission is conventionally performed as direct flight, whereas the ISO case contains for each mission two flight segments connecting the origin to the destination airport via a stopover at the refueling airport. As the short-term effects of ISO is of interest in this study, it is assumed that each ISO mission is performed by the same aircraft type as used for the direct flight ("self-substitution") and no further changes of the aircraft fleet need to be considered. Mission data was taken from Sabre ADI flight schedule database for the first quarter of 2010 and flight frequencies were scaled up to the period of one year. As previous studies have revealed that only wide-body aircraft actually show a fuel saving potential in self-substitution on mission lengths above 2500 NM (Linke et al., 2012), this study is limited to the global wide-body aircraft fleet. Region-dependent passenger load factors were calculated based on IATA economics statistics.

In preparation for the inventory calculation, the stopover locations had to be defined; using an exhaustive search algorithm the respective airport was determined by optimization for each ISO mission assuming that that location is selected for the stopover which leads to the maximum fuel savings for the specific mission. The airports' geographical coordinates were obtained from the EAD database which was filtered for only major airports with at least one asphalt-surfaced runway and an instrument landing system (ILS) assuming that certain equipment needs to be installed such that commercial wide-body airplanes are able to perform an intermediate stop there. Meteorological data was taken from ECMWF for a grid of .75° x .75° for the period of one year (2012). The statistical wind distributions mentioned above were used to account for the effect of wind by considering annual mean air distances between every airport pair. These air distances were used to obtain the respective reduced emission profiles from the database. For the sake of simplicity only orthodromic (great circle) routes were assumed.

4 RESULTS

The introduction of ISO affects the amount and the distribution of engine exhaust emissions thus leads to a change of the climate impact. In the following the some results of the study are presented. In a first step for each mission the optimum stopover airport was determined. For 86,8% of all simulated long-haul flights appropriate airports were found that lead to positive fuel savings compared to the direct flight. It is assumed that as soon as positive savings can be achieved by a stopover the flight is operated in ISO mode. The remaining flights are conducted in direct mode. Table 1 shows the 20 most affected airports together with the number of additional landings and take-offs due to ISO.

Rank	ICAO	Airport name	Location	Flights	
1	CYQX	Gander International Airport	Gander, Newfoundland, Canada	56090	6,31%
2	CYYT	St. John's International Airport	St. John's, Newfoundland, Canada	46387	5,22%
3	LPLA	Lajes Airport	Lajes, Azores, Portugal	27680	3,12%
4	CYYR	Goose Bay Airport	Goose Bay, Labrador, Canada	26432	2,97%
5	BGBW	Narsarsuaq Airport	Narsarsuaq, Greenland	23685	2,67%
6	PADK	Adak Island Airport	Adak (Island), Alaska, USA	19239	2,17%
7	YBRM	Broome International Airport	Broome, Western Australia, Australia	14586	1,64%
8	CYFB	Iqaluit Airport	Iqaluit, Nunavut, Canada	12401	1,40%
9	GVSV	Cesária Évora Airport	São Vicente, Capeverde	11878	1,34%
10	CYVP	Kuujjuaq Airport	Kuujjuaq, Québec, Canada	11856	1,33%
11	LTFH	Carsamba Airport	Samsun, Turkey	11644	1,31%
12	PLCH	Cassidy International Airport	Banana, Kiritimati (Island), Kiribati	10959	1,23%
13	WAPP	Pattimura Airport	Ambon, Indonesia	10946	1,23%
14	GVFM	Nelson Mandela International Airport	Praia, Santiago (Island), Capeverde	10923	1,23%
15	USNR	Raduzhny Airport	Raduzhny, Russia	9950	1,12%
16	CYDF	Deer Lake Airport	Deer Lake, Newfoundland, Canada	9604	1,08%
17	PABR	Wiley Post-Will Rogers Memorial Airport	Barrow, Alaska, USA	8874	1,00%
18	PACD	Cold Bay Airport	Cold Bay, Alaska, USA	8797	0,99%
19	UHMA	Ugolny Airport	Anadyr, Russia	8658	0,97%
20	UOOO	Norilsk Alykel Airport	Norilsk, Russia	7495	0,84%
				348086	39,17%

Table 1: Top 20 most frequented ISO airports with number of additional landings and take-offs

It is not surprising that these airports are mainly located in regions which are crossed by long-haul flights, including Newfoundland, Greenland, Siberia as well as some islands in the Atlantic and Pacific Oceans. Overall 440 individual airports were identified that serve as stopover locations for ISO missions. Approximately 40% of all intermediate stops can be accommodated by the 20 most frequented airports. These findings are consistent with results from previous studies, including Linke et al. (2011) and Langhans et al. (2013), however, this study includes the effect of wind for the first time.

Based on the identified ISO airports emission inventories were calculated both for the direct flight scenario and for the ISO mode scenario. The difference of these inventories with regard to fuel consumption is shown in figure 2. Positive peaks (large differences to reference case) can be found in those regions that were identified before, as additional emissions are produced near airports accommodating intermediate stops.

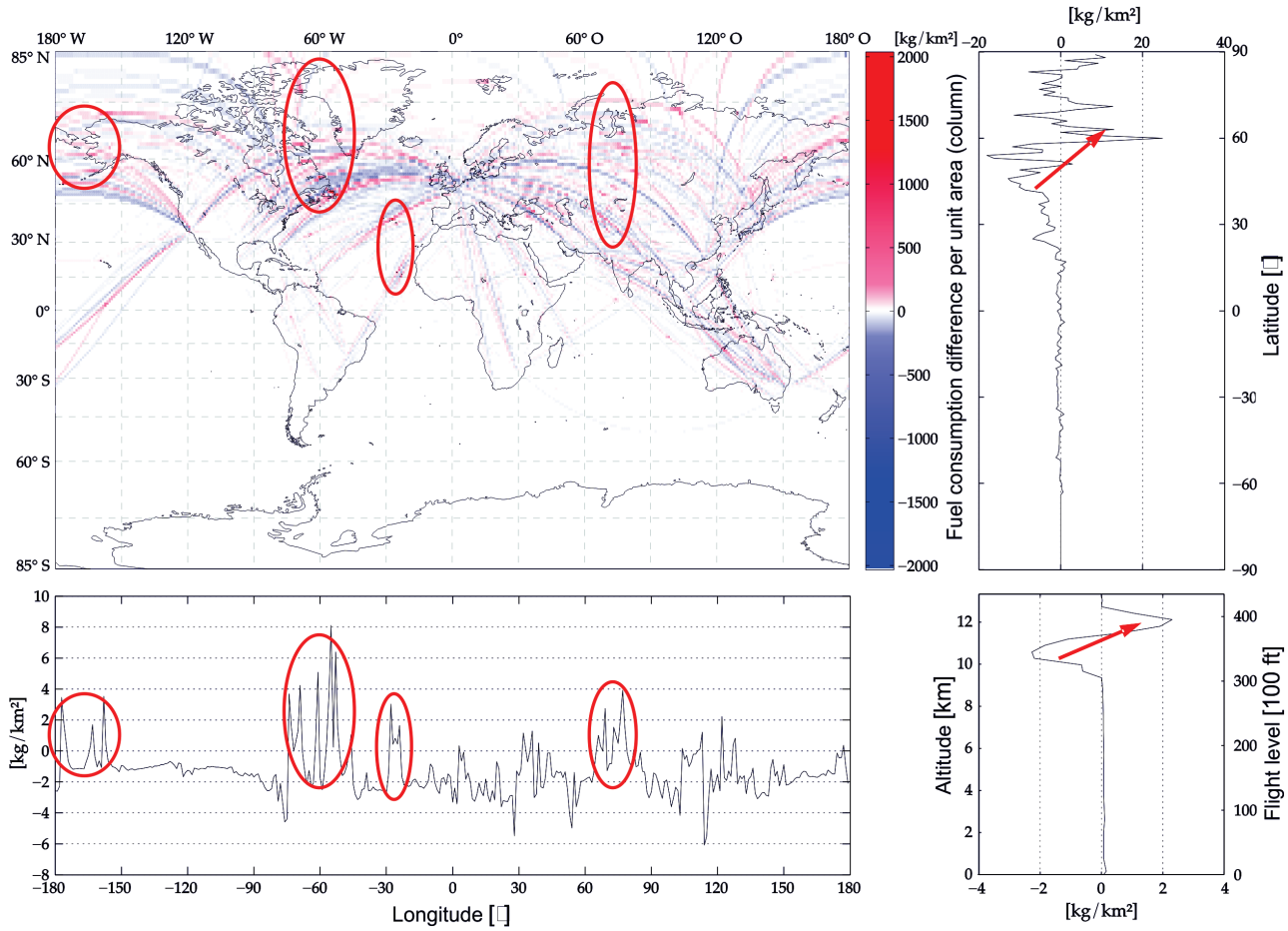

Figure 2: Redistribution of global fuel consumption due to ISO on long-haul missions (differences from direct flight scenario) in the first quarter of 2010; top left: geographical distribution of changes in the fuel sums per column; top right: latitude profile (zonal); bottom left: longitude profile (meridional); bottom right: altitude profile

From the latitude and altitude profiles a shift of emissions towards higher latitudes and altitudes can be observed. The altitude shift can be explained by higher initial cruise flight levels in the ISO case than in the direct flight. The reason for this is the reduced take-off weight (TOW) on the ISO mission corresponding to a higher optimum altitude. In this study it is assumed that pilots try to fly as close as possible to the optimum altitude for fuel economy reasons.

Overall, the introduction of Intermediate Stop Operations could save approximately 3 million tons of fuel per year representing 4.8% of the overall fuel consumption in the reference case. Realizing ISO on a global scale would only require 0.4% extension of the flown ground distance meaning that in general airports can be found that are suitably located and do not require large detours. While CO_2, H_2O and SO_2 can be reduced by 4.8% globally, there is a 4.6% reduction in global aviation NO_x, an increase by 33.3% of CO and an increase of HC by 43.4%. The latter findings indicate

a potential local air quality issue, especially at highly frequented ISO airports, and should be subject to further investigation.

Figure 3 finally shows the CO_2 inventory projections into the longitude-altitude plane both for the direct flight and the ISO scenario. Obviously most cruise emissions are moved to approximately 12 km altitude due to the shift of initial cruise flight levels to higher altitudes by 4000-6000 ft. It can also be observed that the number of step climbs in ISO mode is reduced due to shorter segment lengths and therefore the altitude band is narrowed from 7000 ft to approximately 3000 ft.

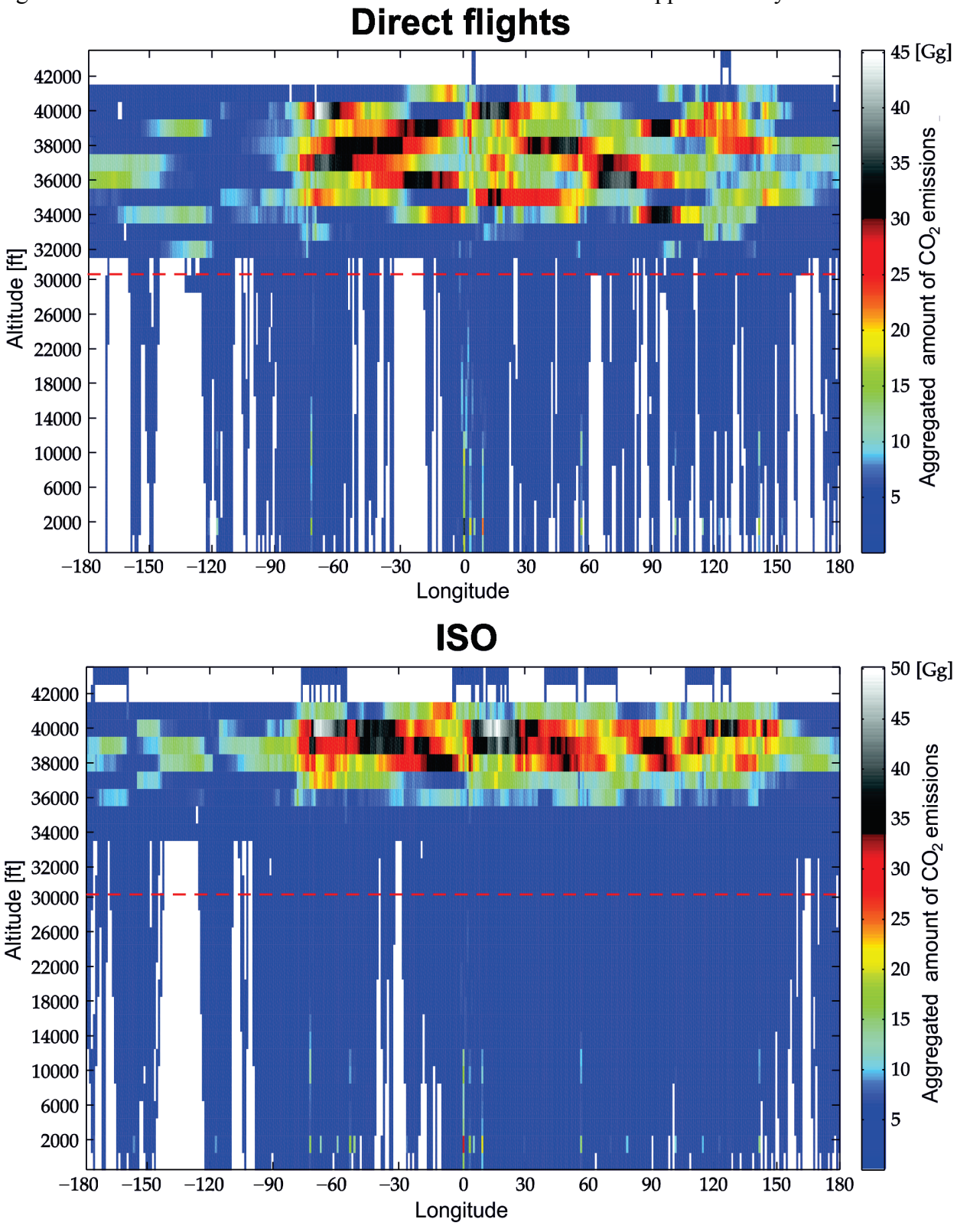

Figure 3: Distributions of CO_2 emissions (absolute values meridionally aggregated) in longitude-altitude plane for the direct flight mode (top) and the ISO mode (bottom)

Finally, a climate impact assessment was made by comparing the climate metrics that were determined by AirClim (see section 2) for the computed emission inventories. As appropriate climate metrics the Average Temperature Response over a period of 100 years (ATR100) was selected as it had been proven to be suitable for the assessment of new operational and technological measures (e.g. Koch, 2013). Using ATR a continuous emission production and the dynamics of the climate system can be considered. As base scenario the Fa1 growth scenario defined by ICAO FESG was selected and the ramp-up of the ISO concept introduction was assumed to last 10 years starting in 2015. The results can be seen in figure 4. Although the absolute amount of emissions of the species CO_2, H_2O, SO_2 and NO_x can be reduced through ISO the Average Temperature Response increases by 2.3% which is one of the major findings of the study. There is a cooling effect of CO_2 due to ISO; however, as most emissions are released in the upper troposphere and lower stratosphere where mixing processes are slower and the radiative forcing of an ozone concentration perturbation is higher, the changes in ozone have a warming effect. Also the cooling effect from methane is reduced due to an increased methane life time, which also leads to retarded ozone depletion (warming) (Grooß et al., 1998).

Figure 4: Climate impact changes (metrics: ATR100) due to ISO separated by contributions of different radiative forcing agents (reference case: percentage of overall ATR; ISO case: relative changes with respect to reference case)

The highest relative changes with respect to the direct flight scenario can be observed for the climate impact of water vapor. The radiative forcing of water vapor generally increases with the altitude at which it is released (Lee, 2010). The upwards shift of flight levels into the lower stratosphere therefore intensifies the greenhouse effect of H_2O. This effect is even increased by a slight shift of emissions to higher latitudes as the tropopause altitude falls towards the poles. For contrails a cooling effect was determined for the ISO concept. The radiative forcing by contrails reaches its maximum just below the tropopause and is dependent on contrail coverage and optical properties. Above the tropopause the radiative forcing by contrails then decreases with increasing altitude (Lee, 2009). The shift to higher altitudes and latitudes therefore is expected to cause the cooling as passing of contrail-prone regions becomes less probable. In combination, these findings show that in contrast to speculations from previous studies a systematic introduction of ISO on a global level would not necessarily have positive implications for the climate. Due to the high fraction of the effect of an ozone concentration perturbation on the overall temperature response this warming effect cannot be compensated by cooling from less CO_2 and contrails.

5 CONCLUSIONS

A method has been presented that allows for the assessment of new operational concepts with respect to their impact on global emissions and climate. The method was applied to analyze the ecological implications of the ISO concept for today's worldwide aircraft fleet. A large-scale air traffic scenario containing all world-wide long-haul flights in 2010 was considered and the effect of wind was accounted for.

Overall, 4.8% of fuel could be saved through ISO globally assuming a full coverage of the operational concept. Airports serving as suitable stopover airports are located mainly in Newfoundland, Greenland, Siberia, Azores and Capeverdes. While most emission species can be reduced by ISO, there would be an increase of 40-50% of HC and CO emissions due to the doubling of descent and landing phases causing a potential local air quality issue. Due to a lower TOW on ISO missions the initial cruise flight levels are shifted up and the altitude band is narrowed as flight segments are shorter and less step climbs are required. This emission relocation causes a warming climate impact

compared to the direct operations by 2.3% in the Average Temperature Response over 100 years as the warming effect caused by the emitted NO_x dominates cooling effects from CO_2 and contrails. The results strongly depend on the balance of the contributions from the various radiative forcing agents to the overall climate response, some of which are scientifically still not completely understood. Therefore, an uncertainty analysis shall be conducted to ensure the robustness of the findings of this study. However, the results are consistent with findings from similar investigations (e.g. Frömming et al., 2012). Furthermore, the results suggest that decreasing cruise altitudes during ISO mode might reduce the negative effects of the concept. As this also reduces the potential fuel savings of the concept a trade-off needs to be done and an optimization could be conducted to determine the optimum altitude for the ISO missions in order to have a combined environmental and fuel saving benefit.

REFERENCES

Airbus Customer Services. Getting to Grips with Aircraft Performance. Tech. rep., Flight Operations Support & Line Assistance, January 2002

Creemers, W., and Slingerland, R. Impact of intermediate stops on long-range jet transport design. 7th AIAA Aviation Technology, Integration and Operations (ATIO) Conference, Belfast, Northern Ireland (2007), AIAA-2007-7849, American Institute of Aeronautics and Astronautics.

Dahlmann, K. Eine Methode zur effizienten Bewertung von Maßnahmen zur Klimaoptimierung des Luftverkehrs. Dissertation, Ludwig–Maximilians–Universität, Munich, December 2011.

DuBois, D., and Paynter, G. Fuel Flow Method 2 for Estimating Aircraft Emissions. SAE Technical Paper 2006-01-1987, Society of Automotive Engineers (SAE), 2006.

Fichter, C. Climate Impact of Air Traffic Emissions in Dependency of the Emission Location and Altitude. Dissertation, Manchester Metropolitan University, 2009.

Frömming, C., Ponater, M., Dahlmann, K., Grewe, V., Lee, D. S., and Sausen, R. Aviation-induced radiative forcing and surface temperature change in dependency of the emission altitude. Journal of Geophysical Research, 117, D19104, doi:10.1029/2012JD018204 (2012)

Green, J. E. Air Travel – Greener by Design: Mitigating the Environmental Impact of Aviation: Opportunities and Priorities. Report of the Science and Technology Sub-Group (July 2005).

Grewe, V., and Stenke, A. AirClim: an efficient tool for climate evaluation of aircraft technology. Atmospheric Chemistry and Physics 8 (2008), S. 4621–4639.

Grooß, Jens-Uwe, J.-U., Brühl, C., and Peter, T. Impact of aircraft emissions on tropospheric and stratospheric ozone. Part I: chemistry and 2-D model results. Atmospheric Environment 32, 18 (September 1998), 3173–3184.

Hein, R., Dameris, M., Schnadt, C., Land, C., Grewe, V., Köhler, I., Ponater, M., Sausen, R., B. Steil, B., Landgraf, J., and Brühl, C. Results of an interactively coupled atmospheric chemistry-general circulation model: Comparison with observations. Annales Geophysicae 19, 4 (2001), 435–457.

Koch, A. Climate impact mitigation potential given by flight profile and aircraft optimization. Dissertation, Hamburg University of Technology (TUHH), November 2013.

Lammering, T., Anton, E., Risse, K., Franz, K., and Hoernschemeyer, R. Gains in Fuel Efficiency: Multi-Stop Missions vs. Laminar Aircraft. 11th AIAA Aviation Technology, Integration, and Operations (ATIO) Conference (2011), AIAA-2011-6885, American Institute of Aeronautics and Astronautics.

Langhans, S., Linke, F., Nolte, P., and Schnieder, H. System analysis for future long-range operation concepts. 27th Congress of the International Council of the Aeronautical Sciences (ICAS), Nice, France (2010).

Langhans, S., Linke, F., Nolte, P., and Gollnick, V. System Analysis for an Intermediate Stop Operations Concept on Long Range Routes. Journal of Aircraft 50, 1 (2013), 29–37.

Lee, D. S., et al. Aviation and Global Climate Change in the 21st Century. Atmospheric Environment (2009).

Lee, D., Pitari, G., Grewe, V., Gierens, K., Penner, J., Petzold, A., Prather, M., Schumann, U., Bais, A., Berntsen, T., et al. Transport impacts on atmosphere and climate: Aviation. Atmospheric Environment 44, 37 (2010), 4678–4734.

Linke, F., Langhans, S., and Gollnick, V. Global fuel analysis of Intermediate Stop Operations on long-haul routes. 11th AIAA Aviation Technology, Integration, and Operations (ATIO) Conference, Virginia Beach, USA (2011), AIAA-2011-6884, American Institute of Aeronautics and Astronautics.

Linke, F., Langhans, S., and Gollnick, V. Studies on the potential of Intermediate Stop Operations for today's airlines. 16th Air Transport Research Society (ATRS) World Conference, Tainan, Taiwan (2012).

Lührs, B. Erweiterung eines Trajektorienrechners zur Nutzung meteorologischer Daten für die Optimierung von Flugzeugtrajektorien. Diploma thesis, Hamburg University of Technology (TUHH), November 2013

Martinez-Val, R., Roa, J., Perez, E., and Cuerno, C. Effects of the Mismatch Between Design Capabilities and Actual Aircraft Utilization. Journal of Aircraft 48, 6 (2014), pp. 1921–1927.

Mouillet, V. Session 4: BADA Family 4 – State of the art. BADA User Group Meeting 2013, EUROCONTROL Experimental Centre, Bretigny sur Orge, France, 5th June, 2013.

Poll, D. I. A. On the effect of stage length on the efficiency of air transport. The Aeronautical Journal 115, 1167 (May 2011), Royal Aeronautical Society.

Swaid, M. Entwicklung von Flugplanungsfunktionalitäten zur Flugmissionsanalyse unter realistischen operationellen Bedingungen. Internal report IB-328-2013-37, Deutsches Zentrum für Luft- und Raumfahrt, Lufttransportsysteme, Hamburg, 2013

Swaid, M. Entwicklung eines Routenoptimierungsalgorithmus zur Ermittlung windoptimaler Flugrouten in einem Luftverkehrsstrassensystem. Diploma thesis, Hamburg University of Technology (TUHH), August 2014.

Climate impact assessment of routing strategies: Interactive air traffic in a climate model

H. Yamashita*, V. Grewe, P. Jöckel
DLR-Institut für Physik der Atmosphäre Oberpfaffenhofen, Germany

F. Linke
DLR-Institut für Lufttransportsysteme, Hamburg, Germany

M. Schaefer
DLR-Institut für Antriebstechnik, Köln, Germany. Present affiliation: Bundesministerium für Verkehr und digitale Infrastruktur

D. Sasaki
Kanazawa Institute of Technology, Department of Aeronautics, Hakusan, Japan

Keywords: climate impact, aircraft emissions, flight trajectory optimization

ABSTRACT: This paper describes AirTraf ver. 1.0 for climate impact evaluations that performs global and long-term air traffic simulations with respect to aircraft routing options. AirTraf was developed as a new submodel of the ECHAM5/MESSy Atmospheric Chemistry (EMAC) model. The real flight plan, Eurocontrol's Base of Aircraft Data (BADA) and ICAO engine performance data were employed. Fuel and emissions were calculated by the total energy model based on the BADA methodology and DLR fuel flow correction method. The flight trajectory optimization was performed by the Genetic Algorithm (GA). The AirTraf simulation was demonstrated on-line with the flight time routing option for a specific winter day. 103 trans-Atlantic flight plans were used, assuming Airbus A330-301 aircraft. The results confirmed that AirTraf properly works on-line and GA successfully found the time-optimal flight trajectories, reflecting local weather conditions.

1 INTRODUCTION

Aviation contributes to climate change, e.g. via emissions of CO_2, NO_x, water vapor and particles, which affect climate agents such as contrail-cirrus, ozone, methane, and carbon dioxide (Lee et al., 2010). Mobility becomes more and more important to society and hence air transportation is expected to grow significantly over the next decades. Mitigating the climate impact from aviation is required to cope with the increasing impact of aviation on climate. A number of studies suggested avoiding climate sensitive regions by re-routing horizontally and vertically (Frömming et al., 2012, Matthes et al., 2012, Søvde et al., 2014, Grewe et al., 2014a). This aircraft routing strategy has a great potential in reducing the climate impact, since most of the climate impact arises from non-CO_2 effects, which are short-lived and vary regionally. However, no assessment platform exists, with which different routing options can be assessed.

Here, we describe a new assessment platform AirTraf ver. 1.0 (Yamashita et al., 2015) that is a simplified global air traffic model coupled to the ECHAM/MESSy Atmospheric Chemistry (EMAC) model (Jöckel et al., 2010). The AirTraf simulation was performed in EMAC (on-line) with respect to the flight time routing option for a specific winter day, using real trans-Atlantic flight plans of A330-301. To verify the routing methodologies, we focused on the results for a representative airport pair.

* *Corresponding author:* Hiroshi Yamashita, DLR-Institut für Physik der Atmosphäre, Oberpfaffenhofen, D-82234 Wessling, Germany. Email: hiroshi.yamashita@dlr.de

2 OVERVIEW OF AIRTRAF SUBMODEL

AirTraf was developed as a submodel of EMAC (Jöckel et al., 2010). The EMAC is suitable for the development environment for AirTraf, because we perform global and long-term air traffic simulations considering local weather conditions. Location and altitude at which emissions are released should be also considered. In addition, various submodels of EMAC can be used to evaluate climate impacts.

This section presents a brief description of the AirTraf submodel. The computational procedure consisted of the following components. First, aviation data (flight plans and aircraft/engine performance data) and AirTraf entries (a routing option, etc.) were input (ICAO, 2005, Eurocontrol, 2011). Second, all entries were distributed to many processes. AirTraf was parallelized using a message passing interface (MPI) based on a distributed memory approach. The global flight plan was decomposed into a number of processing elements (PEs) so that each of PEs had a similar work load, while a whole flight trajectory of an airport pair was handled by only one PE. Third, the global air traffic simulation was run according to the time loop of EMAC. AirTraf provides seven routing options: great circle (minimum flight distance), flight time (time-optimal), NO_x, H_2O, fuel (might differ to H_2O, if alternative fuel options can be used), contrail and climate cost functions (Frömming et al., 2013, Grewe et al., 2014a, Grewe et al., 2014b). The great circle and the flight time routing options can be used in AirTraf 1.0. To determine a flight trajectory with respect to a selected routing option, the flight trajectory optimization was performed (except for the great circle option) based on the Adaptive Range Multi-Objective Genetic Algorithm (ARMOGA ver. 1.2.0) developed by D. Sasaki and S. Obayashi (Sasaki et al., 2002, Sasaki and Obayashi, 2004, Sasaki and Obayashi, 2005). In addition, Fuel use, NO_x and H_2O emissions were calculated to the flight trajectory by using a total energy model based on the BADA methodology (Schaefer, 2012) and the DLR fuel flow correction method (Deidewig et al., 1996). Finally, the obtained flight trajectories and global emission fields were output. Other models, e.g. climate metric models, are integrated easily into AirTraf to evaluate a reduction potential of the climate impact corresponding to the routing option.

The following assumptions were made in AirTraf. Earth radius was set as r = 6,371 km, the aircraft performance model of BADA Revision 3.9 (Eurocontrol, 2011) was used with a constant Mach number, and a cruise flight phase was only considered. Potential conflicts of flight trajectories and operational constraints from air traffic control were not regarded (however, a sector demand analysis is maybe performed based on the output data). A detailed description of the AirTraf will be published (Yamashita, et al., in preparation).

3 DEMONSTRATION OF AIRTRAF SIMULATION

3.1 *Geometry definition of flight trajectory*

Figure 1 shows the geometry definition of a flight trajectory from Munich (MUC) to New York (JFK) as an example. This definition was used to represent a flexible flight trajectory (horizontally and vertically). GA provided the values of six design variables (x_1 to x_6) on location within the rectangular domains; the domain was defined by $0.1 \times \Delta\lambda airport$ (short-side) and $0.3 \times \Delta\lambda airport$ (long-side) ($\Delta\lambda airport$ is the difference in longitude between the airports). GA also provided the values of five design variables (x_7 to x_{11}) in altitude direction within the bound [FL290, FL410]. The given eleven design variables determine coordinates of the eight control points (closed circles) and a flight trajectory was represented by a B-spline curve using the control points (bold solid line). Thereafter, waypoints were distributed along the flight trajectory for function evaluations.

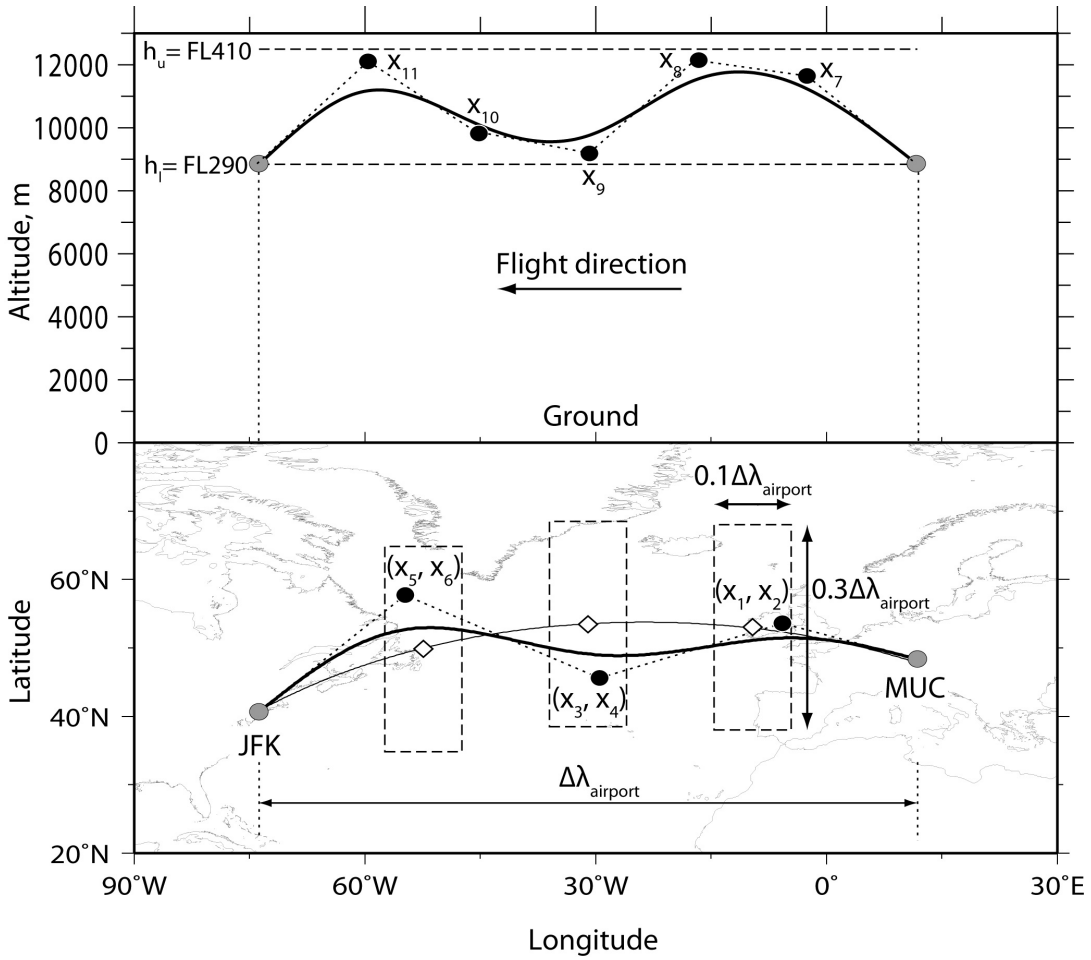

Figure 1 Geometry definition of flight trajectory (bold solid line) on longitude vs altitude (top) and on location (bottom) from MUC to JFK. Control points (closed circle) consist of eleven design variables (x_1, x_2,..., x_{11}). Top: the dashed lines show the lower/upper variable bounds in altitude. Longitude-coordinates for x_7, x_8,..., x_{11} are pre-calculated; the coordinates divide $\Delta\lambda airport$ into six equal parts. Bottom: central points of the rectangular domains (diamond) are calculated on the great circle (thin solid line).

3.2 *Calculation conditions*

Table 1 lists the calculation conditions for the simulation performed for a specific winter day. The weather situation of the day showed a typical weather pattern for winter characterized by a strong jet stream in the North-Atlantic region. We assumed that all flights were operated by A330-301 aircraft with CF6-80E1A2 (2GE051) engines. Altitude changes were considered within the bound [FL290, FL410] (the altitude of the airports was fixed at FL290). The optimization parameters were determined by a benchmark test (Yamashita, et al., in preparation). This simulation was parallelized on 4 PEs of Fujitsu Esprimo P900 (Intel Core i5-2500CPU with 3.30 GHz; 4 GB of memory; peak performance of 105.6 × 4 GFLOPS) at the Institute of Atmospheric Physics, DLR-German Aerospace Center.

Table 1 Calculation conditions for the AirTraf simulation with flight time routing option. The flight plan was provided by the EU FP7 Project REACT4C (REACT4C, 2014).

Parameter	Description/Value
ECHAM5 resolution	T42/L31ECMWF (2.8° by 2.8°)
Duration of simulation	January 1st 1978 00:00:00 - January 2nd 1978 00:00:00 UTC
Time step	12 min
Flight plan	103 trans-Atlantic flights (eastbound 52/westbound 51)
Aircraft type	A330-301
Engine type	CF6-80E1A2, 2GE051 (with 1862M39 combustor)
Flight altitude changes	[FL290, FL410]
Mach number	0.82
Wind effect	Three-dimensional components (u, v, w)
Number of waypoints	101
Load factor	0.62
Optimization	Minimize flight time
Design variable	11 (location 6/altitude 5)
Population size	100
Generation number	100
Selection	Stochastic universal sampling
Crossover	Blend crossover BLX-0.2 ($\alpha = 0.2$)
Mutation	Revised polynomial mutation ($r_m = 0.1$; $\eta_m = 5.0$)

4 RESULTS AND DISCUSSION

To verify the routing methodologies with respect to the flight time routing option, an airport pair was selected for discussion. Table 2 shows the information for the airport pair: Minneapolis (MSP) and Amsterdam (AMS). As indicated in Table 2, the flight time decreased for the eastbound time-optimal flight trajectory compared to that for the westbound flight trajectory.

Figure 2 shows a comparison of the time-optimal flight trajectories and wind fields. The results showed that the eastbound optimal flight trajectory (red line, Fig. 2a) was located to the south of the great circle (black line) to take advantage from the tail winds of the jet stream (red region), while the westbound optimal flight trajectory (blue line, Fig. 2b) was located to the north of the great circle to avoid the head winds (red region). Therefore, the flight time decreased for the eastbound flight, as shown in Table 2.

With regard to the altitude changes, the eastbound optimal flight trajectory was located at FL290, while that for westbound showed large altitude changes, i.e. it climbed, descended and climbed again. The mean flight altitude of these trajectories were h = 8,839 m and h = 10,002 m, respectively (Table 2). To understand the behavior of the altitude changes, Fig. 3 plots the altitude distribution of the true air speed (V_{TAS}) and the tail wind indicator (V_{ground}/V_{TAS}) along the time-optimal flight trajectories. Figure 3c shows that the core tail winds region was located at 8.5 km and the tail winds were most beneficial for the eastbound flight trajectory. On the other hand, the westbound flight trajectory went through the regions where the V_{TAS} was relatively high, as shown in Fig. 3b. In addition, Fig. 3d shows that the middle descent was effective to counteract the head winds. The results confirmed that GA correctly reflects the weather conditions and finds the appropriate flight trajectories corresponding to the flight direction.

To confirm the convergence behavior of the optimizations, Fig. 4 shows the best-of-generation flight time vs the number of objective function evaluations corresponding to the GA runs. The solutions sufficiently converged to each optimal solution. Therefore, GA successfully found the time-

optimal flight trajectories for the airport pair. It is also clear from Fig. 4 that the reduction in computing time can be achieved by sizing the population size and generation number.

Table 2 Information for the flight trajectories between Minneapolis (MSP) and Amsterdam (AMS). Column 6 shows the optimized flight time.

Dep. airport	Arr. airport	Flight direction	Departure time, UTC	Mean flight alt., m	Flight time, s
MSP	AMS	Eastbound	21:35:00	8,839	25,335.6
AMS	MSP	Westbound	12:50:00	10,002	28,869.5

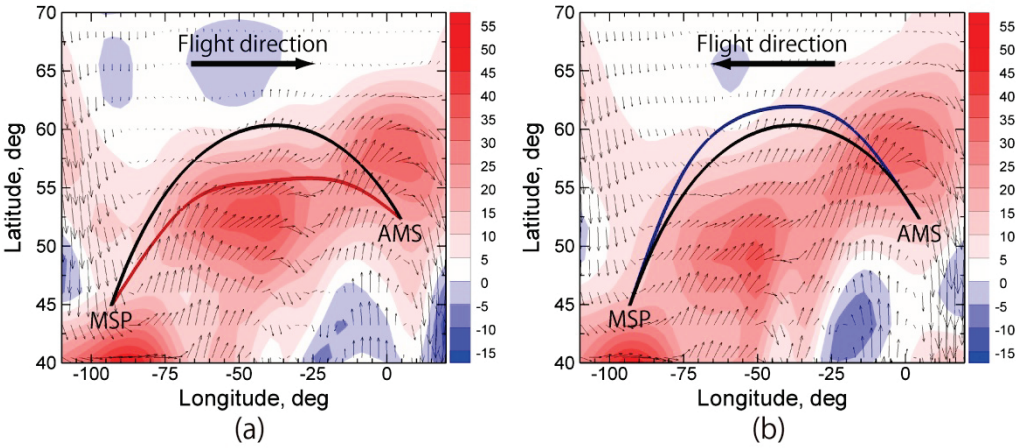

Figure 2 Comparison of trajectories for the time-optimal (red and blue lines) and the great circle cases (black lines) between MSP and AMS. The contours show the zonal wind speed (u) and arrows (black) show the wind speed $(u^2 + v^2)^{1/2}$. (a) The eastbound flight with the wind field at h = 8,839 m at 21:35:00 UTC. (b) The westbound flight with the wind field at h = 10,002 m at 12:50:00 UTC.

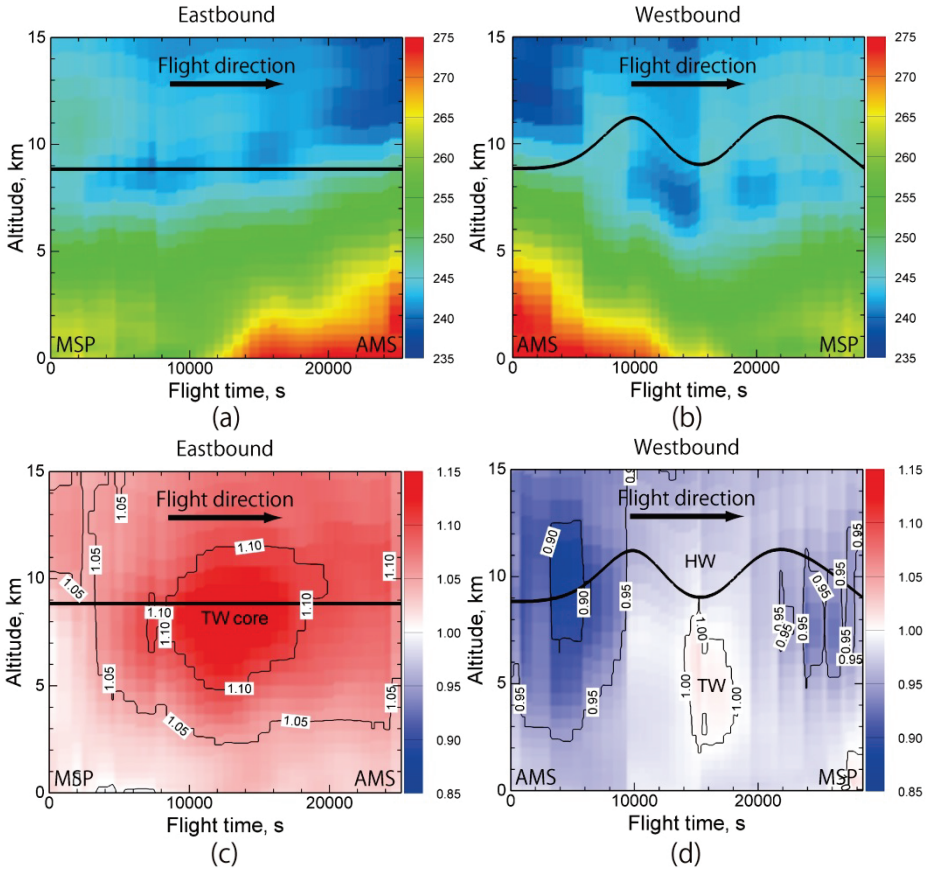

Figure 3 Altitude distributions of the true air speed V_{TAS} (a and b) and the tail wind indicator V_{ground}/V_{TAS} (c and d) along the time-optimal flight trajectories (black line) between MSP and AMS. $(V_{ground}/V_{TAS}) \geq 1.0$ means tail winds (TW, red), while $(V_{ground}/V_{TAS}) < 1.0$ means head winds (HW, blue) to the flight direction. The contours were obtained at the departure time: 21:35:00 UTC (eastbound, a and c); 12:50:00 UTC (westbound, b and d).

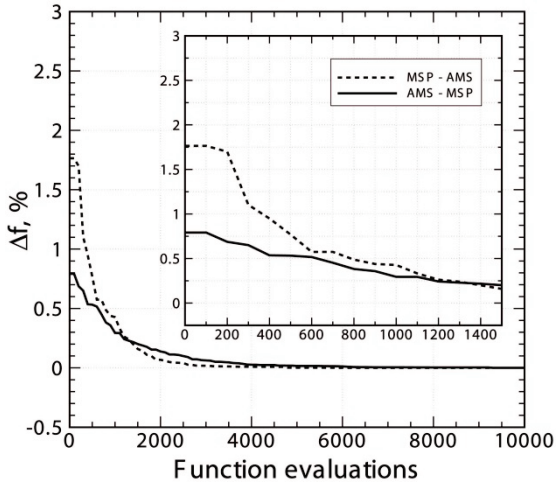

Figure 4 Best-of-generation flight time (in percentage) vs function evaluations (= $np \times ng$), including the enlarged drawing in the early 1,500 evaluations. Population size np = 100 and generation number ng = 100. Δf means the difference in flight time between the solution and the obtained optimal solution (column 6, Table 2).

5 CONCLUSIONS

This paper described the simplified global air traffic submodel AirTraf ver. 1.0 of EMAC. The AirTraf simulation was demonstrated in EMAC (on-line) for a specific winter day by using real trans-Atlantic flight plans of A330-301, and the results for a representative airport pair were discussed. The results confirmed that AirTraf correctly works on-line with respect to the flight time routing option. In addition, we verified that GA successfully found time-optimal flight trajectories considering weather conditions and the solutions sufficiently converged. The fundamental framework of AirTraf has been developed to perform fairly realistic air traffic simulations. To investigate a reduction potential of air traffic climate impacts by aircraft routing, AirTraf is coupled with various submodels of EMAC and objective functions corresponding to other routing options will be integrated.

6 ACKNOWLEDGEMENTS

This work was supported by the DLR Project WeCare. The authors wish to thank Prof. Dr. Shigeru Obayashi of the Institute of Fluid Science, Tohoku University for his invaluable comments on this work. The authors wish to acknowledge our colleagues, especially Prof. Dr. Robert Sausen for his support of this project.

REFERENCES

Deidewig, F., Döpelheuer, A., and Lecht, M.: Methods to assess aircraft engine emissions in flight, ICAS Proceedings, 20, 131–141, 1996.

Eurocontrol: User Manual for the Base of Aircraft Data (BADA) Revision 3.9, EEC Technical/Scientific Report No.12/04/10-45, 2011.

Frömming, C., Ponater, M., Dahlmann, K., Grewe, V., Lee, D., and Sausen, R.: Aviation-induced radiative forcing and surface temperature change in dependency of the emission altitude, Journal of Geophysical Research: Atmospheres (1984–2012), 117, 2012.

Frömming, C., Grewe, V., Jöckel, P., Brinkop, S., Dietmüller, S., Garny, H., Ponater, M., Tsati, E., and Matthes, S.: Climate cost functions as basis for climate optimized flight trajectories: Tenth USA/Europe Air Traffic Management Research and Development Seminar, Chicago, Illinois USA, available at:

http://www.atmseminar.org/seminarContent/seminar10/papers/239-Frömming_0126130830-Final-Paper-4-15-13.pdf (last access: January 2015), 2013.

Grewe, V., Champougny, T., Matthes, S., Frömming, C., Brinkop, S., Søvde, O. A., Irvine, E. A., and Halscheidt, L.: Reduction of the air traffic's contribution to climate change: A REACT4C case study, Atmospheric Environment, 94, 616–625, 2014a.

Grewe, V., Frömming, C., Matthes, S., Brinkop, S., Ponater, M., Dietmüller, S., Jöckel, P., Garny, H., Tsati, E., Dahlmann, K., et al.: Aircraft routing with minimal climate impact: the REACT4C climate cost function modelling approach (V1.0), Geoscientific Model Development, 7, 175–201, 2014b.

ICAO: ICAO Engine Exhaust Emissions Data, Tech. rep., Doc 9646-AN/943 (Issue 18 is used for this study), 2005.

Jöckel, P., Kerkweg, A., Pozzer, A., Sander, R., Tost, H., Riede, H., Baumgaertner, A., Gromov, S., and Kern, B.: Development cycle 2 of the modular earth submodel system (MESSy2), Geoscientific Model Development, 3, 717–752, 2010.

Lee, D., Pitari, G., Grewe, V., Gierens, K., Penner, J., Petzold, A., Prather, M., Schumann, U., Bais, A., Berntsen, T., et al.: Transport impacts on atmosphere and climate: Aviation, Atmospheric Environment, 44, 4678–4734, 2010.

Matthes, S., Schumann, U., Grewe, V., Frömming, C., Dahlmann, K., Koch, A., and Mannstein, H.: Climate optimized air transport, in Atmospheric physics, 727–746, Springer, 2012.

REACT4C: EU FP7 Project: Reducing Emissions from Aviation by Changing Trajectories for the benefit of Climate, http://www.react4c.eu, (last access: January 2015), 2014.

Sasaki, D. and Obayashi, S.: Development of efficient multi-objective evolutionary algorithms: ARMOGAs (adaptive range multi-objective genetic algorithms), Tech. rep., Institute of Fluid Science, Tohoku University, 2004.

Sasaki, D. and Obayashi, S.: Efficient search for trade-offs by adaptive range multi-objective genetic algorithms, Journal of Aerospace Computing, Information, and Communication, 2, 44–64, 2005.

Sasaki, D., Obayashi, S., and Nakahashi, K.: Navier-Stokes optimization of supersonic wings with four objectives using evolutionary algorithm, Journal of Aircraft, 39, 621–629, 2002.

Schaefer, M.: Development of forecast model for global air traffic emissions, Ph.D. thesis, DLR, 2012.

Søvde, O. A., Matthes, S., Skowron, A., Iachetti, D., Lim, L., Owen, B., Hodnebrog, Ø., Di Genova, G., Pitari, G., Lee, D. S., et al.: Aircraft emission mitigation by changing route altitude: A multi-model estimate of aircraft NOx emission impact on O3 photochemistry, Atmospheric Environment, 95, 468–479, 2014.

Yamashita, H., Grewe, V., Jöckel, P., Linke, F., Schaefer, M., and Sasaki, D.: Towards climate optimized flight trajectories in a climate model: AirTraf, available at: http://www.atmseminar.org/seminarContent/seminar11/papers/433-yamashita_0126151229-Final-Paper-5-6-15.pdf (last access: July 2015), 2015.

Yamashita, H., Grewe, V., Jöckel, P., Linke, F., Schaefer, M., and Sasaki, D.: Climate assessment platform of different aircraft routing strategies in the chemistry-climate model EMAC 2.41: AirTraf 1.0 (in preparation for Geosci. Model Dev.).

The impact of shipping on air pollution in North Sea coastal areas – situation today and in the future

V. Matthias*, A. Aulinger, J. Bieser, M. Quante
Helmholtz-Zentrum Geesthacht, Institute for Coastal Research, Geesthacht, Germany

Keywords: Shipping emissions, North Sea, chemistry transport modelling

ABSTRACT: Ships emit large amounts of pollutants, in particular in North Sea coastal areas, where Europe's biggest harbours are located. Based on AIS ship movement data, a vessel characteristics data base and load dependent emission factors for NO_x, SO_x and particulate matter, a ship emission inventory was created for the North Sea region. The impact of shipping on air pollution in North Sea coastal areas was calculated with the chemistry transport model system CMAQ. It was found that shipping on average contributes about 20-30% to the concentrations of NO_2 and nitrate aerosols and 2-3% to ozone concentrations in large parts of the central European coasts. Because shipping activities will increase in the future and stricter regulations for the emission of nitrogen oxides have not been agreed on, yet, this share of shipping in the concentration of harmful air pollutants is likely to increase further. Scenarios for shipping emissions in 2030 show an increase of nitrogen oxide emissions of more than 20% along the main shipping lanes for the case that no emission reduction measures are taken. This is reflected in an increase of NO_2 and nitrate aerosol concentration changes. However, if much stricter rules for NO_x emissions from ships, the so called TIER III rules, will be applied in 2016 or 2021, the latest, the contribution of shipping to air pollution in 2030 will stay at a similar level as today. On the other hand if all ships reduce their NO_x emissions by 70-80% and follow TIER III standards, significant reductions of oxidized nitrogen compounds in the atmosphere can be expected.

1 INTRODUCTION

Shipping is the backbone of the global trade. Because of the ongoing global energy demand and the share of labour in a globalized world, the volume of transported goods increased steadily with growth rates of 2-3 % p.a. since the mid of the 1980s. This tendency is likely to continue in the next decades unless major changes in the global economy will be seen.

As a consequence, emissions of sulphur oxides (SO_x), nitrogen oxides (NO_x), carbon monoxide (CO), hydrocarbons (HC) and particulate matter (PM) from ships become more and more important for air pollution in coastal areas. SO_x have been regulated in the North Sea since 2007, when this area was designated as a sulphur emission control area (SECA). Since then, the allowed sulphur content in ship fuels was decreased from on average 2.7% before 2007 to 0.1% since 1 January 2015. The situation is different for nitrogen oxides. These are also regulated on a global basis for ships with allowed emission rates that depend on the age of the ship. However, these limits are not very strict which has led to a situation in which ships contribute significantly to enhanced NO_2, nitrate aerosol (NO_3^-) and O_3 concentrations in coastal areas (Matthias et al., 2010, Aulinger et al., 2015, Jonson et al., 2015).

In this paper, we present four different scenarios of shipping emissions for the year 2030. They all rely on the same development of the transported volume of goods in the North Sea region, but they differ in the amount of nitrogen oxides that are emitted by ships. The consequences of the emission scenarios on concentrations of the air pollutants NO_2, NO_3^- and O_3 have been investigated by means of a complex 3-dimensional atmospheric chemistry transport model system. This includes different dates for the implementation of strict NO_x emission limits, the so-called TIER III rules. These rules imply that ships reduce their specific NO_x emissions from 14.4 g/kWh (TIER II limits for ships built after 1 January 2011) to 3.5 g/kWh.

* *Corresponding author:* Volker Matthias, Helmholtz-Zentrum Geesthacht, Institute for Coastal Research, Max-Planck-Straße 1, 21502 Geesthacht, Germany. Email: volker.matthias@hzg.de

2 MODEL SYSTEM

The CMAQ model was used in its version 4.7.1 with the CB05 chemistry mechanism (Byun and Ching, 1999; Byun and Schere, 2006). It was run for an entire year with a spin up time of 2 weeks and a data output time step of one hour. Boundary conditions for the model were from the TM5 global chemistry transport model system (Huijnen et al., 2010). The meteorological fields that drive the chemistry transport model were produced with the COSMO-CLM mesoscale meteorological model for the year 2008 (Rockel et al., 2008). This year was chosen because it did not include very unusual meteorological conditions in central Europe and can therefore be considered to represent average weather conditions in Europe.

The model was setup on a 72 x 72 km^2 grid for entire Europe and subsequently on a nested 24 x 24 km^2 grid for the North and Baltic Seas. The vertical model extent contains 30 layers up to 100 hPa in a sigma hybrid pressure coordinate system. Twenty of these layers are below approx. 2km, the lowest layer extends to ca. 36m above ground. For the study presented, only the simulation results of the innermost nest were evaluated.

3 EMISSIONS

3.1 *Shipping emissions*

Shipping emissions for the North Sea were constructed from a collection of AIS (Automatic Identification System) position data of ships in the North Sea region in 2011. From this, ship movements, ship velocities and, in combination with a vessel characteristics data base, fuel use and emissions of other pollutants could be calculated for all ships sailing in the North Sea region. Emission factors for NO_x, CO, HC and PM are engine load dependent. They are based on test bed measurements performed by Germanischer Lloyd and evaluated by Zeretzke (2013). In combination, ship emission maps with hourly resolution were constructed and fed into CMAQ.

3.2 *Land based emissions*

The model runs were performed with full emissions from all relevant sources in the model domain. Land based emissions in hourly temporal resolution were produced with SMOKE for Europe (Bieser et al., 2011). They are based on officially reported EMEP emissions which are distributed in time and space using appropriate surrogates like population density, street maps or land use. Point sources were considered as far as information from the European point source emission register was available. The vertical distribution of the emissions was calculated online with the SMOKE for Europe model, the results are given in Bieser (2011a).

4 SCENARIOS

Four scenarios for future shipping emissions were constructed. They are related to the year 2030 and they are all based on the same fleet development. This development considers an increase in transport volume of 2.7% p.a. which is mainly due to bigger ships and to a lesser extent by additional ships. A fleet renewal with a replacement of the oldest ships with high NO_x emissions by new ones with lower NO_x emissions that follow at least Tier II rules is also taken into account.
The scenarios were built along two axis, regulation and technology. Regulation included the implementation of strict or less strict rules for NO_x emissions while technologies considered selective catalytic reduction (SCR) to reduce NO_x emission and liquefied natural gas (LNG) as alternative fuel. Here, only the regulation scenarios are presented:

- No ECA: no further regulations concerning NO_x emissions are implemented until 2030
- ECA SCR 21: TIER III rules for NO_x emissions are valid for new builts from 2021 onwards
- ECA SCR 16: TIER III rules for NO_x emissions are valid for new builts from 2016 onwards
- ECA opt: TIER III rules for NO_x emissions are valid for all ships in 2030

5 RESULTS

5.1 *Emission changes in 2030*

In Fig. 1a NO_x emissions from ships on the North Sea in the year 2011 are shown together with the relative changes in shipping emissions that will happen until 2030 in the four scenarios described above (1b-1e). In the No ECA case NO_x emissions will increase by more than 20% in large areas of the southern North Sea and the English Channel. ECA SCR 21 shows only a small increase in shipping emissions, the ECA SCR 16 scenario reveals a slight decrease compared to today. A clear decrease in NO_x emissions from ships can only be seen in the ECA opt scenario, when all ships follow strict NO_x regulations.

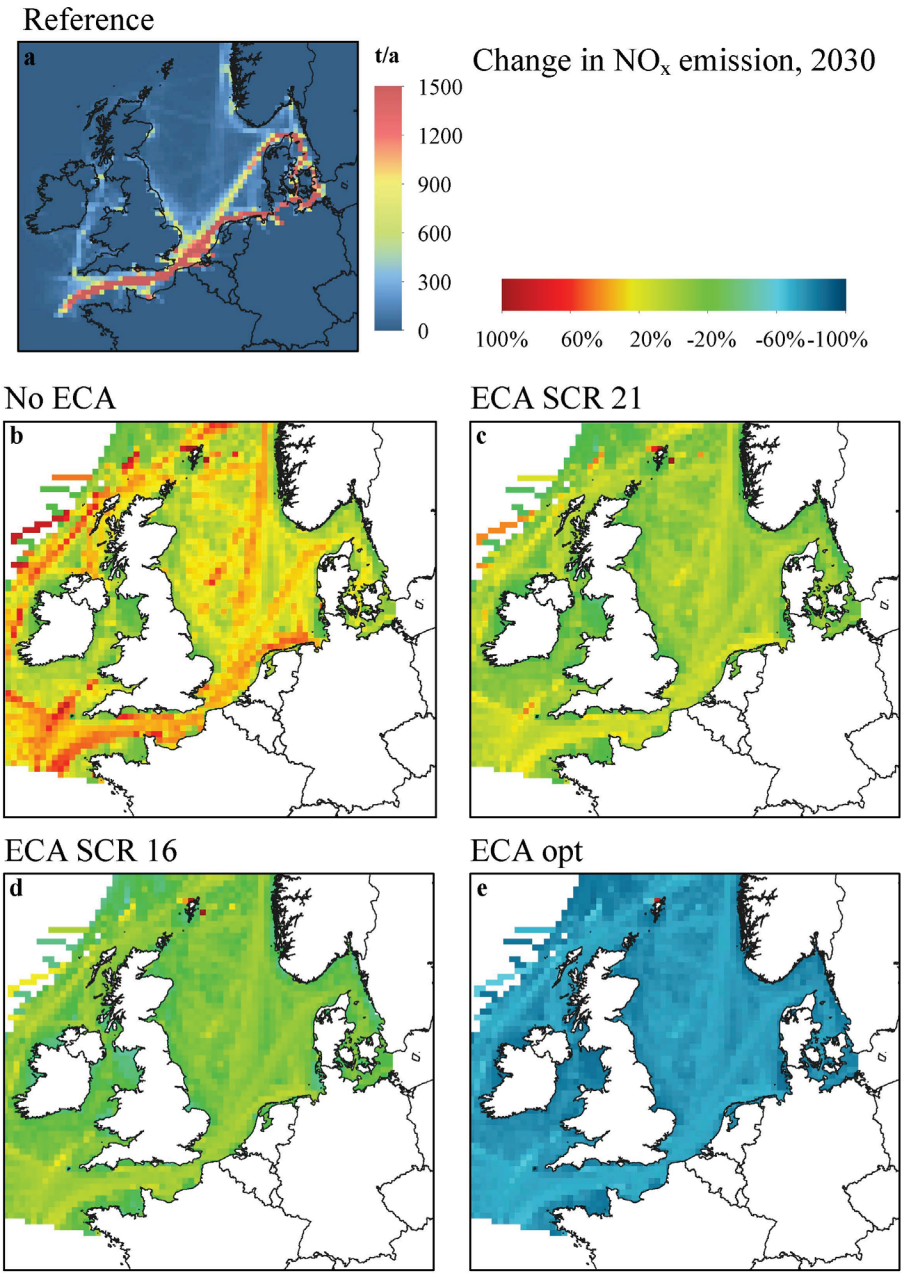

Figure 1: NO_x emissions from shipping in 2011 (a) and relative changes in the scenarios No ECA (b), ECA SCR 21 (c), ECA SCR 16 (d) and ECA opt (e).

5.2 *Situation today*

As a reference, a model simulation for shipping emissions in the year 2011 was performed. All scenario runs are compared to this case and the changes in 2030 are given in relation to the situation in 2011. The contribution of shipping to air pollution is calculated as increase in the concentrations of NO_2, NO_3^- and O_3. These values are given as a reference in Figures 2-4.

5.3 *NO_2 concentration changes in 2030*

Changes in NO_x emissions from ships have a clear impact on the NO_2 concentration levels in the North Sea region. Here, average concentrations in the summer months June, July and August (JJA) are given. While in the No ECA scenario the contribution of ships to the NO_2 concentrations will increase by about 20-30% in large areas around the southern North Sea, only small changes can be seen in the ECA SCR 16 and ECA SCR 21 scenarios (see Fig. 2). In the ECA opt case, significant reductions of more than 50% in the contribution of ships to the NO_2 concentrations are visible.

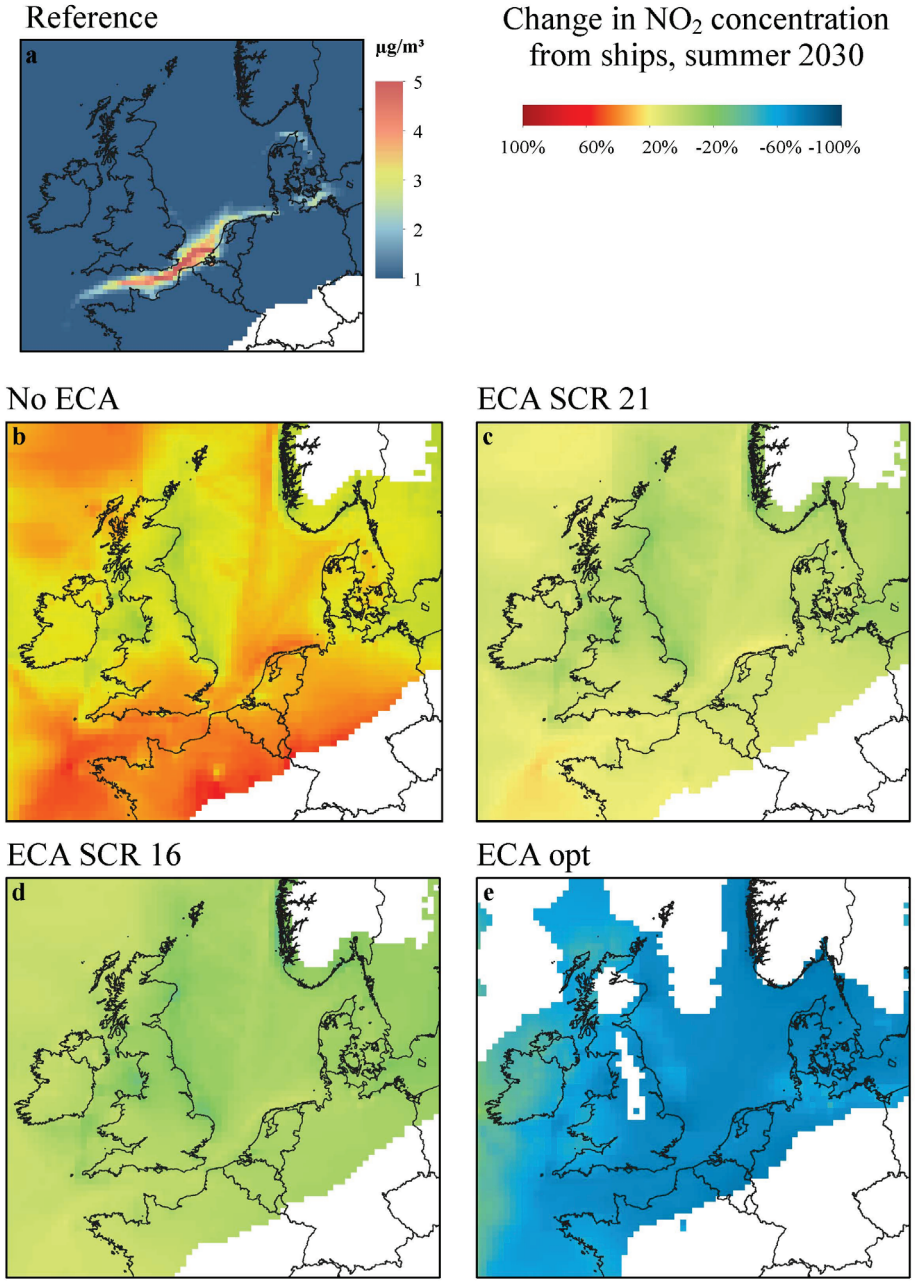

Figure 2: NO_2 concentration increase caused by emissions from shipping in summer 2008 (a) and relative changes to these concentrations in the scenarios No ECA (b), ECA SCR 21 (c), ECA SCR 16 (d) and ECA opt (e).

5.4 *Nitrate aerosol concentrations changes in 2030*

Nitrate aerosols are formed in the atmosphere if sufficient gaseous ammonia is available. Aerosol bound nitrate is not very reactive and can be transported over larger distances compared to gaseous NO_2. Figure 3 shows the concentration changes in the summer months of the year 2030 for the different scenarios and the references case with emissions of the year 2011. The picture is not as clear as for NO_2 because nitrate aerosol concentrations can be very small in summer. Nevertheless, the

general picture is similar to the one for NO_2. The results range from about 30% increase in nitrate aerosol concentrations caused by shipping emissions in the No ECA case to about 50% decrease in the ECA opt scenario.

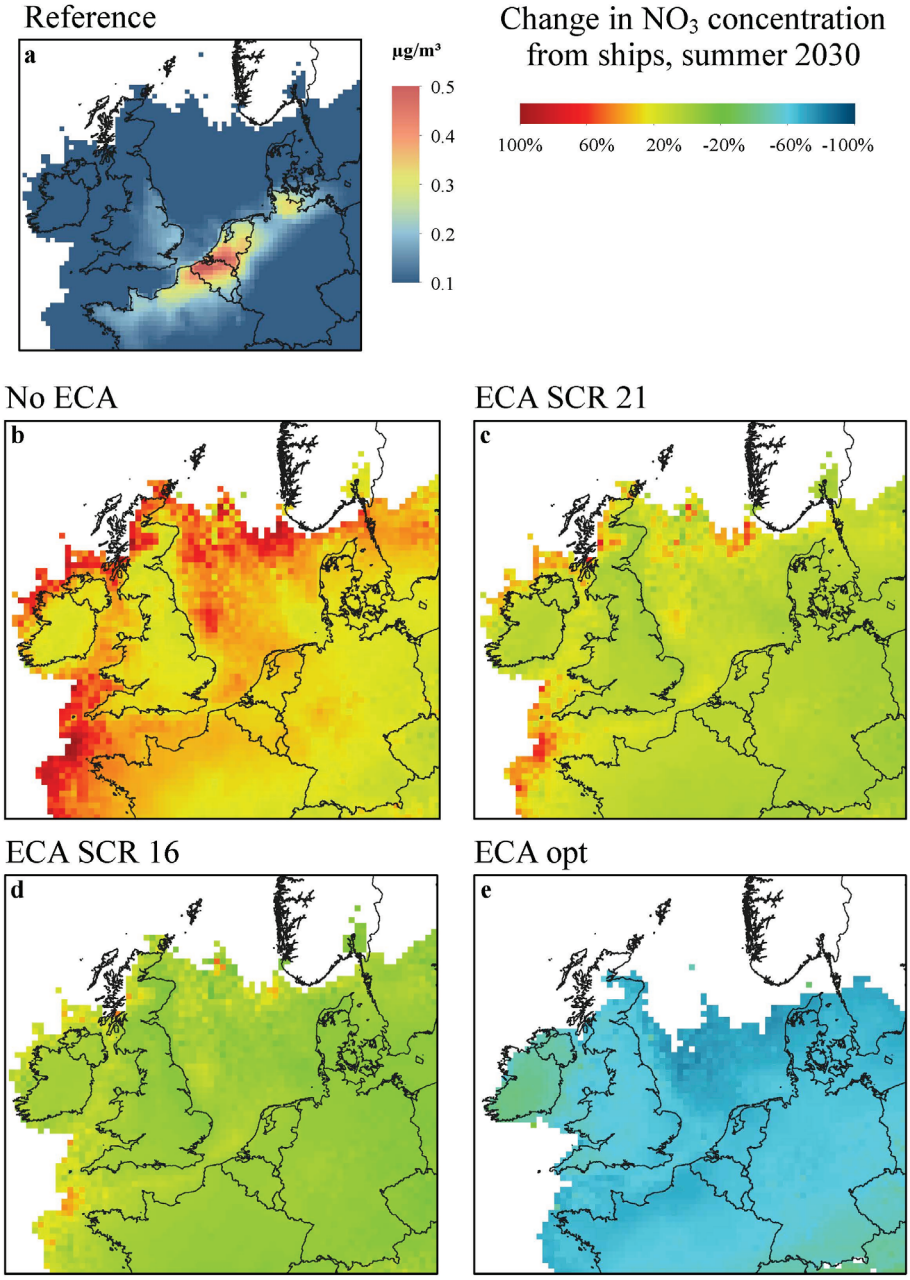

Figure 3: NO_3^- concentration increase caused by emissions from shipping in summer 2008 (a) and relative changes to these concentrations in the scenarios No ECA (b), ECA SCR 21 (c), ECA SCR 16 (d) and ECA opt (e).

5.5 *Ozone concentration changes in 2030*

The effects of NO_x emission changes on ozone concentrations are not as clear as those on NO_2 and nitrate aerosol concentrations. Depending on the availability of volatile organic compounds (VOCs), additional NO emissions can lead to both, enhanced ozone concentrations or decreased ozone concentrations. This can be seen in Figure 4, which again shows the results for the summer months. In the English Channel NO_x emissions are highest and additional NO_x from shipping leads to ozone titration and therefore reduced concentrations. On the other hand, in most other areas NO_x emissions from shipping contribute to enhanced ozone concentrations in the order of 5-10% in the No ECA case. The picture is the other way round in the ECA opt scenario. Here, ozone concentrations increase in the English Channel if NO_x emissions are reduced, while they decrease in all other areas.

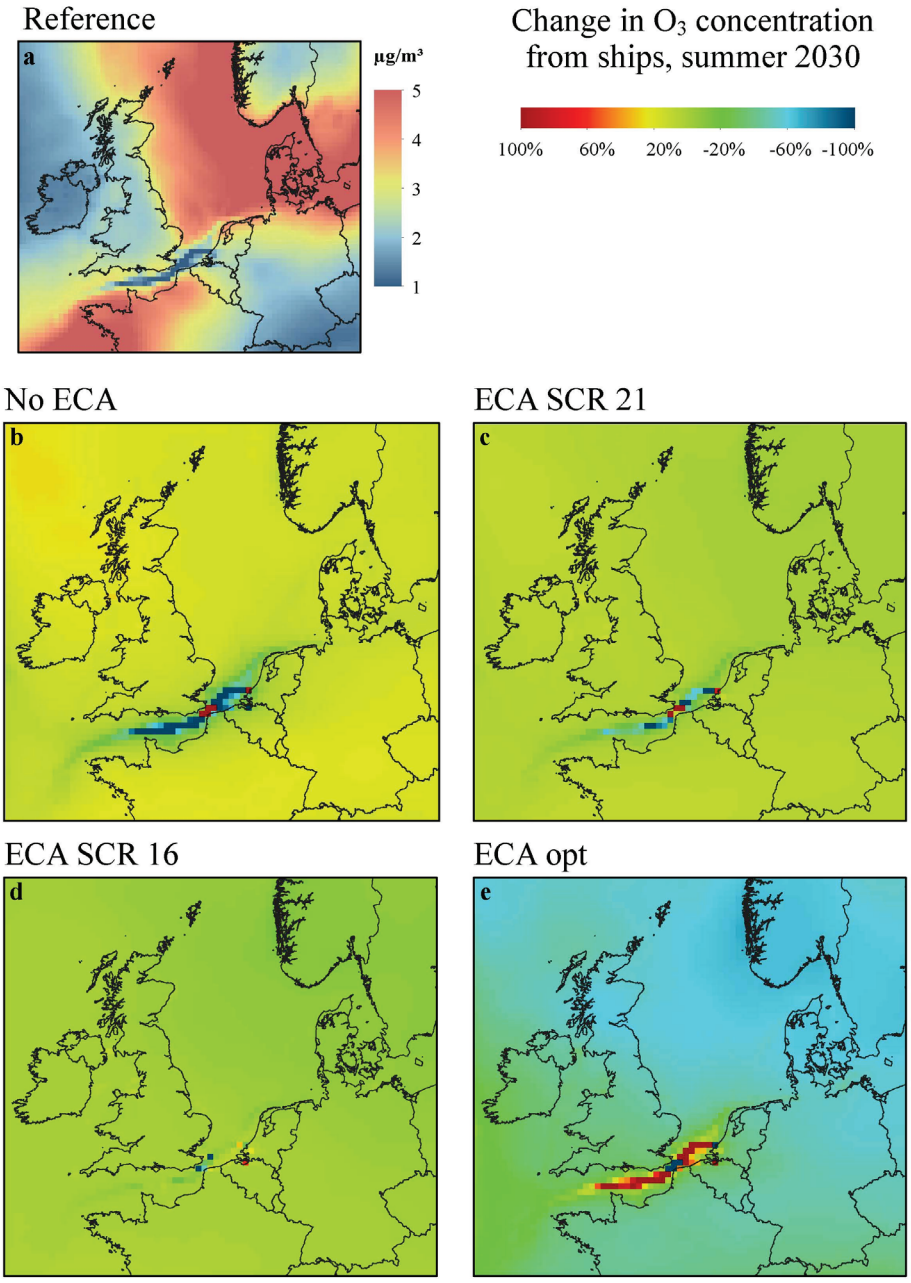

Figure 4: O_3 concentration difference caused by emissions from shipping in summer 2008 (a) and relative changes to these concentration differences in the scenarios No ECA (b), ECA SCR 21 (c), ECA SCR 16 (d) and ECA opt (e).

6 SUMMARY AND DISCUSSION

Shipping contributes significantly to air pollution in North Sea coastal areas. While SO_2 emissions from ships were drastically reduced in recent years, NO_x emissions remain high and are likely to increase further in the future. This is caused by an increase in shipping activities in the North Sea which go along with globalization and steadily increasing transport demands. Four scenarios for different NO_x regulations, ranging from no further regulation compared to 2011 to large emission reductions for all ships, were tested with respect to their impact on NO_2, nitrate aerosol and ozone concentrations in the greater North Sea area.

It was found that the contribution of shipping to NO_2 and nitrate aerosol will increase by 20-30% in large areas of the southern North Sea and its surrounding countries, if no further regulations will be put in place. Regulations that require TIER III limits for new builts from 2016 or 2021 onwards will lead an almost equal contribution of shipping to NO_2 and nitrate aerosol concentrations com-

pared to 2011. This means that the emission reduction from new ships will be compensated by increasing ship activities. Only the scenario in which TIER III limits apply to all ships shows a significant reduction of NO_2 and nitrate aerosol concentrations.

For ozone, the situation is more complex. NO_x emission reductions lead to a small decrease of ozone production, except in areas where NO_x emissions are high. Here titration effects lead to ozone destruction. This can be seen in the English Channel.

The effects of shipping on air pollutants like NO_2, nitrate aerosol and ozone have always to be seen in connection with pollutants from other sources. There are significant interactions between pollutants from different sources which have an impact on the contribution of one single source to the total concentration. NO_x and O_3 form a permanent cycle that is influenced by the availability of VOC, CO, methane and other pollutants and that depends heavily on meteorological conditions. The prevalence of nitrate aerosol also depends on temperature and the occurrence of ammonia which is not yet bound to sulfuric acid to form ammonium sulphate aerosol. By this, sulphur emission reductions have indirect effects on nitrate aerosol formation.

In this study, land based emissions were kept constant for the scenarios for 2030. This is not very likely but it was assumed in order to separate the effects of changing emissions from ships from other effects of emission changes. If land based emissions decrease further, the impact of shipping on NO_2 and nitrate aerosol concentrations is likely to be higher than shown here.

REFERENCES

Aulinger, A.; Matthias, V.; Zeretzke, M.; Geyer, B.; Bieser, J., and Quante, M., 2015: The impact of shipping emissions on air pollution in the Greater North Sea region. Part I: Current emissions and concentrations, Atmos. Chem. Phys. Discuss. 15, 11277 - 11323.

Bieser, J.; Aulinger, A.; Matthias, V.; Quante, M., and Builtjes, P., 2011: SMOKE for Europe - adaptation, modification and evaluation of a comprehensive emission model for Europe, Geoscientific Model Development 4(1), 47 - 68.

Bieser, J.; Aulinger, A.; Matthias, V.; Quante, M., and Denier van der Gon, H. A. C., 2011: Vertical emission profiles for Europe based on plume rise calculations, Environmental Pollution 159(10), 2935 - 2946.

Byun, D., and Ching, J., 1999: Science Algorithms of the EPA Models-3 Community Multiscale Air Quality Modeling System, Technical report, US Environmental Protection Agency, Office of Research and Development, Washington DC.

Byun, D., and Schere, K., 2006: Review of the Governing Equations, Computational Algorithms, and Other Components of the Models-3 Community Multiscale Air Quality (CMAQ) Modeling System, Applied Mechanics Reviews 59, 51 - 77.

Huijnen, V.; Williams, J. E.; van Weele, M.; van Noije, T. P. C.; Krol, M. C.; Dentener, F.; Segers, a.; Houweling, S.; Peters, W.; de Laat, a. T. J.; Boersma, K. F.; Bergamaschi, P.; van Velthoven, P. F. J.; Le Sager, P.; Eskes, H. J.; Alkemade, F.; Scheele, M. P.; Nédélec, P., and Pätz, H.-W., 2010: The global chemistry transport model TM5: description and evaluation of the tropospheric chemistry version 3.0, Geoscientific Model Development 3(2), 445 - 473.

Jonson, J. E.; Jalkanen, J. P.; Johansson, L.; Gauss, M., and Denier van der Gon, H. A. C., 2015: Model calculations of the effects of present and future emissions of air pollutants from shipping in the Baltic Sea and the North Sea, Atmospheric Chemistry and Physics 15(2), 783 - 798.

Matthias, V.; Bewersdorff, I.; Aulinger, A., and Quante, M., 2010: The contribution of ship emissions to air pollution in the North Sea regions, Environmental Pollution 158(6), 2241 - 2250.

Rockel, B.; Will, A., and Hense, A., 2008: The Regional Climate Model COSMO-CLM(CCLM), Meteorologische Zeitschrift 17(4), 347 - 348.

Zeretzke, M. Entwicklung eines Modells zur Quantifizierung von Luftschadstoffen, die durch Schiffsdieselmotoren auf See emittiert werden, Master's thesis, Technische Universität Hamburg-Harburg, 2013.

The global impact of the transport sector on atmospheric aerosol and climate in the Representative Concentration Pathways

M. Righi*, J. Hendricks, R. Sausen
DLR-Institut für Physik der Atmosphäre Oberpfaffenhofen, Germany

Keywords: aerosol, land transport, shipping, aviation, future scenarios, global modelling.

ABSTRACT: Using the EMAC global climate-chemistry model coupled to the aerosol module MADE, we simulate the impact of land transport, shipping and aviation emissions on global atmospheric aerosol and climate in 2030. Future emissions of short-lived gas and aerosol species follow the four Representative Concentration Pathways (RCPs) designed in support of the IPCC AR5. We compare the resulting 2030 transport-induced aerosol concentrations to the ones obtained for the year 2000 in a previous study with the same model configuration. The simulations suggest that black carbon (BC) and aerosol nitrate are the most relevant pollutants from land transport in 2000 and 2030 and their impacts are characterized by very strong regional variations during this time period. Europe and North America experience a decrease in the land-transport-induced particle pollution, although in these regions this sector remains a major source of surface-level pollution in 2030 under all RCPs. In Southeast Asia, however, a significant increase is simulated, but in this region the surface-level pollution is still controlled by other sources than land transport. Shipping-induced air pollution is mostly due to aerosol sulfate and nitrate, which show opposite trends towards 2030. Sulfate is strongly reduced as a consequence of sulfur reduction policies in ship fuels in force since 2010, while nitrate tends to increase due to the excess of ammonia following the reduction in ammonium sulfate. The continuous growth in air traffic in the future leads to increasing impacts in all scenarios, affecting BC and sulfate concentrations in the northern mid-latitudes at cruise level with some effects also close to the surface. The aerosol-induced climate impact of the transport sectors is dominated by aerosol-cloud effects and, with the exception of aviation, is projected to decrease between 2000 and 2030, nevertheless still contributing a significant radiative forcing to Earth's radiation budget.

1 INTRODUCTION

The emissions from transport are growing faster than those from the other anthropogenic sectors. According to several scenarios, this growth is projected to continue in the future, due to increases in world population, economic activities and related mobility (Uherek et al., 2010; Eyring et al., 2010; Lee et al., 2010). The transport sectors have a substantial impact on climate which goes beyond the well-known CO_2 effect, and includes a wide range of other effects like ozone formation and methane destruction via NO_x emissions, direct and indirect aerosol effects from sulfate and BC, and, in the case of aviation, the formation of contrail and contrail-cirrus clouds, as well as the perturbation of natural cirrus clouds due to BC.

This work represents the follow-up of the study by Righi et al. (2013, hereafter R13, presented at TAC-3), where we quantified the transport effects on aerosol and climate in the year 2000. Here, we focus on the year 2030 in the four RCPs (Moss et al., 2010), the scenarios developed in support of the IPCC AR5. As in the companion paper, we perform numerical simulation with the EMAC-MADE global aerosol model, which is able to track both aerosol mass and number perturbations, and to simulate the aerosol-cloud and aerosol-radiation interactions, hence allowing the estimation of aerosol radiative forcing effects.

* *Corresponding author:* Mattia Righi, DLR-Institut für Physik der Atmosphäre, Oberpfaffenhofen, D-82205 Wessling, Germany. Email: mattia.righi@dlr.de

2 AEROSOL AND AEROSOL-PRECURSORS EMISSIONS IN THE RCPS

The RCPs provide future projections of the emissions of short-lived species until 2100. The emissions of air pollutants in these scenarios are estimated considering changes in driving forces (fossil fuel and fertilizer consumption) and including both air quality control policies and climate policies. The four RCPs were established based on the projected global anthropogenic radiative forcing (RF) in 2100, spanning the whole range of possible climate policies, from the low RCP2.6 to the no-climate-policy high RCP8.5 scenario. It is important to note that they do not cover the full range of air pollution projections available in the literature and do not include, for instance, a business-as-usual scenario. All RCPs assume a correlation between growing economy (in terms of gross domestic product, GDP) and more stringent air pollution control strategies and mitigation measures. As a consequence, they are all characterized by a globally declining trend of air polluting emissions, which is not fully representative of the literature on air quality projections. This has to be considered when interpreting the results of the present work.

3 IMPACTS ON AEROSOL SURFACE-LEVEL CONCENTRATIONS

The impact of each sector is estimated here as the difference between a reference simulation including all sources and a perturbation experiment, in which the emission from the given sector are switched off. This method is applied for each transport sector to each RCP in the year 2030, and the results are compared to the same estimates obtained for the year 2000 in the companion study (R13).

As in 2000, BC and aerosol nitrate are the most relevant pollutants from land transport. The general tendency in the land transport impacts between 2000 and 2030 is a decrease in aerosol surface-level concentrations over the developed countries (USA, European countries and Japan) and an increase in the countries with fast-growing economies (in Southeast Asia). This applies to the total concentrations as well as to the land-transport-induced concentrations. Such decreasing concentration in the developed countries is a common feature in all RCPs, but there are some exceptions. Most importantly, the changes in the aerosol concentrations are different from what could be expected from the RCP rankings: scenarios with the most stringent climate policies and with the strongest long-term reductions in global climate effects (like RCP2.6) show sometimes an opposite behavior in terms of short-lived pollutants from specific sectors and regions. According to our simulations, the largest reductions of the land transport impact on BC surface-level concentration (Fig. 1) are simulated for Europe, in particular for RCP8.5, with local reductions of up to 1 $\mu g/m^3$. Significant reductions (0.1–0.5 $\mu g/m^3$) are also found for the USA, Japan and some large metropolitan areas (especially in South America). This result is not surprising, in view of the findings of R13 for the year 2000, in which land transport was responsible for the bulk of BC surface-level pollution in these regions (up to about 70%). Air pollution control policies in such regions must necessarily address the land transport sector in order to reduce pollution. Compared with the changes in other sources (right column of Fig. 1), it is clear that land transport drives a major portion of the reduction trend in the developed countries in 2030 in all scenarios.

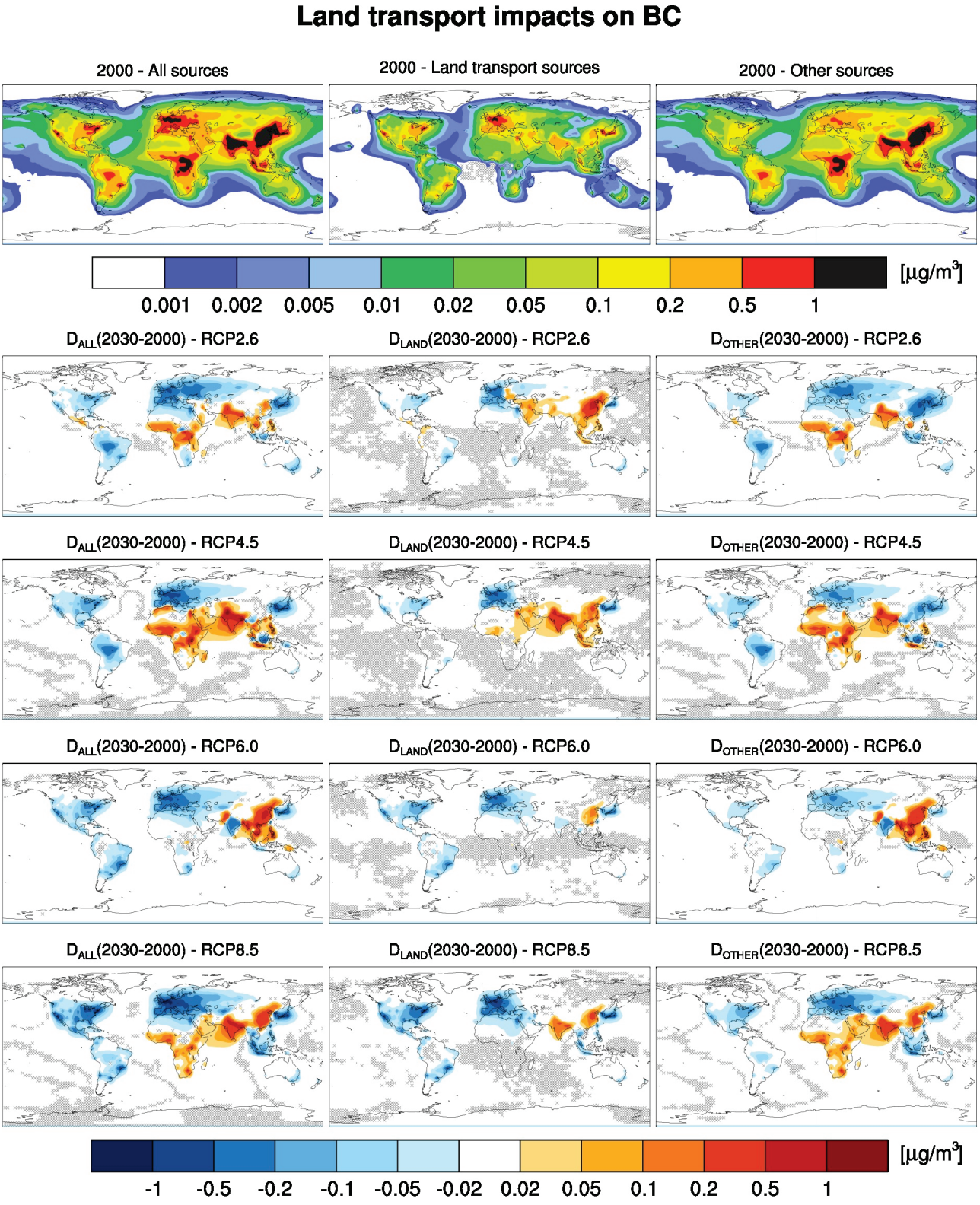

Figure 1. Annual average large-scale mean surface-level concentrations of BC. The first row shows the values for 2000: total concentration (left), the concentration induced by land transport (middle) and the concentration induced by other sources (right). The other rows show the changes in the same quantities between 2000 and 2030 for the four RCPs. Grid points where the difference is not statistically significant according to a univariate t test (5% error probability) are hatched.

Concerning shipping, the simulated pattern of changes shows a clear decrease in shipping induced sulfate, mostly confined to the Northern Hemisphere. This was expected given the recently-implemented limits on shipping fuel sulfur content since 2010. Such regulations are accounted for in the RCPs. Total sulfate is projected to decrease quite strongly in the continental regions and in

the coastal areas (with the exception of southern Asia, southern Africa and South America) in all scenarios, but the contribution of shipping to this trend is only marginal, around 0.5 μg/m^3, whereas the concentration induced by other sources decreases by several micrograms per cubic meter. The shipping impacts on sulfate pollution are strongly correlated with aerosol nitrate effects, given that both compounds are formed depending on the availability of ammonia. The strong reduction in sulfate makes such the competition between sulfate and nitrate for available ammonia particularly relevant for shipping. A lower concentration of SO_2 in the marine boundary layer makes more ammonia available for the formation of ammonium nitrate and therefore results in an increase of the aerosol nitrate concentration.

As reported for the year 2000, the contribution of the aviation sector to the mass concentration changes remains small in 2030. The only remarkable feature is the increase in aviation-induced BC concentration for RCP2.6. This leads to an increase in the overall BC concentration in the tropopause region of the Northern Hemisphere, which would be otherwise characterized by a decrease (right panel). In the other scenarios, aviation-induced BC shows a similar pattern, but relevant changes are found only in the upper-troposphere. The increase in mean aviation-induced particle number concentration (Fig. 3), on the contrary, is quite strong in all scenarios, with values of the order of 1000 cm^{-3} in the northern mid-latitudes UTLS. In this domain, the aviation emissions significantly contribute to the overall changes in particle number concentration between 2000 and 2030, leading to a large increase (1000–3000 cm^{-3}), in particular for RCP2.6 and RCP8.5.

4 CLIMATE EFFECTS

We quantify the aerosol-induced impacts on Earth's radiation budget due to transport emissions by considering the changes in the radiative fluxes at the top of the atmosphere. We analyze the all-sky radiative flux (considering both cloudy and clear-sky conditions) as well as the clear-sky flux only, the latter being derived from radiative flux calculations neglecting the effects of clouds. By comparing the two fluxes one can infer the importance of clouds and cloud modifications for the radiation budged. Based on the uncertainty analysis of R13, we present a range of values for the transport-induced RF, corresponding to different assumptions on the size distributions of the emitted particles

The land-transport-induced aerosol RF (Fig. 2, left panel) shows a reduction of the cooling effect from –80 mW/m^2 in 2000 to about –60 mW/m^2 in 2030. The difference between the all-sky and the clear-sky components reveals that the bulk of the RF impact is due to cloud effect, therefore it is mostly controlled by changes in particle number concentration in the activated size range (around 0.1 to 1 μm). The absolute land-transport-induced change in particle number burden in this size range is quite similar among the scenarios (about $2–3 \cdot 10^{24}$ particles on average), which explains the small differences in 2030 RF among the four RCPs for the land transport sector.

The shipping impacts (Fig. 2, middle panel) are characterized by a strong decrease of the aerosol-induced RF in RCP2.6, dropping from –181 mW/m^2 in 2000 to –53 mW/m^2 in 2030 as a consequence of the aforementioned fuel sulfur control measures for the shipping sector, which significantly affect the sulfate burden. This factor of 3–4 reduction in aerosol forcing is in good agreement with the results of Righi et al. (2011) for future low-sulfur shipping scenarios. Smaller reductions are projected for the other scenarios, consistent with the corresponding changes in tropospheric sulfate burdens. The uncertainty range due to the assumed size distribution of emitted particles is relatively small for the shipping sector, as discussed in R13.

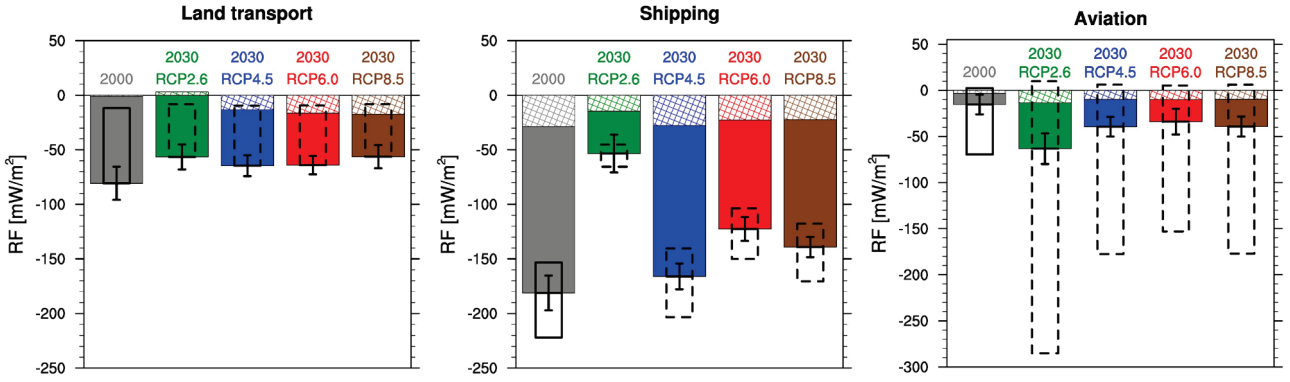

Figure 2. Global mean all-sky RF resulting from the emissions of land transport (left), shipping (middle) and aviation (right) in the year 2000 (gray bars) and for the four RCP scenarios in 2030 (colored bars). The hatched part of each bar is the corresponding clear-sky forcing, calculated neglecting the effects of clouds. The whiskers represent the 95% confidence interval. The boxes correspond to the uncertainty range derived from the assumptions on the size distribution of emitted particles, as calculated by R13 for year 2000 (solid) and rescaled here to the 2030 values (dashed).

Aviation is the only transport sector for which an increasing impact of aerosol on the radiation budget is simulated. RCP2.6 is the scenario with the largest increase, shifting the all-sky forcing from –15 mW/m^2 in 2000 to –63 mW/m^2 in 2030, while values between –30 and –40 mW/m^2 are calculated for the other scenarios. Such large increase with respect to 2000 can be explained by the large increase in aviation sulfate emissions. Considering the uncertainties associated with the size distribution assumptions, extremely large values can be estimated, up to –285 mW/m^2 for RCP2.6, when the NUC size distribution of R13 is assumed (characterized by a large number of sulfate particles emitted in the nucleation mode).

5 SUMMARY AND CONCLUSIONS

This study complements a previous work by R13 with an analysis of transport sector impacts on aerosol and climate under the RCP scenarios in 2030. Using the EMAC-MADE aerosol-climate model we found that the four RCPs project a general decrease in the globally integrated land transport emissions for all species, with only very few exceptions. Large regional differences still occur, in particular between the western countries and the Southeast Asian countries. The most important feature of future shipping is the clear decrease in shipping-induced aerosol sulfate concentration, especially in the Northern Hemisphere, where most of the shipping routes are located. This reduction correlates with an increase in aerosol nitrate, due the competition of the two species for available ammonia. Aviation-induced concentration of BC and aerosol sulfate will increase in the UTLS and close to the source, but their overall impact on the atmospheric composition will still be small in relative terms. On the other hand, we simulated a strong impact of the aviation sector on particle number concentration in the upper-troposphere mid-latitudes, significantly larger than for the year 2000. Land transport and shipping are characterized by a significant reduction in the aerosol-induced RF effects, despite the growth in traffic volume, while aerosol-driven climate impact of aviation in 2030 results is 2 to 4 times larger than in 2000. Large uncertainties however exist, especially due to the assumptions on the size distribution of emitted particles, which play a significant role in the calculation of transport-induced perturbation on particle number concentrations.

REFERENCES

Eyring, V., I. S. A. Isaksen, T. Berntsen, W. Collins, J. J. Corbett, O. Endresen, R. G. Grainger, J. Moldanova, H. Schlager, and D. S. Stevenson, D. S., 2010: Transport impacts on atmosphere and climate: shipping. Atmos. Environ., 44, 4735–4771.

Lee, D. S., D. W. Fahey, P.M. Forster, P. J. Newton, R.C. N. Wit, L. L. Lim, B. Owen, and R. Sausen, 2010: Transport impacts on atmosphere and climate: Aviation, Atmos. Environ., 44, 4678–4734.

Moss, R. H., J. A. Edmonds, K. A. Hibbard, M. R. Manning, S. K. Rose, D. P. van Vuuren, T. R. Carter, S. Emori, M. Kainuma, T. Kram, G. A. Meehl, J. F. B. Mitchell, N. Nakicenovic, K. Riahi, S. J. Smith, R. J. Stouffer, A. M. Thomson,J. P. Weyant, T. J. and Wilbanks, 2010: The next generation of scenarios for climate change research and assessment., Nature, 463, 747–56.

Righi, M., J. Hendricks, and R. Sausen, 2013: The global impact of the transport sectors on atmospheric aerosol: simulations for year 2000 emissions, Atmos. Chem. Phys.,13, 9939—9970.

Uherek, E., T. Halenka, J. Borken-Kleefeld, Y. Balkanski, T. Berntsen, C. Borrego, M. Gauss, P. Hoor, K. Juda-Rezler, and J. Lelieveld, 2010: Transport impacts on atmosphere and climate: land transport. Atmos. Environ., 44, 4772–4816.

Aircraft emissions of NO_x: radiative forcing from long-term stratospheric changes of H_2O and O_3

G. Pitari*, G. Di Genova, E. Mancini
Department of Physical and Chemical Sciences, Università degli Studi dell'Aquila, L'Aquila, Italy

I. Cionni
ENEA, Ente per le Nuove Tecnologie, l'Energia e l'Ambiente, Rome, Italy

O.A. Søvde
Center for International Climate and Environmental Research - Oslo (CICERO), Oslo, Norway

L. Lim
Faculty of Science and Engineering, Manchester Metropolitan University, Manchester, UK

Keywords: aviation NO_x, CH_4 long-term response, stratospheric H_2O and O_3, radiative forcing.

ABSTRACT: Two independent chemistry-transport models with troposphere-stratosphere coupling are used to quantify the different components of the radiative forcing (RF) from aircraft emissions of NO_x, i.e., the University of L'Aquila climate-chemistry model (ULAQ-CCM) and the University of Oslo chemistry-transport model (Oslo-CTM3). The tropospheric NO_x enhancement due to aircraft emissions produces a short-term O_3 increase with a positive RF (+17.3±2.1 mW/m^2) (the uncertainty range represents the spread between the two models). This is partly compensated by the CH_4 decrease due to the OH enhancement (-9.4±1.0 mW/m^2). The latter is a long-term response calculated using a surface CH_4 flux boundary condition (FBC). This induces a long-term response of tropospheric O_3 due to less HO_2 being available for O_3 production, compared with the reference case where a constant CH_4 surface mixing ratio boundary condition is used (MBC) (-3.92±0.01 mW/m^2). The CH_4 decrease induces a long-term response of stratospheric H_2O (-1.2±0.1 mW/m^2). The latter finally perturbs HO_x and NO_x in the stratosphere, with a more efficient NO_x cycle for mid-stratospheric O_3 depletion and a decreased O_3 production from HO_2+NO in the lower stratosphere. This produces a long-term stratospheric O_3 loss, with a negative RF (-1.4±0.1 mW/m^2), compared with the CH_4 MBC case. Other minor contributions to the net NO_x RF are those due to NO_2 absorption of UV-A (+0.5±0.1 mW/m^2), increasing sulphate due to more efficient OH oxidation of SO_2 (-0.2 mW/m^2) and increasing nitrates formed via NO_3 + BVOC or HNO_3 heterogeneous reactions (-3.1 mW/m^2). These aerosol contributions have been calculated only in the ULAQ-CCM. According to these model calculations, aviation NO_x emissions for 2006 produced a small global net cooling effect of -1.3±0.8 mW/m^2 (an average of ULAQ-CCM and Oslo-CTM3 results). The ULAQ-CCM's calculated RF is -2.1 mW/m^2 (O_3 column changes of +0.32 and -0.056 DU in troposphere and stratosphere, respectively), whereas the Oslo-CTM3's calculated RF is -0.5 mW/m^2 (O_3 column changes of +0.45 and -0.082 DU in troposphere and stratosphere, respectively).

1 INTRODUCTION

Aviation alters the composition of the atmosphere globally and can thus drive climate and O_3 changes (Sausen et al., 2005; Lee et al., 2010). Aircraft emissions may impact the atmospheric composition both directly (mainly via emissions of CO_2, H_2O, NO_x, SO_2, soot) and indirectly (by increasing tropospheric O_3 and OH and decreasing the CH_4 lifetime; with formation of contrails and with indirect effects on upper tropospheric cirrus cloudiness, i.e., contrail-cirrus and soot-cirrus). Aircraft NO_x emissions, in particular, play a significant role in tropospheric and lower stratospheric chemistry, by enhancing the O_3 production and the OH concentration (Köhler et al., 2008; Hoor et al., 2009). The chemical reaction with OH, in turn, acts as the main sink for atmospheric CH_4, so that NO_x emissions by the aircraft will decrease the CH_4 lifetime. The lowering of CH_4 atmospheric abundance induces a cooling that may partially counteract the warming due to the other greenhouse

* *Corresponding author:* Giovanni Pitari, Department of Physical and Chemical Sciences, Università degli Studi dell'Aquila, Via Vetoio, 67100 L'Aquila, Italy. Email: gianni.pitari@aquila.infn.it

gases (CO_2, stratospheric H_2O, tropospheric O_3) from aviation, as well as the warming due to upper tropospheric cloud formation (contrails and aviation cirrus cloudiness) (Holmes et al., 2011). The aircraft impact on atmospheric O_3 is particularly complex, because a superposition of short- and long-term effects takes place, via direct NO_x emissions (short-term) and via OH driven CH_4 changes, which can feedback on HO_x chemistry, and finally on O_3 (long-term) (Wild et al., 2001; Holmes et al., 2011).

A new insight in the present study is the evaluation of the long-term stratospheric O_3 response associated with CH_4 lifetime changes produced by the aviation induced tropospheric OH perturbation. In this case, we have followed an innovative approach, by not using the IPCC simplified parametric formulas to calculate long-term negative RFs associated with the CH_4 RF (i.e., tropospheric O_3 and stratospheric H_2O), but through an explicit numerical experiment where surface CH_4 is calculated using a flux boundary condition. In this way, the calculated OH change due to aircraft NO_x emissions produces a CH_4 lifetime change that may be directly translated onto the CH_4 mixing ratio distribution. Therefore, the calculated O_3 RF results are the sum of both the short- and long-term responses and the effects on stratospheric H_2O and O_3 are explicitly calculated.

The main purpose of the present study is to compare the explicitly calculated long-term effects of aviation NO_x emissions with the results of IPCC parametric formulas and to assess the net RF from the different components (both short- and long-term effects). Two independent chemistry-transport models with troposphere-stratosphere coupling have been used to explicitly quantify the different components of the radiative forcing (RF) from aircraft NO_x emissions, i.e., the University of L'Aquila climate-chemistry model (ULAQ-CCM, used here in CTM mode) and the University of Oslo chemistry-transport model (Oslo-CTM3). For a complete discussion of the adopted aircraft emissions we refer to Søvde et al. (2014) and Pitari et al. (2015), as well as for a full description of the two models.

2 AIRCRAFT EMISSIONS AND NUMERICAL EXPERIMENTS SETUP

The aircraft emissions used in this study was generated for the EU FP7 project REACT4C ("Reducing Emissions from Aviation by Changing Trajectories for the benefit of Climate"). These were generated by the aviation emissions model FAST (Lee et al., 2005; Lee et al., 2009), which has been approved by the Modelling and Database Group (MDG) of the International Civil Aviation Organization (ICAO)'s Committee on Aviation Environmental Protection (CAEP) (ICAO, 2013). Aircraft movements from the CAEP Round 8 (CAEP/8) MDG work programme for the year 2006 were used as the basis of the emissions calculation. These were calculated using radar data from North American and European airspace, and for the rest of the world, the Official Airline Guide (OAG) schedule data. Routes were assumed to follow great circle trajectories and to correct for this assumption, CAEP/8 empirical factors (ICAO/CAEP, 2009) were applied to the distance and fuel consumption. The aircraft fleet was divided into 42 representative types, for which fuel flows were estimated with the PIANO aircraft performance model. FAST then used the fuel flow data to calculate NO_x emissions, which were based on the relationship between sea-level NO_x certification data and emissions at altitude (Lee et al., 2005). A 3D grid of $1\times1^\circ$ horizontal spacing and 2,000 ft vertical spacing of fuel, CO_2 , NO_x, particles and distance was generated by the FAST gridding utility. With this inventory, the calculated global fuel use and NO_x emissions are 178 Tg/yr and 0.71 Tg-N/yr, respectively.

Simulations with no aircraft (NO-AIRCRAFT, NA) and with aircraft emissions (AIRCRAFT EMISSION, AE) were performed with both ULAQ-CCM and Oslo-CTM3 models. These simulations were conducted for the 2006 time-slice and two experimental setups for CH_4; one with a fixed CH_4 surface mixing ratio boundary condition (MBC) and the other with a surface flux boundary condition (FBC). In the MBC case, NA and AE experiments were run for 10 years, allowing the aircraft perturbation to reach a satisfactory statistical steady-state. In the FBC case, NA and AE experiments were run for a much longer time period (i.e., 50 years), allowing CH_4 mixing ratios to adjust to the OH field, which is in turn perturbed by aircraft NO_x emissions. Background surface fluxes (NO_x, CO, VOCs, FBC-CH_4) and aircraft emissions are kept fixed in the CTMs at the values representative of year 2006, as well as surface mixing ratios of long-lived species relevant for O_3 photochemistry (CFCs, HCFCs, HFCs, N_2O and MBC-CH_4) (Søvde et al., 2014; Pitari et al., 2015).

3 RESULTS AND DISCUSSION

Any attempt to assess the long-term atmospheric response to upper tropospheric NO_x emissions from global aviation should calculate the atmospheric CH_4 distribution that allows surface CH_4 to respond freely to tropospheric perturbations of its main sink process, i.e., oxidation by OH. The usual modeling approach of adopting a fixed surface mixing ratio can still be used to calculate aviation induced changes in CH_4 lifetime, but this method cannot provide information on the tropospheric mass changes of CH_4 resulting from upper tropospheric NO_x emissions. In addition, correction factors are needed in the MBC approach to provide a meaningful estimate of the lifetime perturbation, due to the missing feedback of lower tropospheric CH_4 changes on HO_x chemistry (see for example IPCC, 1999; Myhre et al., 2011).

Table 1. Summary of CH_4 model calculations and the AE-NA differences (annual global averages).

Model	Exp	Surface mixing ratio [ppbv]	Tropospheric mixing ratio [ppbv]	Mass burden [Tg]	Lifetime [years]	Exp	Tropospheric mixing ratio change [ppbv]	Lifetime change [%]
ULAQ-CCM	FBC	1754	1732	4760	8.35	FBC AE-NA	-18.7	-1.17
ULAQ-CCM	MBC	1754	1735	4765	8.36	MBC AE-NA	-0.27	-0.81
Oslo-CTM3	FBC	1774	1754	4820	7.47	FBC AE-NA	-23.7	-1.32
Oslo-CTM3	MBC	1769	1756	4826	7.67	MBC AE-NA	-0.13	-0.96

A summary of CH_4 model calculations and AE-NA differences for ULAQ-CCM and Oslo-CTM3 models is presented in Table 1. The use of a fixed CH_4 surface mixing ratio (MBC) does not allow calculation of the tropospheric CH_4 mass distribution changes - only the lifetime perturbation. The latter is however underestimated by a factor of approximately 1.41±0.03 (average from the two models), due to the missing feedback of CH_4 changes with the HO_x chemistry (IPCC, 1999). The direct effect of aircraft perturbation on tropospheric NO_x is discussed in detail in Søvde et al. (2014) and Pitari et al. (2015). For the 2006 aircraft emissions, the models calculated a maximum change in the order of 0.07 – 0.15 ppbv on an annual basis and this is located at the northern mid-latitudes between ~200 and 300 hPa.

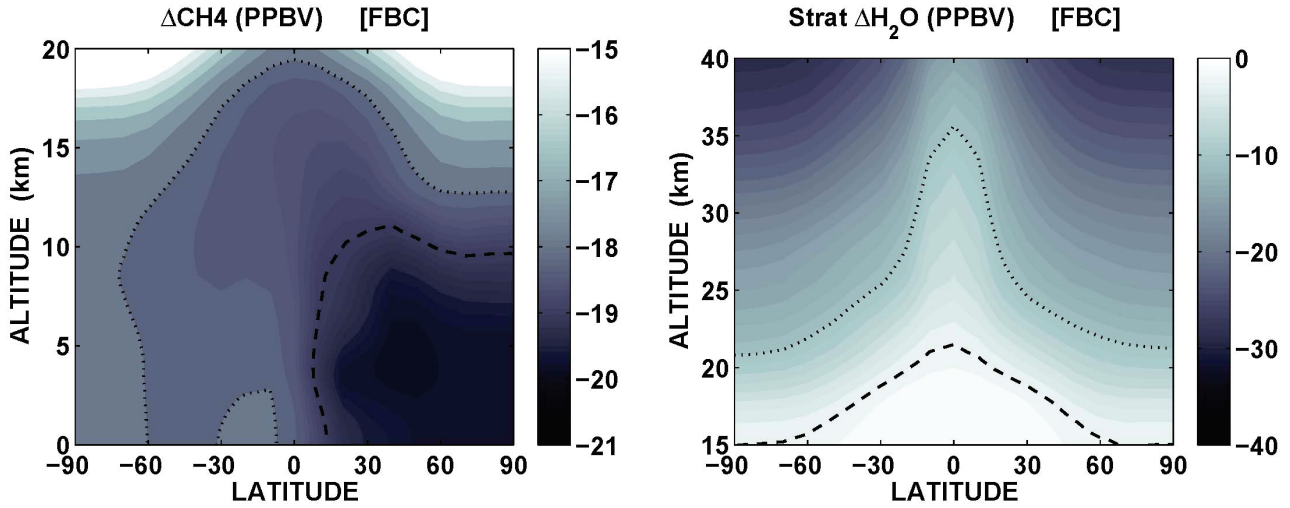

Figure 1. Left panel: annual zonal mean of tropospheric CH_4 mixing ratio changes (AE-NA) (ppbv). Dashed and dotted lines highlight contour lines of -19 and -17 ppbv, respectively. Right panel: annual zonal mean of stratospheric H_2O mixing ratio changes (AE-NA) (ppbv). Dashed and dotted lines highlight contour lines of -2 and -10 ppbv, respectively. Both panels are for the FBC model experiment. [ULAQ-CCM results].

The direct "instantaneous" effect of this NO_x enhancement is the increased photochemical production of O_3 and OH, the latter largely from the reaction of NO + HO_2 → NO_2 + OH. The model results show that the annually averaged maximum increase of these two species is 4 – 5 ppbv for O_3 and 0.20 – 0.25 $\times 10^6$ molec/cm^3 for OH. The instantaneous OH perturbation plays a key role in the global atmospheric chemistry by decreasing the CH_4 lifetime and then linking together short- and long-term effects of aircraft emissions. This is clearly visible in Fig. 1 (left panel), where the CH_4 mixing ratio aircraft perturbation (FBC) is shown. A non-negligible inter-hemispheric gradient of

the CH_4 perturbation is visible. This is expected from the OH change even though CH_4 is quite well-mixed in the troposphere due to its long lifetime. Conservation of the global hydrogen mass among the main H reservoirs (CH_4, H_2O and H_2), requires the average tropospheric CH_4 change due to aircraft NO_x emissions to be conserved in the stratosphere as the sum of $\Delta CH_4 + 0.5\Delta H_2O + 0.5\Delta H_2$, thus becoming the driver for photochemical changes of stratospheric water vapour (Fig. 1, right panel). The good isolation of the tropical pipe produces a significant horizontal gradient of the calculated ΔH_2O in the mid-lower stratosphere. An extensive evaluation of water vapour transport in the lower stratosphere (using available balloon, aircraft and satellite observations) has been made using the calculated mean age-of-air and tape-recorder signal as indicators (not shown). The stratospheric H_2O perturbation becomes the main driver for long-term changes of stratospheric O_3, as a result of less O_3 production in the lower stratosphere (HO_2 decreases) and a mid-stratospheric increase of the NO_x catalytic cycle for O_3 destruction (NO_2 increases).

Table 2. Summary of NO_x-related long-term RF components relative to CH_4, from ULAQ-CCM and Oslo-CTM3, and comparison with IPCC-type estimates.

Species	Model	Global changes H_2O, O_3 [DU] CH_4 [Tg]	RF-NET [mW/m^2]	RF/RF-CH_4 [%]	RF/RF-CH_4 [%] (IPCC, 2013)
CH_4	ULAQ CTM3	-52 -66	-8.38 -10.35	-	-
H_2O stratosphere	ULAQ CTM3	-0.63 -0.69	-1.34 -1.45	16.0 14.0	15 ± 10
O_3 troposphere	ULAQ CTM3	-0.12 -0.13	-3.91 -3.93	46.7 38.0	50 ± 27
O_3 stratosphere	ULAQ CTM3	-0.08 -0.14	-1.10 -1.34	13.1 13.0	-
O_3 total	ULAQ CTM3	-0.20 -0.27	-5.61 -6.30	59.8 50.9	50 ± 27

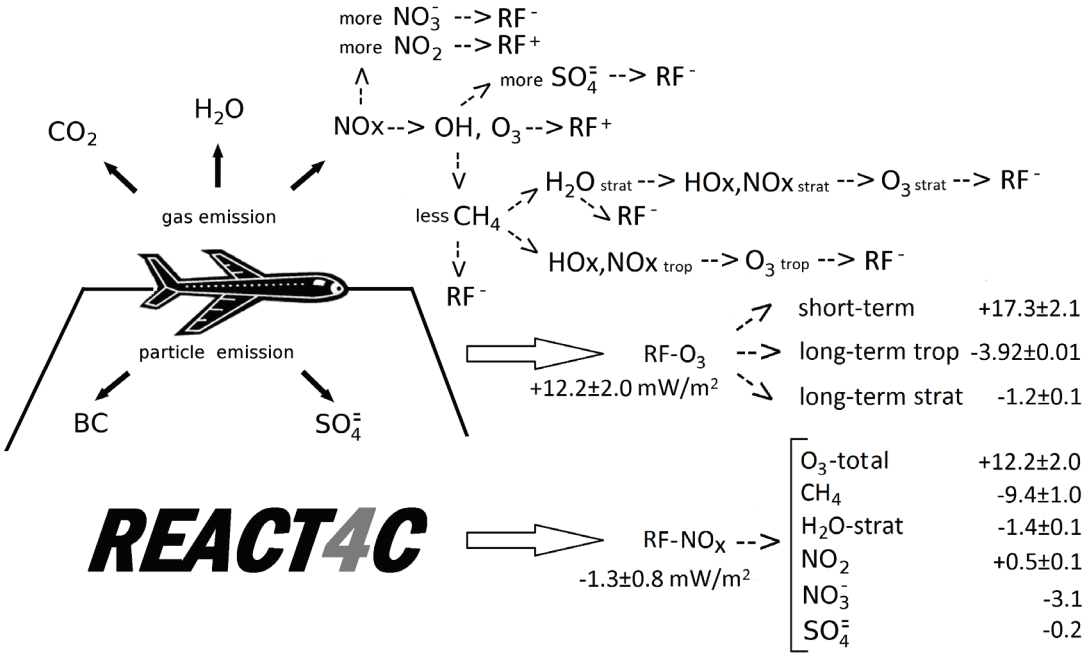

Figure 2. Summary of the annual globally averaged RF results (mW/m^2) from the ULAQ radiative code applied offline to the 3D monthly mean output of ULAQ-CCM and Oslo-CTM3. [Model average; the uncertainty range represents the spread between the two models].

The ULAQ radiative transfer code is applied offline to the monthly averaged fields of O_3, CH_4 and stratospheric H_2O from the two models (see Pitari et al., 2015 for more details). The O_3 RF breakdown between tropospheric and stratospheric contributions makes it possible to calculate the long-term effects for the two regions by comparing the results of MBC and FBC model experiments. In

the MBC case, where CH_4 is fixed at the surface, the lifetime change due to the NO_x-driven OH enhancement is not able to trigger a significant (and realistic) CH_4 decrease and therefore, the associated loss of stratospheric H_2O. This means that in the MBC case, the O_3 RF is a pure "instantaneous" response to aviation NO_x, whereas the difference between MBC and FBC gives an indirect estimate of the long-term impact of aviation NO_x on both tropospheric and stratospheric O_3. Table 2 presents a summary of the NO_x-related long-term RF components relative to CH_4, from ULAQ-CCM and Oslo-CTM3 models and these are compared with the IPCC-type estimates. The CH_4 RF computed through the radiative transfer code (Chou et al., 2001) is approximately 20% higher with respect to the parameterizations based on the average tropospheric mixing ratio and the lifetime change. The difference is mainly due to the inclusion of the solar near-infrared contribution in the 4-10 μm wavelength band, and partly due to the inhomogeneity of the CH_4 spatial distribution. Figure 2 shows the overall summary of offline radiative calculations made with the 3D output from the two models. The impact on secondary aerosols (sulphates and nitrates) is produced by the tropospheric OH enhancement (resulting in a more efficient SO_2 oxidation in SO_4) and also by the increasing nitrate formation from NO_3 + BVOC (biogenic organics) and HNO_3 heterogeneous reactions on the surface of soil dust or sea salt particles (Ayres et al., 2015). These aerosol contributions have been calculated using the ULAQ-CCM aerosol module.

4 CONCLUSIONS

Two independent chemistry-transport models with troposphere-stratosphere coupling have been used to quantify the different radiative forcing components from NO_x aircraft emissions, by taking into account both the short-term tropospheric O_3 response and the long-term responses due to OH-driven changes of tropospheric CH_4 and then in tropospheric HO_x chemistry and stratospheric H_2O, and finally on stratospheric O_3. A broadband radiative transfer model has been applied offline, to calculate the tropopause RF from the perturbed greenhouse gases (i.e., O_3, CH_4 and H_2O), as well as from NO_2 absorption of UV-A, indirect SO_4 increase due to the tropospheric OH enhancement and additional NO_3 aerosol formation from NO_x and HNO_3. The resulting net RF related to aircraft NO_x emissions is calculated as a small negative residual (-1.3±0.8 mW/m^2), with -2.1 mW/m^2 in the ULAQ-CCM and -0.5 mW/m^2 in Oslo-CTM3.

Acknowledgements. The authors acknowledge funding of the European Commission REACT4C project, under Grant No. ACP8-GA-2009-233772.

REFERENCES

Ayres, B.R., et al., 2015. Organic nitrate aerosol formation via NO_3 +BVOC in the Southeastern US. Atmos. Chem. Phys. Disc. 15, 16235-16272, doi: 10.5194/acpd-15-16235-2015.

Chou, M.-D., M.J. Suarez, X.-Z. Liang, and M.M.-H. Yan, 2001. A thermal infrared radiation parameterization for atmospheric studies. NASA/TM-2001-104606, 19; pp. 55.

Holmes, C.D., Q. Tang, and M.J. Prather, 2011. Uncertainties in climate assessment for the case of aviation NO. P. Natl. Acad. Sci. USA 108, 10997–11002, doi:10.1073/pnas.1101458108.

Hoor, P., J. Borken-Kleefeld, D. Caro, O. Dessens, O. Endresen, M. Gauss, V. Grewe, D. Hauglustaine, I.S.A. Isaksen, P. Jöckel, et al., 2009. The impact of traffic emissions on atmospheric ozone and OH: results from QUANTIFY. Atmos. Chem. Phys. 9, 3113-3136, doi:10.5194/acp-9-3113-2009.

Köhler, M.O., G. Rädel, O. Dessens, K.P. Shine, H.L. Rogers, O. Wild, and J.A. Pyle, 2008 Impact of perturbations to nitrogen oxide emissions from global aviation. J. Geophys. Res. 113 (D11), D11305, doi:10.1029/2007JD009140.

ICAO, 2013. International Civil Aviation Organization. http://www.icao.int/environmental-protection/Pages/modelling-and-databases.aspx.

ICAO/CAEP, 2009. International civil aviation organization (icao) / committee on aviation environmental protection (caep), agenda item 4: Modeling and databases task force (modtf) goals assessment results. ICAO/CAEP Working Paper, Steering Group Meeting, Salvador, Brazil, 22–26 June 2009.

IPCC, 1999. Aviation and the global atmosphere. Intergovernmental Panel on Climate Change, J. Penner, et al., Eds., Cambridge University Press, Cambridge, UK.

IPCC, 2013. Climate change 2013: Chapter 6. The physical science basis, T.F. Stocker et al., Eds. Cambridge University Press, UK.

Lee, D. S., B. Owen, C. Fichter, L.L. Lim, and D. Dimitriu, 2005. Allocation of International Aviation Emissions from Scheduled Air Traffic-present Day and Historical, Report to UK Department for Environment, Food and Rural Affairs, London.

Lee D.S., D.W. Fahey, P.M. Forster, P.J. Newton, R.C.N. Wit, L.L. Lim, B. Owen, and R. Sausen, 2009. Aviation and global climate change in the 21st century, Atmos. Environ. 43, 3520-3537.

Lee, D.S., G. Pitari, V. Grewe, K. Gierens, J. Penner, A. Petzold, M. Prather, U. Schumann, A. Bais, T. Berntsen, et al., 2010. Transport impacts on atmosphere and climate: Aviation, Atmos. Environ. 44, 4678–4734.

Myhre, G., K. Shine, G. Readel, M. Gauss, I. Isaksen, Q. Tang, M. Prather, J. Williams, P. van Velthoven, O. Dessens, et al., 2011. Radiative forcing due to changes in ozone and methane caused by the transport sector, Atmos. Environ. 45(2), 387-394.

Pitari, G., D. Iachetti, G. Di Genova, N. De Luca, O.A. Sovde, Ø. Hodnebrog, D.S. Lee, and L. Lim, 2015b: Impact of coupled NO_x/aerosol aircraft emissions on ozone photochemistry and radiative forcing, Atmosphere, 6, 751-782; doi:10.3390/atmos6060751.

Sausen, R., I. Isaksen, V. Grewe, D. Hauglustaine, D.S. Lee, G. Myhre, M.O. Köhler, G. Pitari, U. Schumann, F. Stordal, and C. Zerefos, 2005. Aviation radiative forcing in 2000: An update on IPCC (1999), Meteorol. Z. 14, 555-561.

Søvde, O.A., S. Matthes, A. Skowron, D. Iachetti, L. Lim, Ø. Hodnebrog, G. Di Genova, G. Pitari, D.S. Lee, G. Myhre, and I.S.A. Isaksen, 2014. Aircraft emission mitigation by changing route altitude: A multi-model estimate of aircraft NO_x emission impact on O_3 photochemistry, Atmos. Environ. 95, 468-479, doi: 10.1016/j.atmosenv.2014.06.049.

Wild, O., M.J. Prather, and H. Akimoto, 2001. Indirect long-term radiative cooling from NO_x emissions, Geophys. Res. Lett. 28, 1719-1722, doi:10.1029/2000gl012573.

Influence of Fuel Sulfur Content on Contrail Formation in the Near-Field of a Commercial Aircraft

J. C. Khou*, W. Ghedhaïfi, X. Vancassel, E. Montreuil
Onera – The French Aerospace Lab, F-91761 Palaiseau, France

F. Garnier
Ecole de Technologie Supérieure, Montreal, QC H3C 1K3 Canada

Keywords: Contrail, soot, activation, sulphur, simulation

ABSTRACT: Contrails may contribute to the radiative forcing due to aviation. In this context, investigation of contrails formation in the near field of an aircraft may be helpful to provide strategies in order to reduce their impact. In this study, we perform three-dimension RANS simulations of contrails produced by commercial aircraft in cruise conditions. A realistic geometry (here a Boeing 737) is taken into account including engine core and bypass flows which allows several possible parametrical studies and avoids using parameterizations for the description of the plume's dilution. The objective is to simulate the early development of contrails in the near-field's plume whose dilution is obtained by a spatial simulation of the dynamical flow around the aircraft. A coupling is carried out with a microphysical model implemented in the CFD code CEDRE to simulate particle growth using an Eulerian approach. The implemented microphysics model is capable of simulating water condensation onto soot particles, taking into account their activation by adsorption of sulfuric species and scavenging of volatile particles.

1 INTRODUCTION

Air traffic continuous growth over the past decades aroused environmental concerns regarding the impact of aircraft engine emissions. The consequences of such have been largely studied in recent years, but the level of scientific understanding of the role played by contrails and induced cirrus clouds remains poor (Lee et al, 2010). Condensation trails forming conditions can be fairly well determined from a thermodynamic point of view, by using the revised Schmidt-Appleman criterion (Schumann, 1996). Based on usual physics laws of conservation, it provides the atmospheric temperature and relative humidity threshold values for water saturation to be reached in the expanding plume. This method is robust to determine atmospheric regions of contrail occurrence and persistence and in this respect helps improving estimates of environmental impact. This impact is also related to contrail optical thickness that depends on the actual microphysical properties of the plume, amongst other parameters. The knowledge of ice crystals number density as well as their size distribution in water supersaturated aircraft plumes is therefore highly desirable in order to refine contrails and contrail-cirrus atmospheric impact. Direct in-flight measurements can provide relevant information on plumes microphysical properties (e.g. Schumann et al., 2002) but are difficult to achieve from a technical point of view. Besides, field campaigns require a large set of instruments and partners ranging from scientists to air traffic control. Plume microphysical modelling has proved to be a viable option to complete, validate and analyse in-situ measurements results (Kärcher et al, 1998). They can lead to a better understanding of physical and chemical plume processes (e.g. Yu and Turco, 1998). In this respect, 0D trajectory box models have shown interesting ability to improve physical understanding and insights of possible environmental impact reduction through fuel composition for instance (Rojo et al., 2015). However they only partly account for the influence of the early stages of plume mixing, since they assume an average dilution, unless when they are coupled to fluid flow solvers in a multi 0D approach (Vancassel et al., 2014).

The plume dilution in the atmosphere is a complex process, leading to a spatially inhomogeneous distribution of vapours and primary particles, whose fate is controlled by local thermodynamic con-

* *Corresponding author:* Weeded Ghedhaïfi, Onera – The French Aerospace Lab, F-91761 Palaiseau, France, Email: weeded.ghedhaïfi@onera.fr

ditions, hence by mixing in the fresh plume. Three-dimension CFD codes solving Navier-Stokes equations codes can deal with such complexity but generally use simplified microphysics and parameterized solutions to describe the wing-tip vortices and its initial interaction with the engine jets (e.g. Paoli et al, 2013).

In this paper, we report the results of the efforts made to simulate contrail formation using a realistic Boeing B737 aircraft geometry, including engine core and bypass flows. The calculations include 3D aerodynamics, chemistry and microphysics coupled calculations. We also present the outcome of the refinements added in the microphysical modelling, emphasizing the role of soot particle activation through sulphuric acid deposition, since it is a growth factor when burning sulphured fuels (e.g. Gysel et al., 2003).

2 MODEL OVERVIEW

2.1 *Fluid Flow Solver*

The CEDRE numerical code used for this study is a parallel, three-dimensional, multi-species, and compressible Navier–Stokes solver (Refloch et al, 2011). The numerical method is based on a cell-centered finite-volume approach for general unstructured grids, especially appropriate when complex geometries are used.

The mass-conservation equations related to the 3D compressible Navier–Stokes equations in CEDRE are:

$$\frac{\partial}{\partial t}\left(\rho y_k\right)+\frac{\partial}{\partial x_j}\left(\rho u_j y_k\right)=\frac{\partial}{\partial x_j}\left(\rho D_k \frac{\partial y_k}{\partial x_j}\right)+\dot{w}_k \tag{1}$$

$$\frac{\partial}{\partial t}\left(\rho u_i\right)+\frac{\partial}{\partial x_j}\left(\rho u_i u_j\right)=-\frac{\partial p}{\partial x_i}-\rho g\,\delta_{i3}+\frac{\partial}{\partial x_j}\left(\mu S_{ij}^d\right),\ i=1,\ldots,3 \tag{2}$$

$$\frac{\partial}{\partial t}\left(\rho e_t\right)+\frac{\partial}{\partial x_j}\left(\rho u_j h_t\right)=\frac{\partial}{\partial x_j}\left(\rho c_p \kappa \frac{\partial T}{\partial x_j}+\sum_k h_k D_k \frac{\partial y_k}{\partial x_j}+\mu S_{ij}^d u_i\right) \tag{3}$$

where the variables are velocity vector $(u_1,u_2,u_3)^T$; pressure p; total energy $e_t=e+\frac{1}{2}u_i u_i$, where e is the internal energy; total enthalpy $h_t=e_t+\frac{p}{\rho}$; temperature T; the deviator strain-rate tensor $S_{ij}^d=\left(\frac{\partial u_i}{\partial x_j}+\frac{\partial u_j}{\partial x_i}\right)-\frac{2}{3}\frac{\partial u_l}{\partial x_l}\delta_{ij}$; and dynamical viscosity μ. The species are governed by their mass fraction y_k, their diffusion coefficient in the mixture D_k, and their mass transfer rate $\dot{w}_k$. The thermal diffusivity is represented by κ. We adopted a high-resolution spatial Reynolds-Averaged Navier–Stokes (RANS) method. In the RANS approach, equations are averaged so that any variable may be decomposed into a mean part and a fluctuation part. For compressible flows, a density-weighted time average decomposition (also called Favre average) has been used, leading to a new set of equations that can be found in Khou et al (2015).

2.2 *Microphysical model*

The plume mixture has been assumed to be initially made of air, water vapor, and soot particles. Air and water vapor have been considered as ideal gases. Soot was assumed to be spherical, for the sake of simplicity as their fractal-like structure is complex to account for, especially in a CFD code. The freezing process has been supposed to be immersion freezing from a liquid thin layer and we assumed that turbulence did not promote any ice growth particular direction. Therefore the assumption that soot particles were initially spherical is a reasonable simplification, although collision processes on aggregates may be enhanced in comparison with spherical particles. Gas and particles

have been assumed to be in dynamical and thermal equilibrium. Particles were defined through an Eulerian approach and followed in the plume with a passive scalar transport equation given by:

$$\frac{\partial}{\partial t}\left(\overline{\rho}\widetilde{N}_p\right)+\frac{\partial}{\partial x_j}\left(\overline{\rho}\widetilde{u}_j\widetilde{N}_p\right)=\frac{\partial}{\partial x_j}\left(\mu\frac{\partial\widetilde{N}_p}{\partial x_j}-\overline{\rho}\widetilde{u_j''N_p''}\right) \tag{4}$$

where $\widetilde{N}_p$ represents the particle-number density (number of particles per unit volume). Soot particles distribution at the engine exit was monodisperse with a diameter of 20 nm. Soot particles have been considered to be coated by sulphuric acid prior to freezing by adsorption of gaseous sulphuric acid formed in the plume. We implemented a chemical kinetics scheme following Kärcher et al (1996) to work out the concentration of sulphuric acid formed from sulphur species initially in the fuel. About 22 species and 60 reactions were considered using mostly Arrhenius reaction rates. The activation process has been considered from the work reported for instance in Wong and Miake-Lye (2008). The surface covered in sulphur species (referred to as the activated surface) was given by

$$\theta_{ads}=\frac{n(SO_3)_{\text{ads}}+n(H_2SO_4)_{\text{ads}}}{\sigma_0} \tag{5}$$

where σ_0 is the number of available sites per surface unit of soot particle and $n(X)_{ads}$ is the number density of gaseous sulphur species adsorbed at the soot surface, calculated as follows:

$$\frac{dn_{ads}}{dt}=\frac{\pi}{4}\alpha c n_{soot}d_{soot}^2(1-\theta_{ads})\left(n(H_2SO_4)+n(SO_3)\right) \tag{6}$$

where α is the accommodation coefficient, c the molecules average thermal speed, n_{soot} the soot particles number density, d_{soot} their diameter and n(X) the concentration of gaseous X species in the plume. The main assumption used in this work is that contrail formation is driven by ice heterogeneous nucleation on activated soot particles. All emitted soot particles have been considered as potential ice nuclei but water vapour deposition has been scaled by the coated fraction θ_{ads}. Growth has been evaluated using a modified Fick's law dedicated to mass transfer on particles whose radius r_p is of the order of the mean free path λ. The mass transfer rate $\overline{\dot{w}}_{ice}$ [kg.m^{-3}.s^{-1}] is given by:

$$\overline{\dot{w}}_{ice}=\frac{4\pi\widetilde{N}_p\ r_p D_{vap}\ M_{H_2O}}{R\overline{T}}\left(\overline{p}_{vap}-\overline{p}_{vap}^{sat/ice}\right)G\left(r_p\right)\Pi\left(\overline{p}_{vap}^{sat/liq},r_p\right) \tag{7}$$

where M_{H_2O} is the water molar mass and R the ideal gas constant, D_{vap} the diffusion coefficient of water vapor in air. Furthermore, the mass transfer depends on saturation conditions and, more precisely, on the difference between the water-vapor partial pressure in the plume $\overline{p}_{vap}$ and the saturation vapor pressure above ice $\overline{p}_{vap}^{sat/ice}$. $\widetilde{N}_p$ is the particle-number density and r_p is the particle radius. The function G takes into account the transition of the uptake from the gas kinetic to diffusion regimes. The function Π in Equation (7) first starts mass transfer onto the dry particles when water liquid saturation is reached in the plume, since ice formation from immersion freezing requires a liquid coating.

$$\Pi\left(\overline{p}_{vap}^{sat/liq},r_p\right)=\begin{cases}0 \text{ when } \overline{p}_{vap}\le\overline{p}_{vap}^{sat/liq} \text{ and } r_p=r_s\\ 1 \text{ when } \overline{p}_{vap}\ge\overline{p}_{vap}^{sat/liq} \text{ or } r_p>r_s\end{cases} \tag{8}$$

where $\overline{p}_{vap}^{sat/liq}$ is the saturation vapor pressure above liquid water.

3 RESULTS AND DISCUSSION

The simulations have been performed on a simplified B737 aircraft geometry (see Figure 1, left). Engine outputs were modelled with a core flow and a bypass flow. The computational domain dimensions are given by referring to the wingspan b. It is a box of lengths 4.5b, 2b and 2b, in the axial, horizontal and vertical directions, respectively. The mesh used (see figure 1, right) contained

about 30 million cells, with refinement areas in order to capture key physical processes, occurring especially at the engine exit (jet) and the wing tip (vortex). The initial atmospheric conditions were chosen so that a contrail was expected to form in the plume. The ambient temperature was 219K and the relative humidity has been set to 30% or 60%, so that sensitivity could be done. The aircraft operated at typical cruise conditions either from an atmospheric point of view or from the engine emissions and exhaust gas temperature.

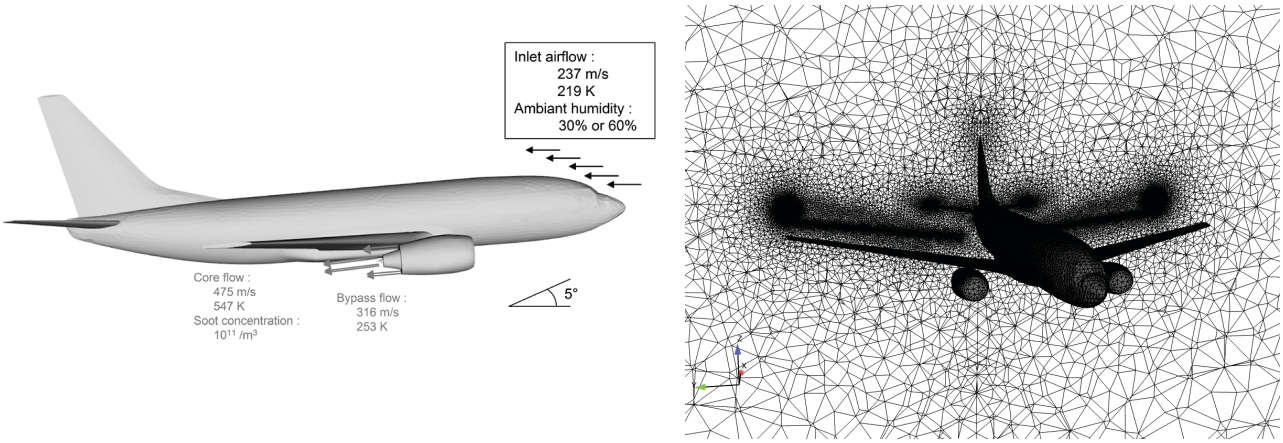

Figure 1: Aircraft geometry and initial conditions used to simulate contrail formation (left) and associated 30 million cells mesh (right)

Simulations were performed for three different fuel sulphur contents. We chose 350 and 700 ppm as they are typical of the FSC range of average value. We also used 5500 ppm, well above the legally admitted level (3000 ppm) so that comparisons with previously published work could be made (Kärcher, 1998). Figure 2 illustrates some of the obtained results. The left panel describes the evolution of the averaged soot activated surface in the plume for the three tested FSC. Results are in good agreement with 0D studies from the literature (Kärcher, 1998; Wong and Miake-Lye, 2008) since the trends are similar. About 20% of the soot surface is activated 130m downstream the engine exit, for the 350 ppm case. When the FSC is doubled, the fraction increases up to 40% although adsorption is a non-linear process. For the maximum FSC tested, the soot particles are entirely activated, meaning that 100% of the surface is covered in sulphuric acid or sulphur trioxide molecules. The rate of soot activation also increases with increasing FSC. As a consequence, more surface area is available for water vapour deposition and ice crystal final sizes at 0.5s in the plume are larger for larger FSC used. However, as reported in Schumann et al (2002), the final size is not so much affected. The variation between the 300 and 5500 ppm case is about 39% but only 16% between the 700 and the 5500 ppm.

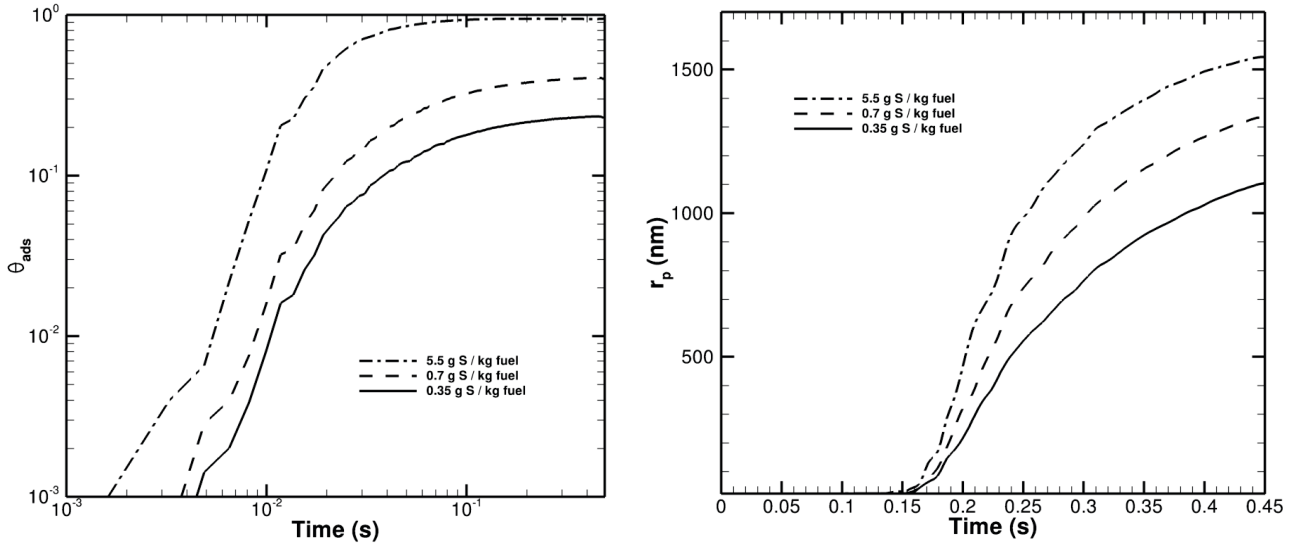

Figure 2: Evolution of the soot particles activated surface fraction in the plume (left) for three different fuel sulphur content and respectively radius of ice crystals in the plume (right)

The fuel sulphur content does not modify the probability that a contrail forms. It does not seem to modify ice crystal properties that much but it modifies the mass transfer rate since it scales as the activated surface. Figure 3 (left) shows the effect of the FSC on the evolution of the contrail optical depth.

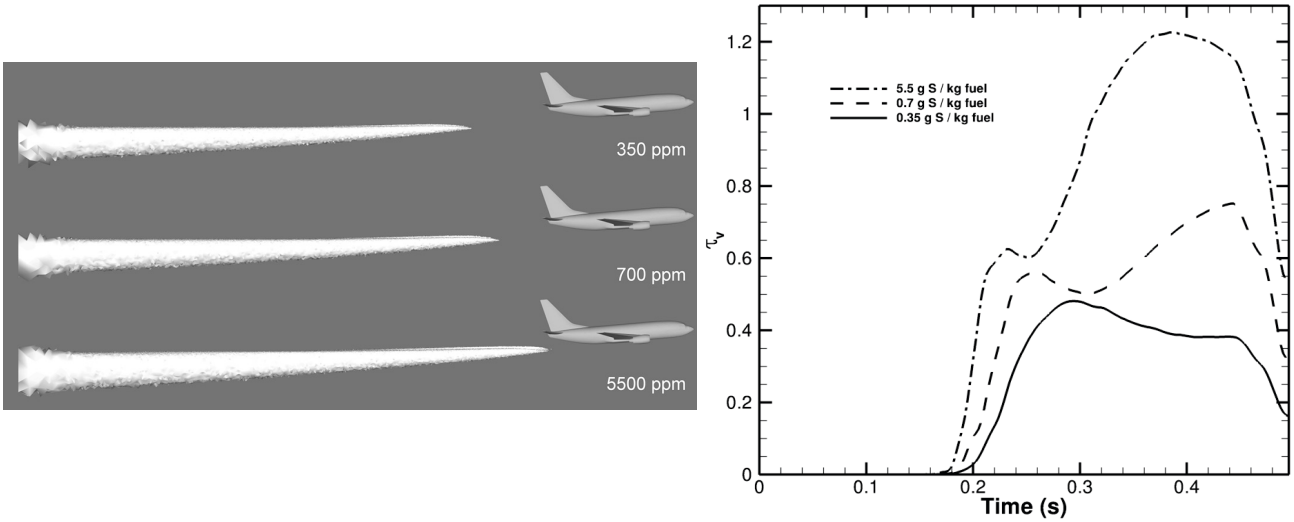

Figure 3: Influence of fuel sulphur content on contrail onset based on a visibility criterion (left) and evolution of the optical thickness for three FSC (right)

4 ACKNOWLEDGMENTS

Financial support for this work was provided by the Direction Générale de l'Aviation Civile through the TC2 project ("Condensation Trails and Climat"). This work was granted access to the High Performance Computing (HPC) resources of Très Grand Centre de Calcul (TGCC) under the allocation 2014 - t2014017254 made by Grand Equipement National de Calcul Intensif (GENCI).

REFERENCES

Gysel, M., Nyeki, S., Weingartner, E., Baltensperger, U., Giebl, H., Hitzenberger, R., Petzold, A., and Wilson, C. W., 2003: Properties of jet engine combustion particles during the PartEmis experiment: Hygroscopicity at subsaturated conditions. Geophys. Res. Lett., 30, 1566, doi:10.1029/2003GL016896.

Kärcher, B., Hirschberg, M. M., and Fabian, P., 1996: Small-scale chemical evolution of aircraft exhaust species at cruising altitudes., J. Geophys. Res., vol. 101.

Kärcher, B, 1998: Physicochemistry of aircraft-generated liquid aerosols, soot, and ice particles: 1. Model description, J. Geophys. Res., 103(D14), 17111–17128, doi:10.1029/98JD01044.

Kärcher, B., Busen, R., Petzold, A., Schröder, F. P., Schumann, U., and Jensen, E. J., 1998: Physicochemistry of aircraft-generated liquid aerosols, soot, and ice particles: 2. Comparison with observations and sensitivity studies, J. Geophys. Res., vol. 103, 17129–17147.

Lee, D. S., Pitari, G., Grewe, V., Gierens, K., Penner, J. E., Petzold, A., Prather, M. J., Schumann, U., Bais, A., Berntsen, T., Iachetti, D., Lim, L. L., and Sausen, R., 2010: Transport impacts on atmosphere and climate: Aviation, Atmos. Environ., vol. 44, 4678–4734.

Paoli, R., Nybelen, L., Picot, J., and Cariolle, D., 2013: Effects of jet/vortex interaction on contrail formation in supersaturated conditions, Phys. Fluids (1994-present), vol. 25, 053305.

Refloch, A., Courbet, B., Murrone, A., Villedieu, P., Laurent, C., Gilbank, P., Troyes, J., Tessé, L., Chaineray, G., Dargaud, J. B., Quémerais, E., and Vuillot, F., 2011: Cedre Software, Aerosp. Lab J., 1–10.

Rojo, C., Vancassel, X., Mirabel, P., Ponche, J. L., Garnier, F., 2015: Impact of alternative jet fuels on aircraft-induced aerosols, Fuel, 144, 335

Schumann, U., 1996: On conditions for contrail formation from aircraft exhausts, Met. Zeit., vol. 5, 4–23.

Schumann, U., Arnold, F., Busen, R., Curtius, J., Kärcher, B., Kiendler, A., Petzold, A., Schlager, H., Schröder, F. and Wohlfrom, K-H., 2002: Influence of fuel sulfur on the composition of aircraft exhaust plumes: the experiments SULFUR 1–7, J. Geophys. Res., Vol. 107, No. D15.

Vancassel, X., Mirabel, P., Garnier, F., 2014 : Numerical simulation of aerosols in an aircraft wake using a 3D LES solver and a detailed microphysical model. Int. J. of Sustainable Aviation, 1 (2), pp.139-159.

Wong, H., Yelvington, P. E., Timko, M. T., Onasch, T. B., Miake-Lye, R. C., Zhang, J., Waitz, I. A., 2008: Microphysical Modeling of Ground-Level Aircraft-Emitted Aerosol Formation: Roles of Sulfur-Containing Species, J Prop. Power, Vol. 24, No. 3 (2008), pp. 590-602.doi: 10.2514/1.32293.

Yu, F., Turco, R. P., 1998: The formation and evolution of aerosols in stratospheric aircraft plumes: Numerical simulations and comparisons with observations, J. Geophys. Res., 1998, 103, D20, 25915.

A numerical study of contrail-to-cirrus transition using 3D large-eddy simulations

R. Paoli*, O. Thouron, D. Cariolle
CERFACS, Toulouse, France

Keywords: contrail cirrus, LES, atmospheric turbulence, radiative transfer

ABSTRACT: We present a numerical study of contrail-to-cirrus transition during the first hour of contrail lifetime using fully 3D large-eddy simulations. We analyze the effects of atmospheric turbulence and radiative transfer in determining the contrail structure, the mean properties and radiative forcing. We perform a parametric study of contrail cirrus in terms of turbulence intensity, RHi and radiative set-up, and additional off-line calculations to analyze the sensitivity to ice radiative proprieties. We present a possible strategy for developing contrail cirrus parameterizations for global models based on the results from detailed LES.

1 INTRODUCTION

According to the latest estimates, contrail cirrus are among the most uncertain contributors of aviation to the Earth radiative forcing (RF, see Lee et al, 2009). They form when the initially linearly shaped contrails spread out due to the combined action of atmospheric turbulence, wind shear, radiative transfer and other atmospheric processes, and may ultimately become indistinguishable from natural cirrus. Contrail-to-cirrus transition is challenging to reproduce with cloud-resolving models because it requires large computational domains to accommodate the lateral and vertical spreading of the contrail and high-resolution to capture all relevant scales. Compared to contrail evolution during the vortex phase, contrail cirrus have then been studied to a much lesser extent in the literature. Unterstrasser and Gierens (2010) analyzed this problem using two-dimensional large-eddy simulations (LES) with bulk ice microphysics while Lewellen (2014) employed a quasi-3D LES approach with bin ice microphysics. While these approaches allows for the exploration of a large set of parameter space, they usually rely on simplified representation and/or numerical treatment of the wake vortex dynamics. Lewellen (2014) did carry out a limited set of 3D LES on stretched grids and ad-hoc re-initialization of the atmospheric turbulence but the effects of these choices on the turbulent kinetic energy or the structure functions of the resulting field were not investigated the authors' knowledge.
The present work is part of a larger project that aims at evaluating the atmospheric impact of contrail cirrus using a chain of fully 3D models that cover the contrail lifetime. Here, the specific objectives are: (i) to identify the role of atmospheric turbulence and radiative transfer in determining the 3D contrail characteristics in a limited set of atmospheric situations, and (ii) identify the relevant dynamical, microphysical properties to represent the contrail radiative properties and help GCM modelers to derive contrail cirrus parameterizations.

2 LES OF CONTRAIL-CO-CIRRUS TRANSITION

2.1 *Computational set-up*

We use the atmospheric mesoscale model Meso-NH developed by CNRM and Laboratoire d'Aérologie in Touluse. It solves Navier-Stokes equations in the anelastic approximation with turbulence closure based on the transport of turbulent kinetic energy. Additional transport equations include water vapor and ice that is treated with a Eulerian bulk approach. Detailed of the model can be found in http://mesonh.aero.obs-mip.fr/mesonh. In order to simulate the contrail-to-cirrus transition an atmospheric turbulence field is first generated on a large atmospheric domain using the stochas-

* *Corresponding author:* Roberto Paoli, CERFACS, 42 Avenue G. Coriolis, 31057 Toulouse, France. Email: paoli@cerfacs.fr

tic forcing technique described by Paoli et al (ACP, 2014). Then the jet and vortex phases are simulated on a smaller subdomain (Picot et al, 2015). The flow-field at a contrail age of 5 minutes is then extruded in the axial direction, copied back to the larger domain, and used as initial condition for the contrail cirrus simulations (beginning of the diffusion phase). This procedure was first tested on 4 km x 4 km x 4 km domain (mesh 1) with uniform 4 m resolution and then used on an 10 km x 10 km x 4 km domain (mesh 2) with uniform 10 m resolution for most of the cases analyzed in this study (see Figure 1).

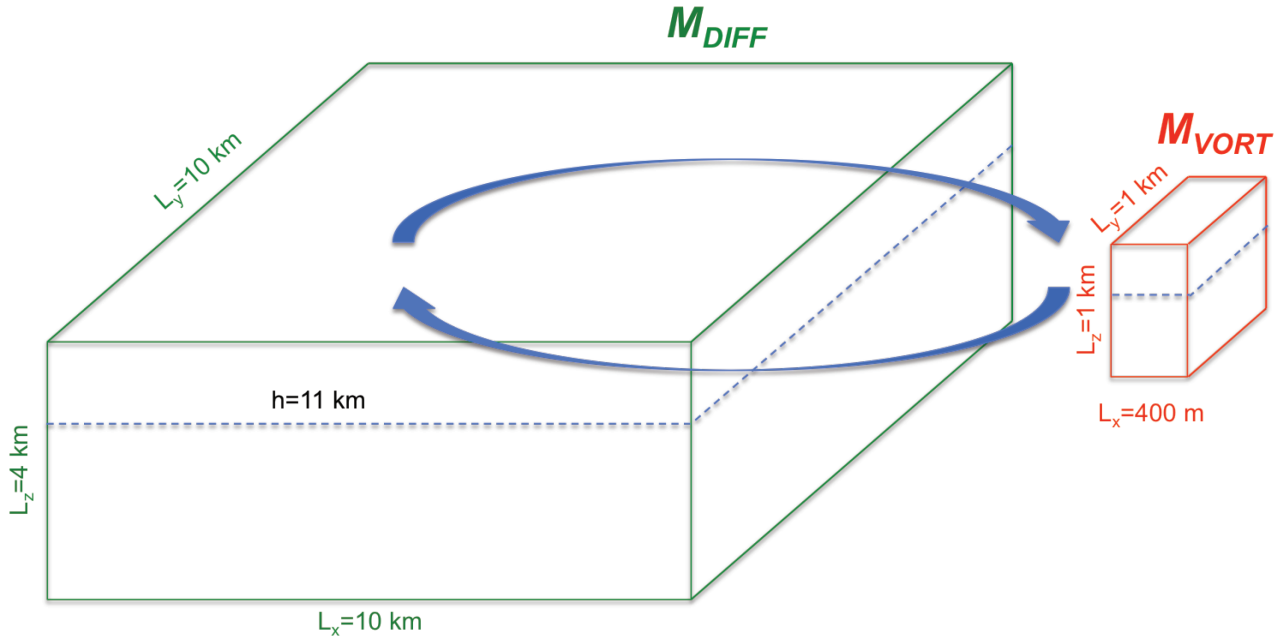

Figure 1: SKETCH of the computational set-up of for the LES of contrail-to-cirrus transition.

2.2 *Analysis*

We varied the ambient turbulence intensity and RHi, without and with the radiative transfer activated. In the latter case, we considered two idealized setups that mimic flights over a standard ocean surface in night and day (noon) conditions.

Figure 2 shows how the radiative transfer affects the contrail structure. When it is switched off, the contrail is distributed on almost independent vertical layers following the characteristic pattern of turbulent stratified flows. When the transfer is activated, the contrail tends to distribute into single vertical layer creating ice puffs of high/low ice concentration that are symptomatic of stronger vertical mixing in the cloud.

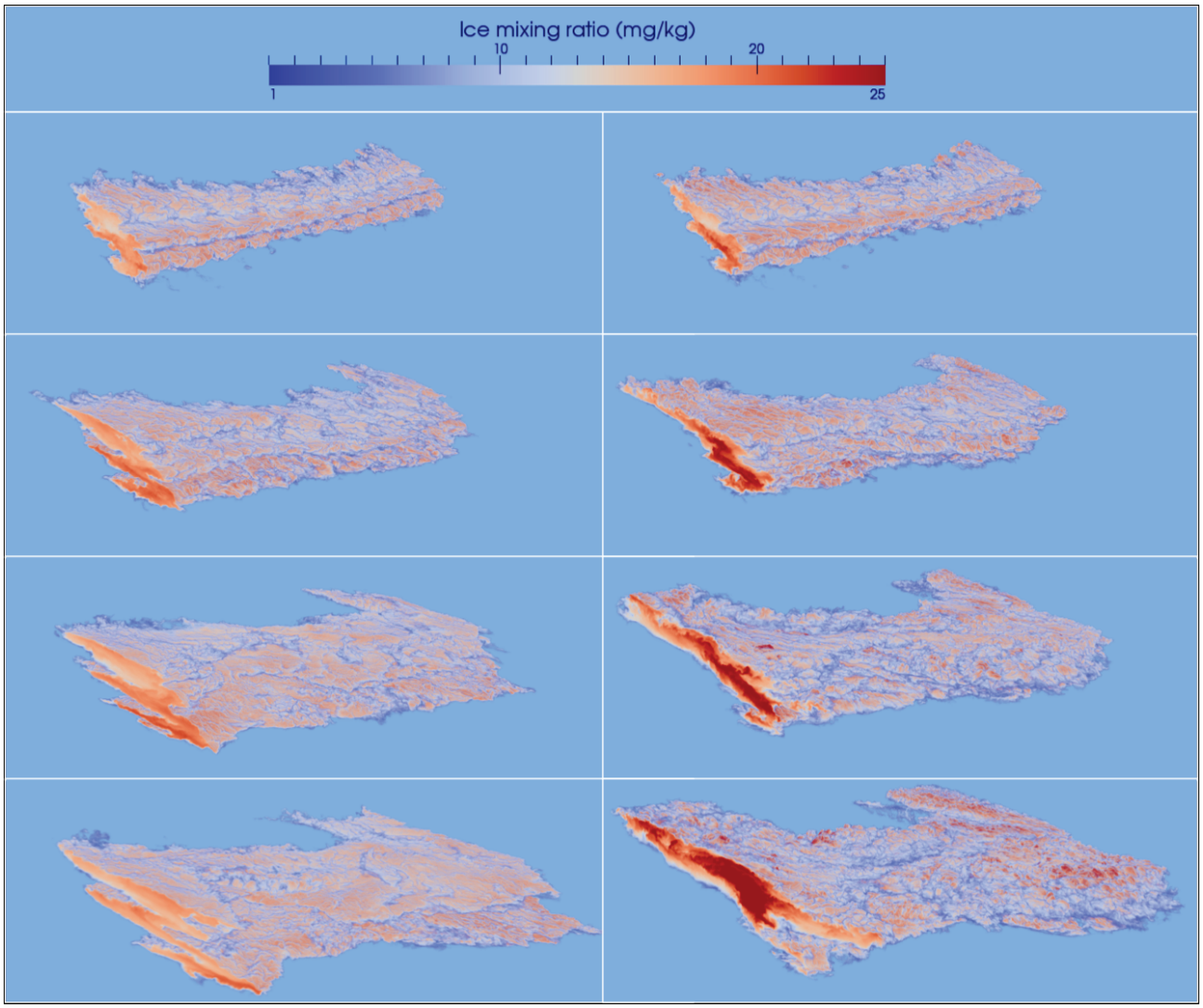

Figure 2: Evolution of contrail mixing ratio without (left panels) and with (right panels) radiative transfer activated (mesh 1, RHi=130%). From top to bottom: contrail ages of 10 min, 20 min, 30 min, and 40 min.

Figure 3 shows the evolution of ice water path (IWP) in the sensitivity study (mesh 2). It can be seen that the turbulence increases the cloud fraction as the contrail mixes more efficiently with the supersaturated ambient air but this effect is inhibited when radiative transfer is activated. The sensitivity of optical depth τ to the various configurations is analyzed in Figure 4. For a given RHi, the mean τ in the LW band is slight affected by the radiative set-up (even though the distribution inside the cloud is different). On the other hand, the mean optical depth in the SW band is sensitive to the ambient humidity with mean τ increasing of a factor of three --from 0.08-0.09 for RHi=110% to 0.22-0.27 for RHi=130%.

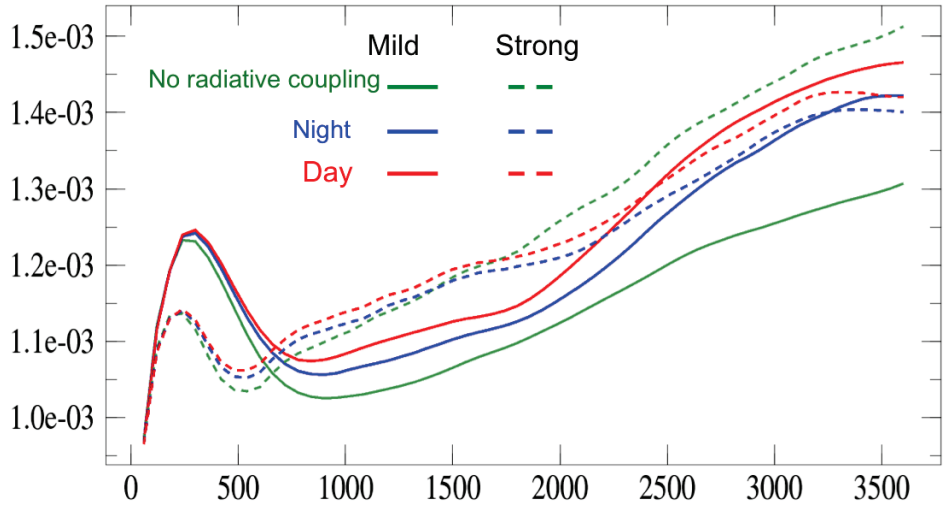

Figure 3: Evolution of contrail ice water path obtained in the sensitivity analysis (only cases with RHi=130% are shown).

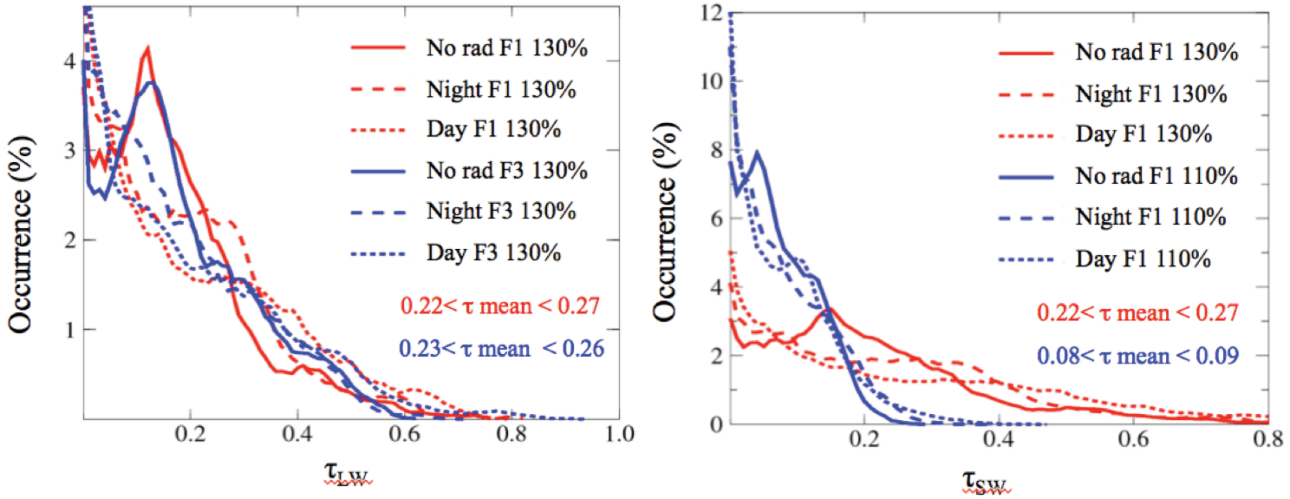

Figure 4: Evolution of contrail ice water path obtained in the sensitivity analysis (only cases with RHi=130% are shown).

Finally we evaluated the contrail radiative forcing that is calculated here as the difference of net flux at contrail top in the presence of ice particles minus the net flux in clear sky (Figure 5). In the SW band, the RF is negative because of the cooling effect of albedo whereas in the LW band, the strong absorption inside the contrail leads to a warming and a positive RF. As expected, both effects increase with the ambient RHi. The SW and LW components tend to balance although a slight warming persists.

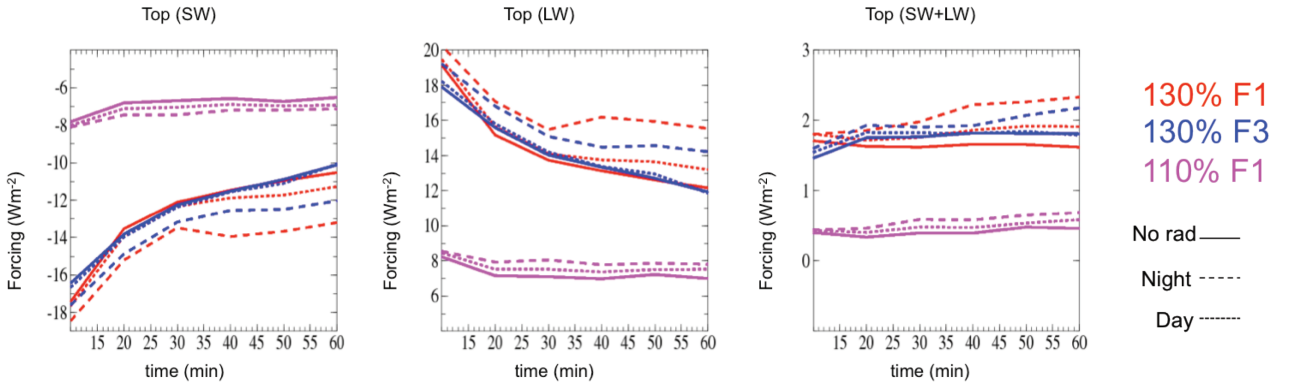

Figure 5: Contrail RF in ths SW and LW band and net RF for the sensitivity analysis.

We completed the analysis by running a series off-line radiative calculations at various contrail ages by changing the surface albedo, the microphysical properties (shape) of ice particles and their radiative properties (Single Scattering Albedo, Asymmetry Factor, Extinction). We found a large

sensitivity of RF when using the different parameterizations of Fu-Liu, Ebert-Curry and Gayet (not shown). To propose guidelines for GCM parameterizations, we reported in Figure 6 the optical depth as a function of ice water path at different contrail ages. The figure shows that τ decreases with age and, as opposed to what is typically assumed in GCM parameterizations, it also decreases with the IWP. We repeated the exercise by running a new set of LES by halving the initial particle concentration N and obtained the same trend. To fit the data we then derived an empirical law of the form $\tau(t)$(t) =a(t,N)·IWP+ τ(clear sky) where the coefficient depends on the contrail age and the initial particle concentration.

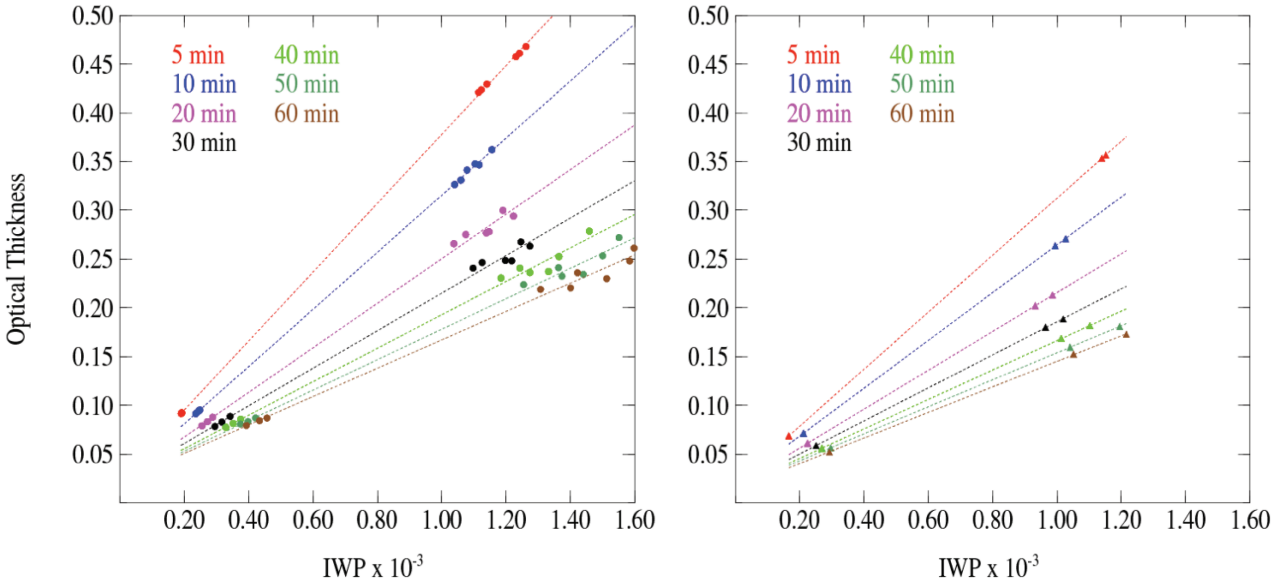

Figure 6: Optical depth as a function of IWP for different LES at different contrail ages. Left panel: baseline initial particle concentration N, right panel: N/2.

3 CONCLUSIONS

We performed 3D ELS of contrail-to-cirrus transition using a chain of models to cover the first hour of contrail age. Given the computational cost of each simulation (as low as 0.5 x109 grid points) we limited the parametric study to ambient turbulence, RHi and initial particle concentration. Additional analysis includes the sensitivity of radiative forcing to the ice radiative properties using off-line radiative calculations. Overall the results are in line with expectations (e.g. RF>0 in the LW and RF>0 in the SW). We proposed some guidelines to develop contrail parameterizations for GCM based on LES results by relating the optical depth to the IWP with an empirical law that accounts for the contrail age and concentration.

REFERENCES

Lee D.S., D. W. Fahey, P.M. Foster, P.J. Newton, R.C.N. Wit, L.L. Limn, B. Owen, and R. Sausen, 2009: Aviation and global climate change in the 21th century. Atmos. Environ. 43, 3520–3537.

D.C. Lewellen, 2014: Persistent contrails and contrail cirrus. Part II: Full lifetime behavior. J. Atmos. Sci. 71, 4420–4438.

Paoli R, O. Thouron, J. Escobar, J. Picot, and D. Cariolle, 2014: High-resolution large-eddy simulations of sub-kilometer-scale turbulence in the upper troposphere lower stratosphere. Atmos. Chem. Phys. 14, 5037–5055.

Picot J, R. Paoli, O. Thouron, and D. Cariolle, 2015. Large-eddy simulation of contrail evolution in the vortex phase and its interaction with atmospheric turbulence. Atmos. Chem. Phys. 15, 7369–7389.

Unterstrasser S and K. Gierens 2010: Numerical simulations of contrail-to-cirrus transition –Part 1: an extensive parametric study. Atmos. Chem. Phys. 10, 2017–2036.

Angle dependent extinction of solar radiation by individual condensation trails

J. Rosenow *, H. Fricke
Technische Universität Dresden, Institut für Luftfahrt und Logistik, Germany

Keywords: Condensation trails, solar radiative forcing, angle dependence
ABSTRACT: In this work, a continuous model is developed to estimate the solar scattering and absorption properties and their dependence on the position of the sun. The initial microphysical properties of realistic condensation trails are calculated using a flight performance model yielding precise information about altitude, true air speed, fuel flow and emission of water vapor and heat. The evolution of the contrail microphysical properties during the diffusion regime is calculated with a Gaussian plume model. The radiation field around the contrail is calculated with the radiative transfer library libRadtran using a discrete ordinate radiative transfer solver for solar radiation. Finally, radiative extinction due to the condensation trail is calculated utilizing a Monte Carlo simulation for the consideration of multiple scattering. This radiative extinction model is calibrated and tested for a wide range of realistic parameter settings. Radiative extinction strongly depends on the irradiation angle and on the geographical orientation of the condensation trail both determining the distance photons travel through the condensation trail. Furthermore, strong forward scattering, defined by the particle shape and wavelength cause a reduced cooling effect at noon, when the main part of solar radiation is irradiating perpendicular to the condensation trail axis. The results facilitate the possibility of improve both, the trajectory management and the network structure towards an air traffic system with reduced environmental impact due to contrails.

1 INTRODUCTION

Long living condensation trails (short: persistent contrails) are ice crystals at flight level developed behind an aircraft (Schumann 2005) in an ice-supersaturated environment (Schmidt 1941, Brewer 1946, Appleman 1953, Schumann 1996, and Sussmann et al. 2001). The water condenses at soot particles, from the exhaust of the aircraft. In the Earth-atmosphere energy budget, contrails seem like a restriction in the atmospheric energy exchange (Myhre et al. 2013, Lee et al. 2009), because they scatter incoming shortwave solar radiation partly back to the sky and they absorb and emit outgoing longwave terrestrial radiation partly back to the Earth's surface Myhre et al. 2013, Minnis et al. 1999, Sausen et al. 2005 and Burkhardt et al. 2011). The impact of a single contrail on the extinction of solar radiation (solar radiative forcing RF_{solar}) is calculated in this study considering the angle dependence of solar radiation due to time of day and flight path.

1.1 *State of the art*

The radiative forcing of contrails has been estimated several times. For example, using a global climate model as done by Burkhardt et al. 2011. Or by observing contrails and interpreting the incoming and outgoing radiation with the help of satellite data as shown by Graf et al. 2012, Schumann et al. 2013 and Vázques-Navarro et al. 2015. The influence of contrails on the Earth-atmosphere energy balance has been first approximated by Hansen et al. 1997, Meerkötter et al. 1999, Myhre et al. 2001, Petty 2002, Marquart et al. 2003, Ponater et al. 2006, Solomon et al. 2007 and Corti et al. 2009 treating contrails as plane parallel layer with constant properties. However, considering the contrail as horizontally homogenous layer, ignores the realistic three dimensional structure of a contrail (Schulz 1997 and Gounou et al. 2007). All above publications neglect multiple scattering. A detailed study of angle dependent photon transport through a three-dimensional defined realistic condensation trail by Gounou et al. 2007 and Forster et al. 2011 demonstrated the importance of considering large solar zenith angles. Due to an application of a Monte Carlo code for photon transport as used by Forster et al. 2011 effects like multiple scattering are already consid-

* *Corresponding author:* J. Rosenow, Technische Universität Dresden, Institut für Luftfahrt und Logistik, D-01069 Dresden, Germany. Email: Judith.Rosenow@tu-dresden.de

ered. However, the latest estimations of realistic contrails are still based on a radiative transport calculation of the whole atmosphere with an additional contrail. They are using a coarse spatial grid within the contrail. From a meteorological point of view, which is the estimation of the contrail influence on the energy budget, the latest results are very useful and the extinction properties of the contrail without an atmospheric environment are not of interest. However, for an optimization of the aircraft trajectory and flight performance with respect to minimize contrail impact on radiative forcing, those calculations are insufficient. Here, photon transport through the contrail is estimated separately from the radiative transfer processes through the atmosphere. Hence, a feedback of the flight performance on the contrail radiative forcing is possible.

2 MODEL

The influence of a condensation trail on the energy budget of the Earth-atmosphere system strongly depends on the properties of the contrail, which are influenced by the aircraft generating the contrail (Schumann 2000 and Jeßberger et al. 2013).

2.1 *Aircraft performance model*

The flight profile is generated with the help of the Enhanced Jet Performance Model (EJPM) derived by Kaiser 2015 for an Airbus A320 aircraft. The EJPM optimizes fuel consumption and the lift to drag ratio using a maximum specific range. For the current study, it provides the required Thrust F, fuel flow m_f, true air speed v_{TAS} and altitude z.

2.2 *Contrail life cycle model*

The characteristics of the flight profile and the model atmosphere Mid-Latitude Winter by Anderson et al. 1986 allow the calculation of the initial dimensions and microphysical properties of the contrail. For persistent contrail formation, the model atmosphere is manipulated by an ice-supersaturated layer between z = 9.5 km and z = 11.5 km. Because the exhaust is captured in the wake vortices of the aircraft, the initial characteristics of the contrail are defined at the beginning of the dispersion regime of the wake vortices with the help of the "Probabilistic Two-Phase Wake Vortex Decay and Transport Model" (P2P) by Holzäpfel 2003. Here, an eddy dissipation rate of $\varepsilon = 5 \cdot 10^{-5}\ m^2\ s^{-3}$ is assumed due to missing turbulence information. The initial contrail height is defined as the distance between emission height at flight level down to the altitude the vortex fall during the vortex regime, plus two times the vortex radius. The vortex radius r is defined as the radius, where the tangential velocity v_t (r) has reached a value of $(\sqrt{e})^{-1/2}$ of the tangential velocity in the vortex core v_t (r_c). This fraction corresponds to the position of one standard deviation 1σ within the Gaussian distribution function, where also a value of $(\sqrt{e})^{-1/2}$ times the maximum value of the function is reached.

The life cycle of the contrail is described by a Gaussian plume model as described by Schumann et al. 1995 and applied by Rosenow et al. 2012. To overcome computational costs in the radiative forcing calculations, an elliptical cross section is assumed. Therewith, the calculation of radiative extinction due to the contrail is sufficient for the directions coming from one octant. Other directions of incoming photons are considered by reflecting the results of the Monte Carlo simulation in the slice planes to the other octants. The Gaussian plume model results in a continuous calculation of the contrail microphysics (ice particle size r_p and ice water content IWC) at every position within the contrail. Hence, for every point within the contrail and for each wavelength the solar radiative extinction properties (scattering and absorption efficiencies Q_{sca} , Q_{abs} and asymmetry g parameter for the scattering phase function) can be calculated using parameterizations from Wyser et al. 2000. Here, non-spherical particle shapes typically found in midlatitude cirrus clouds are considered without particle size distribution.

2.3 *Radiative transfer model*

Solar radiances at contrail altitude are calculated utilizing the radiative transfer model libRadtran (Mayer et al. 2011). With libRadtran, diffuse and direct solar radiances coming from all directions in space with a discretization of 2° are calculated at 10.5 km altitude over Berlin, Germany, on 21st of June 2012. No clouds and a default aerosol concentration are considered. The surface library of

the International Geosphere Biosphere (IGBP) from the NASA CERES/SARB Surface Properties Project is used for surface reflectivity. The Discrete Ordinate Radiative Transfer (DISORT) solver with 256 streams, developed by Stamnes et al. 1988 with the correlated-k scheme LOWTRAN of Ricciazzi et al. 1998 is used to overcome computational costs due to narrow absorption bands even in the solar spectrum. The calculations are done for 21 bands between wavelengths of λ = 275 nm and λ = 2200 nm.

2.4 *Radiative forcing model*

For radiative extinction of solar radiances calculated with libRadtran, 107 photons are traced in a Monte Carlo simulation. This simulation is necessary to consider multiple scattering events. For radiative extinction Beer's law

$$I = I_0 exp\left(\int_{s_1}^{s_2} -\beta_{ext}\,(s)ds\right)$$

is solved, where I and I_0 denote the extinguished and the original radiances [W m^{-2} sr^{-1} nm^{-1}], respectively, β_{ext} describes the volume extinction coefficient [m^{-1}] and s the thickness of the extinguishing medium [m], or the position within. Using the geometrical cross section of a particle $[m^2] A_p = \pi \cdot r_p^2$ (r_p...particle radius [m]) and the number density of particles n_p [m^{-2}] as function of location s (Gaussian distribution), Beer's law becomes:

$$I = I_0 exp\left(\int_{s_1}^{s_2} -Q_{ext}\,\mathrm{A_p n_p}(s)ds\right).$$

Considering the corresponding hemispheres of the entering and leaving photons, a calculation of the impact of a contrail on the Earth's energy system is possible. Therefore, three counters are generated each collecting forward scattered, backward scattered and absorbed photons. The number ratios of photons between incoming and collected photons in each counter are weighted by the irradiated length (here, six times the standard deviation 6σ) and the sine on the angle α between the incoming photons and flight path as projection of the perpendicular irradiated area on the flight path (compare Figure 1).

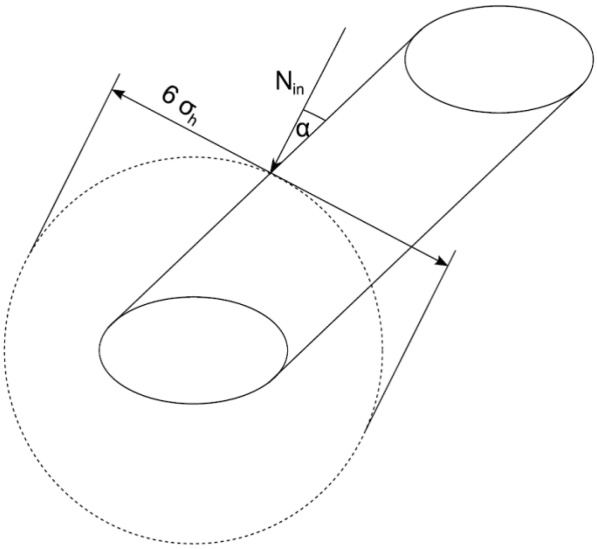

Figure 1: Geometry of the Monte Carlo simulation. Photons start uniformly distributed perpendicular to the direction of arrival along line with a width of 6σ_h.

Hence, the intermediate results of the Monte Carlo simulation for each hemisphere are weighted number ratios of forward scattered S_f, backward scattered S_b and absorbed S_a photons. Because they are weighted by the irradiated width 6σ, they have the unit [m]. These weighted number ratios of extinguished photons are multiplied with the solar radiances I_0 [W sr^{-1} m^{-2} nm^{-1}] coming from the particular direction and the corresponding solid angle Ω [sr]. These resulting quantities are forward scattered P_f, backward scattered P_b and absorbed P_a powers [W m^{-1} nm^{-1}] per meter contrail and per nanometer. With these quantities, the solar radiative forcing can be calculated:

$$RF_{solar} = P_{\downarrow\uparrow a} + P_{\uparrow b} - P_{\downarrow b}$$

where the arrows are indicating the direction of irradiance. Note, for all calculations, diffuse and direct solar radiation coming from all directions in space are considered.

3 CALCULATIONS

To visualize the angle dependence of solar radiative extinction due to a contrail, Figure 2 and Figure 3 show the weighted number of forward scattered S_f and backward scattered S_b photons, respectively, coming from different directions above the contrail. These directions are described by their solar zenith angle θ (as deviation from the vertical direction) and by their solar azimuthal angle φ (as deviation from South). Here, the contrail constitutes the North- South- axis. Figure 2 and Figure 3 show two phenomena. First, the strong forward scattering defined by the high asymmetry parameter g = 0.74 in the Heyney Greenstein Phase scattering function explains differences between forward and backward scattering (i.e. between Figure 2 and 3) as already shown by Wyser et al. 2000. And second, extinction depends on the travel distance through the contrail, especially through the contrail core. Hence, the larger the angle θ (towards horizontal photon transport), the larger is the extinction. For large solar zenith angles, the influence of the azimuthal angle φ becomes significant, deciding on whether the contrail cross section or the longitudinal axis is irradiated.

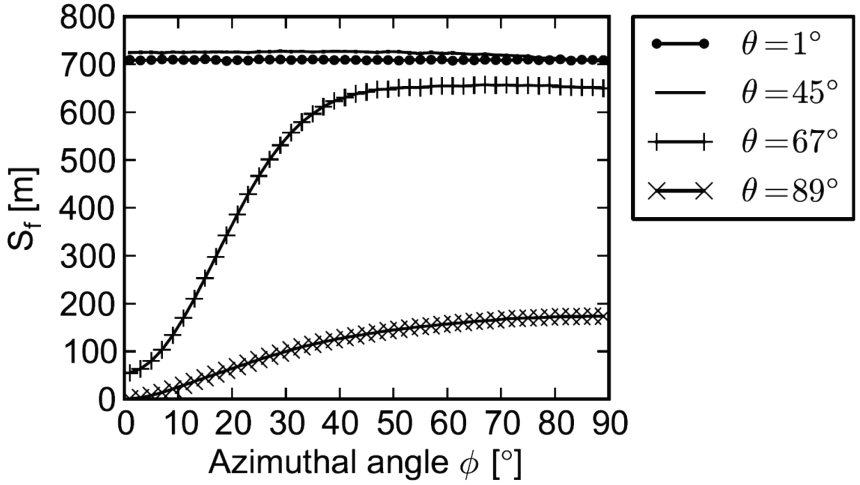

Figure 2: Number ratios of forward Sf scattered photons to the total number of 107 photons, weighted by the sine of the angle between incident photons and contrail axis and by the width 6σ were the photons are starting from. The angular dependent simulation is done for a solar wavelength λ = 550 nm. The optical properties of the contrail are described in Table 1.

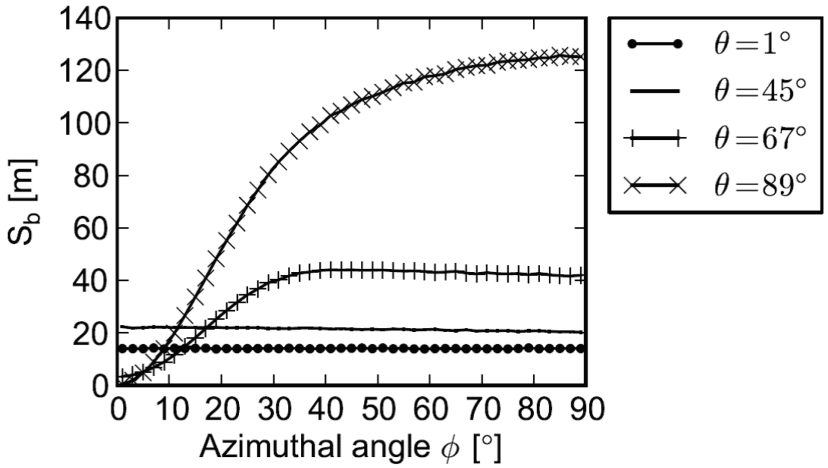

Figure 3: The same as in Figure 2, except backward scattered photons S_b are considered.

The relevance of multiple scattering is shown in Figure 4. The larger the distance traveled through the contrail, the higher the number of scattering events. In the worst case, each photon is scattered 1.6 times on average. Thus, multiple scattering cannot be neglected.

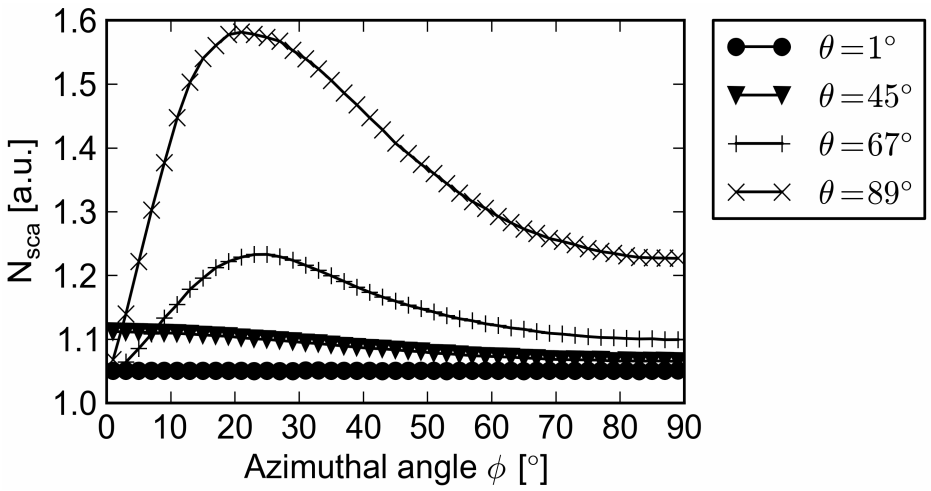

Figure 4: The average number of scattering events per scattered photon N_{sca} for several solar zenith angles θ and for all azimuthal angles φ. The angular dependent simulation is done for a solar wavelength λ = 550 nm after a lifetime of 20 hours in a strong turbulent environment with $\varepsilon = 10^{-4}$ m^2 s^{-3}.

The influence of the flight path on the radiative extinction is shown in Figure 5 and Figure 6, where the backscattered powers (required for the estimation of the radiative forcing $RF_{550\,nm}$) are calculated for different solar zenith angles and solar azimuthal angles during the day. In Figure 5, the contrail constitutes the North-South axis. In Figure 6, the contrail is along the East-West axis. Hence, different combinations of zenith and azimuthal angles for direct solar radiation are expected, resulting in different extinguished powers and radiative forcing. In Figure 5 (North-South), during sunrise and sunset (for φ = 90 ° and φ = 270 °) the sun irradiates the contrail longitudinal axis. In Figure 6 (East-West), during sunrise and sunset direct solar radiation irradiates the contrail cross section while horizontal photon transport takes place. As shown in Figure 2 and Figure 3, the influence of the azimuthal angle φ increases with increasing zenith angle θ (towards a horizontal irradiation). For small angles α (facing the contrail cross section) the irradiated area is minimized. Hence, the extinguished powers are reduced but are not converging to Zero, because of the amount of diffuse solar radiances coming from all directions. In general, Figure 5 and Figure 6 show that strong forward scattering reduces the backscattered power $P_{\downarrow \mathrm{b}}$ during midday, when solar zenith angle θ is small. The absorbed power $P_{\downarrow\uparrow a}$ corresponds to the available radiances, particularly the direct radiation, which increases until 12 a.m.. Due to small solar absorption efficiency $RQF_{a,550\,nm}$, small values of absorbed power $P_{\downarrow\uparrow a}$ are expected.

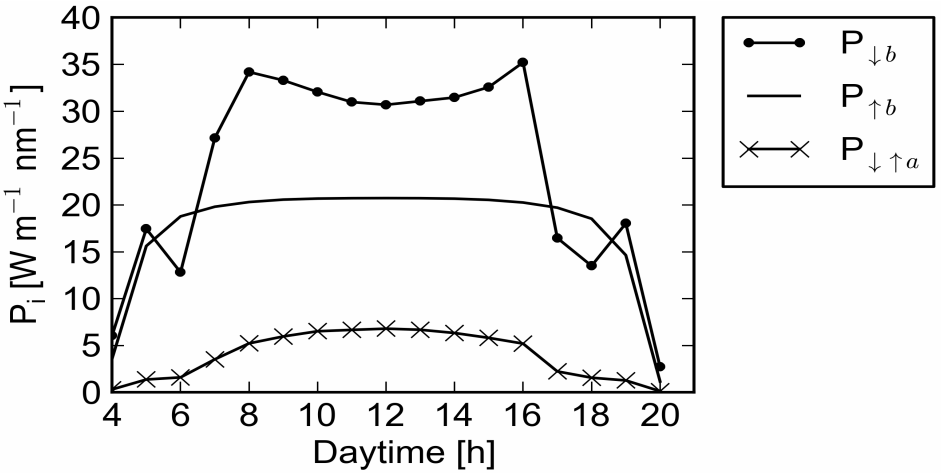

Figure 5: Backscattered power for diurnal variations of upward ($P_{\uparrow b}$) and downward ($P_{\downarrow \mathrm{b}}$) solar radiation ($\lambda$ = 550 nm) and absorbed power of downward and upward radiation ($P_{\downarrow\uparrow a}$) for constant contrail properties according to Table 1. The contrail constitutes the North-South axis.

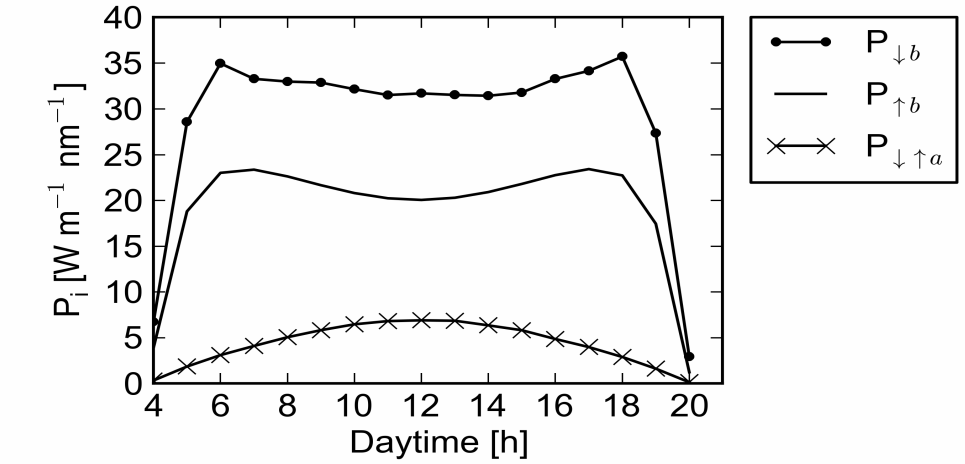

Figure 6: Backscattered powers depending on diurnal variations of upward ($P_{\uparrow b}$) and downward ($P_{\downarrow b}$) solar radiances (λ = 550 nm) and absorbed power of downward and upward radiation ($P_{\downarrow\uparrow a}$) for constant contrail properties. The contrail constitutes the North-South axis.

3.1 *Verification*

To verify the radiative forcing model, a comparison with the results of other publications is done. Mostly, the optical thickness τ is used for the description of optical contrail properties, measured vertically through the atmosphere. In the present case of treating the contrail by a Gaussian plume without defined boundaries, the optical thickness strongly depends on the contrail irradiated width. The larger the irradiated width, the smaller the optical thickness, because the share of photons traveling through the contrail core is reduced. This phenomenon is illustrated in Figure 7, where the optical thickness is shown for a contrail with optical and microphysical properties shown as described in Table 1.

Table 1: Contrail properties used in the Monte Carlo simulation assuming a strong turbulent environment with $\varepsilon = 10^{-4}$ m^2 s^{-3} and a contrail age of 20 hours.

Width for starting photons	$6\sigma_h = 10188$ m
Horizontal standard deviation	$2\sigma_h = 3396$ m
Vertical standard deviation	$2\sigma_v = 148$ m
Ice particle radius	$r_p = 10^{-5}$ m
Solar absorption efficiency	$Q_{abs,550\,nm} = 0.009$
Solar scattering efficiency	$Q_{sca,550\,nm} = 1.96$
Solar asymmetry parameter	$g_{550\,nm} = 0.74$

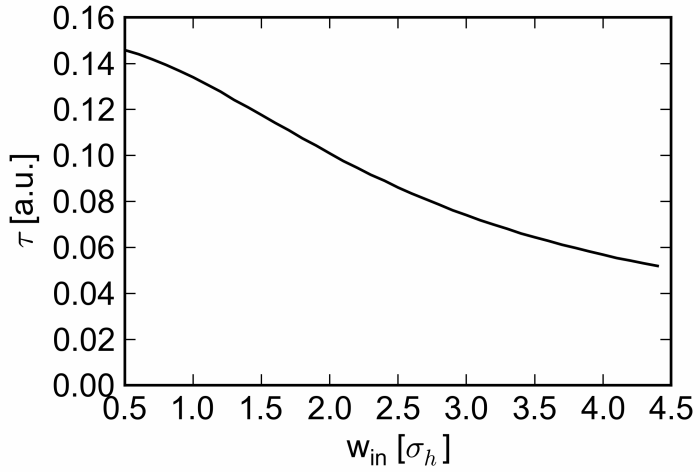

Figure 7: Optical thickness τ for vertical photon transport for a contrail with the same optical and microphysical properties as used in Table 1 as function of the irradiated width. Due to the definition of the contrail by a Gaussian plume, τ decreases with increasing irradiated width without converging to a constant value.

Hence, a comparison of the optical thickness is impossible unless the corresponding contrail width is published additionally, as done by Gounou et al. 2007, Forster et al. 2011 and Vázques-Navarro et al. 2015. This width can be interpreted as the irradiated width used in the current study. Hence, the number ratio of extinguished to evaluated photons, which is $S_{ext} = S_f + S_b + S_a$ can be used for comparison with other publications, if their optical thickness is multiplied with the contrail width. Forster et al. 2011 published values of the optical thickness of a nonsheared contrail for several contrail ages. These are multiplied with the corresponding contrail width and compared with the present weighted number ratios. The results are in the same order of magnitude (compare Table 2). Differences occur due to different atmospheres, unknown turbulence and different contrail ages.

Table 2: Comparison of weighted number ratios S_{ext} for a wavelength of $\lambda = 550$ nm of different ages of contrail lifetime with the product of mean optical depth and contrail width by Forster et al. 2011. The mean turbulent environment of $\varepsilon = 5 \cdot 10^{-5}$ m^2 s^{-3} is assumed.

Contrail width [m]	S_{ext} [m] Forster et al. 2011	Standard deviation [m]	S_{ext} [m] current study
960	223.6	778.5	342.5
1680	403.2	1078.5	453.0
2880	720.0	1330.3	585.3
4320	1036.8	1539.9	677.5
6000	1020.0	1718.9	739.1
6480	528.4	1976.7	889.5

The influence of the solar zenith angle on radiative extinction can be compared with Gounou et al. 2007 as well as with Forster et al. 2011. Here, the shape of the extinction depending on solar zenith angle should be similar to the results observed in the present study considering a single wavelength λ = 550 nm. Figure 8 shows the typical minimum of radiative forcing at solar zenith angles around $\theta \approx 70°$, although, direct and diffuse radiation are considered. A flight path along the North-South axis is chosen, even though no differences compared to the East-West contrail are detected, probably because diffuse and direct radiances are considered.

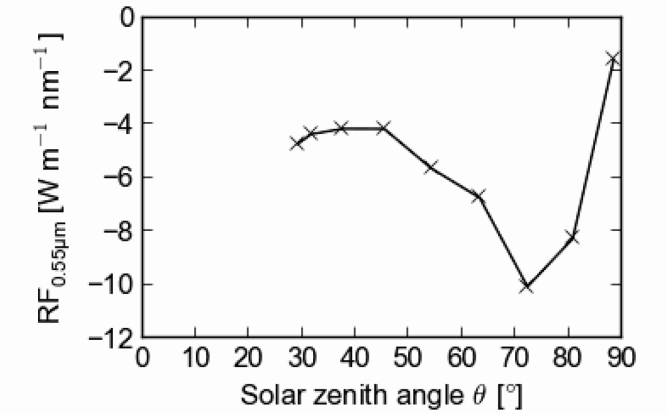

Figure 8: Radiative forcing at λ = 550 nm as function of the solar zenith angle θ for comparison with other works considering the optical properties of individual contrails depending on solar zenith angle. The shape of the curve is similar to the Figures 3 and 9 of Gounou et al. 2007 [35] as well as Figures 5, 6, 10 and 11 of Forster et al. 2011 [36].

To compare the estimated solar radiative forcing, radiative extinction is calculated for the contrail described in Table 3 again, over Berlin on 21st of June 2012, 12 a.m. with solar zenith angle θ = 29 ° and azimuthal angle φ = 2 ° and is integrated over 21 solar bands between wavelengths of λ = 275 nm and λ = 2200 nm.

Table 3: Contrail properties used in the Monte Carlo simulation of the whole solar spectrum assuming a mean turbulent environment with $\varepsilon = 5 \cdot 10^{-5}$ m2 s-3 and a contrail age of 20 hours.

Width for starting photons	$6\sigma_h = 9178$ m
Horizontal standard deviation	$2\sigma_h = 3059$ m
Vertical standard deviation	$2\sigma_v = 119$ m
Ice particle radius	$r_p = 9.6 \cdot 10^{-6}$ m

The scattering and absorption efficiencies are calculated according to Key et al. 2002 using parameterizations from Yang. Considering both, diffuse and direct solar radiation coming from all directions in space, a radiative forcing of $RF = 932.15$ W m^{-1} per meter contrail is calculated (the RF shown in Figure 9 is integrated). Although the estimation of the real contrail width is impossible, the result is divided by the assumed width of the contrail core, $2 \cdot \sigma_h = 3059.8$ m yielding a radiative forcing of $RF = 0.305$ W m^{-2}. The positive sign of that result seems surprisingly, however, considering a single wavelength $\lambda = 550$ nm, a negative RF occurs (compare Figure 8). Respecting the whole solar spectrum with relevant contributions of solar radiances results in a positive RF. For wavelengths $\lambda > 750$ nm diffuse upward radiances exceed diffuse downward radiances, probably because atmospheric absorption and reemission is already taking place. The increased absorption for these wavelengths in Figure 10 gives evidence for this green house effect. Hence, the amount of downward scattered and absorbed radiation exceeds upward scattered radiances and warm the atmosphere (compare Figure 10).

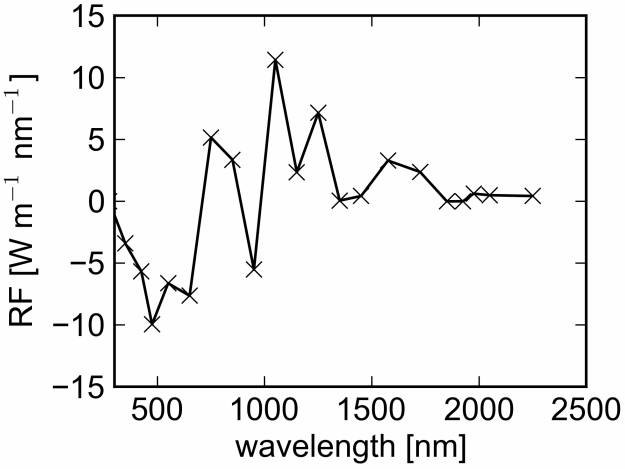

Figure 9: Solar wavelength specific radiative forcing per meter contrail and per nanometer for a contrail described in Table 3. For wavelengths $\lambda > 750$ nm radiative forcing is positive due to increased atmospheric absorption and reemission.

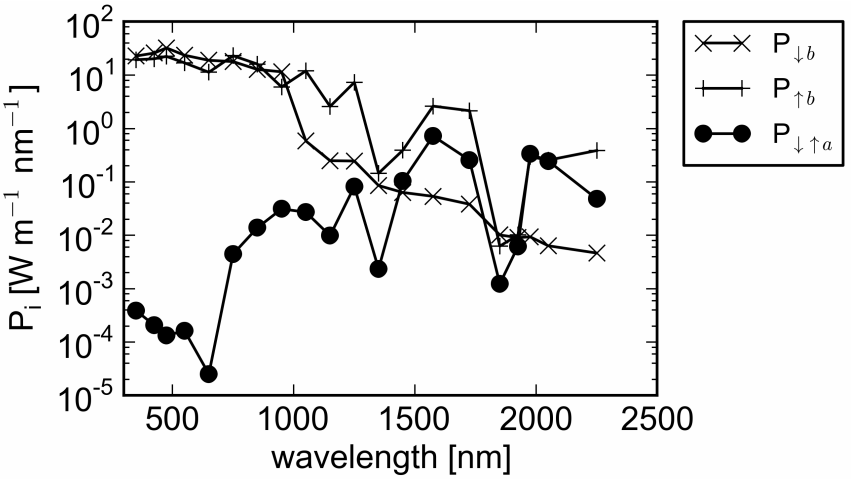

Figure 10: Wavelength specific upward scattered, downward scattered and absorbed powers per meter contrail and per nanometer for a contrail described in Table 3. For wavelengths $\lambda > 750$ nm downward scattered and absorbed radiances exceed upward scattered radiances, resulting in a positive radiative forcing (compare Figure 9).

4 DISCUSSION AND CONCLUSION

In this study, a model has been developed and tested, to calculate the angle dependence of solar radiative extinction due to an aircraft induced condensation trail. Thereby, multiple scattering had been considered and evaluated as not negligible for large solar zenith angles. The contrail is described by a Gaussian plume, allowing the continuous calculation of extinction through the contrail.

However, it does not give the exact dimensions of the contrail, complicating the determination of the optical thickness and the radiative forcing for comparison with other publication. Whenever possible, comparisons are done, and similar results are received. Differences in radiative extinction due to flight path and day time are shown, yielding first hints for air traffic management, to avoid flying during sunrise and sunset (large solar zenith angles) and when possible prefer flight paths along North-South, instead of East-West. The results can influence an airline network structure, when external costs are internalized. The consideration of diffuse and direct radiances, integrated over the solar spectrum show a positive radiative forcing over Germany, even on the longest day of the yea at noon. An advantage of the here developed approach is the combination of photon extinction calculations within the contrail (Monte Carlo simulations) with the results of the radiative transport calculations of the atmosphere (with LibRadtran) so that changes in day time or flight direction can be realized easily and without high computational costs.

REFERENCES

Appleman, H., 1953: The formation of exhaust condensation trails by jet aircraft, Bull. Amer. Meteor. Soc. 34, 14–20.

Brewer, A.W., 1946: Condensation trails. Weather 1, 34–40.

Burkhardt, U. and B. Kärcher, 2011: Global radiative forcing from contrail cirrus, Nature Climate Change 1, 54–58.

Corti, T. and T. Peter, 2009: A simple model for cloud radiative forcing, Atmospheric Chemistry and Physics 9, 5751–5758.

Forster, L., C. Emde, B. Mayer, and S. Unterstrasser, 2011: Effects of Three- Dimensional Photon Transport on the Radiative Forcing of Realistic Contrails, American Meteorological Society, 2243–2255.

Gounou A., and R. J. Hogan, 2007:A sensitivity study of the effect of horizontal photon transport on the radiative forcing of contrails, Journal of Atmospheric Sciences 64, 1706–1716.

Graf, K., U. Schumann, H. Mannstein, and B. Mayer, 2012: Aviation induced diurnal North Atlantik cirrus cover cycle, Geophysical Research Letters 39, L16804 (2012).

Hansen, J.E., M. Sato, and R. Ruedy, 1997: Radiative forcing and climate response, J. Geophysical Research 102, 6831–6684.

Holzäpfel, F., 2003: Probabilistic Two-Phase Wake Vortex Decay and Transport Model". Journal of Aircraft 40, 323-331.

Jeßberger, P., C. Voigt, U. Schumann, I. Sölch, H. Schlager, S. Kaufmann, A. Petzold, D. Schäuble, and F. G. Gayet, 2013: Aircraft type influence on contrail properties, Atmospheric Chemistry and Physics 13, 11965–11984.

Kaiser, M., 2015: Optimierung von Flugtrajektorien strahlgetriebener Verkehrsflugzeuge bei konkurrierenden SESAR Zielfunktionen mittels Entwicklung eines hochpräzisen Flugleistungsmodells, Dissertation, Technische Universität Dresden.

Key, J. R., P. Yang, B. A. Baum, and S. L. Nasiri, 2002: Parameterization of shortwave ice cloud optical properties for various particle habits. J. Geophys. Res. 107, 4181.

Lee, D.S., D. W Fahey, P. M. Forster, P. J. Newton, R. C.N. Witt, L. L. Lim, B. Owen, and R. Sausen, 2009: Aviation and global climate change in the 21st century, Atmospheric Environment 43, 3520–3537.

Marquart, S., 2003: Klimawirkung von Kondensstreifen: Untersuchungen mit einem globalen Zirkulationsmodell. Dissertation, University of Munich, Department of Physics.

Mayer, B., A. Kylling, C. Emde, U. Hamann, and R. Buras, 2011: libRadtran user's guide. Technical report, Technische Universität München.

Meerkötter, R., U. Schumann, P. Minnis, D. R. Doelling, T. Nakajima, and Y. Tsushima, 1999: Radiative forcing by contrails, J. Geophysical Research 17, 1080–1094.

Minnis, P., U. Schumann, D. R. Doelling, K. M. Gierens, and D. W. Fahey, 1999: Global distribution of contrail radiative forcing, Geophysical Research Letters 26, 1853–1856.

Myhre G. and F. Stordal, 2001: On the tradeoff of the solar and thermal infrared impact of contrails, Geophysical Research Letters 28, 3119–3122.

Myhre, G., D. Shindell, F.-M. Bréon, W. Collins, J. Fuglestvedt, J. Huang, D. Koch, J.-F. Lamarque, D. Lee, B. Mendoza, T. Nakajima, A. Robock, G. Stephens, T. Takemura, and H. Zhang, 2013: Anthropogenic and Natural Radiative Forcing. In: Climate Change 2013: The Physical Science Basis. Contribution of Working Group I to the Fifth Assessment Report of the Intergovernmental Panel on Climate Change, Cambridge University Press.

Ponater, M., S. Pechtl, R. Sausen, U. Schumann, and G. Hüttig, 2006: Potential of cyroplane technology to reduce aircraft climate impact: A state-of-the-art assessment, Atmospheric Environment 40, 6928–6944.

Petty, G.W., 2002: Area-Average Solar Radiative Transfer in Three-Dimensionally Inhomogeneous Clouds: The Independently Scattering CloudletModel". J. Atmos. Sci. 59, 2910–2929.

Ricchiazzi, P., S. Yang, C. Gautier, and D. Sowle. "SBDART: A research and Teaching software tool for plane-parallel radiative transfer in the Earths atmosphere", Bulletin of the American Meteorological Society 79, 2101-2114.

Rosenow, J., M. Kaiser, and H. Fricke, 2012: Modeling Contrail life cycles based on highly precise flight profile data of modern aircraft, International Conference on Research in Airport Transportation (ICRAT), Berkley

Sausen, R., I. Isaksen, V. Grewe, D. Hauglustaine, D. S. Lee, G. Myhre, M.O. Köhler, G. Pitari, U. Schumann, F. Stordal, and C. Zerefos, 2005: Aviation radiative forcing in 2000: An update on IPCC (1999). Meteorologische Zeitschrift 14, 555–561.

Schmidt, E,. 1941: Die Entstehung von Eisnebel aus den Auspuffgasen von Flugmotoren, Schriften der Deutschen Akademie der Luftfahrtforschung, Verlag R. Oldenburg, München/Berlin 44, 1–15.

Schultz, J., 1997: On the effect of cloud inhomogeneity on area averaged radiative properties of contrails, Geophysical Research Letters 25, 1427–1430.

Schumann, U., 1996: On conditions for Contrail formation from aircraft exhaust, Meteorologische Zeitschrift 5, 4–23.

Schumann, U., 2000: Influence of propulsion efficiency on contrail formation, Aerospace Science and Technology 4, 391–401.

Schumann, U., 2005: Formation, properties and climatic effects of contrails. C.R. Physique 6, 549–565.

Schumann, U. and K. Graf, 2013: Aviation-induced cirrus and radiation changes at diurnal timescales, Journal of Geophysical Research 118, 1–18.

Solomon, S., D. Quin, M. Manning, M. Marquis, K. Averyt, M. M. B. Tignor, H. L. Miller Jr., and Z. Chen, 2007: Climate change 2007: The Physical Science Basis. Cambridge University Press.

Stamnes, K., S.-C. Tsay, W. Wiscombe, and K. Jayaweera, 1988: Numerically stable algorithm for discrete-ordinate-method radiative transfer in multiple scattering and emitting layered media, Applied Optics 27, 2502–2509.

Sussmann, R. and K. M. Gierens, 2001: Differences in early contrail evolution of two-engine versus four-engine aircraft: Lidar measurements and numerical simulations. J. Geophysical Research 106, 4899–4911.

Vázquez-Navarro, M., H. Mannstein, and S. Kox, 2015: Contrail life cycle and properties from one year of MSG/SEVIRI rapid-scan images. Atmos. Chem. Phys. Discuss. 15, 7019–7055.

Wyser, K., D. Mitchell P. Yang, K. N. Liou. 2000: Parameterization of the scattering and absorption properties of individual ice crystals, Journal of Geophysical Research 105, 4699–4718.

Study of a contrail cluster observed during the ML-CIRRUS campaign

M. Vázquez-Navarro*, L. Bugliaro, U. Schumann, M. Wirth
DLR-Institut für Physik der Atmosphäre Oberpfaffenhofen, Germany

Keywords: Contrail cluster, cirrus, Meteosat, modelling, lidar

ABSTRACT: A contrail cluster has been probed with the HALO aircraft during the ML-CIRRUS campaign over Germany on 10 April 2014. This paper presents a synergistic analysis of this situation combining ACTA and COCS contrail and cirrus results from MSG/SEVIRI satellite retrievals, contrail cirrus model predictions (CoCiP) and airborne lidar optical depth measurements (WALES). ACTA has been extended to follow contrail clusters. The results give insight in the capabilities of the various methods. The contrail cluster formed in otherwise cloud-free air, lasted for more than 6 h, with optical depth up to 0.6.

1 INTRODUCTION

Aviation impacts climate through carbon dioxide, nitrogen oxides and aerosol emissions from aircraft. However, a larger impact is thought to come from the formation of persistent contrails and aviation-induced (or contrail) cirrus (Lee et al, 2009). Unfortunately, properties and radiative forcing of persistent contrails are difficult to determine because contrails spreading out to cirrus lose their typical linear shape and can thus hardly be identified as anthropogenic in their origin (Mannstein and Schumann, 2005). The net effect of contrails including contrail cirrus on the global scale is believed to be a small warming effect (Stocker et al, 2013). On the regional scale this effect can be much stronger. Especially clusters of spreading persistent contrails that can form in areas of heavy air-traffic and live for several hours can affect regional climate and have even the potential for producing a considerable fraction of the global radiative forcing due to persistent contrails (Haywood et al, 2009).

Here, we study a contrail cluster observed on 10 April 2014 during the Mid-Latitude Cirrus (ML-CIRRUS) campaign that took place in March-April over Europe with the HALO research aircraft HALO operated by DLR to investigate natural and anthropogenic cirrus clouds in mid latitudes. The contrail cluster under study was formed in the early morning over Northern France and drifted towards Belgium and Germany in the course of the day. We use three independent but complementary approaches. First, the cluster is observed using data from the SEVIRI radiometer aboard the Meteosat Second Generation (MSG) satellite (Schmetz et al, 2012). With its spectral channels in the solar and thermal spectral range and thanks to its high temporal resolution of 5 min in rapid scan mode it is possible to track the cluster and to derive the evolution of its optical properties. To this end, we apply the COCS algorithm (Kox et al, 2014) to the contrails detected by ACTA (Vázquez-Navarro et al, 2010) and to the contrail cluster pixels identified by an extended version of the ACTA algorithm. Second, to investigate the evolution of the cluster before it was observable with MSG/SEVIRI and the conditions that led to its formation, the CoCiP model (Schumann, 2012) was applied to this event. CoCiP is a Lagrangian model that simulates the lifecycle of contrails from their formation behind individual aircraft until final dissipation for given aircraft route information. Finally, for a quantitative evaluation of the contrail optical thickness derived from both MSG/SEVIRI and CoCiP, data from the WALES lidar installed in the HALO research aircraft was considered. DLR's WALES lidar (Wirth et al, 2009) is a multi-wavelength airborne instrument that performs water vapor DIAL (Differential Absorption Lidar) measurements at up to 4 wavelengths around 935 nm at the same time. Additional channels at 532 nm and 1064 nm allow for the characterization of aerosols and clouds. At 532 nm a High Spectral Resolution Lidar (HSRL) capability

* *Corresponding author:* Luca Bugliaro, DLR-Institut für Physik der Atmosphäre, Oberpfaffenhofen, D-82205 Wessling, Germany. Email: luca.bugliaro@dlr.de

(Esselborn et al, 2008) is implemented to allow for the collocated measurements of humidity and (cirrus) optical thickness.

The comprehensive approach presented here distinguishes this study from previous work devoted to contrail clusters (Minnis et al, 1998; Duda et al, 2004; Haywood et al, 2009, Laken et al, 2011; Minnis et al, 2013).

2 CONTRAIL DETECTION AND TRACKING

Contrails can be detected in satellite data exploiting their linear shape (Mannstein et al, 1999). When relative humidity over ice is high enough, linear contrails can evolve into cirrus clouds, so called contrail cirrus. This transition process can be observed with the ACTA algorithm (Vázquez-Navarro et al, 2010) that is able to track a given contrail, initially detected with in high spatial resolution satellite data like MODIS or AVHRR, using data from MSG/SEVIRI until it loses its typical linear shape.

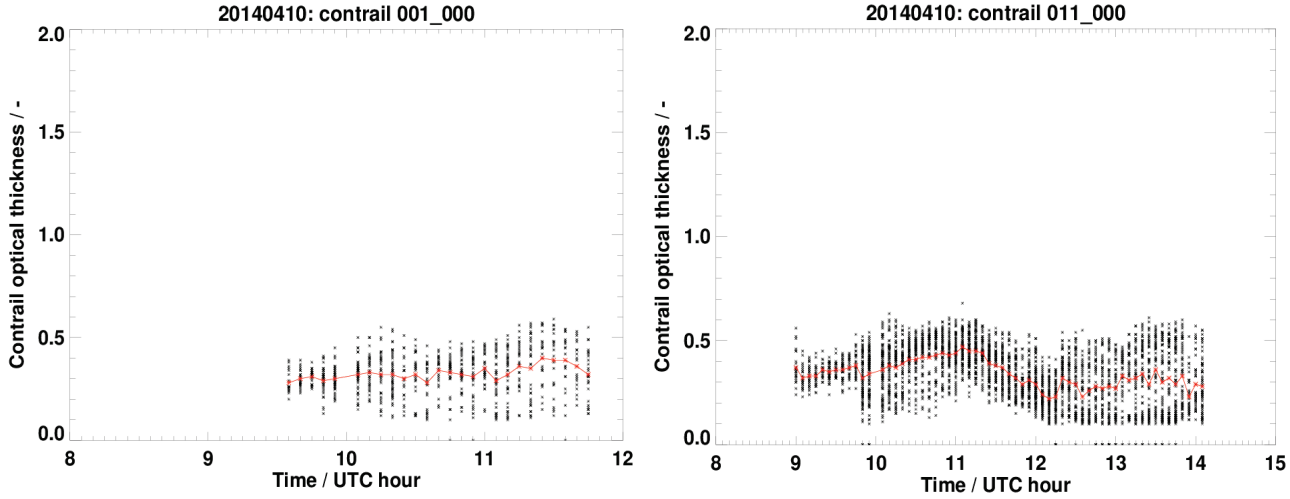

Figure 1: Temporal evolution of the contrail optical thickness for two selected contrails tracked by ACTA. Black crosses represent the values of the single pixels in one contrail at a particular time. The red line connects the mean optical thickness as a function of time.

In total, 12 contrails could be identified and tracked between 9:00 UTC and 14:05 UTC. Their lifetime was very heterogeneous, from 5 min (they could be identified and tracked in only two MSG/SEVIRI slots) to 5 h. Their optical thickness is determined using COCS (Kox et al, 2014). COCS is a neural network trained with MSG/SEVIRI brightness temperatures and brightness temperature differences (BTDs) to reproduce CALIPSO/CALIOP cirrus cloud optical thickness ("cirrus" includes all ice clouds). It shows that the contrail optical thickness was always smaller than 0.6, with mean values between 0.2 and 0.4. Figure 1 shows two examples of the long-lived contrails detected this way: Black crosses are the values of the single pixels in one contrail at a particular time, the red line represents mean optical thickness values of the contrail as a function of time. Please notice that the lower detection limit of COCS is set 0.1 here (the false alarm rate of COCS for optical thicknesses smaller than this value is high). Mean optical thickness of the contrail in the left panel of Fig. 1 remains constant at around 0.3 as a function of time. The contrail in the right panel of Fig. 1 has an optical thickness of 0.3 when it is first detected, increases to 0.5 at 11:05 UTC and decreases then again to 0.2 at 12:10 UTC and then remains approximately constant until 14:05 UTC. In both cases the scattering of the values around the mean seems to increase with time thus indicating that pixels of a single contrail can evolve quite differently: the second contrail, for instance, consists at the end of its lifetime (as determined by ACTA) of pixels with high optical thickness (>0.5) and pixels with optical thickness close to 0.1.

3 CONTRAIL CLUSTERS DETECTION AND TRACKING

After 14:00 UTC ca. the ACTA algorithm is no longer able to track the contrails because their linear structure is less remarkable due to spreading and overlap with other contrails. Instead, a contrail cluster can be observed where single contrails can no longer be easily identified. To further analyze the development of these contrails the tracking procedure must be deeply modified.

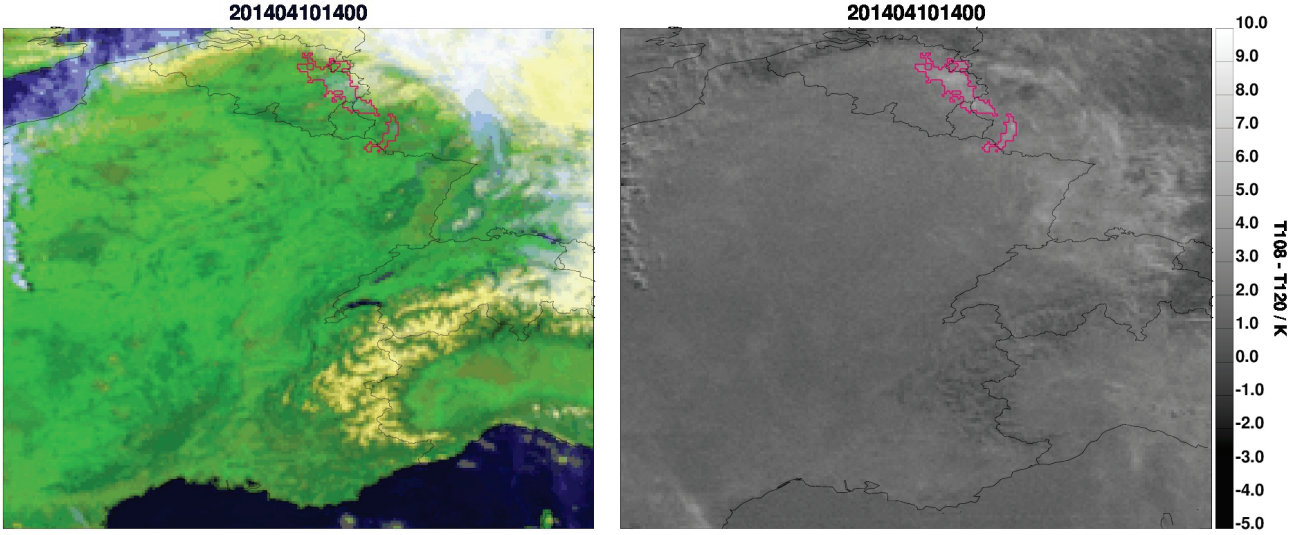

Figure 2: (left) RGB colour composite showing Central Europe. (right) BTDs between 10.8 and 12.0 µm in K for the same region as in the left panel. In both panels the cluster contours are plotted pink.

The new algorithm, called ACTA2 in this paper, is an algorithm designed for the tracking of thin cirrus clouds such as the cirrus clouds formed through the clustering of aged contrails. It is based on the usual 10.8 - 12.0 µm BTD. In the first image (which was already focused in space and time on the contrail cluster to be investigated), all pixels are identified where BTD > 1 K. Then, the largest connected region is selected to represent the contrail cluster. Further time steps recall the earlier position of the cloud and identify the same cloud through a combination of the following criteria: overlap (with the cloud detected on the previous image), size (the largest connected region) and BTD threshold. The BTD threshold for subsequent images is dependent on the previous maximum values (continuity of the BTD values). An example is shown in Figure 2: on the left hand side a false color composite depicts the region under investigation. This RGB image, where bluish/violet colors represent high and thin cirrus clouds, is produced by combination of solar and thermal information. The BTD between the SEVIRI channels centered at 10.8 and 12.0 µm (i.e. only thermal information) is shown on the right hand side together with the contours of the cluster that are provided by ACTA2. From this picture it is evident that a) thin cirrus is more clearly visible in thermal data alone and b) any linear structure is missing and c) that the cluster optical thickness is really low. Thus, it is clear that ACTA could not find any contrails after 14:00 UTC.

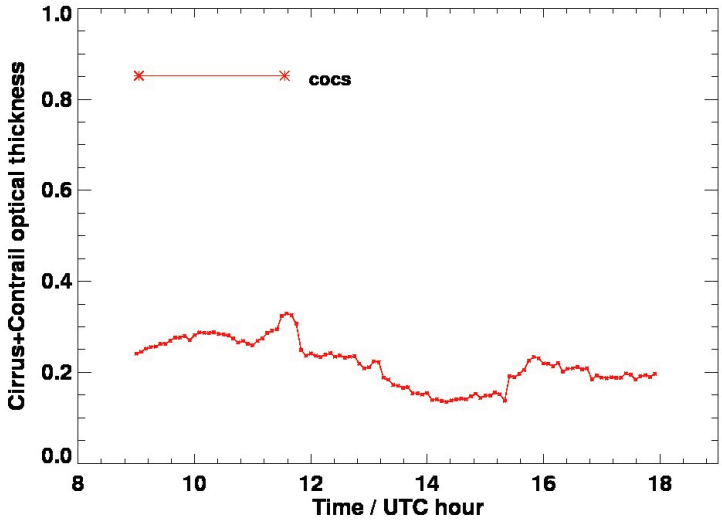

Figure 3: Temporal evolution of the mean contrail cluster optical thickness obtained with ACTA2 (tracking) and COCS.

As for ACTA (see Sect. 2), when the cluster has been identified, cloud optical thickness can be determined using COCS. To increase the response of COCS, we lower the detection limit of COCS from 0.1 to 0.05. Since the contrail cirrus pixels have been already identified by ACTA2, we reset the lower limit of COCS to 0.05 (from 0.1) to infer cloud optical thickness. Figure 3 shows the temporal development of the contrail cluster optical thickness from 9:00 UTC to 18:00 UTC ca. It can be seen that the tracking is possible now for a much longer period of time. The contrail cluster lives for 9 h approximately according to this procedure and counts to the longer lived contrails observed in Vázquez-Navarro et al, 2015. Its optical thickness varies between 0.15 and 0.35. Abrupt changes in optical thickness are mainly due, on one side, to the fact that from time to time new pixel areas with lower/higher optical thickness are added to the cluster by ACTA2; on the other side, COCS/ACTA2 might fail for portions of the cluster when their optical thickness is too low. In general, the cluster becomes optically thicker in the morning and reaches a first maximum at 10:00 UTC (0.3) and a second maximum at 11:45 UTC (0.35) before it starts becoming optically thinner again. The minimum optical thickness of 0.1 is reached ca. 14:15 UTC. Afterwards an increase up to 0.25 at 16:00 UTC is observed.

These values of the optical thickness are slightly smaller than those retrieved e.g. by Minnis et al (2013, optical thickness range: 0.32 - 0.43) and is located in the lower optical thickness range of the contrail cluster described by Duda et al (2004) over the Great Lakes (optical thickness range: 0.1 - 0.6).

4 CONTRAIL CLUSTER FORMATION AND EVOLUTION WITH COCIP

Contrail cirrus optical depth maps were computed using the Contrail Cirrus Prediction Model "CoCiP". CoCiP is a Lagrangian model which traces individual contrail segments forming along flight routes for given aircraft route information. CoCiP simulates the lifecycles of contrails from their formation behind individual aircraft until final dissipation. The model uses ambient meteorology fields (temperature, humidity, wind etc. as functions of pressure in space and time) input from numerical weather prediction (NWP) analysis data. The model is described and discussed in Schumann (2012), with recent changes and validation results in Schumann et al (2015).

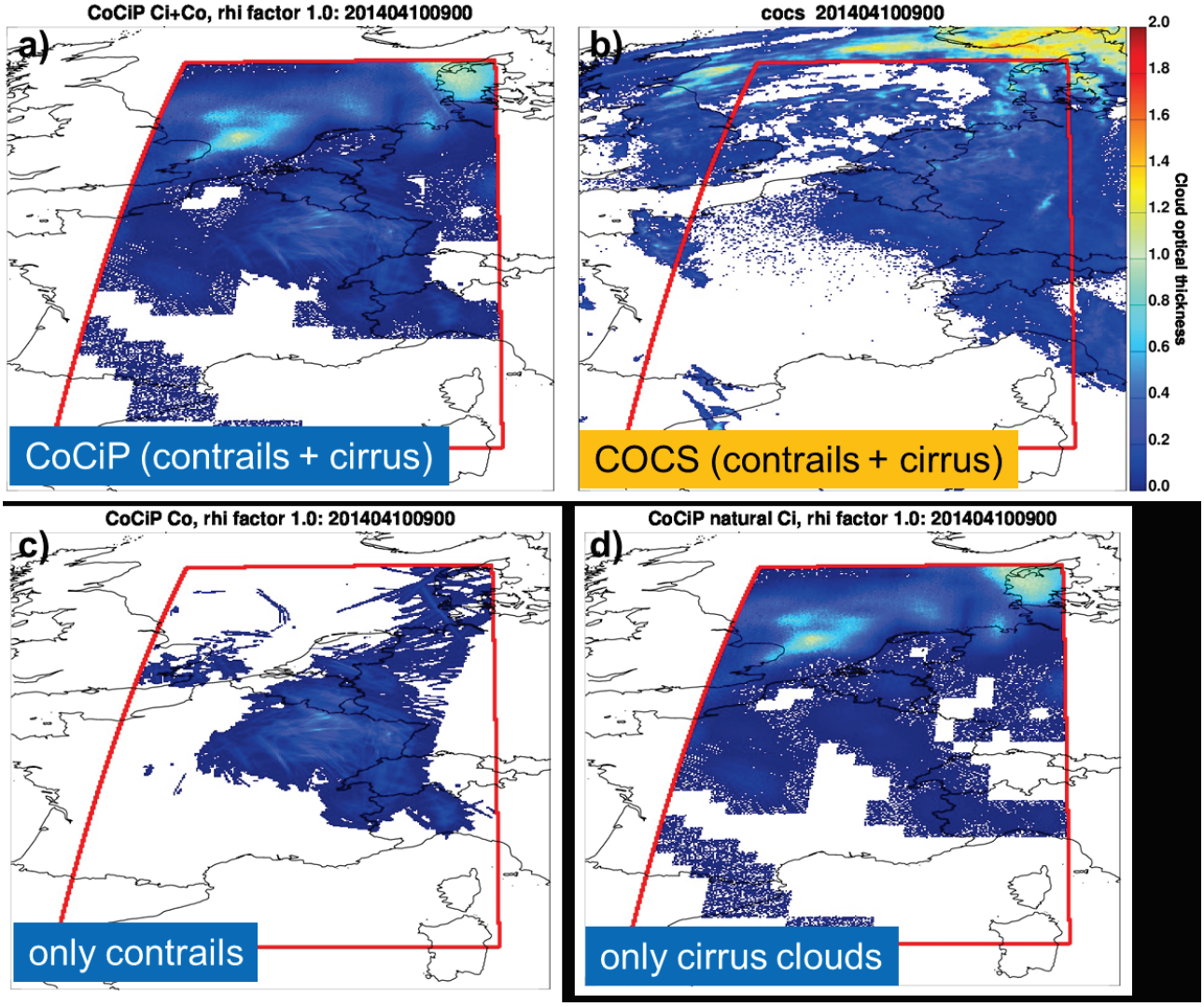

Figure 4: Optical thickness (at 550 nm) of cirrus from observation (COCS) and computation (CoCiP) at 9 UTC 10 April 2014. a) Computed contrail cirrus. b) Observed cirrus. c) Computed contrails only. d) Computed background cirrus only.

The NWP data for ML-CIRRUS were provided by the Integrated Forecast System (IFS) of the European Center for Medium Range Weather Forecasts (ECMWF). The NWP data have 1 h time resolution, combining 6-h analysis data with hourly forecast data starting from these analyses. The data used cover the ML-CIRRUS domain (60°W to 20°E, 20°N to 70°N) with 0.5° horizontal resolution and 137 vertical levels. The specific simulations used for comparison with COCS on 10 April 2014 start at 0 UTC 9 April 2010, allowing for the development of aged contrails. The absolute humidity provided by the NWP output to CoCiP is increased by a factor 1/RHic to allow for subgrid scale cirrus formation. The analyses are run with RHic=1 except for parameter studies. The model runs in its offline mode for given NWP data, without changing ambient humidity when contrails form (Schumann et al, 2015).

Table 1: Traffic data used for CoCiP-COCS comparisons of 10 April 2014

Acronym	Description
ADSB	Ground based ADS-B (Automatic Dependent Surveillance – Broadcast) transponder data from FlightRadar24
DFS	Upper air German air space radar data from DFS (Deutsche Flugsicherung)
UK	Radar data for British air space from EUROCONTROL

The air traffic data specify the aircraft type, and the sequence of waypoints in space and time of routes flown by each individual aircraft. Here we use a combination of observed aircraft movement data as specified in Table 1. Aircraft type data (wing span, mass, fuel consumption) are estimated

using BADA data from EUROCONTROL as explained in Schumann (2012). The fuel specific parameters (combustion heat and water emission index) are set for kerosene. The soot number emission index is set to 0.357×10^{15} kg^{-1}, consistent with the earlier CoCiP applications (Schumann and Graf, 2013; Schumann et al, 2013).

From the numerical simulation, CoCiP generates output every 5 min in the form of longitude-latitude maps of optical depth (at 550 nm) of contrails alone or of the sum of contrails and cirrus clouds ("cirrus" includes all ice clouds). The optical depth includes contributions from all individual contrails depending on the distance between the center line of contrails and the map coordinates on a fine grid with 940×2550 longitude×latitude grid cells in the domain 0-10°E, 40-57°N. This spatial resolution of about 1 km fits much better to the satellite data spatial resolution of approx. 3 x 5 km^2 over Central Europe. The optical depth of cirrus is computed based on the vertical integral of extinction above 6 km altitude, extinction is computed for given cirrus ice water content from the NWP input and an effective radius (Schumann et al, 2011). The effective radius of cirrus particles is estimated as in the ECMWF IFS using an empirical function of temperature and ice water content (Sun and Rikus, 1999). These optical thickness maps from CoCiP are used for comparison with the optical depth derived with COCS from MSG/SEVIRI. The computed optical depth of contrails is sensitive to the model parameters, in particular to the ambient humidity provided by the NWP data (modified by the parameter RHIc) and the soot emissions index (Schumann et al, 2013).

The comparison of CoCiP optical thickness for all cirrus clouds (Fig. 4a) with the corresponding COCS optical thickness from MSG/SEVIRI (Fig. 4b) at 09:00 UTC shows a good correlation with a similar but slightly phase shifted cloud pattern, Southern France and the Mediterranean being free of cirrus. Single contrails are visible in both panels, CoCiP predicts them over North Eastern France, in COCS data they can be found further in the North East. Considering contrail cirrus in Fig. 4c and natural cirrus in Fig. 4d one can observe that cirrus cover in Easter Switzerland and North West of Switzerland is almost exclusively due to air traffic. This is confirmed by the temporal evolution of the cloud field (not shown) as computed by CoCiP. It can also be observed that the contrail cluster is advected in the correct direction. However, the optical thickness of CoCiP contrails appears to be slightly larger than the observed one.

5 VALIDATION OF CIRRUS OPTICAL THICKNESS WITH WALES

The HALO aircraft flew through the contrail cluster investigated in this study in the afternoon of April 10, 13:30-16:30 UTC, and performed in-situ and remote sensing measurements in the context of the ML-CIRRUS campaign. In particular, the HALO flew a remote sensing leg for lidar observations between 15:49 and 16:02 UTC. During this time, cirrus optical thickness was derived using the HSRL channel at 532 nm (Esselborn et al, 2008) of the DLR Water vapor lidar WALES (Wirth et al, 2009). After collocation of the airborne measurements with the MSG/SEVIRI pixels in space and time including parallax correction, the cirrus optical thickness was compared as shown in Fig. 5. Since the cirrus optical thickness is very low in this case (see red lines in Fig. 5), the lower limit of COCS was reduced from 0.1 to 0.05. This is justified by the fact that cirrus detection is in this case trivial since all pixels sensed by the lidar were cirrus pixels. This way, the sensitivity of COCS in such a low optical thickness range could be investigated. It turns out that the shape of the WALES (red) and COCS (blue) curves is very similar although maxima and minima do not always perfectly correspond in time (please notice that there might be a temporal shift of at most 2.5 min between the two instruments). Due to its higher sensitivity, WALES can also measure cirrus cloud optical thickness down to 0.01, in contrast to COCS. Nevertheless, COCS optical thicknesses are in the correct range for this episode. Comparing to the temporal evolution of the contrail cluster in Sect. 3, one sees that HALO was flying above a rather thin portion of the cluster, whose mean optical thickness at this time was larger than 0.3 (according to COCS and ACTA2).

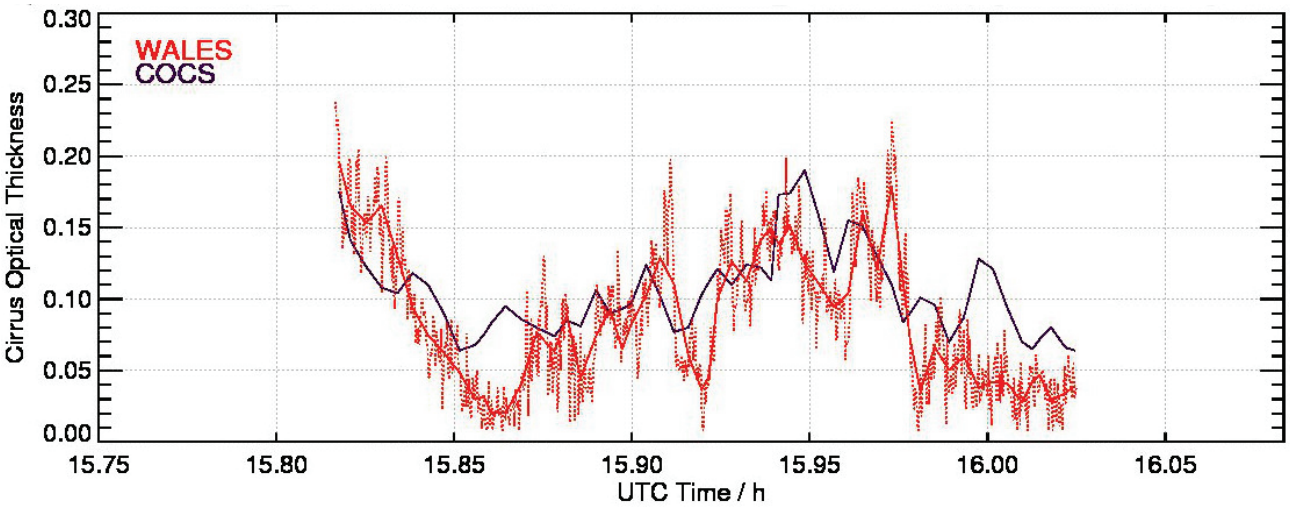

Figure 5: Comparison of the cirrus optical thickness from WALES (red) and the COCS algorithm (blue). The red dotted lines represents the local lidar result with high spatial and temporal resolution, the red solid curve shows the pixel-mean value of the cirrus optical thickness in collocated MSG/SEVIRI pixels.

For CoCiP a comparison to WALES data for the same 23-min-period is shown in Fig. 6. For this plot only contrail cirrus optical thickness is considered because it was emphasized above that the cloud is of anthropogenic origin (in fact, cirrus optical thickness vanishes over the HALO flight path). Lower values of RHIc correspond to higher relative humidity in the CoCiP model and thus to higher optical thicknesses. The CoCiP data shows high sensitivity to relative humidity, especially for thin cirrus clouds. The comparison is hindered by the fact that the cloud sensed by WALES is located at another position in the CoCiP model field than in reality due to the phase shift of the prediction, and by the shortness of the lidar flight leg. After a steep decrease, where RHIc=1.1 turns out to be too low, CoCiP optical thickness remains low from 15:51 to 15:54 UTC (between 0 and 0.2). In this part of the leg it is hard to spot the RHIc factor that best fits the measurements. From 15:54 to 15:57 UTC CoCiP optical thickness increases again, together with WALES optical thickness, and the RHIc=1.0 factor seems to best fit the data. After 15:57 UTC the cloud characteristics are definitely different in the model data w.r.t. to measurements since all CoCiP optical thicknesses strongly increase to values around or above 1.0 while WALES always shows values below 0.22. From the two-dimensional spatial distribution of the optical thickness field over the entire area processed with CoCiP (not sown) the RHIc factor 1.0 appears to produce the best overall agreement with COCS, whose good agreement with WALES is shown in Fig. 5. Thus, under the meteorological and cirrus conditions of 10 April 2014, CoCiP results compare best with COCS and WALES results for RHIc=1.0. A model overestimate in optical depth may be caused by too high values of the humidity used by CoCiP or too many soot particles causing contrail-ice nucleation.

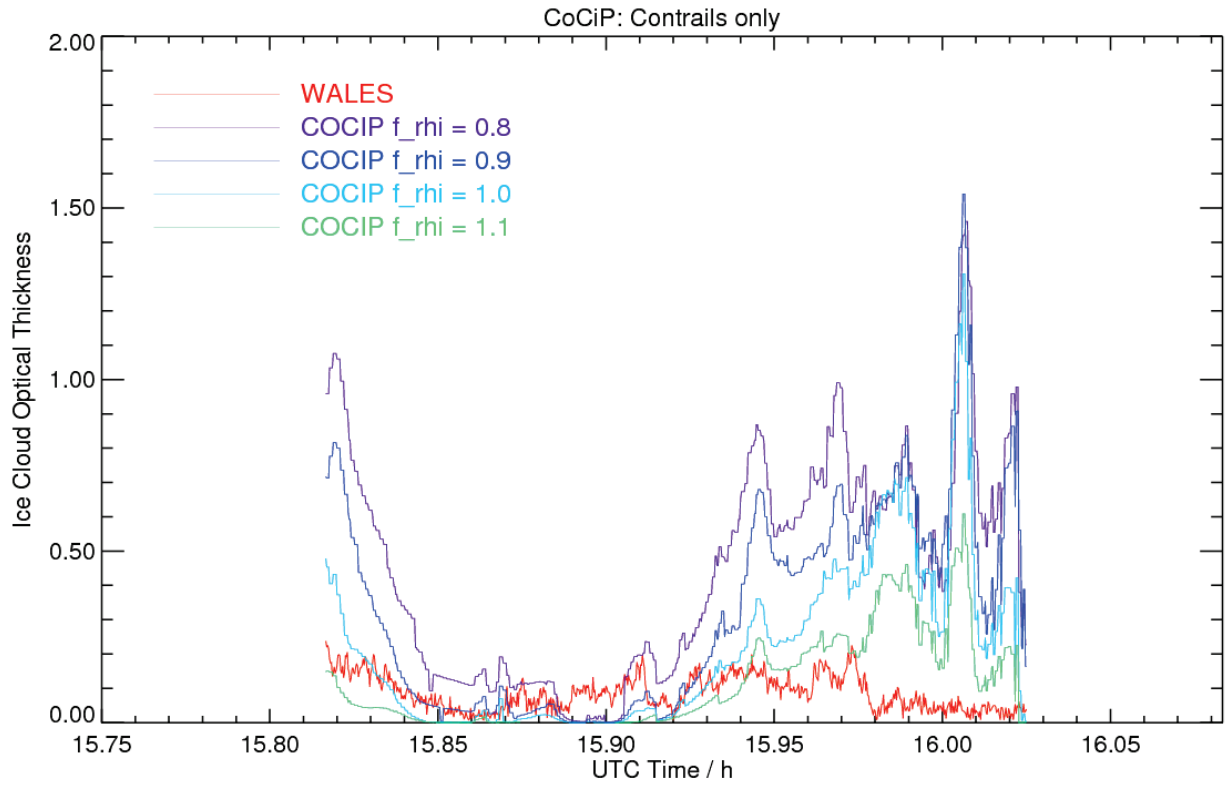

Figure 6: Contrail-cirrus optical thickness from CoCiP for four different values of f_rhi=RHIc (blueish colored lines), and cirrus optical thickness from WALES (red line).

6 CONCLUSIONS

The tracking of the contrail cluster on 10 April 2014 using the novel ACTA2 algorithm shows a cluster composed of 12 contrails with mean optical thickness up to 0.6 and lifetime of 9 h, . Modelling results using CoCiP suggest that this cluster is of anthropogenic origin and consists of contrails forming in essentially cloud free air mass. The forecast skills of the model are good in general but the simulated optical thickness is too high in this case when compared to airborne HSRL lidar measurements. The satellite retrieval COCS is able to discriminate such small optical thicknesses (0.05 - 0.22) in remarkably good comparison with the lidar measurements.

REFERENCES

Duda, D. P., P. Minnis, L. Nguyen, and R. Palikonda, 2004: A case study of the development of contrail clusters over the Great Lakes. J. Atmos. Sci, 61, 1132–1146.

Esselborn, M., M. Wirth, A. Fix, M. Tesche, and G. Ehret, 2008: Airborne high spectral resolution lidar for measuring aerosol extinction and backscatter coefficients, Appl. Opt. 47, 346–358, doi: 10.1364/AO.47.000346.

Haywood, J. M., R. P. Allan, J. Bornemann, P. M. Forster, P. N. Francis, S. Milton, G. Rädel, A. Rap, K. P. Shine, and R. Thorpe, 2009: A case study of the radiative forcing of persistent contrails evolving into contrail-induced cirrus. J. Geophys. Res. 114, D24201, doi:10.1029/2009JD012650.

Kox, S., L. Bugliaro, and A. Ostler, 2014: Retrieval of cirrus cloud optical thickness and top altitude from geostationary remote sensing. Atmos. Meas. Tech. 7, 3233–3246, doi:10.5194/amt-7-3233-2014.

Laken, B. A., E. Pallé, D. R. Kniveton, C. J. R. Williams, and D. A. Kilham, 2012: Contrails developed under frontal influences of the North Atlantic. J. Geophys. Res. 117, D11201, doi:10.1029/2011JD017019.

Lee, D. S., Fahey, D. W., Forster, P. M., Newton, P. J., Wit, R. C. N., Lim, L. L., Owen, B., and Sausen, R., 2009: Aviation and global climate change in the 21st century, Atmos. Environ. 43, 3520–3537, doi:10.1016/j.atmosenv.2009.04.024.

Mannstein, H. and U. Schumann,2005: Aircraft induced contrail cirrus over Europe, Meteorol. Z. 14, 549–554, doi:10.1127/0941-2948/2005/0058.

Mannstein, H., R. Meyer, and P. Wendling, 1999: Operational Detection of Contrails from NOAA-AVHRR-Data. Int. J. Remote Sens. 20, 1641–1660.

Minnis, P., D. F. Young, D. P. Garber, L. Nguyen, W. L. Smith, and R. Palikonda, 1998: Transformation of contrails into cirrus during SUCCESS. Geophys. Res. Lett. 25(8), 1157 – 1160, doi:10.1029/97GL03314.

Minnis, P., S.T. Bedka, D. P. Duda, K.M. Bedka, T. Chee, J.K. Ayers, R. Palikonda, D.A. Spangenberg, K.V. Khlopenkov, and R. Boeke, 2013: Linear contrail and contrail cirrus properties determined from satellite data. Geophys. Res. Lett. 40, 3220–3226.

Schmetz, J., P. Pili, S. Tjemkes, D. Just, J. Kermann, S. Rota, and A. Ratierk, 2002: An introduction to Meteosat Second Generation (MSG), Bull. Am. Meteorol. Soc. 83, 977–992.

Schumann, U., B. Mayer, K. Gierens, S. Unterstrasser, P. Jessberger, A. Petzold, C. Voigt, and J.-F. Gayet, 2011: Effective radius of ice particles in cirrus and contrails. J. Atmos. Sci. 68, 300-321, doi: 10.1175/2010JAS3562.1.

Schumann, U., 2012: A contrail cirrus prediction model. Geosci. Model Dev. 5, 543–580, doi: 10.5194/gmd-5-543-2012.

Schumann, U., and K. Graf, 2013: Aviation-induced cirrus and radiation changes at diurnal timescales. J. Geophys. Res. 118, 2404-2421, doi: 10.1002/jgrd.50184.

Schumann, U., P. Jeßberger, and C. Voigt, 2013: Contrail ice particles in aircraft wakes and their climatic importance. Geophys. Res. Lett. 40, 2867-2872 doi: 10.1002/grl.50539.

Schumann, U., J. E. Penner, Y. Chen, C. Zhou, and K. Graf, 2015: Dehydration effects from contrails in a coupled contrail-climate model. Atmos. Chem. Phys. 15, in press, 2015.

Stocker, T.F., D. Qin, G.-K. Plattner, M. Tignor, S.K. Allen, J. Boschung, A. Nauels, Y. Xia, V. Bex, and P. M. Midgley, 2013: Climate change 2013: The physical science basis, Intergovernmental Panel on Climate Change, Working Group I Contribution to the IPCC Fifth Assessment Report (AR5)(Cambridge Univ. Press, New York).

Sun, Z., and L. Rikus, 1999: Parametrization of effective sizes of cirrus-cloud particles and its verification against observations, Q. J. R. Meteorol. Soc. 125, 3037-3055.

Vázquez-Navarro, M., H. Mannstein, and B. Mayer, 2010: An automatic contrail tracking algorithm, Atmos. Meas. Tech. 3, 1089–1101, doi:10.5194/amt-3-1089-2010.

Vázquez-Navarro, M., H. Mannstein, and S. Kox, 2015: Contrail life cycle and properties from 1 year of MSG/SEVIRI rapid-scan images. Atmos. Chem. Phys. 15, 8739-8749, doi:10.5194/acp-15-8739-2015.

Wirth, M., A. Fix, P. Mahnke, H, Schwarzer, F. Schrandt, and G. Ehret, 2009: The airborne multiwavelength water vapor differential absorption lidar WALES: system design and performance, Appl. Phys. B 96, 201–213, doi:10.1007/s00340-009-3365-7.

Simulating Contrails with COSMO-ART Based on Real Time Flight Tracks

S. Gruber*, B. Vogel, H. Vogel
Institute of Meteorology and Climate Research, KIT, Germany

J. Bechtold, M. Jung, H. Pak
Institute of Air Transport and Airport Research, DLR, Cologne, Germany

Keywords: contrails, COSMO-ART, ADS-B, two moment scheme, regional scale

ABSTRACT: Condensation trails (contrails) from aircrafts are among the most obvious indications showing anthropogenic activities impacting the atmosphere. A parameterization to simulate the formation and life cycle of contrails has been implemented into the high resolution regional numerical model system COSMO-ART (Baldauf et al., 2011; Vogel et al., 2009).
Depending from the Schmidt-Appleman criterion (Schumann, 1996), that decides whether the environmental conditions are favorable for the formation of contrails, the parameterization computes additional ice water content and number concentrations. The following life cycle, consisting of processes like advection, deposition of water vapor and sublimation is described using the two moment cloud microphysical scheme of Seifert and Beheng (2006), in which the new parameterization scheme is embedded. This method allows also the treatment of so called contrail cirrus that is basically aged contrails which more and more develop into wide spread and optical thin cirrus.
A basic data set provided by the German Aerospace Center - Institute of Air Transport and Airport Research contains the spatial and temporal high resolved trajectories of a limited number of sample flights over Central Europe.
First model results are compared with satellite pictures for the simulated days. Besides the conditions for formation and the life cycle of contrails and contrail cirrus, the influence on the upper troposphere cloud coverage of these man-made clouds over Germany is examined.

1 INTRODUCTION

Besides the modification of profiles for radiative active gases like carbon dioxide and nitric oxides by direct emissions, air traffic causes changes in the microphysical and optical properties of high level clouds by contrails (Schumann, 1996) and the indirect aerosol effect (Hendricks et al., 2005). The latter two phenomena are not well understood till now, but nevertheless quite easily to observe. They occur mostly in the upper troposphere and lower stratosphere. In both areas, that are, apart from this, quite pristine, important processes influencing the radiative budget of the atmosphere take place, as they offer favorable conditions for cirrus clouds.

Contrails, contrail cirrus and contrail induced cloudiness influence the radiative budged in a way that is comparable to thin natural cirrus clouds (Sausen et al., 2005). But important properties like the optical depth or the spatial and temporal extent of occurrence is still not investigated well enough and also not quantified. It is assumed, that the influence of aged contrails and contrail induced cirrus is of a stronger importance than the one originating from young, line shaped contrails (Eleftheratos et al., 2007).

Former studies mainly used global circulation models to simulate line shaped and aged contrails e.g. (Marquart et al., 2003). The global influence can be examined, although averaging in time and area is required. In this context, a global mean of contrail coverage of 0.1 - 2 % seems to be negligible (IPCC, 2013). But still, there are estimations for situations with up to 10 % for example over Central Europe. Compared to a globally mean radiative forcing of about 6 – 15 mW m^{-2}, local impacts of more than 300 mW m^{-2} seem to be possible (Burkhardt and Kärcher, 2011).

* *Corresponding author:* Simon Gruber, Institute of Meteorology and Climate Research, Karlsruhe Institute of Technology (KIT), D-76344 Eggenstein-Leopoldshafen, Germany. Email: simon.gruber@kit.edu

Another group of projects calculates single contrails with large-eddy models (Lewellen et al., 2001; Unterstrasser, 2014). Here, the process of forming and the vortex dynamics are represented fairly exact. Parameter studies allow investigating how and under which conditions contrails are persistent and how microphysical and optical properties change during a contrail life cycle. An obvious drawback of this method is that it is not applicable on a larger spatial area.

The here presented study combines both approaches. The regional atmospheric model COSMO-ART (Baldauf et al., 2011; Vogel et al., 2009) is used, that allows besides high spatial and temporal resolution also the treatment of processes that deal with the influence of aerosols and trace gases. The model is extended by a parameterization based on recent results from large-eddy-simulations (Unterstrasser, 2014; Schumann, 2012) for taking into account the formation of contrails.

2 DATA SET

For testing the developed methods, one single day was picked because of its relatively high density of contrails combined with apart from this, mostly cloud-free conditions (Fig. 1 (a)). Despite of a thick band of clouds over the North- and Baltic Sea, lots of line shaped contrails and diffuse cirrus clouds can be seen. Especially the last mentioned consist to a large extent of contrail induced cloudiness, as shown later.

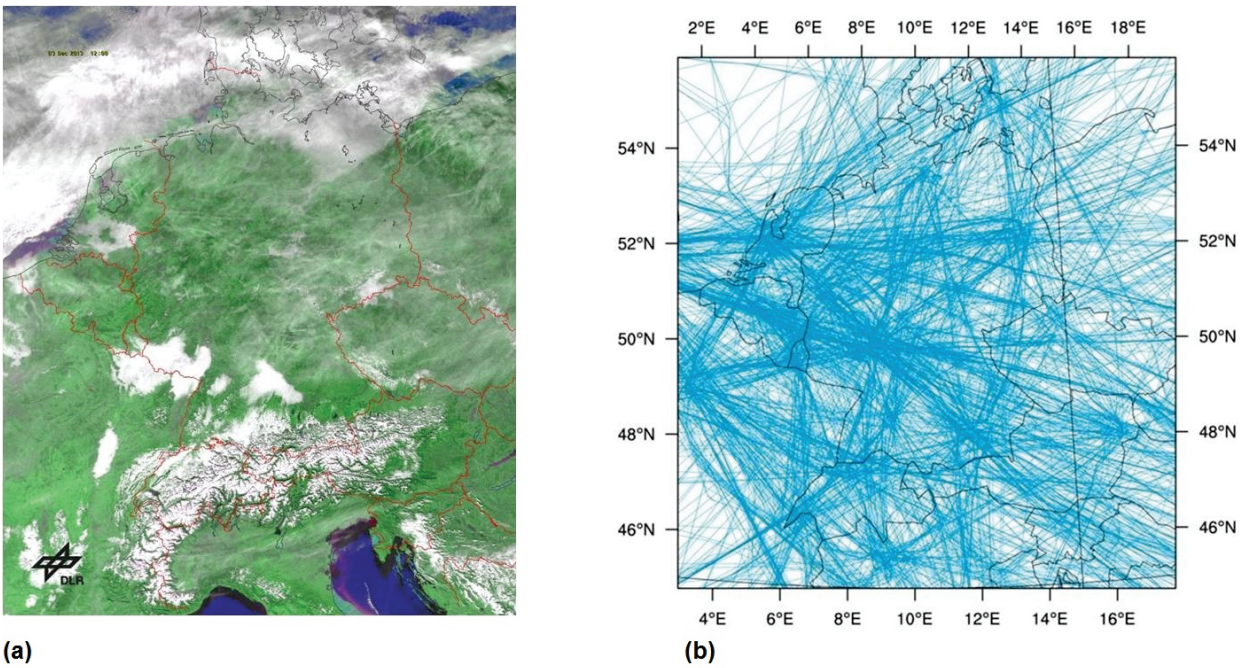

FIGURE 1: (a) Satellite product for Central Europe, 3 December 2013, 12 UTC; (b) Trajectories generated from ADS-B data for the COSMO-DE domain, 3 December 2013, 08 UTC – 16 UTC.

Compared to many global modeling studies, this project uses a new kind of data set. Instead of statistical calculations for globally averaged fuel consumption (Ferrone, 2011), the basic data consists of exact flight trajectories, available over a limited area, that are recorded from real time based data (flightradar24, 2015) and provided by the Institute of Air Transport and Airport Research, DLR, Cologne, Germany. In Fig. 1 (b), all read in trajectories are depicted.

The simulation takes place on the COSMO-DE domain, with a horizontal grid size of 2.8 x 2.8 km and 80 vertical levels. As meteorological boundary data, COSMO reanalysis are used.

3 METHODS

The regional non-hydrostatic atmospheric model COSMO-ART (Consortium for Small Scale Modeling, Aerosol and Reactive Trace Gases) with a coupled scheme for the cloud microphysics that uses a two moment approach (Seifert and Beheng, 2006) serves as base to this study. For a better representation of the special characteristics of young contrails, that is at first the small particle di-

ameters and the large number densities, their microphysical processes are treated separately from the natural cloud ice, yet still allowing the possibility for the different classes for cloud ice and contrails to interact with each other. As the contrails microphysics is embedded in the cloud scheme and thus being calculated online, a diagnostic treatment of the relevant processes is avoided.

At first, the Schmidt-Appleman-Criterion (Schumann, 1996) is checked. Depending on environmental pressure and temperature, various parameters affected by engine type and burned fuel, a critical temperature TLC can be calculated in such a way, that environmental temperatures lower than TLC force the mixing of exhaust plume and environmental air to produce supersaturation. In case of lower temperatures, the model allows the formation of a contrail for the distinct grid point at the current time step.

The developed parameterization then provides source terms for contrail ice by following in large parts the contrail prediction model CoCiP (Schumann, 2012). First, using Eq. 1, initial ice mass and numbers are generated:

$$IWC_0 = IWC_A(\dot{m}_F) + q_V - q_{SAT} \quad N_0 = IWC_0 / m_0 \tag{1}$$

Here the entire amount of water vapor causing local supersaturation ($q_V - q_{SAT}$) is converted into contrail ice. An additional source IWC_A considers the impact of the flying aircraft itself. As the engine burns a certain amount of fuel, additional water vapor is set free, quantitatively depending mainly from the fuel flow $\dot{m}_F$. Hence, this term may vary for different engines. The initial number of ice crystals is calculated by assuming a constant diameter ($d_0 = 1$ µm) for the very young particles.

Afterwards, the crystal loss in the wake of the aircraft is taken into account by Eq. 2. Owing to adiabatically warming (ΔT_{AD}) by a sinking movement in the downstream vortex, a certain part of particles (ΔIWC_V) sublimates. The strength of this downwash process depends from vertical velocity (w) and stratification (NBV). Dilution caused by extension of the contrail diameter also reduces the concentration, where also a slight growing of the particles is assumed (Eq. 3).

$$IWC_C = IWC_0 - \Delta IWC_V(\Delta T_{AD}, w, N_{BV}) \tag{2}$$

$$N_C = n_0 f^{1.1}; f = IWC_C / IWC_0 \tag{3}$$

4 RESULTS

The computed ice water path (IWP) for the simulated day at 12 UTC is compared in Fig. 2. In Fig. 2 (a), the IWP of the reference run, that is, without the new contrail parameterization, is displayed. Fig. 2 (b) shows the entire IWP for a simulation with the parameterization switched on. Here, natural IWP as well as additional contributions from contrails, contrail cirrus and contrail induced cloudiness in general is included. Parts of the visible but rather blurred cirrus cloud coverage over Germany and Eastern Europe in Fig 1 (a) is strongly intensified when applying the parameterization. Also, certain patterns like the cirrus over the center of Germany and the high-level cloudiness located south of the Alps seem to be caused by contrails and the resulting contrail cirrus.

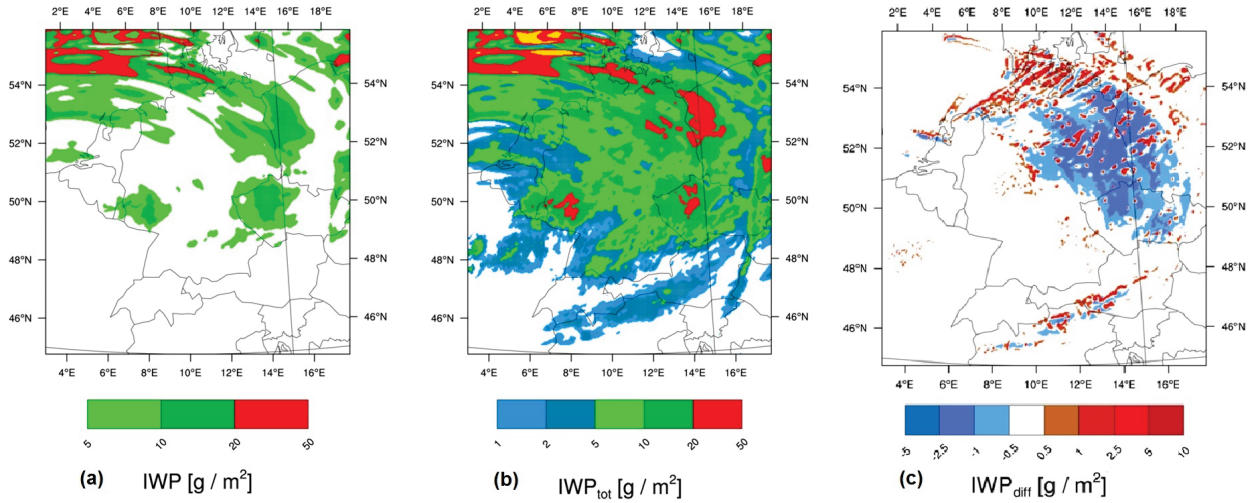

FIGURE 2: 3 December 2013, 12 UTC: Ice water path from the reference simulation (a), for a simulation with contrails (b) and difference in natural ice water path for simulation with and without contrails (c).

The contrail microphysics is treated separately from the one for the natural ice phase, but nonetheless, feedbacks are possible. For example, both hydrometeor classes can compete for the available water vapor. The difference in natural IWP at 12 UTC for two simulations is displayed in Fig. 2. (c) The values from the reference run are subtracted from the results of the simulation with the parameterization switched on. Natural IWP means here, also contrail ice exceeding a certain threshold mass is taken into account, as those crystals are of a circus-like size and occur in a similar number density. Shown here is therefore the quantitative influence of contrails on natural cirrus clouds. The line-shaped structures, depicted in red, consist of additional ice particles that originally occurred in contrails but grew in such an extent, that their mass is comparable to natural crystals. Negative values in blue indicate a reduction in natural cloudiness because of existing contrails. As contrails and contrail cirrus contain water vapor, that now cannot neither be transported nor serve to form cirrus. Compared to the IWP of the reference run in Fig. 2 (a), the additional contrail cirrus reaches IWP up to 10 g m^{-2} and is of a thickness equal to thin natural cirrus.

Concerning their microphysical properties, contrails differ strongly from natural clouds. For the simulated contrail ice in the layer of 10.000 m height at 10 UTC, Fig. 2 shows in (a) the ice water content (IWC), in (b) the particle number density (N) and in (c) the volume radius (r_V). The maximum contrail age here is two hours. At this time, they still consist of lots of very small ice crystals. The number density lays on average above 100 cm^{-3}, whereas the calculated particle radii, with values varying between 1 and 5 µm are about one order of magnitude underneath what is observed in natural cirrus.

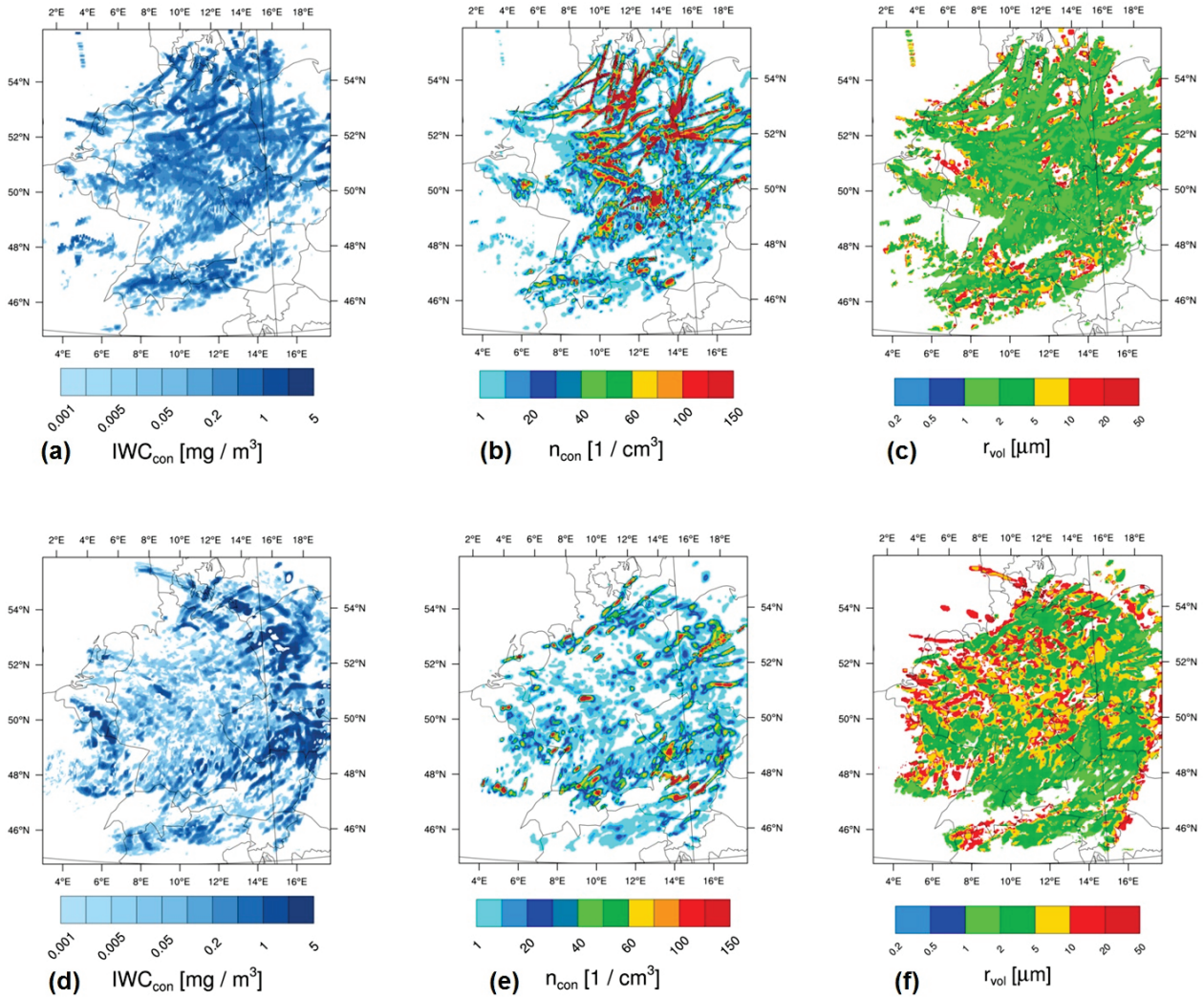

FIGURE 3: 3 December 2013: Properties of young and aged contrails, top row: 10 UTC, 10 300 m, bottom row: 13 UTC, 9 500 m; left: ice water content, center: particle number concentration, right: volume radius.

In Fig. 1 (c) to (d), the same variables like (a) to (c) are depicted, but now with values for three hours later. Therefore, some contrails are up to five hours old and find themselves in a phase of transition to contrail cirrus. Comparing (a) and (d), only small changes in the ice water content are

observed. Obviously, because of the persistent supersaturation with respect to ice over large areas, no significant loss of mass happens. In contrast, the number density decreases strong in (e). As a consequence, the mean particle radii grow about one order of magnitude in (f) compared to (c). This is to be explained with various microphysical processes like diffusional and depositional growth.

5 CONCLUSIONS AND OUTLOOK

Modeling contrails for short time spans on the regional scale brings advantages. Using flight trajectories based on real time is prerequisite for validation. Furthermore, the online coupled microphysics allows examining feedback mechanisms between cloudiness of natural and anthropogenic origin. It was shown, that the model configuration is able to simulate the local occurrence of contrails as well as their life cycle and their influence on natural cirrus clouds.
Partly, the existence of the cirrus-like clouds observed in satellite pictures can only be explained by considering aviation induced cloudiness. A significant change in high level cloud coverage, both positive and negative occurs when taking contrails and contrail cirrus into account.
The presented study is a framework to do some first tests on the developed parameterization. In a further step, the radiative impact of contrails and contrail cirrus is to be investigated. Because of the high spatial and temporal resolution, this project can serve as a base to improve the predictability of the solar radiation budget modified by contrails and contrail cirrus. This gains a certain importance when it comes to estimate the amount of produced energy from photovoltaic systems.

REFERENCES

Baldauf, M., A. Seifert, J. Forstner, D. Majewski, M. Raschendorfer and T. Reinhardt, 2011: Operational convective-scale numerical weather prediction with the COSMO model: description. Mont. Weather Rev. 139, 3887 - 3905.

Burkhardt, U., and B. Kärcher, 2011: Global radiative forcing from contrail cirrus. Nat. Clim. Change 1(1), 54 - 58.

Eleftheratos, K., C. Zerefos, P. Zanis, D. Balis, G. Tselioudis, K. Gierens, and R. Sausen, 2007: A study on natural and manmade global interannual fluctuations of cirrus cloud cover for the period 1984-2004, Atmos. Chem. Phys. 7, 2631 - 2642.

Ferrone, A., 2011: Aviation and climate change in Europe: from regional climate modelling to policy-options, Prom. : van Ypersele, Jean-Pascal.

flightradar24.com, 2015: http://www.flightradar24.com, 02.09.2015.

Hendricks, J., B. Kärcher, U. Lohmann, and M. Ponater, 2005: Do aircraft black carbon emissions affect cirrus clouds on the global scale?, Geophys. Res. Lett, 32.

Lewellen, D., and W. Lewellen, 2001: The effects of aircraft wake dynamics on contrail development, J. Atmos. Sci., 58(4), 390 - 406.

Marquart, S., M. Ponater, F. Mager, and R. Sausen, 2003: Future development of contrail cover, optical depth and radiative forcing: Impacts of increasing air traffic and climate change, J. Clim., 16(17), 2890 - 2904.

Myhre, G., D. Shindell, (...), and H. Zhang, 2013: Anthropogenic and Natural Radiative Forcing. In: Climate Change 2013: The Physical Science Basis. Contribution of Working Group I to the Fifth Assessment Report of the Intergovernmental Panel on Climate Change, Cambridge University Press, Cambridge, United Kingdom and USA.

Sausen, R., I. Isaksen, V. Grewe, D. Hauglustaine, D. Lee, G. Myhre, M. Köhler, G. Pitari, U. Schumann, F. Stordal, et al. , 2005: Aviation radiative forcing in 2000: An update on IPCC (1999), Meteorol. Z., 14(4), 555 - 561.

Schumann, U., 1996: On conditions for contrail formation from aircraft exhausts, Meteorol. Z., NF 5, 4 - 23.

Schumann, U., 2012: A contrail cirrus prediction model, Geosci. Model Dev., 5, 543 - 580.

Seifert, A. and K. D. Beheng, 2006: A two-moment cloud microphysics parameterization for mixed-phase clouds. part 1: Model description, Meteorol. Atmos. Phys., 92, 45 - 66.

Unterstrasser, S., 2014: Large-eddy simulation study of contrail microphysics and geometry during the vortex phase and consequences on contrail-to-cirrus transition, J. Geophys. Res. Atmos., 119, 7537 - 7555.

Vogel, B. H. Vogel, D. Bäumer, M. Bangert, K. Lundgren, R. Rinke and T. Stanelle, 2009: The comprehensive model system COSMO-ART - Radiative impact of aerosol on the state of the atmosphere on the regional scale, Atmos. Chem. Phys., 9, 8661 - 8680.

Contrail predictions for ML-CIRRUS – Method and Experiences

U. Schumann*, K. Graf, L. Bugliaro, A. Dörnbrack, C. Voigt, M. Wirth, H. Ziereis
DLR, Institut für Physik der Atmosphäre, Oberpfaffenhofen, Germany

A. Giez, A. Minikin
DLR, Flugexperimente, Oberpfaffenhofen, Germany

Keywords: Numerical weather prediction, Contrails, Climate, Weather

ABSTRACT: A contrail cirrus prediction method was set up for quasi-operational campaign planning during the ML-CIRRUS project. This paper describes the method and an example of predictions in comparison to satellite data. We found that contrail cirrus can be forecast to some useful degree. Comparisons to remote sensing and in-situ data have been used for validation; details are to be described elsewhere.

1 INTRODUCTION

Cirrus ice clouds and aircraft-induced contrails influence Earth climate and weather. Still, predictions of cover, life time, thickness, and weather and climate impact of such clouds are uncertain (Voigt et al., 2010). Accurate contrail-cirrus predictions are also essential for mitigation of the climate impact of contrails cirrus from aviation by selecting routes with minimum contrail cirrus climate impact (Grewe et al., 2013). For all these purposes, better prediction methods are needed. This requires improved understanding and models validated by high-quality observations.

Existing flight planning tools provide online access to horizontal maps and vertical cross-sections of numerical weather prediction data, including maps of the Schmidt-Appleman threshold temperature distribution (Rautenhaus et al., 2012). However, the amount and life times of contrails depend on a variety of meteorological and air traffic parameters, and require more specific prediction tools therefore.

The Mid-Latitude Cirrus Experiment ML-CIRRUS was performed to investigate natural and anthropogenic cirrus with a suite of in-situ and remote sensing instruments for airborne measurements on the research aircraft HALO operated by DLR (Voigt et al., 2015).

Therefore, we implemented the recently developed Contrail Cirrus Prediction model CoCiP into an existing quasi-operational flight planning environment. This paper describes briefly the methods used, some comparisons to satellite data and report on some of the experiences obtained. A detailed comparison with the suite of HALO data has still to be done.

2 METHOD

2.1 *Forecasts*

CoCiP is a Lagrangian model which traces individual contrail segments forming behind aircraft along given flight routes for given ambient meteorology. CoCiP simulates the lifecycles of contrails from their formation behind individual aircraft until final dissipation. The model is described and discussed in Schumann (2012). CoCiP has been applied in various previous studies, e.g. Schumann and Graf (2013). Recent changes and validation results are described in Schumann et al. (2015).
CoCiP requires input on the expected meteorology and air traffic in the forecast region and period, and the properties of the aircraft used.

Here, the forecast region is the ML-CIRRUS domain (60°W to 20°E, 20°N to 70°N). Forecasts are generated every 12 h during a 4-week period in March/April 2014. Each forecast covers a peri-

* *Corresponding author:* Ulrich Schumann, DLR-Institut für Physik der Atmosphäre, D-82205 Oberpfaffenhofen, Germany. Email: ulrich.schumann@dlr.de

od of 3.5 days with 1 h time resolution.

The required meteorological fields include three-dimensional fields of wind, temperature, humidity, ice water content, and cloud cover as a function of pressure, horizontal position, and time. In addition, two-dimensional fields are needed for surface pressure, outgoing longwave radiation, reflected shortwave radiation, and incoming solar direct radiation. CoCiP interpolates in these fields linearly in space and time to obtain the values at any position.

The NWP data for ML-CIRRUS were provided by the Integrated Forecast System (IFS) of the European Center for Medium Range Weather Forecasts (ECMWF). The NWP forecast data are available with 1 h time resolution. The data used cover the ML-CIRRUS domain with 0.5° horizontal resolution and 137 vertical levels of which 25 levels (69 to 83) cover the static pressure interval in which contrails form (~130-450 hPa) . Within CoCiP, the absolute humidity provided by the NWP output to CoCiP is increased by a factor 1/RHic to allow for subgrid scale contrail cirrus formation. The forecast are run with RHic=0.8 to make sure that no contrail is missed. This may lead to some overestimation of contrail cover and contrail optical depth which the user has to take into account. The model runs in an offline mode for given NWP data, without changing ambient humidity when contrails form (Schumann et al., 2015).

CoCiP simulates contrail segments for each flight from departure until arrival for a maximum life time, set to 12 h in these forecasts. As a consequence, the first 12 hours of contrail forecast may miss older contrails.

Air traffic is defined by input to CoCiP, including the aircraft type, and the sequence of waypoints of routes flown in space and time by each individual aircraft in the forecast domain. Since we have no operational air traffic forecast for the coming days available, forecast are run with "historical" air traffic data, here for the year 2006, as obtained from the Aviation and Climate Change Research Initiative (ACCRI) project (Wilkerson et al., 2010; Brasseur et al., 2015).

For each aircraft type, the aircraft parameters influencing contrail formation are to be known. Wing span and average operational aircraft mass are estimated using BADA data from EUROCONTROL. The fuel consumption is computed inside CoCiP for given aircraft type as a function of flight level, speed and mass. The emission indices for water vapor and heat are well known for kerosene. The number of soot particles emitted from aircraft contributing to ice nucleation in contrails is not well known. Here, we use a fixed approximate soot number emission index EISOOT= 3.57×10^{14} kg^{-1}. The so-called overall propulsion efficiency, as needed for the Schmidt-Appleman criterion, is estimated from the BADA data for typical fuel consumption and thrust values. It varies between 0.2 and 0.4.

From the contrail simulation results and from the NWP input data, CoCiP generates hourly output in two forms of longitude-latitude maps of optical depth (at 550 nm): one for contrails alone, and one for the combination of contrails and cirrus, i.e., contrail cirrus. In these computations, cirrus is defined by the ice water content from the NWP data above 4.5 km altitude. The map of optical depth is computed on a fine grid with 1200×1000 longitude×latitude grid cells (about 5 km horizontal resolution) and includes contributions from cirrus and from all contrails in the neighborhood contributing to the optical depth at a grid point . The optical depth of contrails is computed from the sum of the contributions from each contrail. For each contrail, the optical depth along the center line of the contrail is computed as a function of ice particle number and mean effective cross-section of contrail ice particles. The contribution of a contrail to a grid point depends on a Gaussian function of the distance between both relative to the contrail width. For cirrus, the optical depth of cirrus is computed as the vertical integral of extinction, here above 4.5 km altitude. The cirrus extinction is computed for NWP-given cirrus ice water content using an effective radius (Schumann et al., 2011). The effective radius of cirrus particles is estimated consistent with the ECMWF IFS from an empirical function of temperature and ice water content (Sun and Rikus, 1999).

The hourly maps of optical depth of contrails and of contrail-cirrus are made available for experiment planning as part of the DLR mission support tool in the internet, extending earlier developments (Rautenhaus et al., 2012; Voigt et al., 2010).

2.2 *Post-Mission Analysis*

After the campaign, a data base of realistic air traffic data has been setup from various sources, and CoCiP was rerun with hourly ECMWF-NWP data including assimilated observation data. These NWP data are a combination of 6-h analysis data with hourly forecast data starting every 12 h from

the analysis at 0 and 12 UTC. The forecast data include radiation and cloud cover values which were missing in the analysis output. Checks have shown that the forecast data are roughly consistent with the analyses data at the 6-h-analysis time intervals. However, the H_2O mixing ratio interpolated in 6-h analysis data differs by up to 15 % from the forecast results. As a consequence, the 6-h analysis data tend to underestimate relative humidity and cirrus formation. This is a consequence of the nonlinear pressure-temperature relationship for saturation. We also checked whether linear or logarithmic interpolation vertically in pressure gives better results. We found that both give similar results, and use linear interpolation for simplicity.

For illustration, Figure 1 shows the backward trajectories of air parcels arriving at the HALO aircraft flight route positions during the ML-CIRRUS science flights, with colored lines identifying trajectories of air parcels with high humidity. The trajectories were computed by integrating the advection equation of an air parcel backward in time using bi-linearly space-time interpolated wind from the forecast data and a second-order Runge-Kutta scheme in time for 600 s time step. The 24-h backward trajectories cover the full ML-CIRRUS domain. Hence, the domain size is just large enough for analysis of this experiment. The trajectories for air with high relative humidity are shorter. Hence, contrail analysis could be done on a smaller domain, but analysis of tracers (nitrogen oxides and soot, e.g.) result from emissions over the whole domain (and beyond).

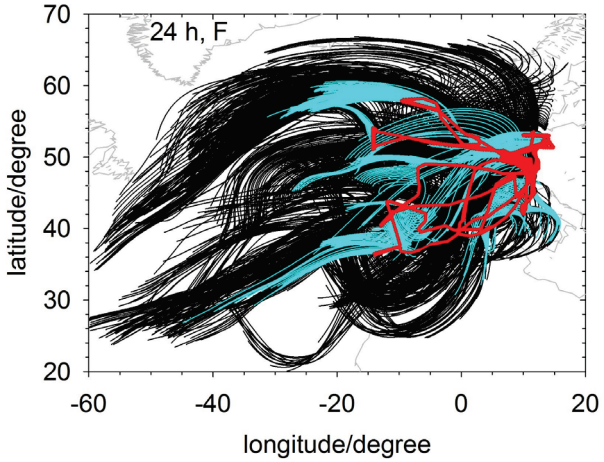

Figure 1. 24-h backward trajectories (black) from HALO positions (red) and backward trajectories in air masses with relative humidity over ice (RHi) exceeding 90 % (cyan).

As explained, accurate traffic data are essential input required for CoCiP. Unfortunately, a single comprehensive source of aircraft data for the ML-CIRRUS domain (mainly Europe and North Atlantic) is not available. Instead, one has to search, collect, buy, combine and mix scattered traffic data from various sources in an approximate manner. For ML-CIRRUS, waypoint data were obtained from various sources as shown in Table 1.

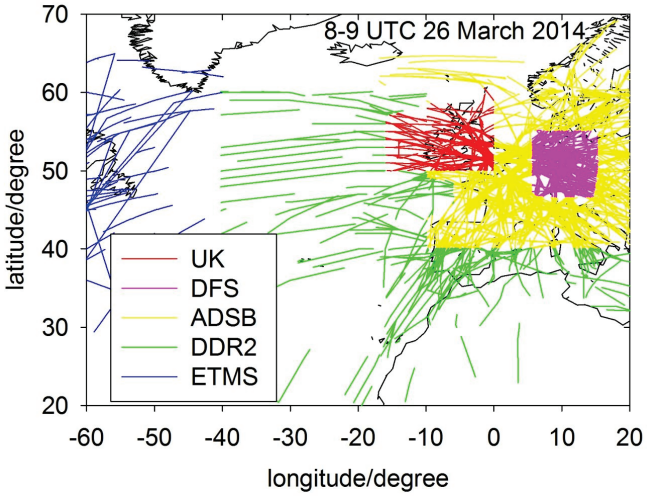

Figure 2. Traffic data combination from various sources in the ML-CIRRUS domain. Example for traffic during one hour (8-9 UTC 26 March 2014).

Table 1. Traffic data used for forecast or analysis during ML-CIRRUS

Acronym	Description	Time period
ACCRI	Global historical waypoint data from a combination of observations and simulations for 2006 as provided by FAA/VOLPE within the Aviation Climate Change Research Initiative (ACCRI) project	2006
ADSB	Ground based Automatic Dependent Surveillance – Broadcast (ADS-B) transponder data, collected and delivered by FlightRadar24	25 March – 15 April 2014
ETMS	Enhanced Traffic Management System (ETMS) product of the Federal Aviation Administration (FAA), used here to define the traffic west of 40°W over the North Atlantic between North America and UK	22 March – 16 April 2014
DDR2	Demand Data Repository version 2 (DDR2) service data, from EUROCONTROL, containing a mixture of flight plan and radar observation data for Europe, including in and outgoing international traffic, used to complete the traffic over Europe.	24 March – 14 April 2014
DFS	Upper air space data from Deutsche Flugsicherung (DFS), for German air space	18 March – 15 April
UK Radar	Eurocontrol radar data for the British air space	25-26 March and 10-11 April

We are grateful to the support of all the data providers from FAA, VOLPE, DFS, EUROCONTROL, and Flightradar24.

The accuracy of the traffic data was checked by comparing HALO positions reported in these sources with the position measured onboard HALO. The DFS data, for example, were found to be highly accurate (better than 100 m horizontally and 50 m vertically) but limited to the German air-space. Similarly, UK Radar data are accurate but limited to British air space and available for a few days only. The ADSB data are also accurate when available, but it is not clear how far the data cover routes near the oceanic coasts; in a few cases timing errors have been noted (local instead of universal time). The ETMS data cover well the northern part of the North Atlantic, but miss the Shannon radar control zone data. Hence, we use a hand-woven mixture of data as shown for example, in Figure 2.

3 OPERATIONS EXPERIENCES AND VALIDATION EXAMPLES

Before and during the mission, CoCiP was run twice a day to provide 3.5-d forecasts of contrail cover, using operational ECMWF forecasts at 0 and 12 UTC and historical traffic data. The forecast output was made available in an internet tool for experiment planning.

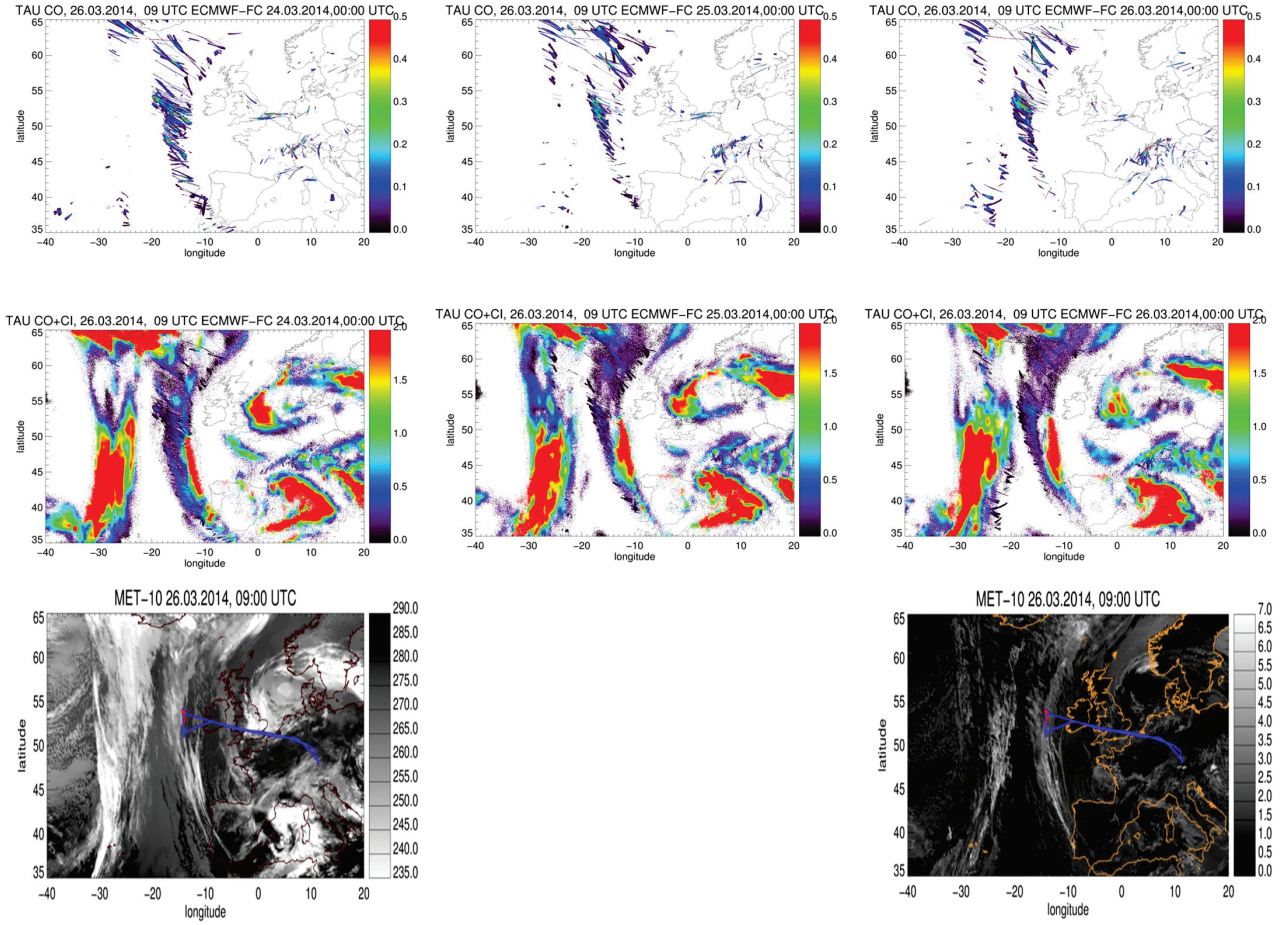

Figure 3. Maps with about 3-, 2-, and 1-day forecast of optical depth (at 550 nm, color scales identify values between 0 and 2) of contrails (top panel) and contrail cirrus (middle), compared to Meteosat-SEVIRI IR brightness temperatures (bottom left, grey scales) at 10.8 µm and from 10.8-12 µm difference (bottom right) at 9 UTC 26 March 2014. The blue lines in the lower panels follow the HALO flight track this day.

For example, starting 22 March and persisting in the early morning of 24 March 2014, ECMWF-IFS driven CoCiP predictions suggested that good observation conditions for contrail cirrus were to be expected near the eastern end of the Oceanic traffic corridor across the North Atlantic near Shannon (9°W, 53°N) during the morning hours of 26 March 2014. The weather at that time was controlled by a warm conveyor belt between 10°W and 35°W transporting humidity from the lower atmosphere in the subtropical North Atlantic north up to about 60°N near Iceland and from there southward towards Ireland. The belt caused an elongated cirrus band. The upper troposphere was predicted to contain ice supersaturated air masses. For the expected traffic in the flight corridor, many long-lived contrails should form. The late morning period (8:30-12 UTC) was of interest because the low traffic density at this time allows for flights in North-South direction across the corridor under Shannon Radar control with the chance to observe aged contrails that were generated during the early morning hours (3-8:30 UTC) drifting with the mean wind from about north into the control zone. Because of radar control limitations, HALO was allowed to operate in that region only east of 14 °W. Based on this information, and in view of the project objective of aged contrail cirrus observations, it was decided to prepare for the first ML-CIRRUS science mission flight with HALO for this occasion.

The coming days were exciting because we had little experience to assess the reliability of the newly implemented forecast method. (A noteworthy contrail outbreak was predicted and observed in satellite data over the North Atlantic already on the afternoon of 25 March 2014.) Some intermediate results indicated the risk that HALO could just miss cirrus because cirrus formation conditions might be low east of 14°W but better further west. However the last predictions as of the morning of 26 March 2014 confirmed the first prediction obtained 2 or even 3 days earlier in that contrail cirrus should be observable between 10°W and 14 °W at the latitude of Shannon, where HALO should operate.

At about 10 UTC 26 March, it became clear that the forecast quality was excellent. The mission scientists reported that HALO was indeed measuring in and above cirrus and young and aged contrails. Figure 3 includes MSG-SEVIRI satellite pictures. The lower left panel clearly shows white areas in the 10.8 µm infrared brightness temperature (BT), indicative for high thick cirrus clouds. The lower right panel with 10.8-12 µm BT difference is sensitive to thin cirrus clouds with many small ice particles, as to be expected for contrail cirrus. Indeed the figure shows line patterns oriented in about east-west direction and local maxima in the BT values, indicating the presence of aged contrail cirrus lines (possibly from many aircraft flying the same route) and thin cirrus with many small ice particles. These observations verify the validity of the contrail cirrus predictions, at least for this case.

Experiences during the coming weeks made it obvious that the one- and two-day contrail forecasts are persistent with often only small differences. The predictions formed a reliable source for general mission planning. Still, most recent forecasts and satellite observations results were transmitted via satellite link to the crew for onboard campaign optimization.

CoCiP was also used to compute contrail, cirrus and trace concentrations, and vertical extinction profiles along the HALO flight paths. The model results are included in the HALO mission data bank. The results are available for comparison to in-situ data. The data are also useful for identifying aircraft and other sources for measured air properties.

The predictions have been compared with HALO observation data from lidar (Gross et al., 2015) (see Figure 4), with satellite data from COCS (Figure 5), and from many in-situ measurements (partly preliminary results) (Voigt et al., 2015). Comparisons to satellite data (Vázquez-Navarro et al., this conference) allowed quantifying the contrail cirrus predictability. The correlation between optical depth of predicted and observed cirrus (including contrails) is of the order 70 % for 3.5-day predictions on average over the whole ML-CIRRUS domain and period with notable reductions during a period with high dust load. Comparisons to vertical lidar backscatter profiles were sometimes in good agreement but by far not always. Variations of the humidity in the model (parameter RHic) show that the comparisons to lidar are highly sensitive to the relative humidity predictions. Comparisons to nitrogen oxides measurements show that dilution of emissions for aircraft are reasonably well simulated in CoCiP. Details are to be reported elsewhere.

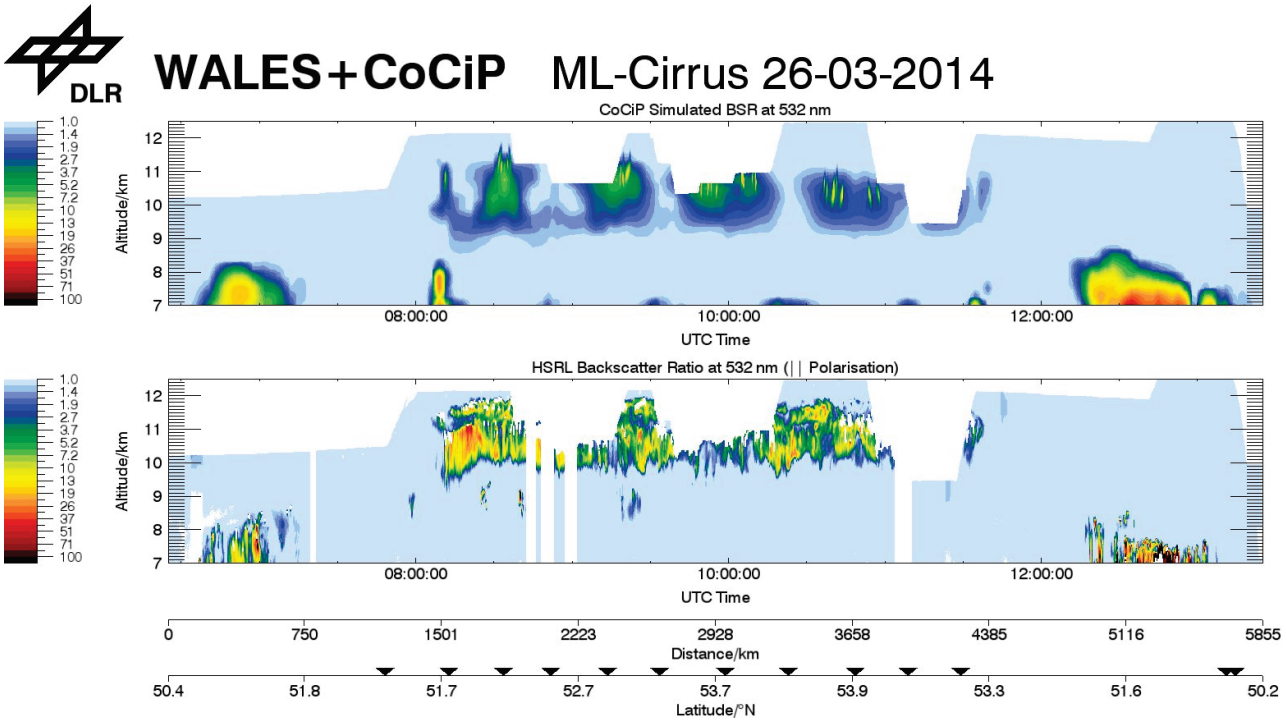

Figure 4. Backscatter ratio (color scale) from the atmosphere with cirrus relative to Rayleigh scattering from the clear atmosphere as a function of altitude and measurement time along thGHALO flight path. The backscatter values are derived from high-spectral resolution lidar observations with WALES (Gross et al., 2015) (lower panel) and from computations from ECMWF cirrus and CoCiP contrail properties (upper panel). The backscatter is plotted in color for altitudes from 7 km above sea level to about 500 m below the HALO aircraft flightpath (white above that altitude).

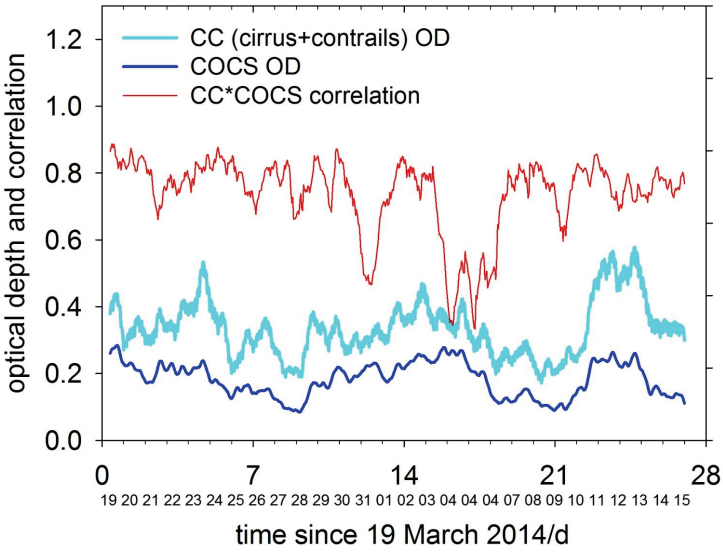

Figure 5. Optical depth of cirrus clouds in the solar range (near 550 nm) derived from satellite infrared MSG-SEVIRI data by means of the COCS algorithm (Kox et al., 2014) and from contrail-cirrus model forecast using CoCiP with ECMWF data versus time for 28 days of the ML-CIRRUS period (19 March-15 April 2014). The blue and cyan curves show hourly mean values on the ML-CIRRUS domain. The red curve shows the mean correlation coefficient of pixelwise optical depth values from COCS and from CoCiP on average over the ML-CIRRUS domain. During the period 29 March to 7 April, large parts of the domain where influenced by Sahara dust aerosol.

REFERENCES

Grewe, V., C. Frömming, S. Matthes, S. Brinkop, M. Ponater, S. Dietmüller, P. Jöckel, H. Garny, E. Tsati, O. A. Søvde, J. Fuglestvedt, T. K. Berntsen, K. P. Shine, E. A. Irvine, T. Champougny, and P. Hullah (2013), Aircraft routing with minimal climate impact: the REACT4C climate cost function modelling approach (V1.0), Geosci. Model Dev. Discuss., 6, 4345-4416, doi:10.5194/gmdd-6-4345-2013.

Gross, S., A. Schaefler, M. Wirth, and A. Fix (2015), Airborne differential absorption and high spectral resolution lidar measurements for cirrus cloud studies, paper presented at ILRC27, 6 -10 July 2015, New York, USA.

Kox, S., L. Bugliaro, and A. Ostler (2014), Retrieval of cirrus cloud optical thickness and top altitude from geostationary remote sensing, Atmos. Meas. Tech., 7, 3233-3246, doi:10.5194/amt-7-3233-2014.

Rautenhaus, M., G. Bauer, and A. Dörnbrack (2012), A web service based tool to plan atmospheric research flights, Geosci. Model Dev., 5, 55-71, doi:10.5194/gmd-5-55-2012.

Schumann, U. (2012), A contrail cirrus prediction model, Geosci. Model Dev., 5, 543–580, doi: 10.5194/gmd-5-543-2012.

Schumann, U., and K. Graf (2013), Aviation-induced cirrus and radiation changes at diurnal timescales J. Geophys. Res., 118, 2404-2421, doi: 10.1002/jgrd.50184.

Schumann, U., J. E. Penner, Y. Chen, C. Zhou, and K. Graf (2015), Dehydration effects from contrails in a coupled contrail-climate model, Atmos. Chem. Phys., 15, 11179-11199, doi:10.5194/acp-15-11179-2015.

Voigt, C., U. Schumann, T. Jurkat, D. Schäuble, H. Schlager, A. Petzold, J.-F. Gayet, M. Krämer, J. Schneider, S. Borrmann, J. Schmale, P. Jessberger, T. Hamburger, M. Lichtenstern, M. Scheibe, C. Gourbeyre, J. Meyer, M. Kübbeler, W. Frey, H. Eichler, T. Butler, M. G. Lawrence, F. Holzäpfel, F. Arnold, M. Wendisch, A. Döpelheuer, K. Gottschaldt, R. Baumann, M. Zöger, I. Sölch, M. Rautenhaus, and A. Dörnbrack (2010), In-situ observations of young contrails – overview and selected results from the CONCERT campaign, Atmos. Chem. Phys., 10, 9039-9056, doi:10.5194/acp-10-9039-2010.

Voigt, C., A. Minikin, U. Schumann, and ML-CIRRUS_team (2015), ML-CIRRUS - the HALO mission on mid latitude cirrus clouds, Geophysical Research Abstracts, 17, EGU2015-2758, http://meetingorganizer.copernicus.org/EGU2015/EGU2015-2758.pdf.

On dehydration effects from contrails in a coupled contrail-climate model

Ulrich Schumann*
DLR, Institut für Physik der Atmosphäre, Oberpfaffenhofen, Germany

Joyce E. Penner, Yibin Chen, Cheng Zhou,
University of Michigan, Department of Atmospheric, Oceanic, and Space Sciences, Ann Arbor, Michigan, USA

Kaspar Graf,
DLR, Institut für Physik der Atmosphäre, Oberpfaffenhofen, Germany

Keywords: Contrail, Climate, Water Vapor, Dehydration, Radiative Forcing

ABSTRACT: The uptake of water by contrails in ice-supersaturated air and release of water after ice particle advection and sedimentation is investigated using a coupled climate-contrail model. Simulations with and without coupling are compared. In the coupled mode, the contrails make the upper troposphere slightly drier which in turn causes thinner contrails. As a consequence, the radiative forcing (RF) by contrails computed in the coupled mode is slightly smaller (about 15 %) than without coupling. As a further effect, many of the contrail ice particles forming in the upper troposphere sediment and release water at lower altitudes, on average 700 m below the mean flight levels. This causes a further drying of the upper troposphere but adds humidity at lower levels. As a consequence, contrails change the entire hydrological cycle in the atmosphere. Contrail formation and contrail ice particle sedimentation causes a reduced total water column and reduced cover of high and low-level clouds. The quantitative effects are small compared to climate noise in the coupled model. Significant changes were found in the simulations only for strongly increased (factor 100) air traffic emissions. Scaled to nominal emissions, the dehydration causes a negative net RF in the global model of order -0.01 W m^{-2}. In total, the RF by contrails is reduced because of humidity exchange between contrails and the background atmosphere and because of dehydration of the upper troposphere. This model study was performed with a 3 times larger soot emission index than in previous studies. The change in soot emission increases the contrail RF which offsets the forcing caused by water coupling and dehydration in the model. Hence, the net contrail-induced RF result is similar to that from previous studies (0.04-0.08 W m^{-2}).

1 INTRODUCTION

Contrail ice particles grow by uptake of humidity from ambient ice-supersaturated air masses and release their water content after sedimentation or advection with the wind into regions with lower relative humidity. Hence, contrails dry or dehydrate the atmosphere at places where they form, and redistribute humidity to places in the atmosphere where they sublimate. The decrease of humidity at flight altitudes may make contrails thinner. Falling ice particles may increase humidity in the lower troposphere where they sublimate and may enhance precipitation from clouds at lower altitudes.

The dehydration effects from contrails are not well known. Burkhardt and Kärcher (2011) studied the dehydration effects within a global climate model. Contrail formation was treated as a subgrid-scale (SGS) process which included a separate cloud class for young contrails. They found that contrail cirrus causes a significant decrease in natural cloudiness, which partly offsets their warming effect. They estimated the cooling from reduced cirrus at about 7 mW m^{-2} and called for further work to more reliably quantify this effect.

Observations and large-eddy simulations show that ice particles precipitating from contrails in ice supersaturated air may form deep fall streaks of quickly falling large ice particles below individual contrails. A nice example is shown in Unterstrasser et al. (2012) based on previous DLR-

* *Corresponding author:* Ulrich Schumann, DLR-Institut für Physik der Atmosphäre, D-82205 Oberpfaffenhofen, Germany. Email: ulrich.schumann@dlr.de

Falcon airborne lidar observations and new large eddy simulation results. The fallstreaks typically have a scale of order 1-2 km vertically and 2-10 km horizontally. Such fall streaks transport huge amounts of water – far more than emitted by the aircraft – to lower levels. The separation between the sizes of individual contrails and the grid sizes in global models makes it difficult to assess the global impact of dehydration from contrails.

This study investigates the following questions: How does exchange of humidity between contrails and ambient air change contrail properties? How strongly do contrails change the atmosphere by dehydration/hydration? Can we quantify the radiative impact of contrail-induced dehydration/hydration?

The potentially important impact of soot with changed ice nucleation properties after processing in contrails (Zhou and Penner, 2015) is not studied in this paper.

2 METHOD

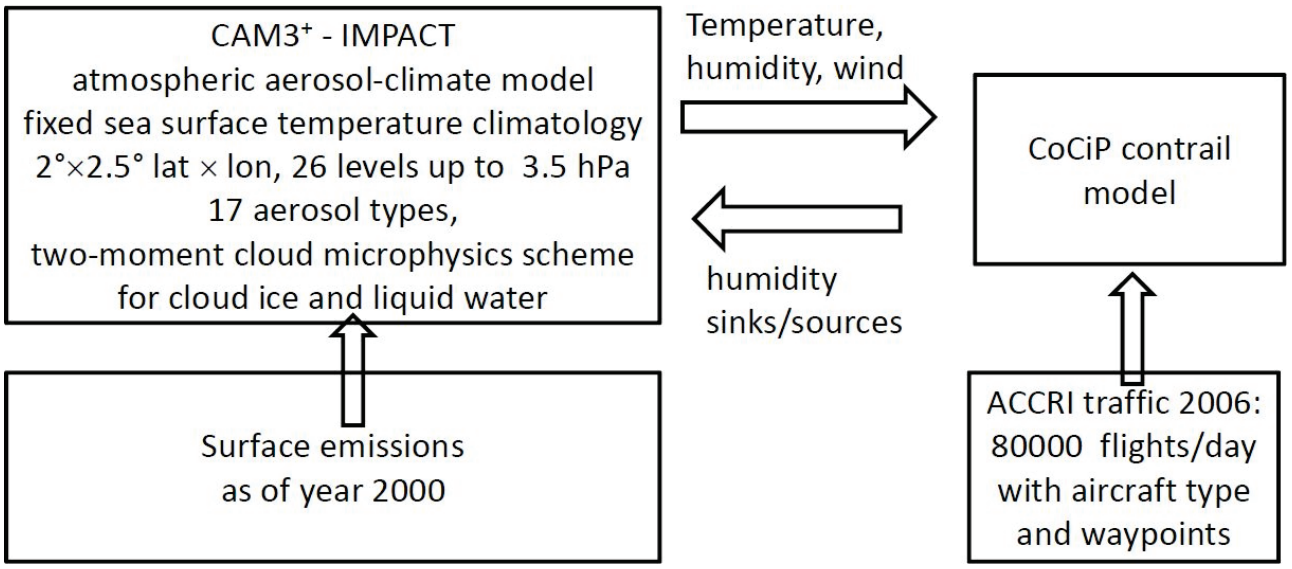

Figure 1: Schematic overview on the coupling method

The method, see Figure 1, is a new combination of CoCiP with CAM3+/IMPACT, with code changes to allow for coupling with exchange of water between contrails and ambient air. CAM3+/IMPACT is a coupled aerosol-general circulation model (Wang and Penner, 2010; Yun and Penner, 2012; Yun et al., 2013). CAM3 is the Community Atmosphere Model version 3, which simulates the atmosphere. IMPACT is the University of Michigan aerosol model. CAM3+ uses a two-moment cloud microphysics scheme for cloud ice, in which mass and number concentrations are predicted by prognostic equations (Liu et al., 2007). The two-moment scheme treats ice nucleation, evaporation, and melting, and allows for ice supersaturation. The cloud fraction calculation accounts for cloud cover formation by ice nucleation, including homogeneous and heterogeneous nucleation of ice. The surface emissions included are for the year 2000 (Penner et al., 2009).

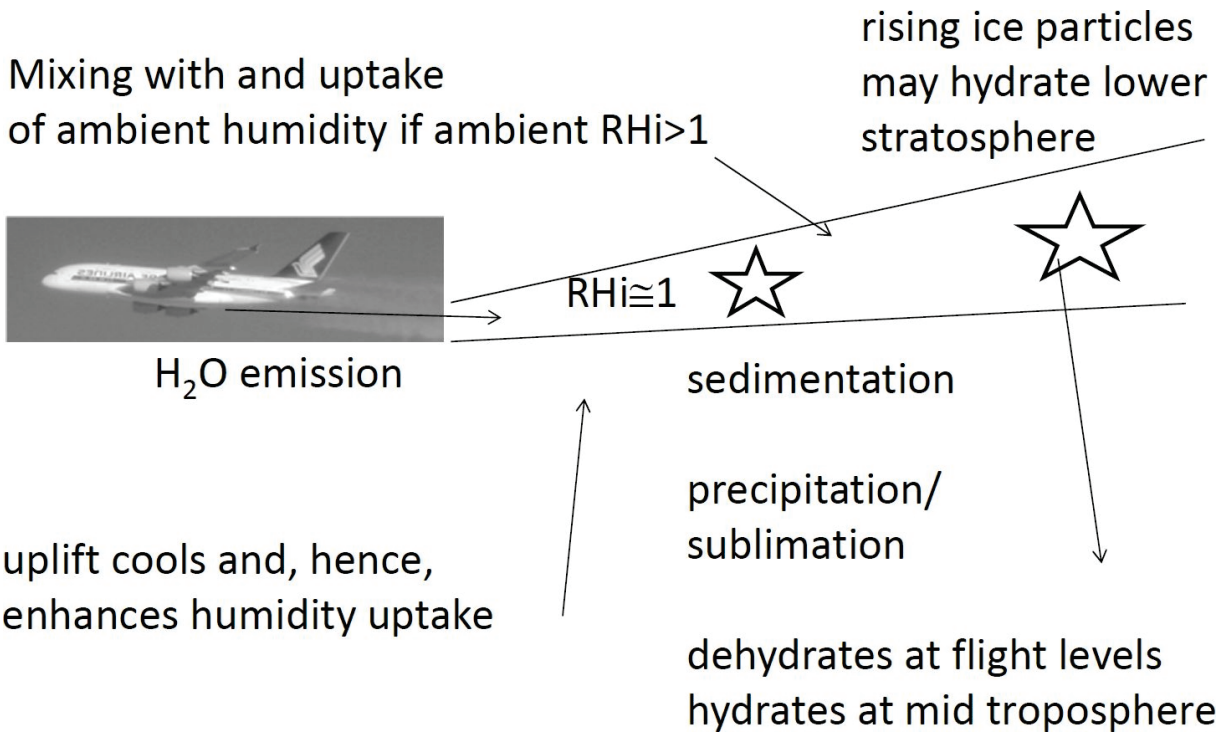

Figure 2. Schematic showing some of the processes simulated in the Contrail Cirrus Prediction Model CoCiP (RHi = relative humidity over ice).

CoCiP is a Lagrangian model which traces individual contrail segments forming along flight routes for many flights. The model is documented and discussed in Schumann (2012). Figure 2 gives an overview on the contrail processes related to dehydration in CoCiP. CoCiP has been applied in various previous studies (Jeßberger et al., 2013; Schumann and Graf, 2013; Schumann et al., 2011; Schumann et al., 2012a; Schumann et al., 2013a; Schumann et al., 2013b; Schumann et al., 2012b; Voigt et al., 2010). The major features and a few modifications are described in Schumann et al. (2015). The modifications result from a correction of a code error in the previous implementation (until October 2012) of the Runge-Kutta scheme used for time integration. The correction causes more reasonable results. Moreover, the soot emission index used, 10^{15} kg^{-1}, is about 3 times higher than in previous CoCiP studies. The higher value is used because recent experimental data indicate that modern aircraft emit more (by number) soot particles acting as contrail ice nuclei than estimated earlier (Schumann et al., 2013b). The absolute humidity provided by CAM to CoCiP is increased by a factor $1/RHi_c$ (RHi_c=0.9) to allow for subgrid scale cirrus formation.

The model is driven by air traffic waypoint data. Here, we use a global data set for the year 2006, including about 80000 flights per day, as provided within the ACCRI project (Brasseur et al., 2015; Wilkerson et al., 2010).

CAM calls CoCiP as a subroutine each time step providing the most recent meteorological fields as input. The fields include three-dimensional (3-D) fields of wind, temperature, humidity, ice water content, and cloud cover as a function of pressure. CoCiP interpolates in these fields linearly in space and time to obtain the values at any position.

In the offline mode, each contrail segment is simulated for the given ambient meteorological fields without changing background meteorology.

The coupled code accounts for emissions exchanged between the background atmosphere and the contrails per time step and per CAM grid cell by tracking 3-D-fields EA, EC and CA. Fig. 3 shows zonal and annual mean values of these fields. EA (engine to atmosphere) records the emission amount emitted from aircraft engines directly to the atmosphere, without processing in contrails. EC (engine to contrail) is the amount emitted from aircraft engines into fresh contrails. Positive CA (contrail to atmosphere) values are the amounts released from contrails to the atmosphere, negative CA values are the amounts taken up by contrails from the atmosphere. If no contrail forms, EA contains all emissions and the contribution to EC is zero. After contrail initiation, in growing contrails, the water contribution to CA becomes negative, because contrail ice grows by uptake of ambient humidity. Later during the contrail life cycle, the contrail provides a positive CA contribu-

tion when ice sublimates releasing water to the atmosphere. The H2O mass passed between CoCiP and CAM is conserved.

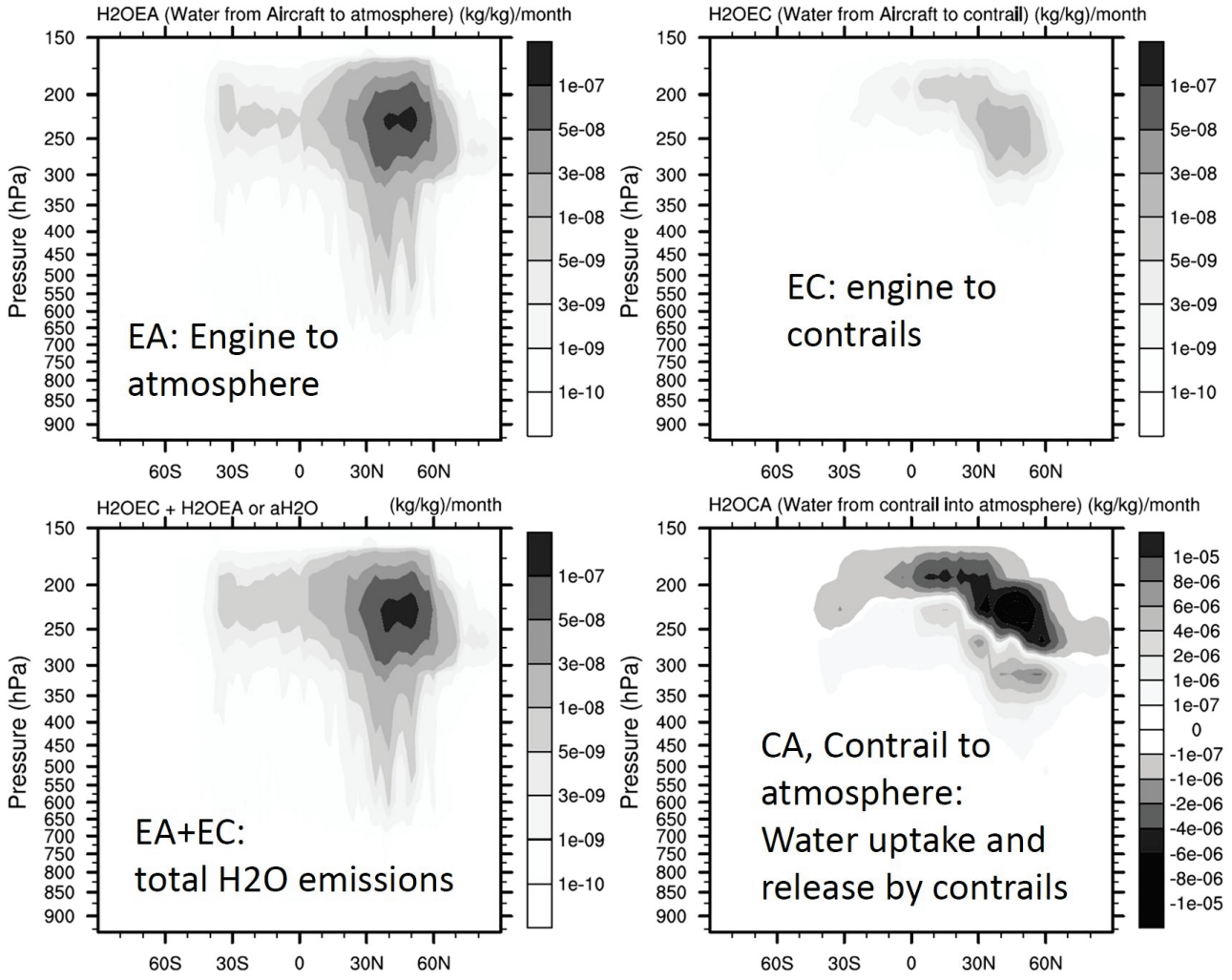

Figure 3. Annual and zonal mean exchange rates of water mass (plotted as mixing ratio per time) between aircraft, contrails and atmosphere in CAM3+/IMPACT/CoCiP.

CoCiP and CAM exchange grid cell mean values from CAM to CoCiP. As a consequence, the mass of H2O uptake (or release, when negative) by a contrail during the time step is spread over the grid cell immediately. Because of the large difference between contrail scales (widths of order 0.1-10 km) and grid scales (of order 200 km), humidity variations at contrail scales cannot be resolved within CAM. A global model with far higher spatial resolution would be required to overcome this problem.

Three runs were performed with CAM3+/IMPACT/CoCiP for this study, see Table 1. Run 0 is the uncoupled (offline) reference case in which CAM runs without aviation emissions while CoCiP is run using nominal aircraft emissions. Here, CoCiP uses the meteorological fields from CAM in the same manner as it used numerical weather prediction results in the past (Schumann and Graf, 2013). Run 1 uses the coupled method (online) and simulates the effects of contrails on the hydrological cycle for nominal aircraft emissions. Run 2 uses aircraft emissions increased by 100 fold to enhance the aviation effects beyond climate noise. The results for runs 0 and 1 are from 30 years of simulation after several years of spin-up. Because of limited computing resources, Run 2 includes just one year restarted from run 1 files. For details see Schumann et al. (2015).

Table 1. Schematic run specification

Run	Coupling method	Emission amounts	Integration period
0	offline	nominal	30 years
1	online	nominal	30 years
2	online	100 × increased	1 year

3 RESULTS

Contrail growth causes dehydration at flight levels, large ice particles sediment, on average by 700 m, eventually sublimate and hydrate the atmosphere at lower levels.

The drying at flight levels changes contrail properties by +5 to -30 % and causes thinner contrails with larger mean age.

Dehydration impacts the entire hydrological system.

The local drying during contrail formation at flight levels causes a ~15 % reduced net RF from contrails (~0.06 instead of ~0.07 W m^{-2}). The change in the global hydrological cycle induced by contrails in the global model causes a net RF of about -0.01 W m^{-2}.

For details see Schumann et al. (2015).

This model study was performed with a 3 times larger soot emission index than in a previous CoCiP application (Schumann and Graf, 2013). The change in soot emissions increases the contrail radiative forcing while the changes caused by water coupling and dehydration in the model decreases the contrail radiative forcing, so that the net result is not much different from previous studies. See Figure 4.

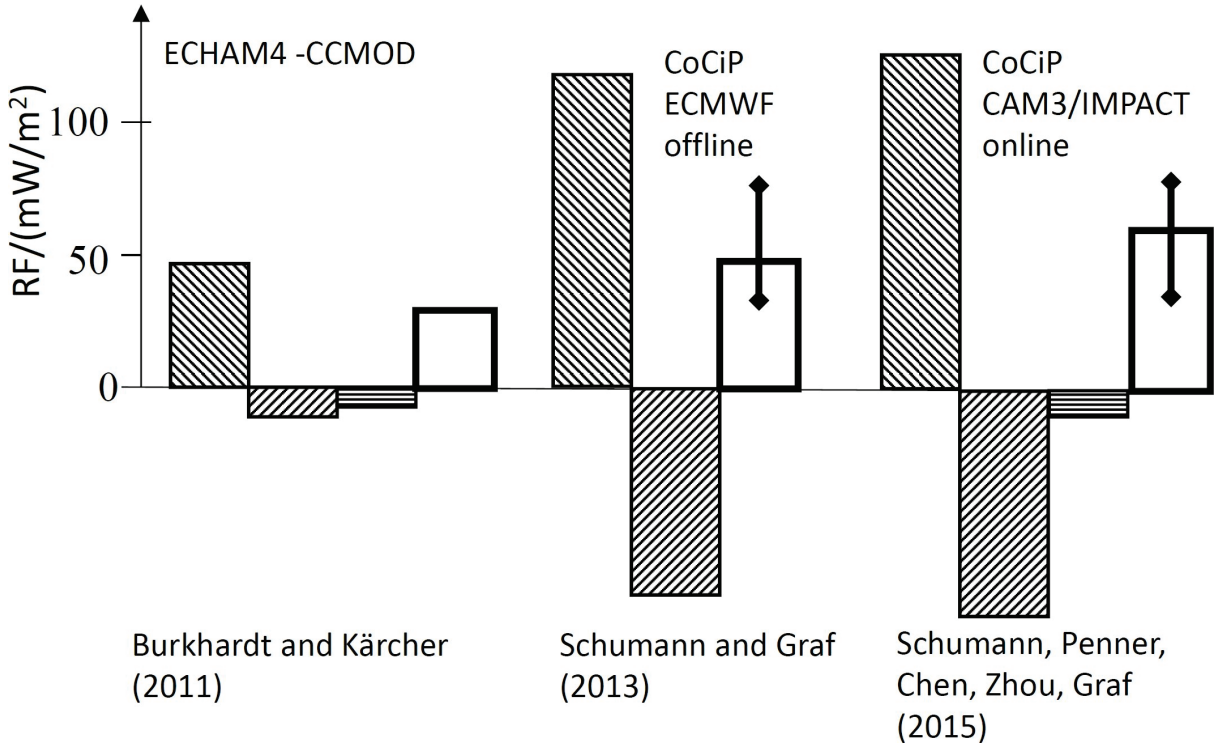

Figure 4. Radiative forcing (RF) from contrail cirrus: Comparison of results from three studies as cited. The first and second bars for each study show the longwave (LW) and shortwave (SW) contrail induced RF. The horizontally striped bars show the RF from global changes caused by dehydration in the global atmosphere, including cirrus changes (Burkhardt and Kärcher, 2011). The white bar shows the net effect from contrails in the coupled models. The vertical bars with diamonds represent best estimates of the range of uncertainty based on statistical uncertainties and on sensitivity studies for a range of model and data analysis parameters. The LW and SW RF from contrails in the present study (Schumann et al., 2015) is larger than the previous CoCiP study (Schumann and Graf, 2013), mainly because of a larger soot emission index.

4 ACKNOWLEDGEMENTS

This research was supported by the Federal Aviation Administration (FAA) within its Aviation Climate Change Research Initiative (ACCRI), by DLR within the DLR projects Climate Compatible Air Transportation System (CATS) and Utilizing Weather-Climate Information in Air Traffic Simulations (WeCare), and by the National Science Foundation (NSF). Computing resources (ark:/85065/d7wd3xhc) were provided by the Climate Simulation Laboratory at NCAR's Computational and Information Systems Laboratory, sponsored by the NSF and other agencies.

REFERENCES

Brasseur, G. P., M. Gupta, B. E. Anderson, S. Balasubramanian, S. Barrett, D. Duda, G. Fleming, P. M. Forster, J. Fuglestvedt, A. Gettelman, R. N. Halthore, S. D. Jacob, M. C. Jacobson, A. Khodayari, K.-N. Liou, M. T. Lund, R. C. Miake-Lye, P. Minnis, S. C. Olsen, J. E. Penner, R. Prinn, U. Schumann, H. B. Selkirk, A. Sokolov, N. Unger, P. Wolfe, H.-W. Wong, D. W. Wuebbles, B. Yi, P. Yang, and C. Zhou (2015), Impact of aviation on climate: FAA's Aviation Climate Change Research Initiative (ACCRI) Phase II, Bull. Amer. Meteorol. Soc., in press, doi: 10.1175/BAMS-D-13-00089.1.

Burkhardt, U., and B. Kärcher (2011), Global radiative forcing from contrail cirrus, Nature Clim. Change, 1, 54-58, doi: 10.1038/NCLIMATE1068.

Jeßberger, P., C. Voigt, U. Schumann, I. Sölch, H. Schlager, S. Kaufmann, A. Petzold, D. Schäuble, and J.-F. Gayet (2013), Aircraft type influence on contrail properties, Atmos. Chem. Phys., 13, 11965-11984, DOI: 10.5194/acp-13-11965-2013.

Liu, X., J. E. Penner, S. J. Ghan, ., and M. Wang (2007), Inclusion of ice microphysics in the NCAR Community Atmosphere Model version 3 (CAM3), J. Clim., 20, 4526–4547., J. Clim., 20, 4526–4547, DOI: 10.1175/JCLI4264.1.

Penner, J. E., Y. Chen, M. Wang, and X. Liu (2009), Possible influence of anthropogenic aerosols on cirrus clouds and anthropogenic forcing, Atmos. Chem. Phys., 9, 879-896, 10.5194/acp-9-879-2009.

Schumann, U., K. Graf, and H. Mannstein (2011), Potential to reduce the climate impact of aviation by flight level changes, in 3rd AIAA Atmospheric and Space Environments Conference, AIAA paper 2011-3376, edited, pp. 1-22, Honolulu, Hawaii.

Schumann, U., K. Graf, H. Mannstein, and B. Mayer (2012a), Contrails: Visible aviation induced climate impact, in Atmospheric Physics – Background - Methods - Trends, edited by U. Schumann, pp. 239-257, Springer, Berlin, Heidelberg, DOI: 10.1007/978-3-642-30183-4_15.

Schumann, U., B. Mayer, K. Graf, and H. Mannstein (2012b), A parametric radiative forcing model for contrail cirrus, J. Appl. Meteorol. Clim., 51, 1391-1406, doi: 10.1175/JAMC-D-11-0242.1.

Schumann, U., and K. Graf (2013), Aviation-induced cirrus and radiation changes at diurnal timescales J. Geophys. Res., 118, 2404-2421, doi: 10.1002/jgrd.50184.

Schumann, U., R. Hempel, H. Flentje, M. Garhammer, K. Graf, S. Kox, H. Lösslein, and B. Mayer (2013a), Contrail study with ground-based cameras, Atmos. Meas. Tech., 6, 3597-3612, doi:10.5194/amt-6-3597-2013.

Schumann, U., P. Jeßberger, and C. Voigt (2013b), Contrail ice particles in aircraft wakes and their climatic importance, Geophys. Res. Lett., 40, 2867-2872 doi: 10.1002/grl.50539.

Schumann, U., J. E. Penner, Y. Chen, C. Zhou, and K. Graf (2015), Dehydration effects from contrails in a coupled contrail-climate model, Atmos. Chem. Phys., 15, 11179-11199, doi:10.5194/acp-15-11179-2015, 2015.

Unterstrasser, S., I. Sölch, and K. Gierens (2012), Cloud resolving modeling of contrail evolution, in Atmospheric Physics - Background - Methods - Trends, edited by U. Schumann, pp. 543-559, Springer, Heidelberg, doi: 10.11007/978-3-642-30183-4_33.

Voigt, C., U. Schumann, T. Jurkat, D. Schäuble, H. Schlager, A. Petzold, J.-F. Gayet, M. Krämer, J. Schneider, S. Borrmann, J. Schmale, P. Jessberger, T. Hamburger, M. Lichtenstern, M. Scheibe, C. Gourbeyre, J. Meyer, M. Kübbeler, W. Frey, H. Eichler, T. Butler, M. G. Lawrence, F. Holzäpfel, F. Arnold, M. Wendisch, A. Döpelheuer, K. Gottschaldt, R. Baumann, M. Zöger, I. Sölch, M. Rautenhaus, and A. Dörnbrack (2010), In-situ observations of young contrails – overview and selected results from the CONCERT campaign, Atmos. Chem. Phys., 10, 9039-9056, doi:10.5194/acp-10-9039-2010.

Wang, M., and J. E. Penner (2010), Cirrus clouds in a global climate model with a statistical cirrus cloud scheme, Atmos. Chem. Phys., 10, 5449-5474, doi:10.5194/acp-10-5449-2010.

Wilkerson, J. T., M. Z. Jacobson, A. Malwitz, S. Balasubramanian, R. Wayson, G. Fleming, A. D. Naiman, and S. K. Lele (2010), Analysis of emission data from global commercial aviation: 2004 and 2006, Atmos. Chem. Phys., 10, 6391-6408, doi:10.5194/acp-10-6391-2010.

Yun, Y., and J. E. Penner (2012), Global model comparison of heterogeneous ice nucleation parameterizations in mixed phase clouds, J. Geophys. Res., 117, 7203–7203, doi:10.1029/2011JD016506.

Yun, Y., J. E. Penner, and O. Popovicheva (2013), The effects of hygroscopicity on ice nucleation of fossil fuel combustion aerosols in mixed-phase clouds, Atmos. Chem. Phys., 13, 4339–4348, doi:10.5194/acp-13-4339-2013.

Zhou, C., and J. E. Penner (2014), Aircraft soot indirect effect on large-scale cirrus clouds: Is the indirect forcing by aircraft soot positive or negative?, J. Geophys. Res., DOI: 10.1002/2014JD021914.

Modelling the chemistry in contrails from the vortex to the diffusion phase using a mesoscale model

H. Clark*, O. Thouron, R. Paoli, D. Cariolle
CERFACS, 42 Avenue Gaspard Coriolis, Toulouse, France

ABSTRACT: Aircraft emit gases and particles directly into the upper-troposphere/lower stratosphere which is a region that is very sensitive to small changes in chemical composition. Through various chemical interactions, the emissions of NO_x, CO_2 and H_2O perturb the concentrations of the radiatively active gases CO_2, O_3, and methane, with consequences for climate. They may also trigger the formation of contrails and contrail induced cirrus, or modify the composition of aerosols, with further effects on climate. With air traffic predicted to increase over the coming years, it is necessary to model these processes to give a better understanding of the effects of aircraft on climate. We present results from the project TC2, which aims to understand the physico-chemical processes throughout the evolution of contrails from the vortex phase (after several seconds) to the diffusion phase (several hours) where true atmospheric variability becomes important. We used the mesoscale model Méso-NH and introduced a specially adapted chemical scheme which included reactions with 13 gaseous species along with ice. Simulations show the interactions between NO_x and atmospheric ozone during the vortex/dissipation phase and will later include heterogeneous reactions on ice surface that convert NO_x species into HNO_3.

1 INTRODUCTION

The region of the upper-troposphere/lower stratosphere (UTLS) is sensitive to small changes in chemical composition. Perturbations to the concentrations of trace gases such as H_2O, O_3 and methane have direct effects on climate with changes in the UTLS having relatively more influence on the radiative budget than changes elsewhere (Reise et al., 2012, Zeng et al., 2008, Gauss et al., 2006) . Aircraft emit radiatively active gases and their precursors into this sensitive region, with potentially important consequences for climate. Other gases and particles emitted by aircraft such as SO_x, hydrocarbons and soot interact through microphysical processes and lead to increased cloudiness which has further effects on climate. With a doubling of air-traffic every fifteen years, the total radiative forcing from aircraft may be significant (Lee et al., 2009). Of the radiative forcing components due to aviation, contrails and aircraft induced cloudiness are one of the more uncertain (Lee et al., 2009). Such uncertainties may be attributed to the difficulty in modelling contrails over the wide range of scales, from several metres to several kilometres and over several seconds to several days, necessary to cover the entire lifecycle of the contrail (Burkhardt et al 2010).

The objective of this study is to model the chemical interactions throughout the lifecycle of a contrail from the emission of gases and particles by the engines, the fine-scale dilution and chemical reactions in the wake, and diffusion on the kilometre scale under different atmospheric conditions. To model the chemical processes within contrails, we need to take into account the main chemical reactions in the gaseous phase between the emitted species and their descendants, reactions in the heterogeneous phase which take place on the surface of the ice particles, and photochemistry which contributes to dissociation of the species emitted or formed. To achieve this we have introduced a chemical scheme into the meso-scale model Méso-NH. The advantage of a meso-scale model is that it allows us to study diffusion under different conditions of wind shear, stratification and turbulence and on scales which are comparable with climate models. The ability of Méso-NH to reproduce turbulence in the UTLS at the sub-kilometre scale has been demonstrated by Paoli et al (2014).

* *Corresponding author:* Hannah Clark, former CERFACS now CNRS Laboratoire d'Aerologie, hannah.clark@aero.obs-mip.fr

2 METHOD

We used a chemical scheme including 48 principal reactions in the gaseous phase among 16 chemical species, along with photochemistry and microphysics. For the moment however, we focus on the homogeneous reactions in the gaseous phase. The chemical scheme is shown in table 1. The reactions highlighted in blue, are the photochemical reactions for which the rate constants were calculated for the atmospheric layer corresponding cruise altitude over the North Atlantic using the model TUV 5.0 (Madronich and Flocke 1998).

K001 = $NO_2 \rightarrow O_3P + NO$	K024 = $HO_2 + HO_2 \rightarrow H_2O_2 + O_2$
K002 = $O_3 \rightarrow O_1D + O_2$	K025 = $HO_2 + HO_2 + H_2O \rightarrow H_2O_2 + H_2O + O_2$
K003 = $O_3 \rightarrow O_3P + O_2$	K026 = $O_3P + NO \rightarrow O_3P + NO_2 \rightarrow NO + O_2$
K004 = $HONO \rightarrow OH + NO$	K028 = $O_3P + NO_2 \rightarrow NO_3$
K005 = $HNO_3 \rightarrow OH + NO_2$	K029 = $OH + NO \rightarrow HONO$
K006 = $HNO_4 \rightarrow 0.65 * HO_2 +$	K030 = $OH + NO_2 \rightarrow HNO_3$
$0.65 * NO_2 + 0.35 * OH + 0.35 * NO_3$	K031 = $OH + NO_3 \rightarrow NO_2 + HO_2$
K007 = $NO_3 \rightarrow NO + O_2$	K032 = $HO_2 + NO \rightarrow NO_2 + OH$
K008 = $NO_3 \rightarrow NO_2 + O_3P$	K033 = $HO_2 + NO_2 \rightarrow HNO_4$
K009 = $H_2O_2 \rightarrow OH + OH$	K034 = $HNO_4 \rightarrow HO_2 + NO_2$
K010 = $HCHO \rightarrow H_2 + CO$	K035 = $OH + HONO \rightarrow H_2O + NO_2$
K011 = $HCHO \rightarrow HO_2 + HO_2 + CO$	K036 = $OH + HNO_3 \rightarrow NO_3 + H_2O$
K012 = $O_3P + OH \rightarrow O_2 + H$	K037 = $OH + HNO_4 \rightarrow NO_2 + H_2O + O_2$
K013 = $O_3P + HO_2 \rightarrow OH + O_2$	K038 = $O_3 + NO \rightarrow NO_2 + O_2$
K014 = $OH + OH \rightarrow H_2O + O_3P$	K039 = $O_3 + NO_2 \rightarrow NO_3 + O_2$
K015 = $O_3P + O_2 \rightarrow O_3$	K040 = $NO + NO + O_2 \rightarrow NO_2 + NO_2$
K016 = $O_3P + O_3 \rightarrow 2.0 * O_2$	K041 = $NO_3 + NO \rightarrow NO_2 + NO_2$
K017 = $O_1D + N_2 \rightarrow O_3P + N_2$	K042 = $NO_3 + NO_2 \rightarrow NO + NO_2 + O_2$
K018 = $O_1D + O_2 \rightarrow O_3P + O_2$	K043 = $NO_3 + NO_2 \rightarrow N_2O_5$
K019 = $O_1D + H_2O \rightarrow OH + OH$	K044 = $N_2O_5 \rightarrow NO_2 + NO_3$
K020 = $O_3 + OH \rightarrow HO_2 + O_2$	K045 = $OH + H_2 \rightarrow H_2O + HO_2$
K021 = $O_3 + HO_2 \rightarrow OH + 2.0*O_2$	K046 = $CO + OH \rightarrow HO_2 + CO_2$
K022 = $OH + HO_2 \rightarrow H_2O + O_2$	K047 = $CH_4 + OH \rightarrow HCHO + H_2O$
K023 = $H_2O_2 + OH \rightarrow HO_2 + H_2O$	K048 = $HCHO + OH \rightarrow HO_2 + CO + H_2O$

Table 1. The HO_x/NO_x chemistry scheme based on 16 species
O_1D, O_3P, O_2, O_3, OH, H_2O, HO_2, N_2, NO, NO_2, NO_3, N_2O5, HNO_3, HONO, CO, CH_2O, and 48 reactions.
Photochemical reactions are shown in blue, where rates were calculated by TUV5 for cruise altitude over the Atlantic.

To simulate the contrail from the vortex phase to the diffusion phase the simulation is performed in two stages. The first step covers the vortex and dissipation phase during the first minutes of evolution of the wake. The second step covers the diffusion regime up to 1 hour later. The two steps are shown in figure 1.

For the first step, the background turbulence was generated by Meso-NH on the domain of Lx = Ly = 10km et Lz = 4km (MDIFF) and a resolution of 10m. This field was merged with the near-field containing the dynamical and microphysical properties of the vortex (u,v,w,P, water vapour, theta, concentrations and effective radius of ice) resulting from a LES simulation using NTMIX under a supersaturation of 130% and a temperature 218K (Picot et al. 2015). The merged field (which contains the near field from NTMIX and the background turbulence), was used as the initial conditions for a Meso-NH simulation on a domain of Lx = 400m, Ly = 1km, Lz = 1km, with a resolution of 2m (Mvort). The first 5 minutes of the evolution of the contrail are performed in this configuration, and the results are discussed here. In the next stage of the simulation, the fields obtained after 5 minutes will be reintroduced into the large domain to run the simulation for several hours for the diffusion phase. Based on emissions indices (Lee et al 2010), we injected 14g/kg of NO for every 1240g/kg of water vapour in the vortex. Background values are shown in table 2.

Simulations were performed for daytime and night time to verify the model with and without photochemistry.

Species	Mixing ratio
NO	$1.x10^{-11}$
O_3	$2.x10^{-7}$
NO_2	$1.x10^{-10}$
OH	$1.5x10^{-14}$
HO_2	$1.x10^{-13}$
H_2O_2	$1.x10^{-14}$
HNO_3	$4.5x10^{-10}$
H_2	$1.x10^{-9}$
CO	$1.x10^{-7}$
CH_4	$1.7x10^{-6}$

Table 2. Background values for different species.

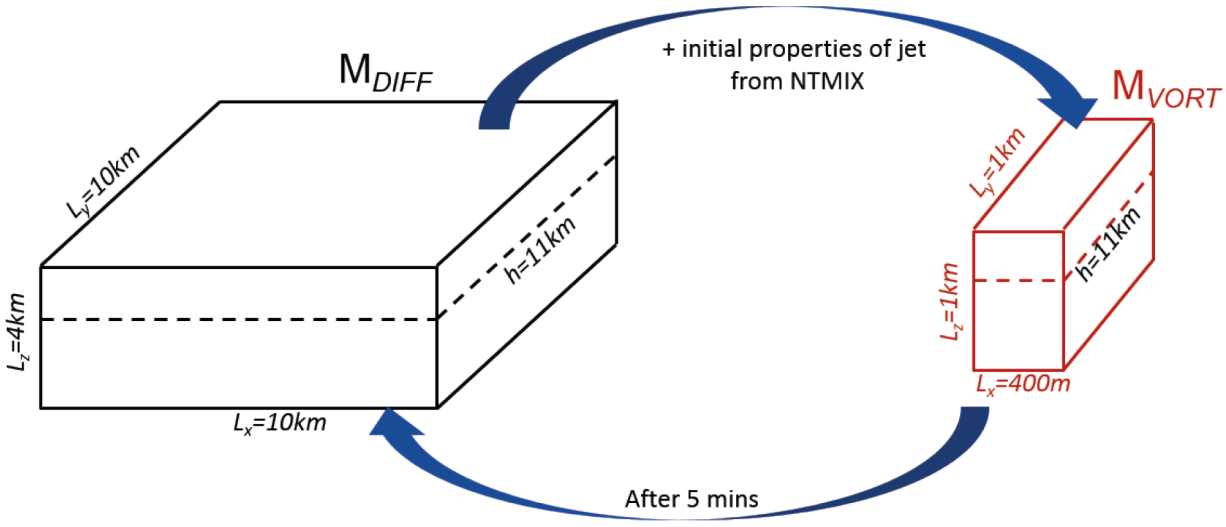

Figure 1. The experimental set-up for the simulation. The Mdiff domain generates the background turbulence and the Mvort domain is used for the vortex and dissipation of the wake.

3 CHEMICAL FIELDS AFTER FIVE MINUTES

Figure 2 presents the evolution over 300s of the potential temperature anomaly introduced by the vortex. The anomaly is relative to the average potential temperature on each vertical level. The vortex descends at rate of about $1.7ms^{-1}$ over 180s. The black contours on 120, 180 and 300s show the concentration of ice and are included to help pick out the temperature anomaly as the field become more dispersed. By 300s, the anomaly in potential temperature is indistinguishable from natural variability and the concentration of ice particles is the only guide as to where the contrail is.

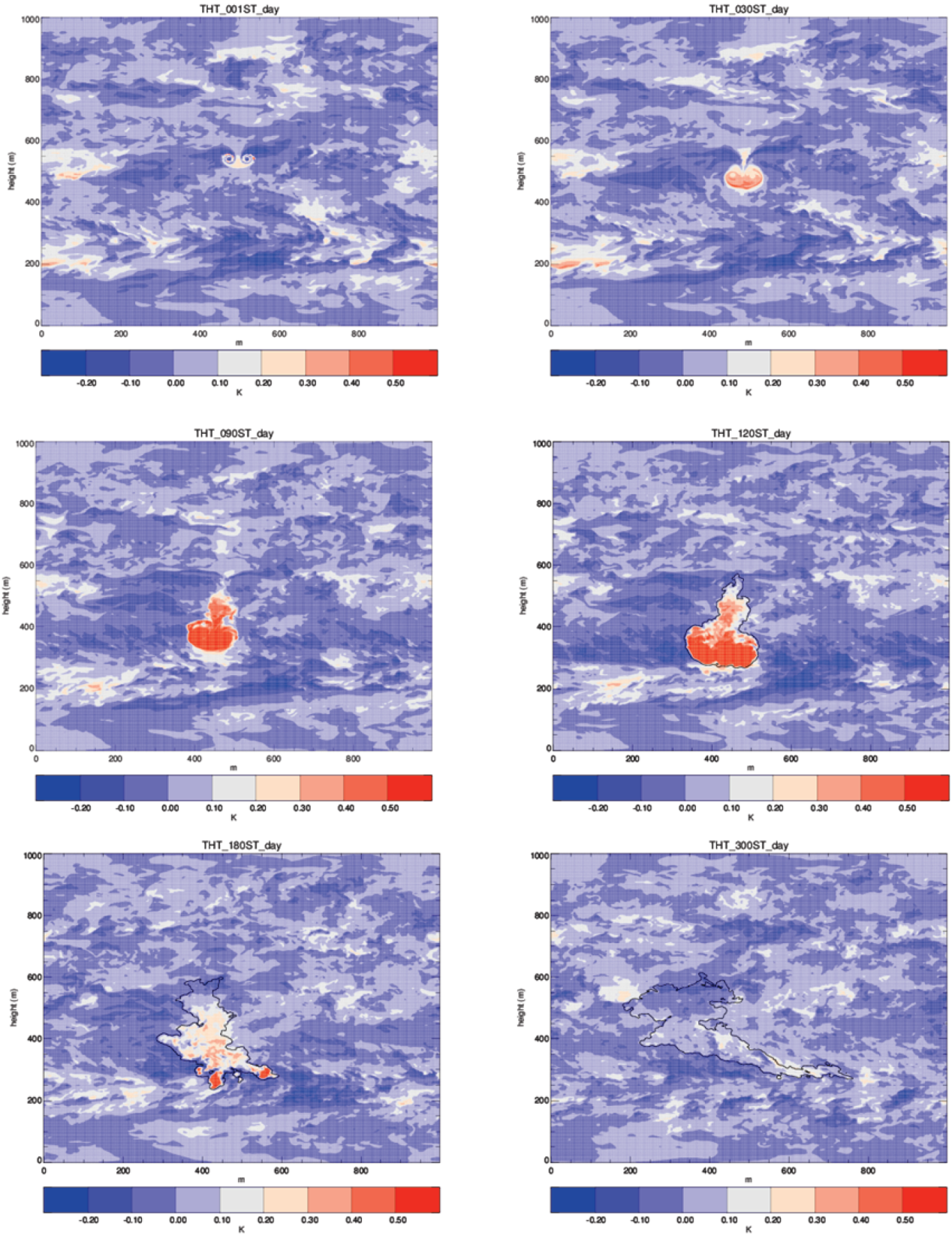

Figure 2. Anomalies of potential temperature (K) from 1 to 300s of simulation with Meso-NH. The black line is a contour of concentration of ice particles used to highlight the position of the vortex as the perturbations due to the vortex become indistinguishable from background variability.

Figure 3, presents the evolution of NO, O_3, NO_2 under daytime conditions. The concentrations of NO and O_3 decrease, and the concentration of NO_2 increases in the vortex according to $NO + O_3 \rightarrow NO_2 + O_2$. There is more ozone during the day than during the night due to the photodissociation $NO_2\ \gamma \rightarrow NO + O$ followed by $O + O_2 \rightarrow O_3$, which results in the formation of ozone (figure 4).

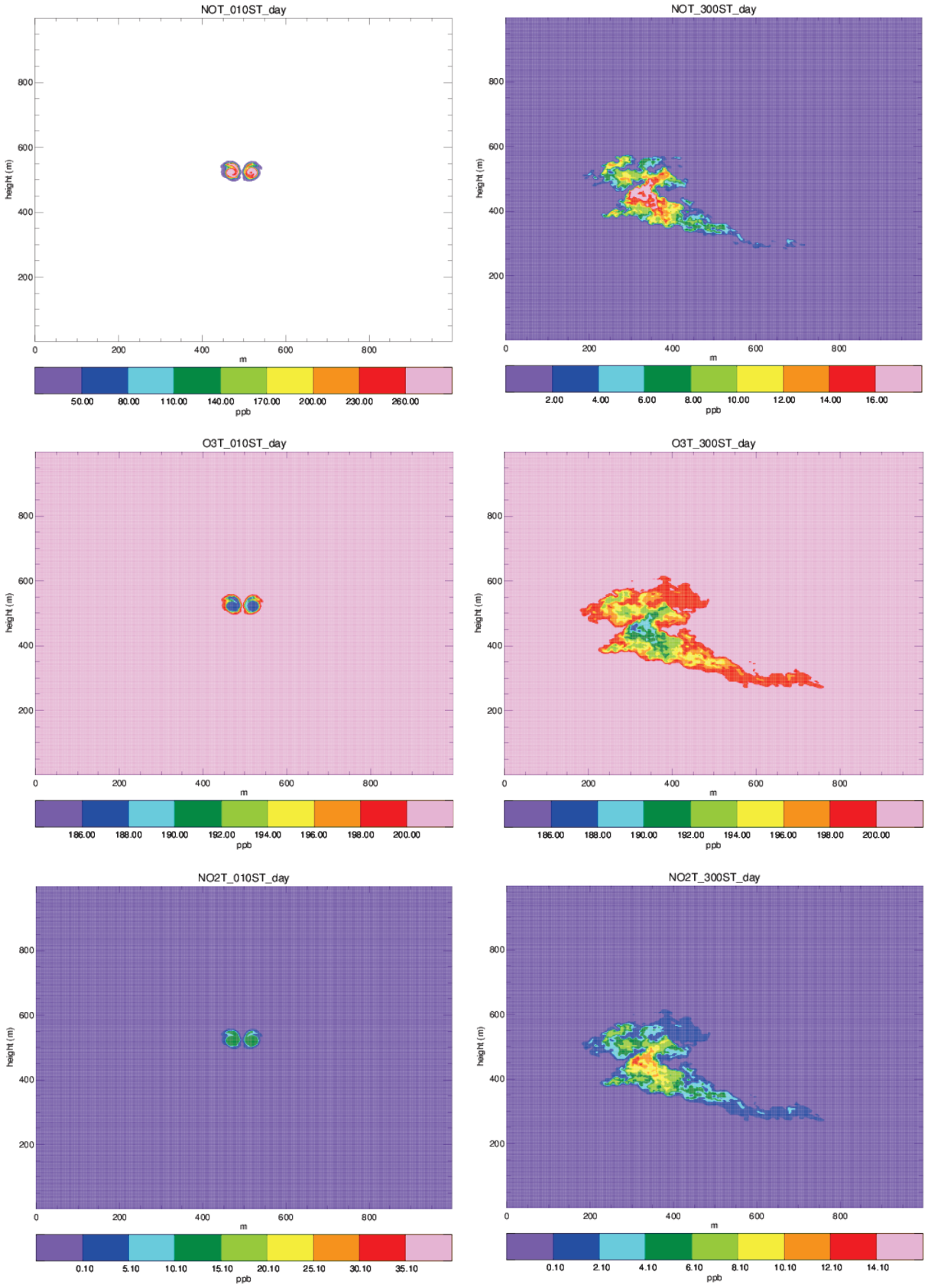

Figure 3. Evolution of NO, O_3 and NO_2 in ppb, after 10s and 120s for the daytime simulation.

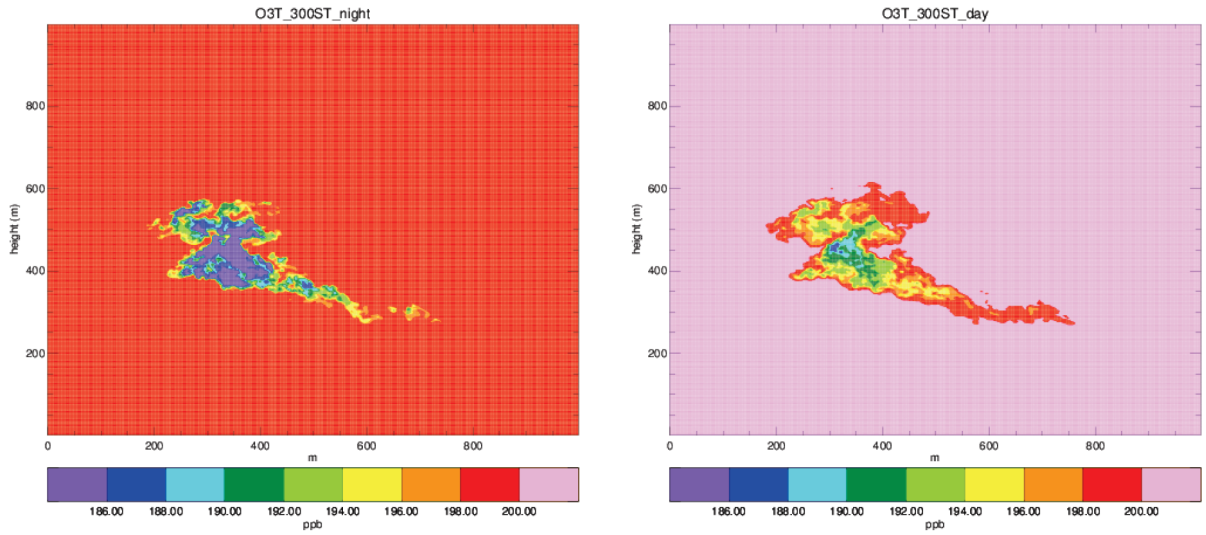

Figure 4. O_3 after 300s day and night (ppb).

In figure 5 we can see that a small quantity of N_2O_5 and NO_3 is produced during the daytime but that much more is produced at night time due to the equilibrium established among the reactions $NO_2 + O_3 \rightarrow NO_3 + O_2$, $NO_3 + NO_2 \rightarrow N_2O_5$ and the photodissociation $NO_3 + \gamma \rightarrow NO_2+O$. In the daytime, there is more ozone, but less NO_2 so less NO_3 is produced. Photodissociation breaks up the NO_3 and therefore only a small amount of N_2O_5 is formed. At night time, there is less ozone, but more NO_2 and resulting in more NO_3. As there is no photodissociation, the NO_3 reacts with NO_2 to form N_2O_5.

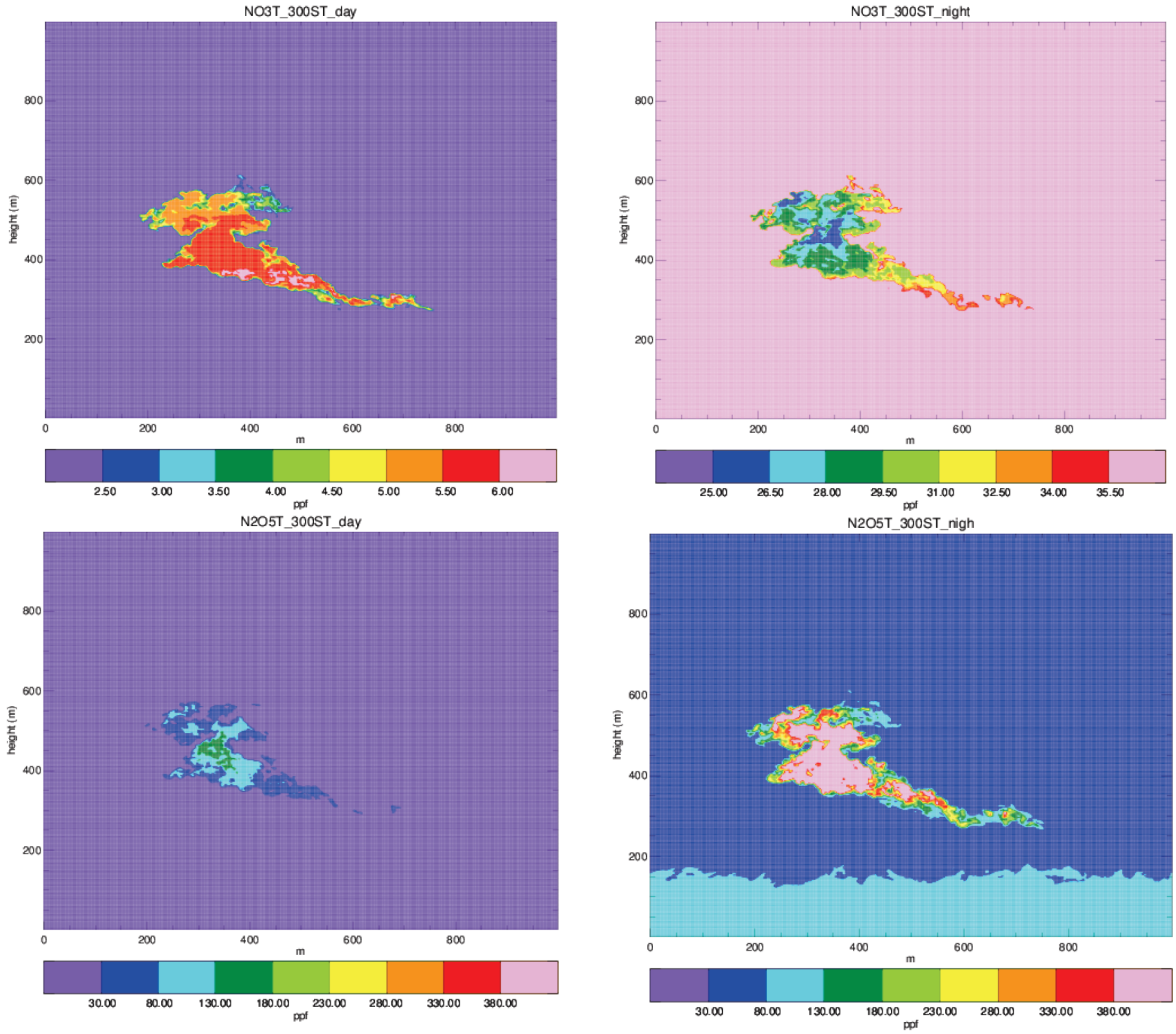

Figure 5. NO_3 and N_2O_5 after 300s day and night (ppf). Note the different contour levels for NO_3 for night and day

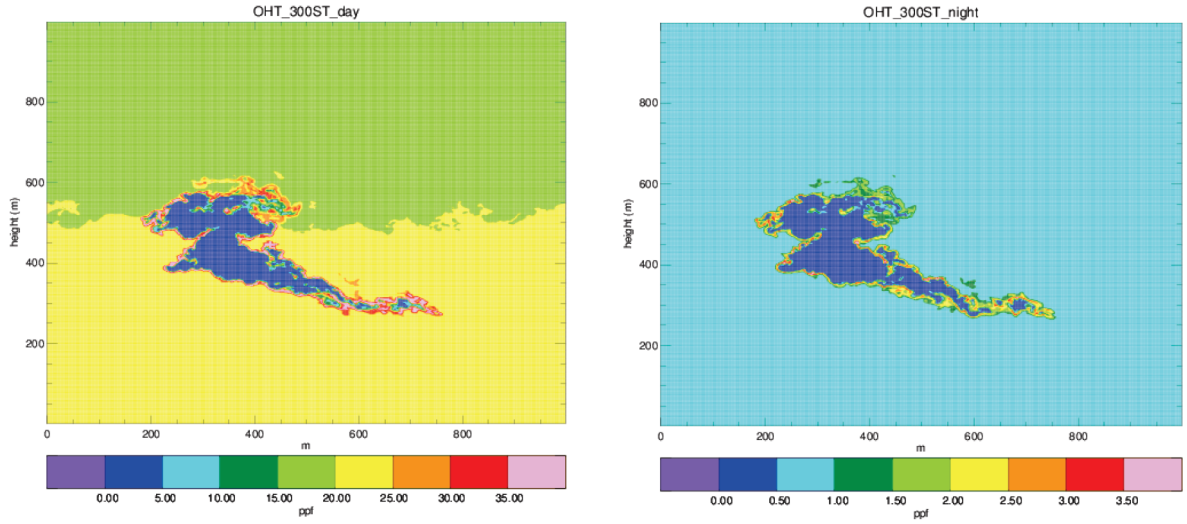

Figure 6. OH (ppf) after 300s day and night.

Figure 6 shows the typical formation of OH around the edge of the vortex according to $NO+HO_2 \rightarrow OH+NO_2$, with an order of magnitude less formed at night. At the centre of the vortex OH is converted to HNO_3 via the reaction $OH+NO_2 \rightarrow HNO_3$ (day) . The formation of HNO_3 in daytime can be seen in figure 7.

4 CONCLUSIONS

We used a multi-scale approach to model the evolution of an aircraft contrail from the vortex phase to the diffusion phase. Dynamical and microphysical quantities were generated by an LES simulation of an aircraft wake and introduced to the Méso-NH mesoscale model running a HO_x/NO_x based chemical scheme. A perturbation in NO was applied based on emissions indices. The behaviour of the model over 300s is largely as expected. The homogeneous chemistry shows important day/night differences in the concentrations of the chemicals formed due to the photolytic reactions. The vortex descends and begins to break up and after 420s, the vortex approaches the boundaries of the small domain. The dynamical, microphysical and chemical fields will then be transferred to the larger domain for a longer simulation with stochastic turbulence. Future plans also include the introduction of heterogeneous chemistry.

REFERENCES

Burkhardt, U., Kärcher, B., and Schumann, U.: Global Modeling of the Contrail and Contrail Cirrus Climate Impact, B. Am. Meteorol. Soc., 91, 479–484, doi:10.1175/2009BAMS2656.1, 2010

Gauss, M., G. Myhre, I. S. A. Isaksen, V. Grewe, G. Pitari et al., Radiative forcing since preindustrial times due to ozone change in the troposphere and the lower stratosphere, Atmos. Chem. Phys., 6, 575-599, 2006.

IPCC, 1999, Aviation and the Global Atmosphere, Cambridge University Press.

Lee, D.S., G. Pitari, V. Grewe, K. Gierens, J.E. Penner, A. Petzold, M.J. Prather, U. Schumann, A. Bais, T. Berntsen, D. Iachetti, L.L. Lim, R. Sausen, Transport impacts on atmosphere and climate: Aviation, Atmospheric Environment 44 (2010) 4678–4734

Lee D.S. D.W. Fahey, P. Forster, P.J. Newton, R.C.N. Wit, L.L. Lim, B. Owen, R. Sausen, Aviation and global climate change in the 21st century, Atmospheric Environment, 43, 3520-3537, 2009.

Madronich, S. and S. Flocke, The role of solar radiation in atmospheric chemistry, in Handbook of Environmental Chemistry (P. Boule, ed.), Springer_Verlag, Heidelberg, pp. 1-26, 1998.

Paoli, R., Thouron, O., Escobar, J., Picot, J., and Cariolle, D.: High-resolution large-eddy simulations of stably stratified flows: application to subkilometer-scale turbulence in the upper troposphere–lower stratosphere, Atmos. Chem. Phys., 14, 5037–5055, doi:10.5194/acp-14-5037-2014, 2014

J. Picot, R. Paoli, O. Thouron , and D. Cariolle, Large-eddy simulation of contrail evolution in the vortex phase and its interaction with atmospheric turbulence, Atmos. Chem. Phys., 15, 7369–7389, 2015

Riese, M., F. Ploeger, A. Rap, B. Vogel, P. Konopka, M. Dameris, and P. Forster, Impact of uncertainties in atmospheric mixing on simulated UTLS composition and related radiative effects, J. Geophys. Res., 117, D16305, doi:10.1029/2012JD017751, 2012

Zeng, G., J. A. Pyle, and P. J. Young, Impact of climate change on tropospheric ozone and its global budgets, Atmos. Chem. Phys., 8, 369–387, doi:10.5194/acp-8-369-2008, 2008.

Uncertainties with respect to contrail coverage modelling in REACT4C

L.L. Lim*, R. Rodríguez De León, D.S. Lee
Faculty of Science and Engineering, Manchester Metropolitan University, UK

O.A. Søvde
Center for International Climate and Environmental Research – Oslo (CICERO), Oslo, Norway

Keywords: REACT4C, contrail coverage, uncertainty

ABSTRACT: The project REACT4C, an EU FP7 funded project, was set out to demonstrate the feasibility of environmentally friendly flight routing. One of the tasks within the project was to provide an analysis of the uncertainties in contrail and contrail-cirrus modelling. An offline contrail coverage model and an offline radiative transfer model were used to estimate the uncertainties due to differences in simulation parameters used to calculate linear contrail coverage. The first difference investigated was the application of two emissions inventories used in REACT4C; AEM and FAST. This showed that the differences seen are largely due to the spatial and vertical distribution of the distance travelled in the inventories, and that there were no linear relationship between distance travelled and contrails radiative forcing (RF). The second investigation was into the application of different temporal resolutions for the emissions inventory. Here, the contrail coverage and RF were found to be sensitive to the diurnal variation of air traffic. Therefore, it is important to know the actual diurnal traffic variation throughout the day, since this can significantly change the RF results, even when it was averaged on a global and annual basis. In contrast, the monthly variation in air traffic did not significantly impact the coverage and RF results. The results presented in this paper informed us on the range of values that we might expect from the assessment of different contrails and contrail-cirrus studies.

1 INTRODUCTION

The project REACT4C was set out to estimate the overall global effect of climate-optimized Air Traffic Management measures. One of the project objectives was to provide an analysis of the uncertainties in contrail and contrail-cirrus modelling. An offline contrail coverage model, the COntrail Modelling and Analysis tool (COMA) (Lim et al., 2012) and the Edwards-Slingo radiative transfer model (Edwards and Slingo, 1996) with the setup of contrail radiative properties as described in De León et al. (2012), were used to achieve this. The focus of this study was to estimate the uncertainties due to two main parameters that are used to calculate contrail and contrail-cirrus coverage, i.e. the aircraft emissions inventory and its temporal resolution. Even though previous studies (for example, Lee et al., 2009) found that the contribution of linear contrails to global radiative forcing (RF) was smaller than some aviation impacts, it is important to firstly understand the uncertainties in linear contrails. This is because contrail-cirrus are made up of young line-shaped contrails and irregularly shaped contrails that formed from aged contrails that persist and spread (Burkhardt and Kärcher, 2011). On a short-term timescale, contrail-cirrus has been shown to make a significant contribution to the total RF from aviation (Lim et al., this proceedings). The magnitude of this contribution may be affected by the uncertainties assessed in this study.

2 DIFFERENCES DUE TO EMISSION INVENTORIES

Two aircraft emission models were used in the REACT4C project; AEM (Skowron et al., 2013), which was used to produce the climate-optimized routing scenarios over the North Atlantic, and FAST (Skowron et al., 2013), which was used to assess the impacts from simplified mitigation sce-

* *Corresponding author:* Ling L. Lim, Faculty of Science and Engineering, Manchester Metropolitan University, Chester St, Manchester M1 5GD, UK. Email: l.lim@mmu.ac.uk

narios. These inventories were extrapolated from 6-weeks of movements data to a year, and have a regular horizontal grid of 1° x 1°. Table 1 shows the main differences between the global AEM and FAST inventories for 2006 that are relevant to contrail coverage calculations. The total distance above 500 hPa is an important criterion for contrail assessments, since contrails are likely to form in regions above this height.

Table 1: AEM and FAST data comparison

	AEM	FAST
Vertical resolution	Up to 47,000 ft at 500 ft intervals	Up to 44,000 ft at 2,000 ft intervals
Distance type	Radar trajectory within US-FAA and EU-EUROCONTROL airspace, great circle for the rest of the world	Great circle globally
Annual total distance	~43.5 billion km	~38.9 billion km
Total distance above 500 hPa	~36.1 billion km (83% of total)	33.7 billion km (87% of total)

The global annual mean contrail coverage for both the AEM and FAST inventories are shown in Figures 1 (a) and (b) respectively. The AEM inventory produced a global contrail coverage that was 10% higher than FAST, even though the distance travelled above 500 hPa was only 7% higher.

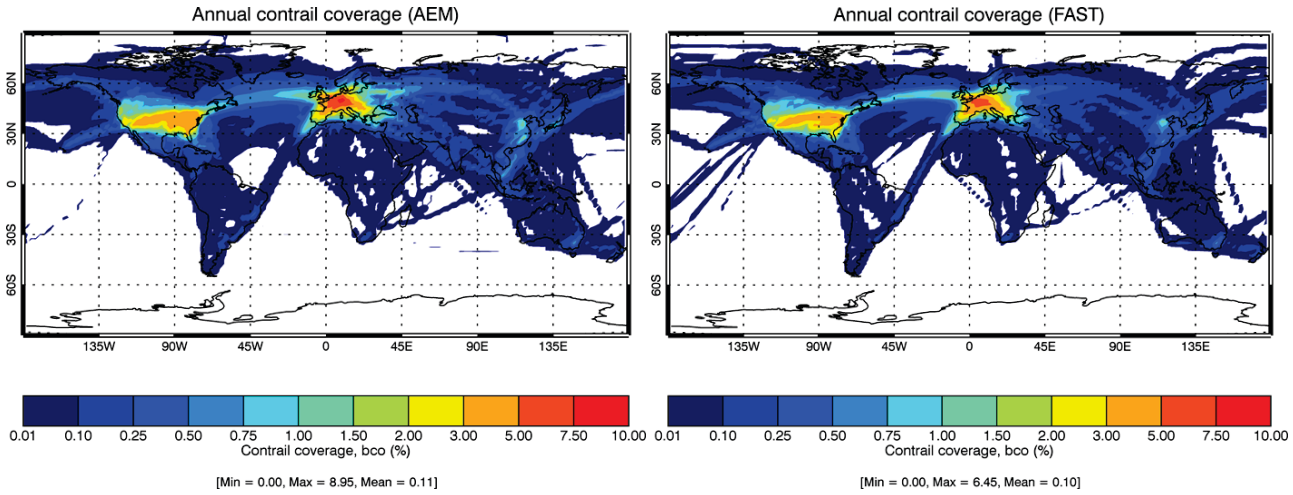

Figure 1: Calculated contrail coverage for the (a) AEM and (b) FAST aircraft emissions inventories

Figures 2 (a) and (b) show the RF distributions due to contrail coverages derived from the AEM and FAST inventories respectively. The global RF difference between inventories for these coverages was 18%. This implied that the relationship between distance travelled and RF is non-linear. We also found that the differences seen here are largely due to the spatial and vertical distributions of the distance travelled in the inventories.

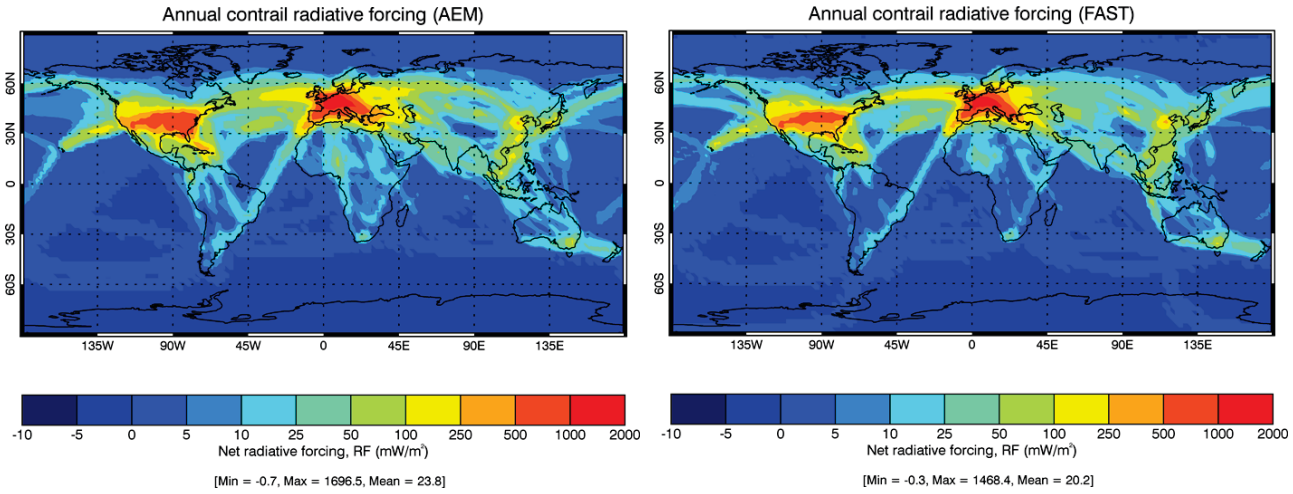

Figure 2: Radiative forcing from the (a) AEM and (b) FAST derived distance travelled

3 DIFFERENCES DUE TO TEMPORAL RESOLUTION

Several case studies were conducted to investigate the differences in contrails RF due to the temporal resolution of the FAST inventory. In this section, we present the contrail coverage and RF results calculated from diurnal and seasonal emissions dataset from a selected case study.

The global coverage differences between time bands were significant, with the highest at 18 UTC, which was 240% higher than the lowest at 06 UTC (Figure 3). In addition, the coverage did not follow the trend observed in the traffic density, where the highest global distance travelled above 500 hPa was at 12 UTC and this was only 47% higher than the lowest at 00 UTC. This indicated that the meteorology at 18 UTC played a stronger role in contrail formation than the traffic density at 12 UTC.

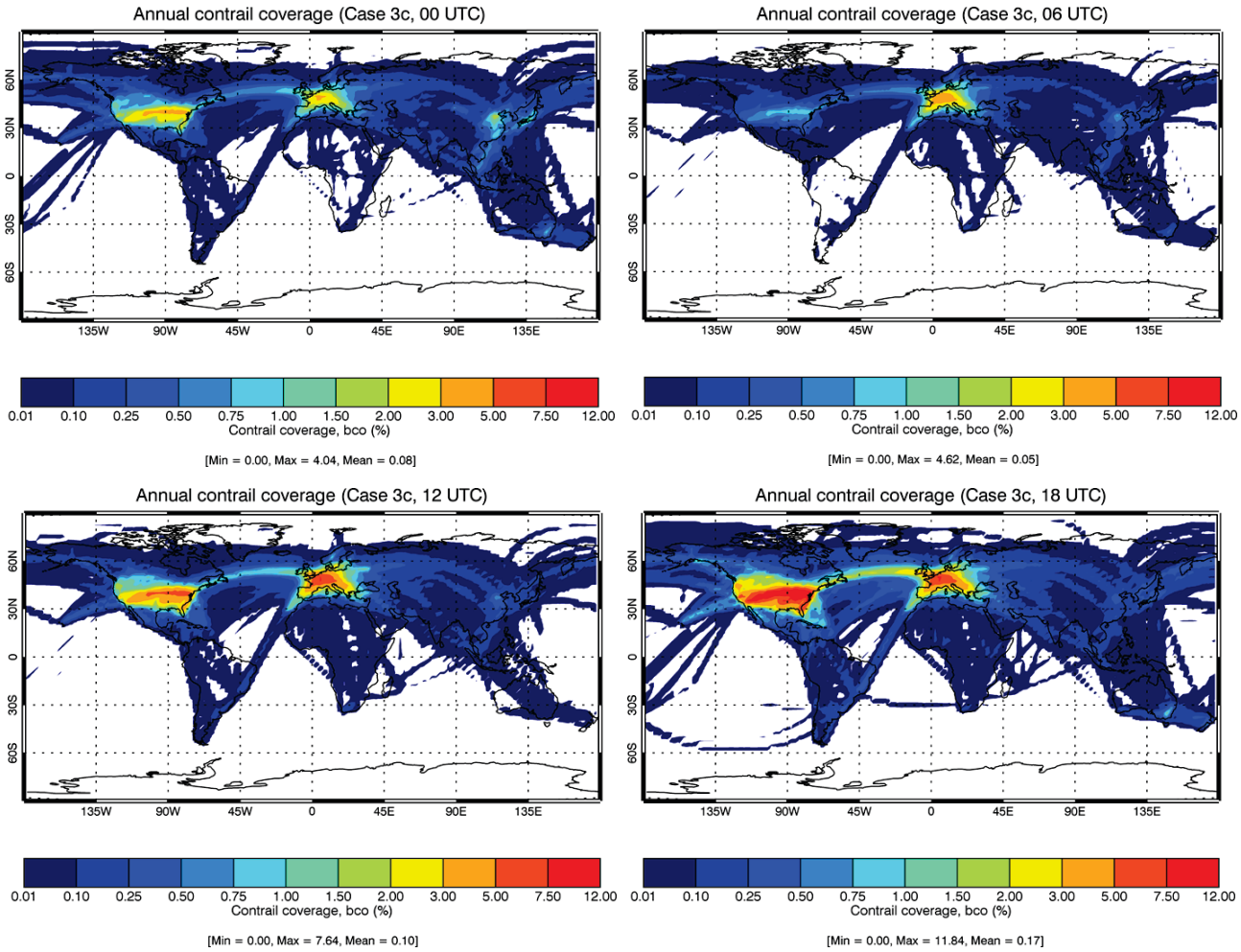

Figure 3: Calculated contrail coverage for (a) 00 UTC, (b) 06 UTC, (c) 12 UTC and (d) 18 UTC

Figure 4 shows that boreal winter forcings were larger than the summer forcings by more than 100%. The smaller global forcings in the summer were due to the lower summer contrail coverage compared with winter, and the longer daylight hours in the northern hemisphere where contrails coverage was also the highest. The difference is related to the fact that the negative RF contribution from the shortwave RF component is enhanced during the boreal summer in the northern hemisphere by the longer daylight times.

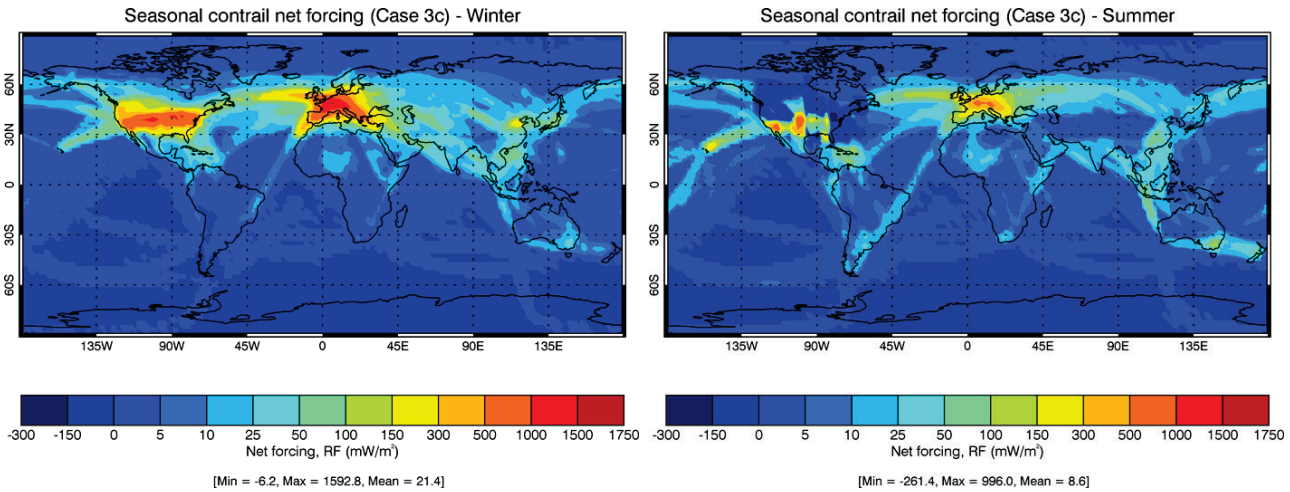

Figure 4: Seasonal radiative forcing for the Northern Hemisphere (a) winter and (b) summer contrail coverages

The temporal resolution case studies showed that the simulated contrail RF is more sensitive to diurnal than seasonal traffic variability, even when the results were averaged on a global and annual basis.

4 SUMMARY

This study found that contrail coverage and RF differences from the application of different emissions inventories are not negligible. In addition, there did not appear to be a linear relationship between distance travelled and the global means values of contrail coverage and RF impacts. In terms of temporal resolution of the inventories, contrail coverage and RF impacts are sensitive to diurnal variability, while the dependence on the monthly traffic variation appears to be not significant. The results presented here informed us on the range of values that might be expected from the assessment of different contrails and contrail-cirrus studies.

ACKNOWLEDGEMENTS

This work was supported by the European Commission Seventh Framework Project, 'REACT4C' (contract no. ACP8-GA-2009-233772, http://www.react4c.eu/). The ICAO-CAEP/MDG (http://www.icao.int/ENVIRONMENTAL-PROTECTION/Pages/modelling-and-databases.aspx) and EUROCONTROL (http://www.inventair.eurocontrol.int/home) are acknowledged for providing aircraft emissions inventories.

REFERENCES

Burkhardt, U. and B. Kärcher, 2011: Global radiative forcing from contrail cirrus. Nature Climate Change 1, 54-58.

De León, R. R., M. Krämer, D.S. Lee and J.C. Thelen, 2012: Sensitivity of radiative properties of persistent contrails to the ice water path. Atmospheric Chemistry and Physics, 12(17), 7893-7901.

Edwards J.M. and A. Slingo, 1996: Studies with a flexible new radiation code I: choosing a configuration for a large-scale model. Q. J. Royal Meteor. Soc. 122, 689-719.

Lee, D.S., D.W. Fahey, P.M. Forster, P.J. Newton, R.C.N. Wit, L.L. Lim, B. Owen and R. Sausen, 2009: Aviation and global climate change in the 21st century. Atmospheric Environment 43, 3520-3537.

Lim, L.L., R. Rodríguez De León, B. Owen, D.S. Lee and J.K. Carter, 2012: Contrail coverage from future air traffic. In: Sausen, R., S. Unterstrasser, A. Blum (eds.), Proceedings of the 3rd International Conference on Transport, Atmosphere and Climate (TAC-3). Deutsches Zentrum für Luft- und Raumfahrt (DLR), Institut für Physik der Atmosphäre, Oberpfaffenhofen, Deutschland, ISSN 1434-8454, ISRN DLR-FB-2012-17, 189-192.

Lim, L.L., D.S. Lee, B. Owen, A. Skowron, S. Matthes, U. Burkhardt, S. Dietmüller, G. Pitari, G. Di Genova, D. Iachetti, I. Isaksen and O. Søvde, (this proceedings): REACT4C: Simplified Mitigation Studies.

Skowron, A., D.S. Lee, and R.R. De León, 2013: The assessment of the impact of aviation NOx on ozone and other radiative forcing responses – The importance of representing cruise altitudes accurately. Atmospheric Environment 74, 159-168.

Ice optical thickness retrieval using SEVIRI-1/2/3 aboard the Meteosat 8-10 satellites: towards a cirrus life cycle analysis

J. Strandgren*, L. Bugliaro, M. Schmidl
DLR-Institut für Physik der Atmosphäre Oberpfaffenhofen, Germany

Keywords: ice clouds, optical thickness, MSG-SEVIRI, remote sensing

ABSTRACT: COCS is a neural network trained with coincident SEVIRI (Spinning Enhanced Visible and Infrared Imager) and CALIOP (Cloud-Aerosol Lidar with Orthogonal Polarization) measurements in order to retrieve the ice optical thickness (IOT) and the ice cloud top altitude using the thermal channels of SEVIRI. In this paper the instrument dependence for the IOT retrieval of COCS is investigated using the three SEVIRI instruments aboard the operational Meteosat Second Generation (MSG) satellites as a first step towards the analysis of the cirrus life cycle. From a combination of qualitative and quantitative analysis using COCS IOT together with SEVIRI false color RGB composites and IOT derived from CALIOP L2 data it is concluded that COCS has a clear instrument dependence and tends to overestimate the amount of thin ice clouds (IOT$\lesssim$0.30) in the tropics when applied to SEVIRI-2/3. COCS seems to be more accurate using SEVIRI-1 data and thus it is further concluded that SEVIRI-1 should be prioritized for natural and contrail cirrus analysis in the tropics unless this feature is alleviated with a re-training of COCS.

1 INTRODUCTION

The "Cirrus Optical properties derived from CALIOP and SEVIRI during day and night" (COCS, Kox et al, 2014) algorithm is a neural network that has been trained with coincident measurements by SEVIRI-1/2 and CALIOP. The SEVIRI instruments (Schmetz et al, 2002) operate in geostationary orbits with 7 thermal and 3 solar channels together with one mixed solar/thermal channel. Since 2004 the instruments have been launched aboard MSG four times (October 2015). CALIOP was launched in 2006 and is a space-borne polarized LIDAR operating in a polar orbit with a vertical resolution of up to 30m (Winker et al, 2009). With COCS the main advantages of the two instruments have been combined i.e. the high temporal resolution and spatial coverage of SEVIRI and the high vertical resolution of CALIOP. COCS takes seven SEVIRI brightness temperatures and brightness temperature differences together with latitude, viewing zenith angle and a land-sea mask as input and provides the IOT and the ice cloud top altitude as output. Since COCS is independent of solar channels and thus solar radiation it can operate during both day and night. To maintain sufficiently high ice cloud detection efficiency together with a low false alarm rate, COCS IOT values lower than 0.1 are considered too inaccurate and are set to zero (Kox et al, 2014).

As a first step towards a cirrus life cycle analysis using COCS in combination with other algorithms, the instrument dependence of the COCS IOT is presented in this paper. As explained above, COCS is trained with data from SEVIRI-1/2, but even though SEVIRI-1/2/3 have the same design and specifications they cannot be identical and COCS can therefore not be assumed to work identically when applied to data from the three respective instruments.

This paper is divided into four sections. Following the introduction, the COCS instrument dependence analysis and the conclusions are presented in section 2 and 3 respectively. Finally an outlook for the next steps towards the cirrus life cycle analysis is presented in section 4.

* *Corresponding author:* Johan Strandgren, DLR-Institut für Physik der Atmosphäre, Oberpfaffenhofen, D-82205 Wessling, Germany. Email: johan.strandgren@dlr.de

2 THE INSTRUMENT DEPENDENCE OF COCS

2.1 *Qualitative comparison between COCS IOT and SEVIRI false color RGB composites*

As a first step the COCS IOT for three MSG SEVIRI scenes were analyzed (2006-05-01, 2010-05-01 and 2015-05-01 at 13:00 UTC), representing the currently operational SEVIRI-1, SEVIRI-2 and SEVIRI-3 instruments respectively. For a qualitative analysis of the COCS ice cloud detection efficiency and false alarm rate the IOT for the three SEVIRI scenes were compared to corresponding false color RGB composites derived using the SEVIRI channels 1, 2 and 9 (0.6, 0.8 and 10.8μm).
The COCS IOT for the three SEVIRI scenes together with the corresponding false color RGB composites can be seen in Fig. 1. From the false color RGBs one gets a good 2D overview of the atmosphere and clouds can easily be separated from clear skies. Furthermore, colder ice clouds can be distinguished from the warmer water clouds, as they appear as white or bluish while the warmer water clouds appear as yellowish. Since the three scenes are from three different years we cannot make a quantitative comparison of the COCS IOT for the three SEVIRI instruments, but we can see that for all three instruments COCS succeeds in identifying the evident ice clouds in the respective RGBs. The frontal systems in the mid-latitudes and the convective clouds along the inter-tropical convergence zone are successfully captured by COCS as well as the cloud free regions at the subsidence zones around the horse latitudes.

For the SEVIRI-2/3 scenes COCS retrieves significantly more thin ice clouds (Fig. 1 center and bottom right) compared to the SEVIRI-1 scene (Fig. 1 top right), especially in the tropics. The IOT-RGB comparison apparently reinforces this impression, that the amount of thin ice clouds in the tropics is overestimated by COCS when applied to the SEVIRI-2/3 data. However it is unclear whether/when thin ice clouds with optical thicknesses in the range 0.0-0.3 should be visible in a false color composite.

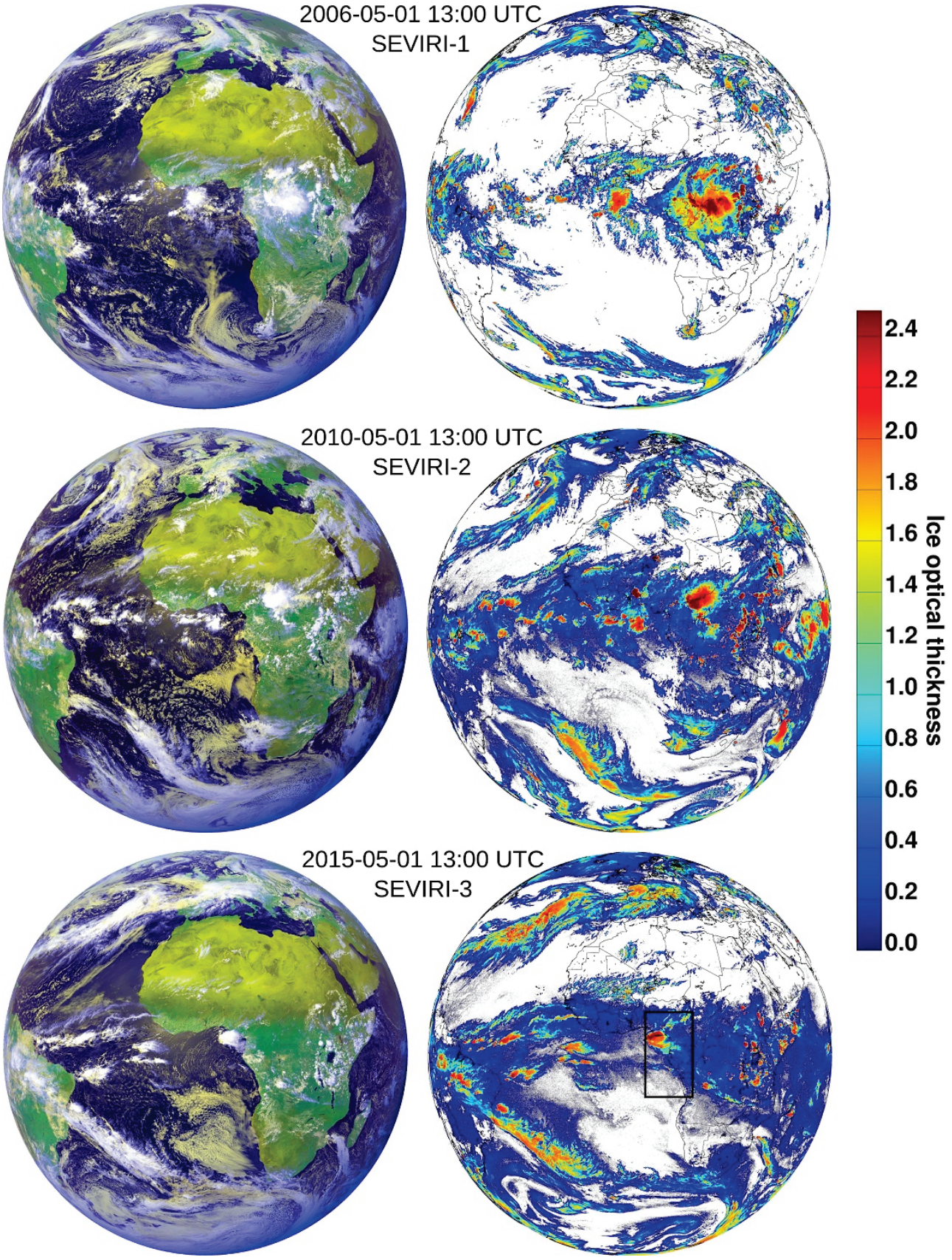

Figure 1: SEVIRI false color RGB composites (left column) and ice optical thickness retrieved by COCS (right column) using SEVIRI-1 (top), SEVIRI-2 (center) and SEVIRI-3 (bottom). Ice clouds are recognized as white or bluish in the false color composites, whereas liquid water clouds are recognized as yellowish. The black rectangle in the bottom right figure shows the region studied in more detail in section 2.2

2.2 *Quantitative comparison between COCS and CALIOP IOT*

To acquire more information on whether COCS in fact overestimates the amount of thin ice clouds in the tropics using the more recent SEVIRI-2/3 instruments, a more quantitative point-by-point comparison between the COCS IOT and IOT derived from the CALIOP L2 cloud layer data on a 5km horizontal grid (CAL_LID_L2_05kmCLay-Prov-V3-30) was made. CALIOP IOT from 10°S to 10°N (12.3°E to 8.5°E) was extracted and matched spatially and temporally to the COCS IOT from the SEVIRI-3 scene (at 2015-05-01 13:00 UTC). The result can be seen in Fig. 2.

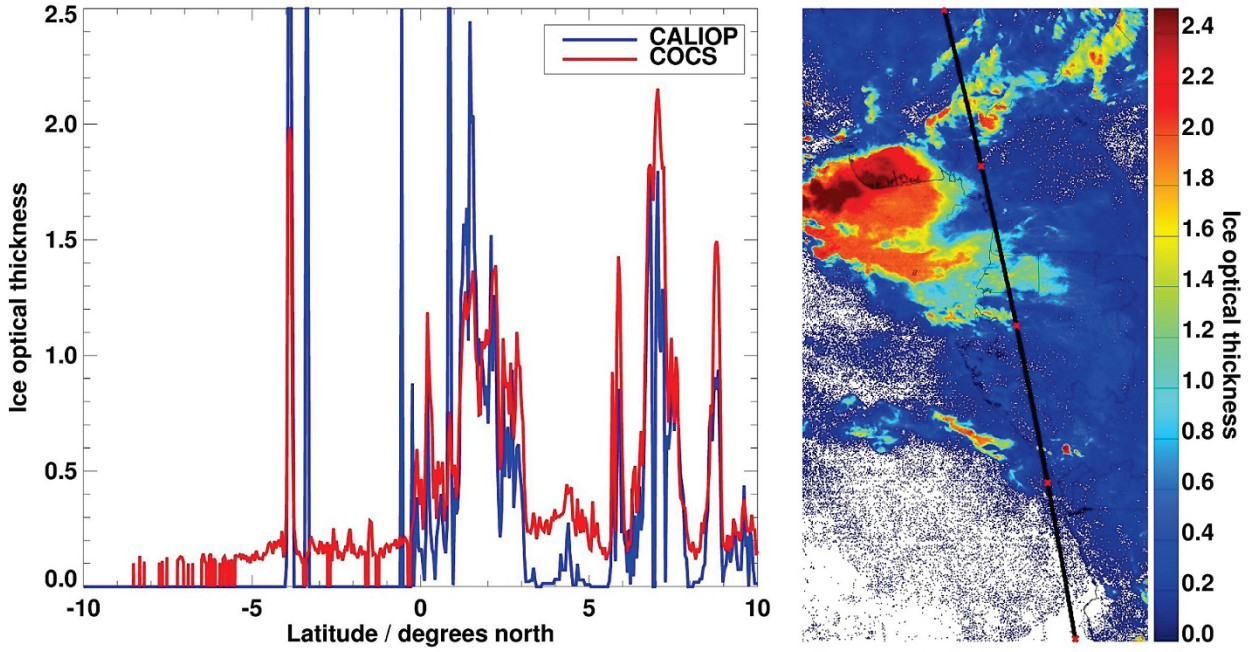

Figure 2: Left: point-by-point comparison between COCS and CALIOP IOT along the CALIOP track in the tropics (from 10°S to 10°N). Right: The CALIOP track on top of the COCS IOT for the region of comparison. Latitudes from 10°S to 10°N are marked with red crosses on the CALIOP track with a 5 degree interval for an easier comparison with the left figure.

From the Fig. 2 it is clear that COCS has high detection efficiency and the respective peaks in the COCS and CALIOP IOT are spatially very well aligned. However, the issue discussed in section 2.1 remains, namely that COCS has a high false alarm rate in the tropics. Where CALIOP detects IOT values less than 0.1 (i.e. no ice cloud according to COCS due to its lower detection threshold at 0.1), COCS generally obtains IOT values ranging from 0.1 to 0.3, resulting in a high false alarm rate of COCS. This pattern can clearly be seen at latitudes< -4°N, -3.5°N<latitudes<-0.5°N and 3°N<latitudes<5.5°N.

3 CONCLUSION

The instrument dependence of the neural network based algorithm COCS is investigated using data from SEVIRI-1/2/3. A qualitative comparison between the IOT derived by COCS and corresponding SEVIRI false color RGB composites was made together with a more quantitative comparison between the COCS IOT and IOT derived from CALIOP L2 cloud layer data. It is concluded that COCS has a clear instrument dependence and tends to overestimate the amount of thin ice clouds (IOT$\lesssim$0.30) in the tropical regions when it is applied to data from SEVIRI-2/3 compared to SEVIRI-1 data. Unless this feature is alleviated with a re-training of COCS it is recommended to prioritize SEVIRI-1 data for natural and contrail cirrus analysis in the tropics using COCS.

It is also concluded that for the training of a neural network like COCS it would be favorable to separate data from the respective SEVIRI instruments and possibly also regions with large climatological differences like the tropics and the mid-latitudes.

4 OUTLOOK

The next steps towards the analysis of the cirrus life cycle are (1) to further analyze the performance of COCS for the three SEVIRI instruments for a better and more complete understanding of the results presented in this paper. (2) To perform a validation and characterization of COCS using simulated SEVIRI brightness temperatures or CALIOP data to understand how COCS performs for different vertical cloud structures; e.g. one layer ice cloud, multiple vertically separated layers of ice clouds, ice clouds above liquid water clouds etc. (3) To develop a sophisticated cirrus tracking algorithm that can work in synergy with COCS and other algorithms in order to monitor the temporal evolution of optical, macro- and microphysical properties of ice clouds.

With respect to (2) above, Fig. 3 shows a comparison between measured and simulated SEVIRI brightness temperatures at 9.7µm (left) and temperature differences between 6.2 and 7.3µm (right). The simulated data have been calculated with the radiative transfer model libRadtran (Mayer and Kylling, 2005) using meteorological data from ECMWF (European Centre for Medium-Range Weather Forecasts) together with spectral surface emissivities from the Moderate Resolution Imaging Spectroradiometer (MODIS) (Seemann et al, 2008). With a generally high correlation between measured and simulated brightness temperatures and temperature differences the simulated data constitutes a potentially good data set for the validation and characterization of COCS. For temperature differences (between 6.2 and 7.3µm) greater than approximately -15°C the correlation is reduced and this feature should be investigated before a validation and characterization of COCS using the simulated data set is made.

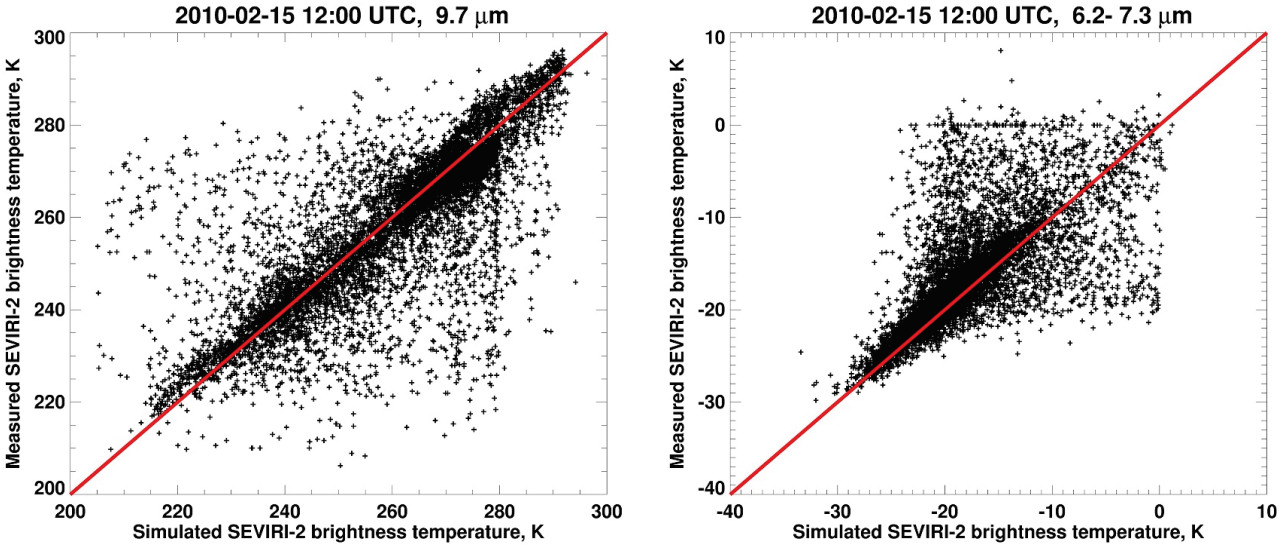

Figure 3: Simulated SEVIRI-2 brightness temperatures ($BT_{9.7\mu m}$) and temperature differences ($BT_{6.2\mu m}$-$BT_{7.3\mu m}$) versus the corresponding measured SEVIRI-2 brightness temperatures and temperature differences.

ACKNOWLEDGEMENTS

The CALIOP L2 data were obtained from the NASA Langley Research Center Atmospheric Science Data Center.

REFERENCES

Kox, S., L. Bugliaro, and A. Ostler, 2014: Retrieval of cirrus cloud optical thickness and top altitude from geostationary remote sensing. Atmos. Meas. Tech., 7, 3233-3246

Mayer, B., and A. Kylling, 2005: Technical note: The libRadtran software package for radiative transfer calculations – description and examples of use. Atmos. Chem. Phys., 5, 1855–1877

Schmetz, J., P. Pili, S. Tjemkes, D. Just, J. Kerkmann, S. Rota, and A. Ratier, 2002: An introduction to Meteosat Second Generation (MSG). Bull. Amer. Meteor. Soc., 83, 977–992,

Seemann, A.W., E.E. Borbas, R.O. Knuteson, G.R. Stephenson, and H.-L. Huang, 2008: Development of a Global Infrared Land Surface emissivity Database for Application to Clear Sky Sounding Retrievals from Multispectral Satellite Radiance Measurements. J. Appl. Meteor., 47, 108-123

Winker, D.M., M.A. Vaughan, A. Omar, Y. Hu, K.A. Powell, Z. Liu, W.H. Hunt, and S.A. Young, 2009: Overview of the CALIPSO Mission and CALIOP data processing algorithms. J. Atmos. Ocean. Technol. 26(11), 2310-2323

Examining the effect of aviation NO_x emissions as a short-lived climate-forcer: assessing the linearity of the NO_x – O_3 chemical system

S. J. Freeman*, L. L. Lim and D. S. Lee
Centre for Aviation, Transport and the Environment, Manchester Metropolitan University, UK

Key words: Aviation, NO_x, CO_2, climate forcers, LinClim, simple climate model (SCM), MOZART 3, chemistry transport model (CTM)

ABSTRACT: As an aircraft travels thought the atmosphere it emits greenhouse gases, primarily CO_2 and NO_x. Both of these gases affect the radiative forcing of the climate, albeit over different timescales. In the attempt to mitigate aviation emissions, studies have shown that the trade-off in reducing either CO_2 or NO_x emissions, by modifying aircraft engines, results in an increase in the other species. Modelling CO_2 emissions is simple, the relationship between emission and atmospheric concentration is linear, however the NO_x – O_3 system in the atmosphere is not linear and therefore more complex to model. This study used the MOZART 3 chemistry transport model (CTM) to ascertain that on the scale at which aviation takes place, the NO_x – O_3 relationship is sufficiently linear to allow the use of a simple climate model (SCM) in the study of both short- and long-term climate forcers over the longer term (>100 years). A scaling method can also be applied during model runs to increase the accuracy of SCM results.

1 INTRODUCTION

Aviation impacts the atmosphere on a global scale and its effects on the climate are still somewhat uncertain. International aviation is currently not included in the Kyoto protocol, and as a result is also not included in international emissions reductions policies (Owen et al., 2010). The main emissions resulting from aviation activity are carbon dioxide (CO_2) and nitrogen oxides (NO_x) (Lee et al., 2010), CO_2 is not particularly reactive; it simply accumulates in the atmosphere and acts as a greenhouse gas, once emitted it becomes well mixed and independent from its source. NO_x on the other hand is particularly reactive and promotes the formation of ozone and destruction of methane in the upper troposphere lower stratosphere region of the atmosphere – where aircraft fly. Measures can be put in place to reduce the amount of CO_2 emitted from an aircraft engine; more complete combustion can be accomplished by increasing the engine pressure ratio, which reduces fuel flow and therefore, CO_2 emissions. However, increasing the engine pressure ratio results in higher combustion temperatures, more dissociation of nitrogen and therefore higher NO_x emissions. Changing the configuration of the combustor to reduce NO_x emissions results in more unburnt hydrocarbons and thus, increased CO_2 emissions (Antoine & Kroo, 2004). Unfortunately, the trade-off of reducing either CO_2 or NO_x results in an increase in the other. The ultimate aim of this work is to determine the trade-offs between a reduction of short-lived climate-forcers (SLCFs) such as aircraft NO_x emissions at the expense of CO_2 emissions, over the long term (>100 years), and therefore examine whether controlling aviation NO_x emissions could help mitigate global climate change.

1.1 *Background atmosphere*

The background atmospheric concentrations of reactive chemical species such as NO_x are heavily influenced by changes in surface emissions. This is particularly relevant when modelling aviation as the magnitudes of the chemical perturbations depend strongly on the background atmosphere into which they are emitted. Of particular interest for this study is the response of ozone (O_3) formation from aviation NO_x emissions. Emissions from the surface determine the state of the background atmosphere – a change in surface emissions changes the concentrations of ozone precursors and therefore the oxidising capacity of the atmosphere (Fry et al., 2012). Thus, the relationship between

* *Corresponding author:* Sarah Freeman, Faculty of Science and Engineering, Manchester Metropolitan University, Chester St, Manchester M1 5GD, UK. Email: S.Freeman@mmu.ac.uk

aviation NO_x emissions and O_3 production is affected by changes in surface emissions of O_3 precursors. Unger et al., (2013) note that studies of future effects of aviation emissions fail to account for changing background conditions, this study attempts to contribute to that understanding.

2 LONG TERM STUDIES AND THE LINCLIM SIMPLE CLIMATE MODEL (SCM)

Figure 1 taken from Daniel et al., (2011) partially inspired this study. It shows that climate is affected differently over short and long time-scales and depends on the species emitted and the magnitude of emission. To model the climate over the long term, the use of a simple climate model (SCM) is necessary. Unlike a full global climate model, simple climate models run instantaneously and inexpensively. They are used to calculate global chemical concentrations and corresponding Radiative Forcing (RF) values for the next several hundred years, making them ideal for studies of long-term climate. The simplicity of SCMs such as LinClim, the SCM used in this study specifically designed to study aviation (Lim et al., 2006), relies on the linearity of the chemical reactions involved in aviation emissions. For CO_2 the calculation is linear, as for every kg of fuel burnt by an aircraft engine, 3.16 kg CO_2 is released. However, the atmospheric NO_x – ozone reactions are not as simple, and non-linearity exists in the system. The purpose of this study is to test the bounds of non-linearity within the NO_x – O_3 system with respect to aviation emissions, using a global CTM, MOZART 3, and therefore justify the use of LinClim SCM in studying the long term effects of aviation.

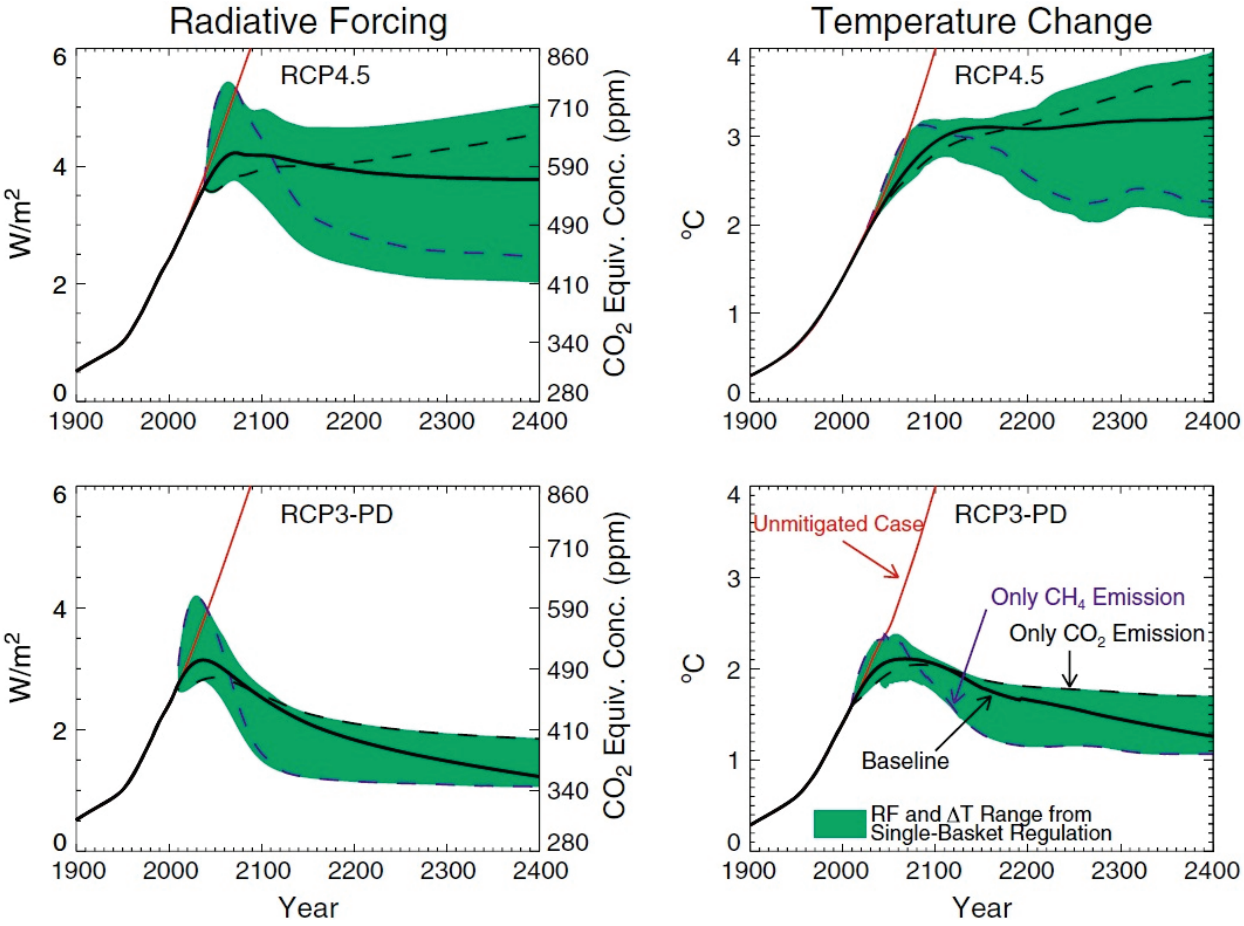

Figure 1: This graph is taken from Daniel et al., (2011) which investigates the approach of grouping emissions in reductions policies. For the purpose of this study the graphs show that different greenhouse gases affect the climate differently over the short and long term. In this case it shows that methane release warms the climate more in the short term, but over the longer term its effects decline while those of CO_2 release continue and increase due to its cumulative nature in the atmosphere.

The LinClim model was designed specifically to model aviation and therefore has a relatively simple representation of the carbon cycle. It relies on a single impulse response function (IRF), which is calibrated to a more sophisticated parent model, creating a parameterization. In general, a single

IRF is used to represent the carbon cycle in SCMs used to study aviation as it is assumed that the forcing from aviation CO_2 is weak enough to allow the system to respond linearly. The single IRF in this case calculates changes in atmospheric CO_2 based on specific emissions scenarios. We propose a series of modifications to LinClim to improve its accuracy, which are discussed later.

3 METHODOLOGY FOR NO_X CALCULATIONS AND THE MOZART 3 CTM

In this study, MOZART 3 CTM will be used to generate ozone concentrations resulting from different aviation scenarios that were emitted into different background atmospheres. The aviation scenarios come from the React4c project (http://www.react4c.eu/). In this study, the React4c base case, which represents aviation in 2006, was scaled up to create possible future aviation scenarios, which were then run on MOZART 3. There were two background atmospheres in the experiment each with different concentrations of surface NO_x emissions. The values were taken from the RCP scenarios and were chosen to represent a possible future 'clean' (RCP3 2100; 20.76 Tg N/yr) and 'dirty' (RCP8 2020; 44.75 Tg N/yr) atmospheric state, regarding NO_x emissions. This experiment was essential as the formation of ozone from aviation NO_x depends heavily on the state of the background atmosphere into which the NO_x is emitted.

4 RESULTS AND DISCUSSION

Ozone forms more readily at flight altitudes than at ground level due to enhanced uv, and its formation is linked, highly sensitively, to precursor emissions and ambient background concentrations at the time and location of formation. The relationship between background atmospheric NO_x and ozone formation from aviation NO_x is a complex one - in the troposphere NO_x is involved in both the formation and destruction of ozone. The results confirm that as aviation NO_x increases, so does ozone burden with a high degree of linearity, in both the RCP3 and RCP8 backgrounds. The relationship between ozone burden and the resulting RF is linear. It is acknowledged that the background NO_x – O_3 relationship is non-linear in the atmosphere, however on the scale at which aviation emissions interact with the background the reaction appears highly linear for aviation emissions of up to 5 Tg N/yr (Figure 2).

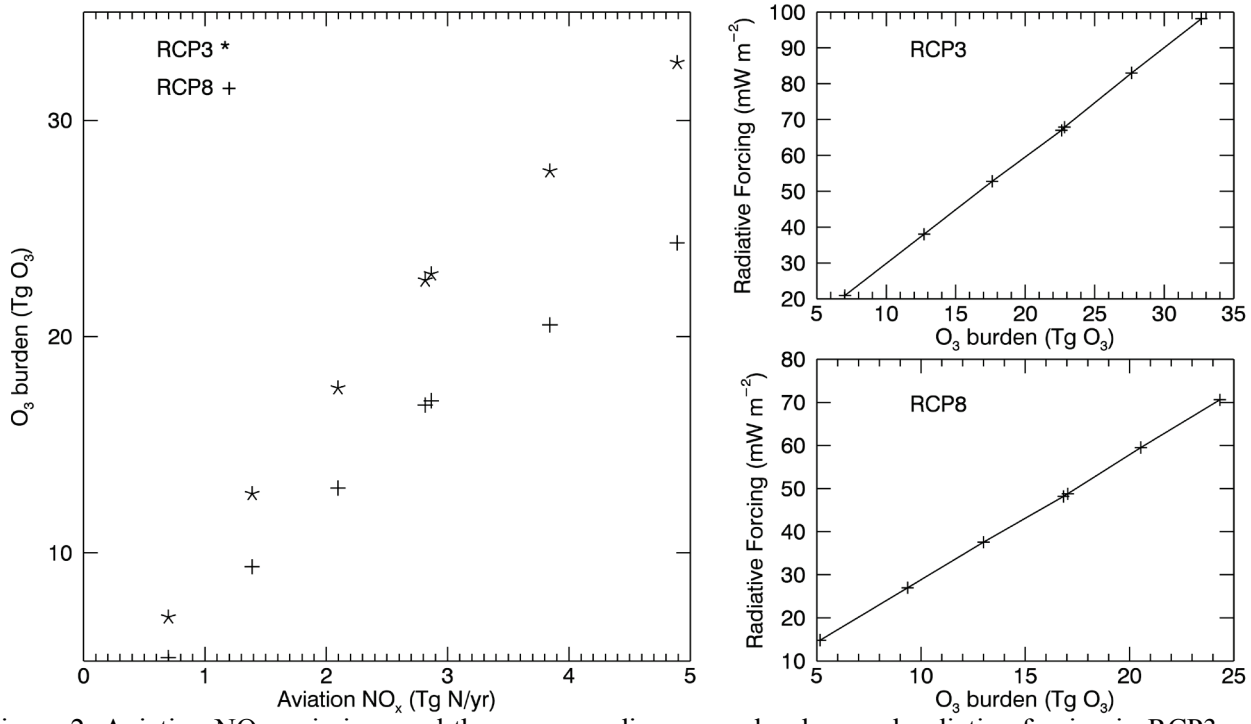

Figure 2: Aviation NO_x emissions and the corresponding ozone burdens and radiative forcing in RCP3 and RCP8 backgrounds. As aviation NO_x emissions increase so does ozone burden in a linear fashion. The resulting RF from ozone burden is show to be linear in both background atmospheres.

Other modelling studies have shown similar results; on the scale at which aviation emits NO_x, its associated interactions with the background atmosphere and subsequent reactions respond linearly, in accordance with the NO_x emission rate. As long as the background atmosphere remains reasonably consistent, this is true on a global scale (Grewe et al., 1999; IPCC 1999; Sausen and Schumann, 2000; Köhler et al., 2008; Khodayari et al., 2014).

The importance of the state of the background atmosphere for ozone formation is evident in the results (Figure 2). The same aviation emissions have a greater effect, in this case lead to the production of more O_3, in a 'cleaner' RCP3 background emissions scenario. Reducing the background concentrations of NO_x increases the ozone production efficiency per aviation-released NO_x molecule (Berntsen & Isaksen, 1999), and the low background NO_x levels allow reactions in the aircraft plume to dominate, with saturation of ozone formation occurring only at much higher, unrealistic levels of aviation.

The results for methane are somewhat similar (Figure 3). The relationship between aviation NO_x emissions and methane lifetime reduction shows some degree of linearity, as aviation NO_x emissions increase, methane lifetime reduction also increases. The new steady state of methane was calculated for each aviation NO_x value according to Fuglestvedt et al., (1999), and shows a linear correlation with the corresponding RF values. The lifetime of methane is reduced substantially more under the RCP3 surface NO_x scenario than the RCP8 (Figure 3). Again, the 'cleaner' atmosphere of RCP3 allows reactions in the aviation plume to dominate locally. The higher OH concentrations of the RCP3 background enables greater ozone formation rates, this then results in a greater decrease in methane lifetime through the reaction:

$$CH_4 + OH \rightarrow CH_3 + H_2O$$

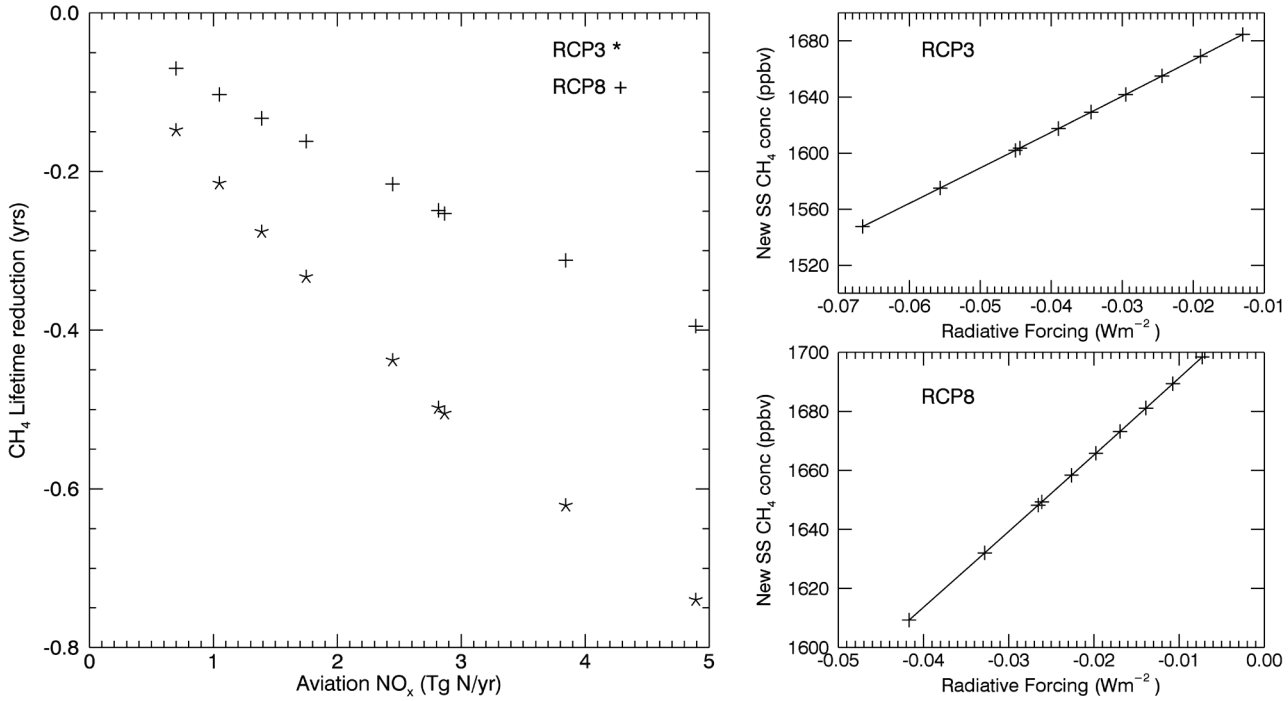

Figure 3: Aviation NO_x emissions and the corresponding methane lifetime change, new steady state and radiative forcing in RCP3 and RCP8 backgrounds. As aviation NO_x emissions increase, methane lifetime is reduced showing a near linear negative correlation. The new steady state of methane, calculated from Fuglestvedt et al., (1999), resulting from aviation NO_x emissions and the corresponding RF show a linear relationship.

As methane is also an ozone precursor, it can be inferred that under the RCP3 background the reduction in ambient methane would eventually contribute to a greater decrease in ozone formation from aviation NO_x than under the RCP8 background, and that this decrease would occur sooner.

5 CONCLUSIONS - LINCLIM MODIFICATIONS FOR FUTURE WORK

The results indicate that on the scale that aviation takes place, the correlation between ozone burden and aviation NO_x emissions shows a high degree of linearity and that the relationship between ozone burden and the resulting RF was completely linear, for aviation NO_x values up to 5 Tg N/yr. Regarding methane, there is a negative correlation between aviation NO_x emissions and methane lifetime and the relationship exhibits some degree of linearity. To account for the non-linearity in the results, particularly that of the NO_x – methane relationship, further LinClim runs will include a scaling factor for the NO_x runs, a series of short runs will be scaled linearly and then combined to make a long-term result.

Another purpose of this work was to determine the extent of modifications necessary to improve the accuracy of LinClim. The first relates to the carbon-cycle. The single IRF currently used in LinClim means that when projecting CO_2 concentrations into the future, the projected concentration is still independent from any change in the background. The current version of LinClim is therefore unsuitable for projecting future atmospheric CO_2 concentration changes resulting from aviation, as the systems that govern background atmospheric CO_2, the biosphere and the oceans, are inherently non-linear (Khodayari et al., 2013). To account for this several modifications to LinClim are proposed, including an update to its carbon cycle and the re-tuning of LinClim to C4MIP results.

This project will go on to investigate the trade-offs between CO_2 and NO_x, using Radiative Forcing (RF), Global Warming Potential (GWP) and Global Temperature change Potential (GTP) metrics. With the proposed modifications, LinClim will be used to extend the modelled effects of aviation CO_2 and NO_x far into the future (over 100 years), in order to ascertain whether reducing one species (NO_x) at the expense of another (CO_2) will improve or worsen the projected climatic effects associated with aviation.

REFERENCES

Antoine, N. E., I. M. Kroo, 2004: Aircraft optimisation for minimal environmental impact. Journal of Aircraft, 41 (4), 790 – 797.

Berntsen, T. K., Isaksen, I. S. A. (1999) Effects of lightning and convection on changes in tropospheric ozone due to NO_x emissions from aircraft. Tellus, 51B, 766 – 788.

Daniel, J. S., S. Solomon, T. J. Sanford, M. McFarland, J. S. Fuglestvedt, P. Friedlingstein, (2011) Limitations of single-basket trading: lessons from the Montreal Protocol for climate policy. Climatic Change, 111. 241 – 248.

Dessens, O., M. O. Köhler, H. L. Rogers, R. L. Jones, J. A. Pyle, (2014) Aviation and climate change. Transport Policy, 34, 14 – 20.

Fry, M. M., Naik, V., West, J. J., Schwarzkopf, M. D., Fiore, A. M., Collins, W. J., Dentener, F. J., Shindell, D. T., Atherton, C., Bergmann, D., Duncan, B. N., Hess, P., MacKenzie, I. A., Marmer, E., Schultz, M.G., Szopa, S., Wild, O., Zeng, G. (2012) The influence of ozone precursor emissions from four world regions on tropospheric composition and radiative climate forcing. J. Geophys. Res, 117, D07306.

Fuglestvedt, J. S., T. K. Berntsen, I. S. A. Isaksen, H. Mao, X. Z. Liang, W. C. Wang, (1999) Climatic forcing of nitrogen oxides through changes in tropospheric ozone and methane: global 3D model studies. Atmospheric Environment, 33, 961 – 977.

Grewe, V., Dameris, M., Hein, R., Köhler, I., Sausen, R. (1999) Impact of future subsonic aircraft NO_x emissions on the atmospheric composition. Geophys. Res. Lett., 26 (1), 47 – 50.

IPCC (1999) Aviation and the global atmosphere. Penner J, Lister DH, Griggs DJ, Griggs DJ, Dokken Dj, McFarland M. (Eds.), Intergovernmental Panel on Climate Change. Cambridge University Press, UK.

Joos, F. M. Bruno, R. Fink, U. Siegenthaler, T. F. Stocker, (1996) An efficient and accurate representation of complex oceanic and biospheric models of anthropogenic carbon uptake. Tellus, 48B, 397 – 417.

Khodayari, A. D. J. Weubbles, S. C. Olsen, J. S. Fuglestvedt, T. Berntsen, M.T. Lund, I. Waitz, P. Wolfe, P.M. Forster, M. Meinshausen, D.S. Lee, L. L. Lim, (2013) Intercomparison of the capabilities of simplified climate models to project the effects of aviation CO_2 on climate. Atmos. Env., 75, 321 – 328.

Köhler, M.O., Rädel, G., Dessens, O., Shine, K.P., Rogers, H.L., Wild, O., Pyle, J.A. (2008) Impact of perturbations to nitrogen oxide emissions from global aviation. J. Geophys. Res., 113, doi:10.1029/2007JD009140

Lee, D. S., G. Pitari, V. Grewe, K. Gierens, J. E. Penner, A. Petzold, M. J. Prather, U. Shumann, A. Bais, T. Berntsen, D. Iachetti, L. L. Lim, R. Sausen, (2010) Transport impacts on atmosphere and climate: Aviation. Atmos. Env, 44, 4678 – 4734.

Lim, L, Lee, D.S., Sausen, R., Ponater, M. (2006) Quantifying the effects of aviation on radiative forcing and temperature with a climate response model. Proceedings of the TAC-Conference, June 26 – 29, 2006, Oxford, UK.

Owen, B., D. S. Lee, L. L. Lim, (2010) Flying into the Future: aviation emission scenarios to 2050. Env.Sci.Technol., 44, 2255–2260, DOI: 10.1021/es902530z

Project React4c – reducing emissions from aviation by changing trajectories for the benefit of climate (http://www.react4c.eu/) last accessed 02.09.2015.

Sausen, R., Schumann, U. (2000) Estimates of the climate response to aircraft CO_2 and NO_x emissions scenarios. Climatic Change, 44, 27 – 58.

Unger, N., Zhao, Y., Dang, H. (2013) Mid-21st century chemical forcing of climate by the civil aviation sector. Geophys. Res. Lett. 40, 641 – 645.

Arctic black carbon from on-road diesel and aircraft emissions

G. Pitari*, G. Di Genova
Department of Physical and Chemical Sciences, Università degli Studi dell'Aquila, Italy

Keywords: black carbon aerosols, global-scale aerosol model, radiative forcing.

ABSTRACT: Market strategies have greatly incentivised the use of diesel engines for land transportation. These engines are responsible for a large fraction of black carbon (BC) emissions in the extra-tropical northern hemisphere with significant effects on both air quality and global climate. A sensitivity study is made with the University of L'Aquila climate-chemistry-aerosol model (ULAQ-CCM) by eliminating on-road diesel emissions of BC (which represent approximately 50% of BC emissions from land transportation). According to the model and using year 2000 emission scenarios, these emissions coupled to large scale atmospheric transport would imply an average tropopause direct radiative forcing (RF) of 53 mWm^{-2} over the Arctic region, with a peak of 160 mWm^{-2} during Arctic springtime months. The calculated Arctic BC optical thickness due to on-road diesel emissions is on average 0.54×10^{-3} at λ=0.55 μm (i.e., 16.5% of the total BC optical thickness over the Arctic), with a peak of 0.96×10^{-3} during springtime. The same model has been used to compare this direct RF with that produced by BC emissions from global aviation. According to the model and using 2006 aviation emission inventories (from the EC project REACT4C), the calculated annually-averaged BC optical thickness change over the Arctic region is 6.5×10^{-6} at λ=0.55 μm, with a tropopause RF=1.6 mWm^{-2}. The tropopause RF ratio between on-road diesel and aircraft BC (33) is much smaller than the mass loading ratio (73), due to the different vertical distribution of BC particles. This produces a much higher radiative efficiency for aircraft BC, approximately 2.3 times larger with respect to on-road diesel BC (i.e., 2700 .vs. 1200 W/g). The corresponding ratio of surface RFs, on the other hand, is approximately one order of magnitude larger with respect to the ratio of tropopause RFs, reflecting the fact that approximately only half of the aircraft BC mass loading resides below the mean Arctic tropopause.

1 INTRODUCTION

Motor vehicles used for land transportation (automobiles, trains, freight traffic, agriculture) contribute in a significant way to emissions of atmospheric pollutants that are relevant for global climate and/or local air quality, namely, CO_2, CH_4, NMHC, CO, NO_x (and O_3 as a photo-chemically produced secondary species), SO_2 and PM (i.e., aerosol particles, mainly carbonaceous and sulphate) (Uherek et al., 2010). Quantifying the climate impact of these species in terms of radiative forcing (RF) is a well assessed exercise only for well-mixed long-lived species (CO_2 and CH_4), whereas it is a much more complex problem (often with uncertain results) for greenhouse gases with shorter lifetimes that may have large spatial gradients (e.g., O_3) and for aerosols that may have highly variable sizes, compositions and spatial distributions (IPCC, 2013).

Among anthropogenic emissions, diesel engines used for land transportation are the most important BC source. Diesel engines are very common in developing countries, East Asia, Eastern Europe and also in Western Europe and the US, where market strategies and policy decisions have encouraged these engines compared to gasoline engines, being more fuel-efficient and thus emitting less CO_2/km. Despite their higher fuel-efficiency diesel engines release more particles, including BC (Twigg, 2007). These engines account for approximately one-third of the global anthropogenic emissions of BC and approximately 17% of the total (Bond et al., 2004). The relative weight of BC diesel emissions may be substantially larger on a regional basis, mainly in western industrialised countries. In the US, for example, diesel engines represent almost 27% of the total BC emissions

* *Corresponding author:* Giovanni Pitari, Department of Physical and Chemical Sciences, Università degli Studi dell'Aquila, Via Vetoio, 67100 L'Aquila, Italy. Email: gianni.pitari@aquila.infn.it

(EPA, 2012). Because of the large warming effect per unit mass of BC emitted, the reduction of diesel engines is a good candidate to mitigate climate forcing (Kopp and Mauzeralla, 2010).

One important aspect of the potential emission reduction of pollutants in northern hemisphere source regions is that these short-lived species may be effectively transported over large spatial scales with significant impact on remote regions. BC transport from NH mid-latitudes over the Arctic region is an important example of this source-receptor problem (Koch and Hansen, 2005). Although the Arctic climate has a complex meteorological system, its major features could be summarised as follows: (a) formation of a strong polar vortex during winter with relatively stable stratification in the troposphere; (b) weakening of the polar vortex in late winter and spring months, allowing greater exchange of low level with upper level air, due to breaking of the vertical stability. Upper level air, in turn, is more efficiently affected by transport from the mid-latitudes due to more intense zonal and southerly winds. BC particles transported to the Arctic polar latitudes and deposited over snow and ice on the surface (Jiao et al., 2014) may have important consequences on the polar surface albedo and on local and global climate forcing.

The main purpose of the present study is to compare the radiative impact of Arctic black carbon from land transportation and aircraft emissions. Aviation BC is largely located in the UTLS with freshly emitted particles of approximately 0.02 μm radius. For a complete discussion of the adopted aircraft emission we refer to Pitari et al. (2015b), as well as for a full description of the University of L'Aquila climate-chemistry coupled model (ULAQ-CCM) adopted in this study. Other model details are given in Pitari et al. (2014), whereas a complete discussion on the adopted BC size distribution and optical parameters for the radiative calculations is made in Pitari et al. (2015a). An effective radius of 0.14 μm has been selected as input to the Mie scattering code (0.05 μm of which due to coating thickness) (Schwarz et al., 2010). The BC complex refraction index is taken from Bond et al. (2013). A single scattering albedo of 0.45 is calculated at λ=0.55 μm, with a refraction index of 1.95 – 0.79i at the same wavelength.

2 BC EMISSIONS AND NUMERICAL EXPERIMENTS SETUP

According to WMO (2011), open biomass burning dominates BC emissions on a global scale (41%), with the largest contribution from the tropics. Total land transportation accounts for 19% of the total and 37% of the anthropogenic fraction; diesel on-road transportation emissions account for 10% of the total and 19% of the anthropogenic fraction. Fig. 1 is adapted from Bond et al. (2004) and shows the on-road diesel percent fraction of total land transportation BC emissions on a regional basis and on-road diesel and total BC emissions in absolute units. The relative contribution of BC emissions from on-road diesel is close to 50% of the total land transport BC emissions in western industrialised countries. The relative contribution of on-road diesel to total BC emissions ranges from 2% in China to 29% in Europe and 48% in the Middle East.

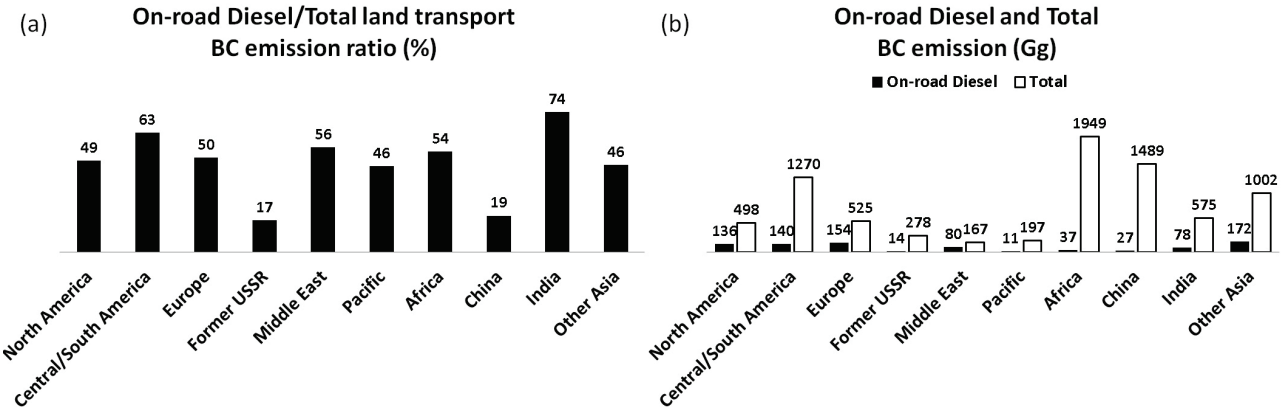

Figure 1. Left panel (a): on-road diesel percent fraction of total land transport BC emissions (regional). Right panel (b): on-road diesel and total BC emissions (Gg/yr) (regional). Adapted from Bond et al. (2004).

This study is organised through a baseline experiment ('base') with anthropogenic fossil fuel emissions of BC, OC and SO_2 from year 2000 scenarios and with (climatological) biomass burning

sources and a perturbed experiment ('pert') where on-road diesel emissions of BC particles are removed from the total land transportation sources, using the regional fractions of Fig. 1a. These fractions represent a contribution of 27% and 29% of total BC emissions over North America and Europe, respectively, and 14% and 17% over India and East Asia, respectively, excluding China (2%), where BC emissions from on-road diesel are relatively low compared to domestic fire or other non-transportation burning sources (Pitari et al., 2015a). A separate sensitivity experiment is made for BC aircraft emissions, using year 2006 emissions provided in the European project consortium EC-REACT4C (Pitari et al., 2015b).

3 RESULTS AND DISCUSSION

The model calculated global BC burden is 0.27 Tg C with an average lifetime of 7.2 d; BC global removal is approximately 65% by wet deposition and 35% by dry deposition (77% and 23%, respectively, over the Arctic region, 65N-90N), consistently with global budgets reported in Koch and Hansen (2005). Global AeroCom statistics reported in Textor et al. (2006) give a mean value of 79% for BC wet deposition among 16 models, with a 10% standard deviation.

According to the model, Europe and Russia together (including both industrial sources and biomass burning) provide the major input to the Arctic BC optical thickness. These sources, along with those from Southeast Asia, also provide substantial input to the Western Arctic BC and over the Atlantic, through coupling of the subarctic westerlies and northward eddy mass fluxes in the atmospheric layers above the surface. The contribution of aircraft emitted BC is negligible in terms of total optical depth (< 1%) but larger in the Arctic upper troposphere and lower stratosphere (UTLS): here the ULAQ model calculates an aircraft contribution of 4.5% on annual basis, using the base case emission scenario adopted from the EC-REACT4C project (Pitari et al., 2015b), with an average soot emission index of 0.013 g/kg-fuel at cruise altitudes. Although the UTLS direct effect of BC aircraft emissions is small, their potential climate impact could be significant through indirect formation of "soot-cirrus" particles, when ice super-saturation conditions are found and ice particle formation may occur via heterogeneous freezing (Hendricks et al., 2005).

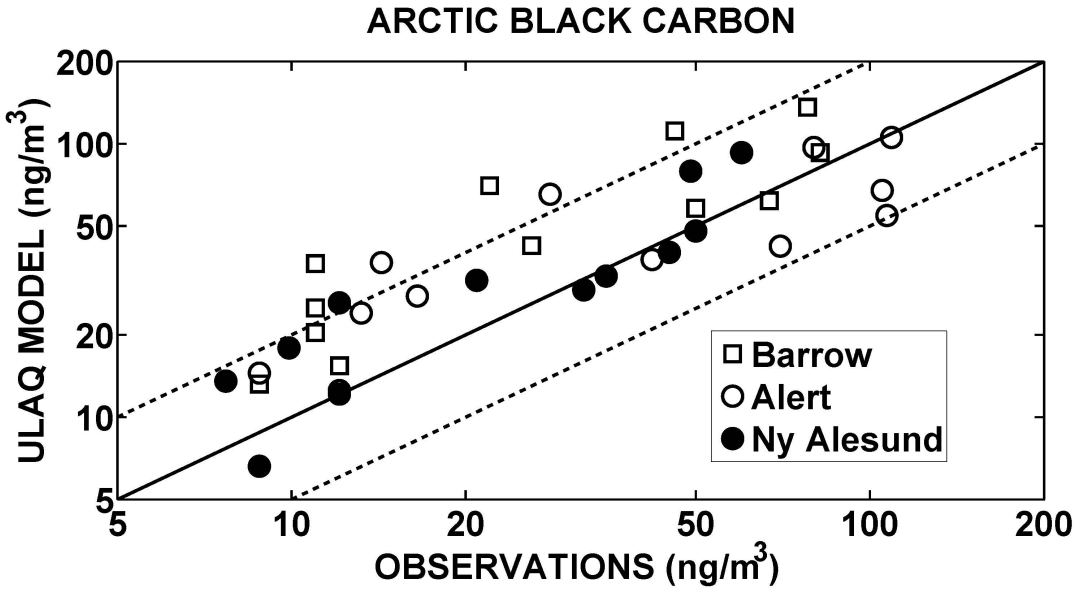

Figure 2. Scatter plot of calculated versus observed monthly mean BC mass concentration values (ng/m^3) at three selected Arctic stations (see legend). Thin (or dashed) lines highlight a factor of 2 deviations.

The BC vertical profile predicted in the ULAQ model over the Arctic region has been compared with available aircraft observations (Schwarz et al., 2010) and is in the uncertainty bar of the measurements at all heights. The model behavior results to be greatly improved respect to previous calculations (Koch et al., 2010), mostly due to a better representation of wet deposition. Fig. 2 shows a comparison of the modelled BC with climatological data collected over three Arctic stations (decadal averages) (Quinn et al, 2011; Sharma et al., 2013). The modelled seasonal changes of BC con-

centration appear to be quite similar to the findings from the ACCMIP model inter-comparison (Lee et al., 2013). For the three considered measurement sites (Barrow, Alert and Ny-Alesund), northern Eurasia has been identified as the major source region, especially in winter/spring. The ULAQ model is consistent at all three stations, except for a significant overestimation at Barrow during springtime months and some overestimation of the summer minimum at all stations. As discussed in the Quinn et al. (2011) report, the models' ability to reproduce observed measurements can be heavily impaired by the treatment of BC microphysical properties and removal rates.
Model-calculated changes in the Arctic averaged optical thickness due to the cancellation of on-road diesel sources closely follow the same seasonal cycle of the baseline reference optical depth, with a rather flat relative decrease during the year (16.5% ± 2%). This is indirect evidence that the greatest amount of BC loading over the Arctic is transported from NH mid-latitude sources and may therefore be significantly affected by changes in anthropogenic fossil fuel burning, both in terms of decadal trends and potential regulating measures of these emissions. A decrease in the relative change in BC optical thickness is calculated during summer months (13% in July-August versus 18% in March-April) and results primarily from the impact of biomass burning sources in Russia during these months (Breider et al., 2014).

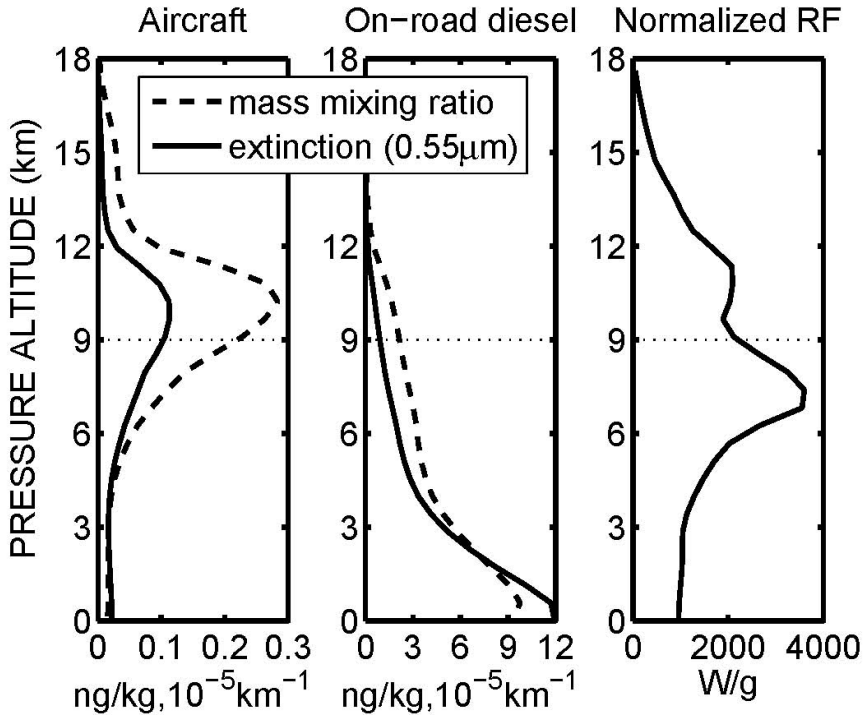

Figure 3. Vertical profiles of mass mixing ratio (dashed line, ng/kg) and extinction at λ=0.55 μm (solid line, 10^{-5} km^{-1}) of Arctic BC, from aircraft emissions (left panel) and from on-road diesel emissions (mid panel) (annual averages). The rightmost panel shows the calculated normalized RF (W/g). The dotted line is for the mean Arctic tropopause height (NCEP value).

A comparison of the vertical distribution of BC over the Arctic from on-road diesel and aircraft emissions is presented in Fig. 3, in terms of mass mixing ratio and extinction at λ=0.55μm (annual averages). The rightmost panel shows the calculated normalized RF. A summary of the ULAQ model calculation is presented in Table 1, including tropopause and surface RF on the Arctic region. The mass loading from aircraft emissions is approximately two order of magnitudes smaller with respect to on-road diesel ones, but the vertical distribution is completely different, with aviation BC in the Arctic region being located for approximately half of the total loading above the tropopause. This produces a much higher radiative efficiency, as visible in Table 1 (approximately a factor of 2.3 larger). The vertical efficiency profile for BC aerosols mainly depends on the location of the absorbing layer with respect to the cloud coverage. Since the cloud albedo is higher than the underlying surface, BC absorbs more from the reflected radiation. The opposite occurs for scattering aerosols, since the enhancement of the reflected radiation by the cloud coverage results in more downward scattering, thus reducing the forcing efficiency. Aerosols within or below clouds

receive less solar radiation, so their efficiency is reduced in any case. To a minor extent, vertical efficiency is also affected by Rayleigh scattering, water vapor and other aerosols. In addition, the behavior of BC aerosols in the stratosphere is to produce a negative RF at the tropopause for the solar shortwave radiation, that is however counteracted by local warming due to positive heating rates with associated positive longwave forcing from the stratospheric temperature adjustment. The large difference of surface RF between aircraft and on-road diesel BC is due to the much larger amount of tropospheric BC in the latter case, thus producing stronger radiation absorption and heating of the surface.

Table 1. Summary of Arctic BC tropopause direct RF (mW/m^2) (annual averages). The last column shows net RF values at the surface.

BC Emission	Mass burden [$\mu g/m^2$]	Mass fraction [%]	RF-SW [mWm^{-2}]	RF-LWadj [mWm^{-2}]	RF-NET [mWm^{-2}]	NRF [W/g]	Surface RF-NET [mWm^{-2}]
Aircraft total	0.59	-	0.52	1.07	1.59	2700	5.3
Aircraft troposphere	0.32	54	0.80	0.0	0.80	2500	5.9
Aircraft stratosphere	0.27	46	-0.28	1.07	0.79	2900	-0.6
On-road diesel total	43	-	46	7.3	53	1200	1187
On-road diesel troposphere	40	94	47.0	0.0	47	1200	1190
On-road diesel stratosphere	2.8	6	-1.5	7.3	5.8	1500	-3.0

4 CONCLUSIONS

The present study makes use of a climate-chemistry model with an interactive aerosol module to explore the sensitivity of the radiative balance in the Arctic region to BC aerosols from on-road diesel and aircraft emissions. The Arctic BC mass loading from aircraft emissions is approximately two order of magnitudes smaller with respect to on-road diesel ones, but the vertical distribution is completely different, with aviation BC being located for approximately half of the total loading above the tropopause. This produces a much higher radiative efficiency, approximately a factor of 2.3 larger. The ratio of surface RFs between on-road diesel and aircraft BC, on the other hand, is approximately one order of magnitude larger with respect to the ratio of tropopause RFs, reflecting the fact that approximately only half of the aircraft BC mass loading resides below the mean Arctic tropopause.

ACKNOWLEDGEMENTS

Part of this work has been completed under the EC project REACT4C, grant No. ACP8-GA-2009-233772. The authors would like to acknowledge Drs. David Lee and Ling Lim of the Manchester Metropolitan University for providing aircraft emission datafiles.

REFERENCES

IPCC, Climate change 2013. Chapter 7. In The physical science basis; T.F. Stocker et al., Eds.; Cambridge University Press: UK.

Bond, T.C., D.G. Streets, K.F. Yarber, S.M. Nelson, J.-H. Woo, and Z. Klimont, 2004: A technology-based global inventory of black and organic carbon emissions from combustion. J. Geophys. Res. 109, D14203, doi:10.1029/2003JD003697.

Bond, T.C., et al., 2013: Bounding the role of black carbon in the climate system: A scientific assessment. J. Geophys. Res. 118, 5380–5552.

Breider, T.J., L.J. Mickley, D.J. Jacob, Q. Wang, J.A. Fisher, R.Y.-W. Chang, and B. Alexander 2014: Annual distributions and sources of Arctic aerosol components, aerosol optical depth, and aerosol absorption. J. Geophys. Res. 119, 4107–4124, doi:10.1002/2013JD020996.

EPA, 2012: Report to Congress on Black Carbon. EPA-450/R-12-001; Department of the Interior, Environment, and Related Agencies.

Hendricks, J., B. Kärcher, U. Lohmann, and M. Ponater, 2005: Do aircraft black carbon emissions affect cirrus clouds on the global scale?. Geophys. Res. Lett. 32, L12814, doi:10.1029/2005GL022740.

Jiao, C., et al., 2014: An AeroCom assessment of black carbon in Arctic snow and sea ice. Amos. Chem. Phys. 14, 2399–2417, doi:10.5194/acp-14-2399-2014.

Koch, D., and J. Hansen, 2005: Distant origins of Arctic black carbon: A Goddard Institute for Space Studies Model E experiment. J. Geophys. Res. 110, D04204, doi:10.1029/2004JD005296.

Koch, D., et al., 2010: Corrigendum to 'Evaluation of Black Carbon Estimations in Global Aerosol Models' published in Atmos. Chem.Phys., 9, 9001-9026, 2009, Atmos. Chem. Phys. 10, 79-81.

Kopp, R.E., and D.L. Mauzeralla, 2010: Assessing the climatic benefits of black carbon mitigation. PNAS 107, 11703–11708.

Lee, Y.H., et al., 2013: Evaluation of preindustrial to present-day black carbon and its albedo forcing from Atmospheric Chemistry and Climate Model Intercomparison Project (ACCMIP). Atmos. Chem. Phys. 13, 2607-2634, doi:10.5194/acp-13-2607-2013.

Pitari, G., V. Aquila, B. Kravitz, A. Robock, S. Watanabe, I. Cionni, N. De Luca, G. Di Genova, E. Mancini, and S. Tilmes, 2014: Stratospheric Ozone Response to Sulfate Geoengineering: Results from the Geoengineering Model Intercomparison Project (GeoMIP). J. Geophys. Res. 119, 2629-2653, doi:10.1002_2013JD020566.

Pitari, G., G. Di Genova, and N. De Luca, 2015a: A modelling study of the impact of on-road diesel emissions on Arctic black carbon and solar radiation transfer, Atmosphere, 6, 318-340, doi:10.3390/atmos6030318.

Pitari, G., D. Iachetti, G. Di Genova, N. De Luca, O.A. Sovde, Ø. Hodnebrog, D.S. Lee, and L. Lim, 2015b: Impact of coupled NO_x/aerosol aircraft emissions on ozone photochemistry and radiative forcing, Atmosphere, 6, 751-782; doi:10.3390/atmos6060751.

Textor, C., et al., 2006: Analysis and quantification of the diversities of aerosol life cycles within AEROCOM, Atmos. Chem. Phys. 6, 1777-1813, SRef-ID: 1680-7324/acp/2006-6-1777.

Quinn, P.K., et al., 2011: The Impact of Black Carbon on Arctic Climate; Arctic Monitoring and Assessment Programme (AMAP): Oslo, Norway.

Sharma, S., J.A. Ogren, A. Jefferson, K. Eleftheriadis, E. Chan, P.K. Quinn, and J.F. Burkhart, 2013: Black Carbon in the Arctic, Arctic Report Card 2013. http://www.arctic.noaa.gov/reportcard/.

Schwarz, J.P., J.R. Spackman, R.S. Gao, L.A., Watts, P. Stier, M. Schulz, S.M. Davis, S.C. Wofsy, and D.W. Fahey, 2010: Global-scale black carbon profiles observed in the remote atmosphere and compared to models. Geophys. Res. Lett. 37, doi:10.1029/2010GL044372.

Twigg, M.W., 2007: Progress and future challenges in controlling automotive exhaust gas emissions. Appl. Catalysis B: Environ. 70, 2–15.

Uherek, E., et al., 2010: Transport impacts on atmosphere and climate: Land transport. Atmos. Env. 44 (37), 4772-4816.

WMO, 2011. Integrated assessment of black carbon and tropospheric ozone; WMO: Geneva, Switzerland.

Aviation impacts on climate: Where are we heading?

L.L. Lim*, K. Walker, B. Owen, D.S. Lee
Faculty of Science and Engineering, Manchester Metropolitan University, UK

Keywords: aviation emissions scenarios, CO_2, radiative forcing

ABSTRACT: Aircraft emit species that directly impact climate such as carbon dioxide (CO_2), and to estimate these impacts, it is necessary for us to know the aviation emissions trends. However, aviation emissions are highly dependent on demand for air travels, and this can be greatly influenced by factors such as economic development, emerging markets, fuel price and availability, and other global issues such as civil unrests, military conflicts and disease outbreaks; making it difficult to produce reliable long-term forecasts. In this preliminary study, we compared several widely used emissions scenarios (aviation and total anthropogenic) that were forecasted back in the 1990s for the present day, with observed data. We found that earlier forecasts of aviation CO_2 emissions compared well to reported levels of aviation emissions derived from kerosene fuel sale data. It was not possible to perform a similar comparison for aviation CO_2 concentrations, but there was good agreement between the background CO_2 concentrations and the global average observation data. We also estimated the radiative forcing (RF) of these scenarios using a simple climate model and found that by 2050, aviation RF was projected to be between 0.04 to 0.12 W/m^2. This implies that aviation's contribution to background RF could increase from 1.5% at present day to about 3.5% by 2050. The results from this preliminary work shows that up to 2012, aviation is within the medium to high growth range of various forecasts and that it is likely to grow at a faster rate post-2030 compared with background emissions. Further work is necessary in this area, which could be used to inform policy makers on whether mitigation efforts are likely to meet the targets set out back in the 1990s or whether more stringent legislations/policies are required to achieve them.

1 INTRODUCTION

Aircraft emit a variety of species that directly impact climate such as carbon dioxide (CO_2), water vapour, nitrogen oxides (NOx) and aerosols, or indirectly by inducing cloud formation (contrails, contrail-cirrus, soot-cirrus). It is necessary for us to know aviation emissions trends in order to estimate the potential climate impacts from aviation. For example, the IPCC Special Report on Aviation (IPCC, 1999) provided forecasts from base year 1992 to 'future' years 2015 and 2050. We are now at a point in time where we can begin to compare these 'forecasts' against reported traffic activities and see how good these estimates actually are. In this paper, we present the results of a preliminary study where we collated existing aviation and total anthropogenic emissions scenarios, assessed the accuracy of earlier forecasts to reported levels of aviation emissions and determined their likely growth trajectory. We then use these emission scenarios and estimate their CO_2 impacts on radiative forcing (RF) using a simple climate model.

2 AVIATION FUEL BURN DATA

Over the years, there have been several widely used emissions scenarios that provided an outlook of future aviation emissions and their contribution to total anthropogenic emissions (IPCC, 1999; Owen et al., 2010; Lee et al., 2013). Aviation emissions are highly dependent on demands and these in turn can be easily influenced by factors such as ticket prices or disease outbreak (e.g. SARS), making it difficult to make reliable long-term forecasts. A selected sample of global civil, military and total fuel burn data for various aviation scenarios are presented in Table 1.

* *Corresponding author:* Ling L. Lim, Faculty of Science and Engineering, Manchester Metropolitan University, Chester St, Manchester M1 5GD, UK. Email: l.lim@mmu.ac.uk

Table 1: A selected sample of global civil, military and total fuel burn data.

Year	Inventory/Scenario	Civil Fuel (Tg yr^{-1})	Military Fuel (Tg yr^{-1})	Total Fuel (Tg yr^{-1})	Comments/Reference
1992	NASA	113.85	25.55	139.41	Table 9.4, IPCC (1999)
1992	ANCAT	114.20	17.08	131.30	Table 9.4, IPCC (1999)
2000	QUANTIFY	n.a.	n.a.	214.00	Normalised to IEA data / Owen et al., (2010)
2015	NASA	288.05	20.59	308.64	Table 9.4, IPCC (1999)
2015	ANCAT	272.32	14.54	287.86	Table 9.4, IPCC (1999)
2016	GIACC S1	302.00	n.a.		GIACC/4-IP/1, ICAO (no date)
2016	GIACC S6	271.00	n.a.		GIACC/4-IP/1, ICAO (no date)
2020	CONSAVE Down to Earth (DtE)	198.00	n.a.		Berghof et al., (2005)
2020	CONSAVE Unlimited Skies (ULS)	287.10	n.a.		Berghof et al., (2005)
2050	CAEP/4-FESG Fc1	253.80	14.40	268.20	Table 9.13, IPCC (1999)
2050	CAEP/4-FESG Fe2	757.70	14.40	772.10	Table 9.13, IPCC (1999)
2050	QUANTIFY A1	766.00	n.a.		Base year normalised to IEA data / Owen et al., (2010)
2050	QUANTIFY B1ACARE	325.00	n.a.		Base year normalised to IEA data / Owen et al., (2010)

The results from Table 1 show that the aviation fuel forecasts were conducted by different organizations (e.g. NASA, ANCAT, CAEP) or to fulfill the requirements of specific research project (e.g. QUANTIFY, CONSAVE). This may lead to different inventory assumptions that could influence any subsequent impact assessment results that have used these inventories (Skowron et al., 2013).

3 CO_2 EMISSIONS DATA

In order to compare CO_2 emissions data from the scenarios discussed in Section 1 with those derived from fuel (kerosene) sales data from the International Energy Agency (IEA) (IEA, 2014); we used a fuel to CO_2 emissions index of 3.15 kg CO_2 per kg fuel. The individual year CO_2 emissions were then linearly interpolated between available data years, so that they can be used in a simple climate model. It can be seen from Figure 1 that the IEA derived CO_2 data were within the range of aviation emission forecasts made in the 1990s (e.g. NASA).

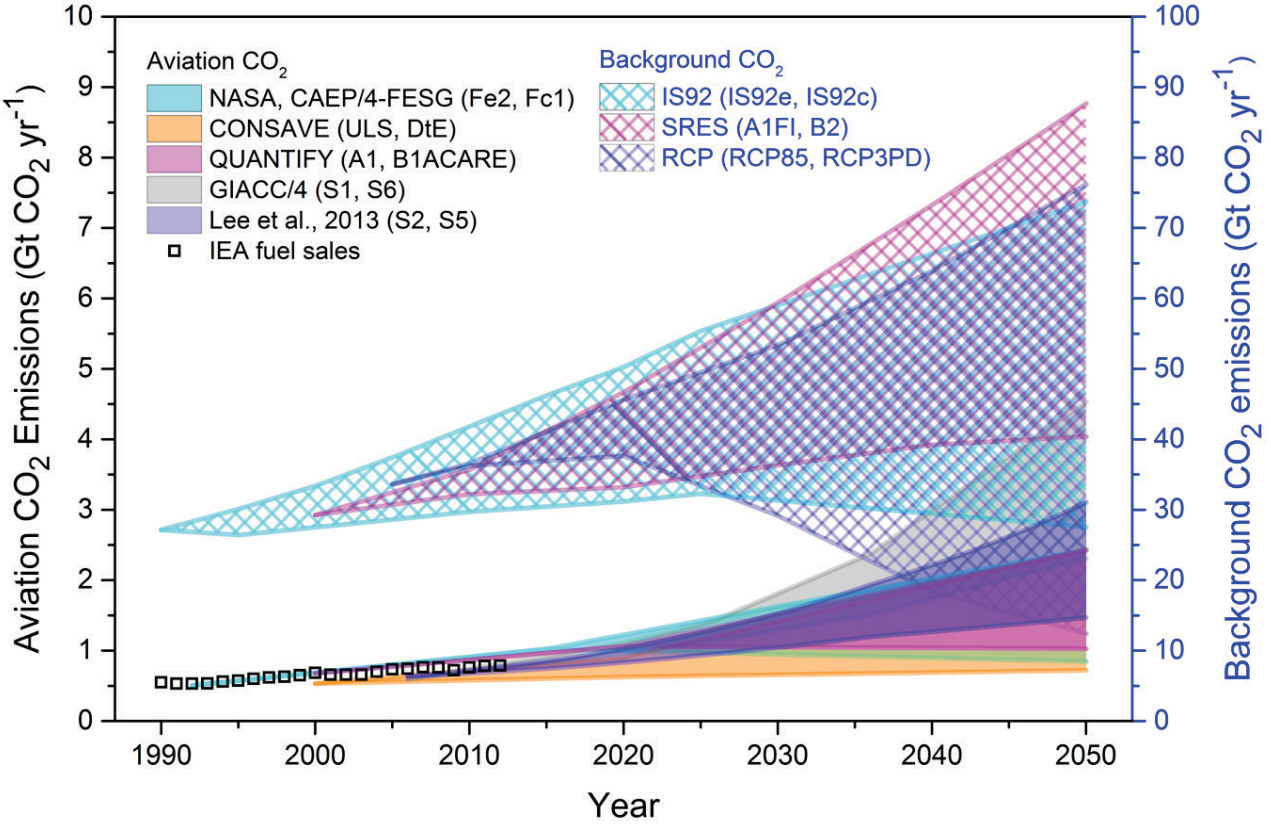

Figure 1: Aviation and background CO_2 emissions from various forecasts and the IEA fuel sales data. The upper and lower range scenarios are denoted in brackets.

Figure 1 also shows the comparison between aviation emission trends and background (all anthropogenic) CO_2 emissions used in previous IPCC assessment reports; Second Assessment Report (IS92) (IPCC, 1996), Third and Fourth Assessment Reports (SRES) (IPCC, 2001 and IPCC, 2007 respectively) and Fifth Assessment Report (RCP) (IPCC, 2013). Some aviation CO_2 emissions

have a projected growth rate exceeding 3% (post-2030) compared to a background annual growth rate of no more than 2.5%.

4 CO_2 CONCENTRATION DATA

The simple climate model, LinClim, (Lim et al., 2007) used historical CO_2 emissions (some were derived from IEA fuel data) to calculate aviation CO_2 concentrations up to 2050. These aviation results are presented alongside background concentrations in Figure 2.

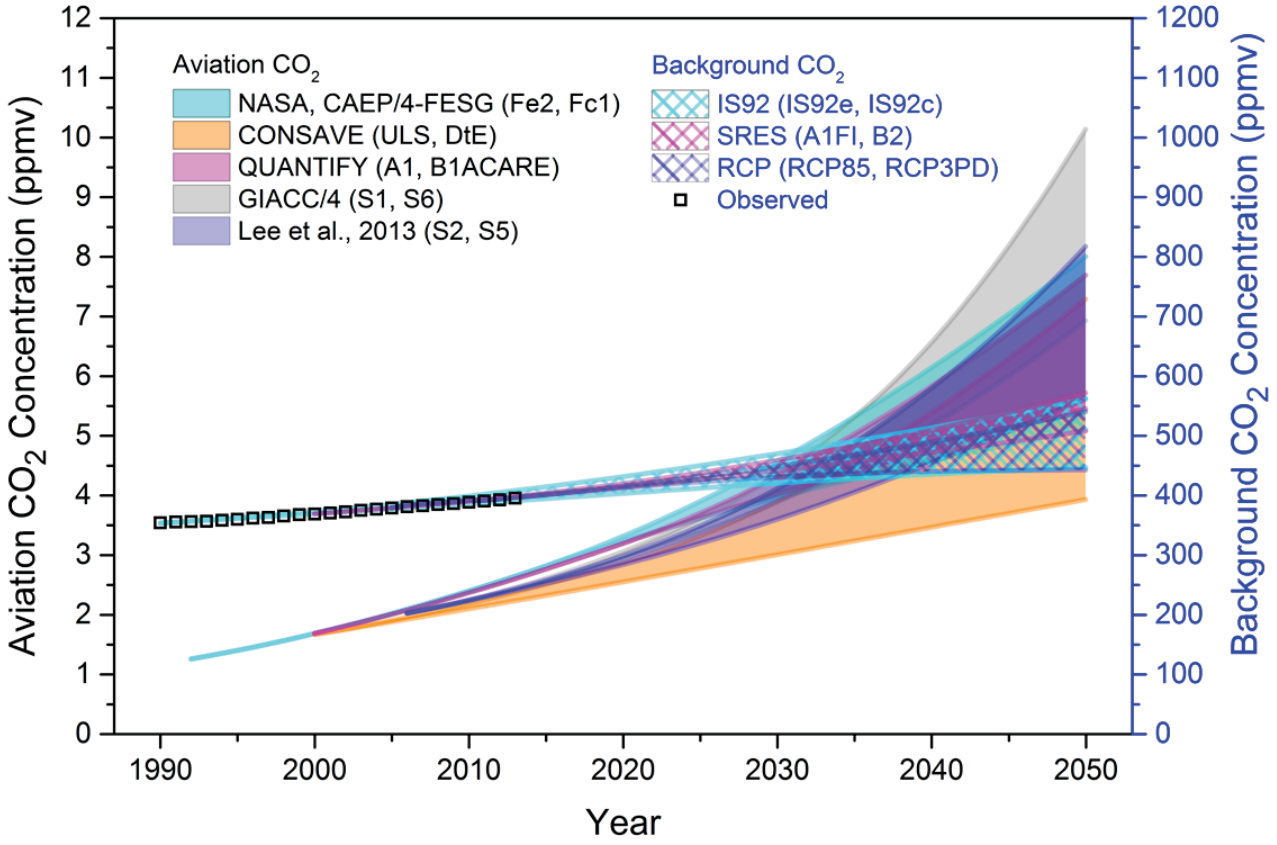

Figure 2: Aviation and background CO_2 concentrations from various forecasts and the observed background CO_2 concentrations. The upper and lower range scenarios are denoted in brackets.

Figure 2 clearly shows that the projected background concentrations developed in the 1990s compared well with observations. The aviation CO_2 contributions to background concentrations are also projected to increase, reaching a high of 4.5% increase per year, while the background an increase of less than 1.5%.

5 CO_2 RADIATIVE FORCING

Aviation emissions depicted in Figure 1 were matched with the relevant background scenarios (for example, QUANTIFY emissions with SRES background) and the resulting RF from LinClim simulations are presented in Figure 3.

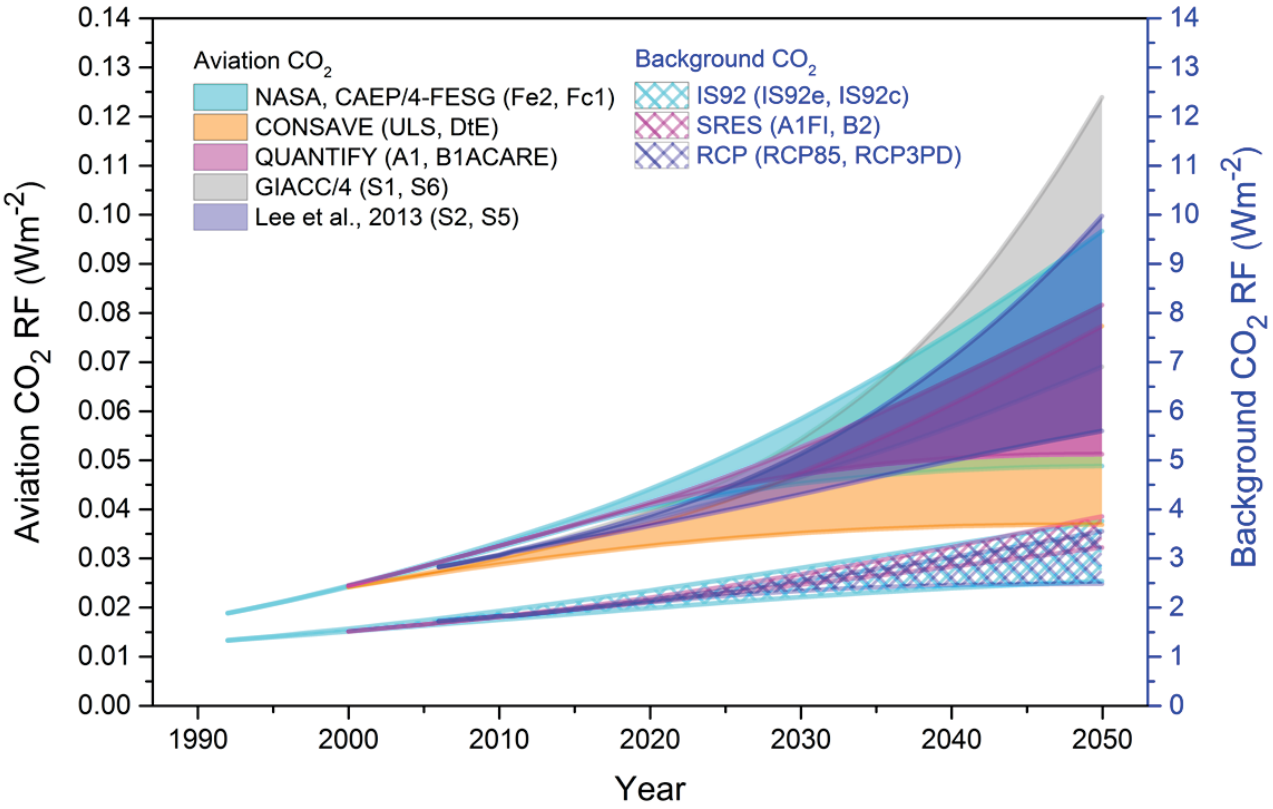

Figure 3: Aviation and background CO_2 RFs from various forecasts. The upper and lower range scenarios are denoted in brackets.

It can be seen from Figure 3 that the range of forecasts for aviation CO_2 RF at 2050 is 0.037 to 0.124 W/m^2. Therefore, according to these forecasts, aviation's contribution to background RF increase from just over 1.5% at present day to about 3.5% by 2050.

6 SUMMARY

The results from this preliminary study show that based on current trends, aviation emissions are still within the medium to high growth range of the various forecasts up to 2012. In addition, these results show that aviation is likely to grow at a faster rate in the future (post-2030), compared with background sources.

ACKNOWLEDGEMENTS

This work was supported by the UK Department for Transport and the Manchester Metropolitan University Research, Enterperise & Innovation Summer Vacation Studentship.

REFERENCES

Berghof, R., A. Schmitt, C. Eyers, K. Haag, J. Middel, M. Hepting, A. Grübler and R. Hancox, 2005: CONSAVE 2050 Final Technical Report. DLR, Köln, Germany.

ICAO, no date: GIACC/4: IP/1, IP/2, IP/3. [Online] [Accessed on 14 October 2015] http://www.icao.int/environmental-protection/GIACC/Giacc-4/CENV_GIACC4_IP1_IP2%20IP3.pdf?Mobile=1&Source=%2Fenvironmental%2Dprotection%2F%5Flay-outs%2Fmobile%2Fdispform%2Easpx%3FList%3Dcaa6919c%2Df115%2D4c3c%2D9586%2D18f6015b43f6%26View%3D8ff2ee57%2D7d03%2D4f91%2Dbfce%2D6da44ff7365f%26RootFolder%3D%252Fenvironmental%2Dprotection%252FGIACC%252FGiacc%2D4%26ID%3D8%26CurrentPage%3D1

IEA, 2014: Oil Information 2012. International Energy Agency, Paris.

IPCC, 1996: Climate Change 1995: The Science of Climate Change. In: Houghton, J.T., L.G. Meira Filho, B.A. Callander, N. Harris, A. Kattenberg, K. Maskell (Eds.), Intergovernmental Panel on Climate Change. Cambridge University Press, Cambridge, UK.

IPCC, 1999: Aviation and the global atmosphere. In: Penner, J.E., D.H. Lister, D.J. Griggs, D.J. Dokken, M. McFarland (Eds.), Intergovernmental Panel on Climate Change. Cambridge University Press, Cambridge, UK.

IPCC, 2001: Climate Change 2001: The Scientific Basis. In: Houghton, J.T., Y. Ding, D.J. Griggs, M. Noguer, P.J. van der Linden, X. Dai, K. Maskell, C.A. Johnson (Eds.), Intergovernmental Panel on Climate Change. Cambridge University Press, Cambridge, UK.

IPCC, 2007: Climate Change 2007: Working Group I: The Physical Science Basis. In: Solomon, S., D. Qin, M. Manning, Z. Chen, M. Marquis, K.B. Averyt, M. Tignor, H.L. Miller (Eds.), Intergovernmental Panel on Climate Change. Cambridge University Press, Cambridge, UK.

IPCC, 2013: Climate Change 2013: The Physical Science Basis. In: Stocker, T.F, D. Qin, G-K. Plattner, M.M.B. Tignor, S.K. Allen, J. Boschung, A. Nauels, Y. Xia, V. Bex, P.M. Midgley (Eds.), Intergovernmental Panel on Climate Change. Cambridge University Press, Cambridge, UK.

Lee, D.S., L.L. Lim and B. Owen, 2013: Bridging the aviation CO_2 emissions gap: why emissions trading is needed. Manchester Metropolitan University.

Lim, L.L., D.S. Lee, R. Sausen and M. Ponater (2007): Quantifying the effects of aviation on radiative forcing and temperature with a climate response model. In: Sausen, R., A. Blum, D.S. Lee, C. Brüning, (Eds.), Proceedings of an International Conference on Transport, Atmosphere and Climate (TAC). Luxembourg, Office for Official Publications of the European Communities, ISBN 92-79-04583-0, 202-207.

Owen, B., D.S. Lee and L.L. Lim, 2010: Flying into the Future: Aviation Emissions Scenarios to 2050. Environ. Sci. Technol. 44, 2255-2260.

Skowron, A., D.S. Lee and R.R. De León, 2013: The assessment of the impact of aviation NOx on ozone and other radiative forcing responses – The importance of representing cruise altitudes accurately. Atmospheric Environment 74, 159-168.

REACT4C: Simplified Mitigation Studies

L.L. Lim*, D.S. Lee, B. Owen, A. Skowron
Faculty of Science and Engineering, Manchester Metropolitan University, UK

S. Matthes, U. Burkhardt, S. Dietmüller
DLR-Institut für Physik der Atmosphäre Oberpfaffenhofen, Germany

G. Pitari, G. Di Genova, D. Iachetti
University of L'Aquila, L'Aquila, Italy

I. Isaksen
Department of Geosciences, University of Oslo, Oslo, Norway

O.A. Søvde
Center for International Climate and Environmental Research – Oslo (CICERO), Oslo, Norway

Keywords: REACT4C, simplified mitigation, aviation non-CO_2

ABSTRACT: The project 'REACT4C' explored the feasibility of operational measures such as flight altitude and route changes to reduce the climate impact from aviation. Simplified mitigation studies were conducted as part of the project to quantify the environmental benefit of simplified Air Traffic Management (ATM) measures and these results were used to formulate general principles of environmentally optimized flight on particular timescales and for specific climate effects. The emissions model, FAST, was used to estimate the global emissions from civil aviation for the year 2006 and two mitigation scenarios, where the cruise altitudes were shifted higher and lower by one flight level or 2,000 ft. It was found that the fuel increased by 1.3% when flying lower and decreased by 0.8% when flying higher. The changes in the atmospheric chemical composition caused by aviation NO_x emissions such as ozone (short- and long-lived), methane and stratospheric water vapour, were identified and quantified by five Chemical Transport Models (CTMs). These resulted in a mean net global radiative forcing (RF) increase of 1.6 mW/m^2 for the 'flying higher' case and a decrease of 2 mW/m^2 for the 'flying lower' case. Similarly, the direct global RF impacts from aerosols and the indirect impacts on cloudiness (soot-cirrus and contrails-cirrus) were also found to be beneficial to climate for the flying lower case, decreasing the RF by 0.2 mW/m^2 for soot-cirrus and 5 mW/m^2 for contrail-cirrus. The biggest contributor to aviation RF on a short-term horizon was the impacts on cloudiness (contrails-cirrus and soot-cirrus). The individual short-term impacts were also compared with the longer-term CO_2 impacts using other metrics such as Global Warming Potential (GWP) and Global Temperature Potential (GTP). It was found that the case for cruising at 'lower' altitudes produced less non-CO_2 effects. However, these mitigation scenarios were idealized and were ultimately used to formulate general principles of climate-optimized flight. The implementation of such simplified measures may not be feasible due to ATM operational restrictions.

1 INTRODUCTION

'REACT4C' (Reducing Emissions from Aviation by Changing Trajectories for the benefit of Climate) was an European Commission Seventh Framework Programme project that set out to explore the feasibility of adopting flight altitudes and routes that may lead to reduced fuel consumption and emissions, and therefore, lessen the environmental impact from aircraft. Another objective was to estimate the overall global effect of such Air Traffic Management (ATM) measures in terms of climate change. In order to achieve this, a set of simplified mitigation studies were devised to quantify the environmental benefit of simplified ATM measures and to use these results to formulate general principles for environmentally optimized flight for defined timescales and climate effects.

* *Corresponding author:* Ling L. Lim, Faculty of Science and Engineering, Manchester Metropolitan University, Chester St, Manchester M1 5GD, UK. Email: l.lim@mmu.ac.uk

2 AIRCRAFT EMISSIONS

The global aircraft emissions model, FAST (Owen et al., 2010), was used to generate a set of emissions inventories for use in other process-based models. These consisted of the 2006 base case and two mitigation scenarios where the cruise altitudes were shifted higher and lower by one flight level, i.e. 2,000 ft. The resulting emissions are shown in Table 1.

Table 1: Global aircraft emissions for 2006 (base case) and the mitigation scenarios

Scenario	Distance (billion km)	Fuel (Tg)	CO_2 (Tg)	NO_x (Tg NO_2)	BC (Tg)
Base case	38.86	178.3	563.4	2.338	0.00407
Lower	38.86	180.7	571.0	2.339	0.00432
Higher	38.86	176.8	558.7	2.358	0.00388

A 1.3% increase in fuel was observed for the flying lower case when compared with the base case. Conversely, a 0.8% decrease was seen for the flying higher case. In general, fuel efficiency increases with higher altitude, although other factors such as aircraft weight may influence an aircraft's optimal altitude.

3 IMPACTS FROM NO_X EMISSIONS

Three global 3D Chemical Transport Models (CTMs) (Oslo-CTM2, Oslo-CTM3, MOZART-3) and two Climate-Chemistry Model (CCMs) running in CTM mode (ULAQ-CTM, EMAC-QCTM) were used to identify and quantify the mitigation possibilities from changes in chemical composition, which are caused by aviation NO_x emissions. The results from this multi-model assessment are fully described in Søvde et al., 2014 and the main results are summarised in Table 2.

Table 2: Mean from the five participating CTMs for changes in global RF in mW/m^2 from aviation NO_x

Scenario	Short-lived O_3	CH_4	Long-lived O_3	Stratospheric H_2O	Net NO_x
Base case	19.5	-8.7	-4.3	-1.3	5.2
Lower	17.9	-8.9	-4.5	-1.3	3.2
Higher	21.0	-8.6	-4.3	-1.3	6.8

The results show that the net radiative forcing (RF) NO_x effects from the flying lower case were smaller than the flying higher case. It can be concluded from these results, which took into account both the short- and long-lived O_3 effects, and the indirect CH_4 and CH_4-induced stratospheric H_2O effects, that shifting cruise altitudes lower is better for atmospheric chemical composition and the effect is largely dominated by short-lived O_3. It should be noted that these results do not account for the effect of aerosols on chemical composition.

4 DIRECT AND INDIRECT IMPACTS FROM AEROSOLS

The ULAQ-CTM was also used to identify and quantify mitigation possibilities due to the direct impact of aerosols (soot and sulphate) and indirectly through cirrus-changes that may be triggered by aircraft aerosols (soot-cirrus). The model setup and base case results are fully described in Pitari et al., 2015 and the results from the mitigation scenarios are summarised in Table 3.

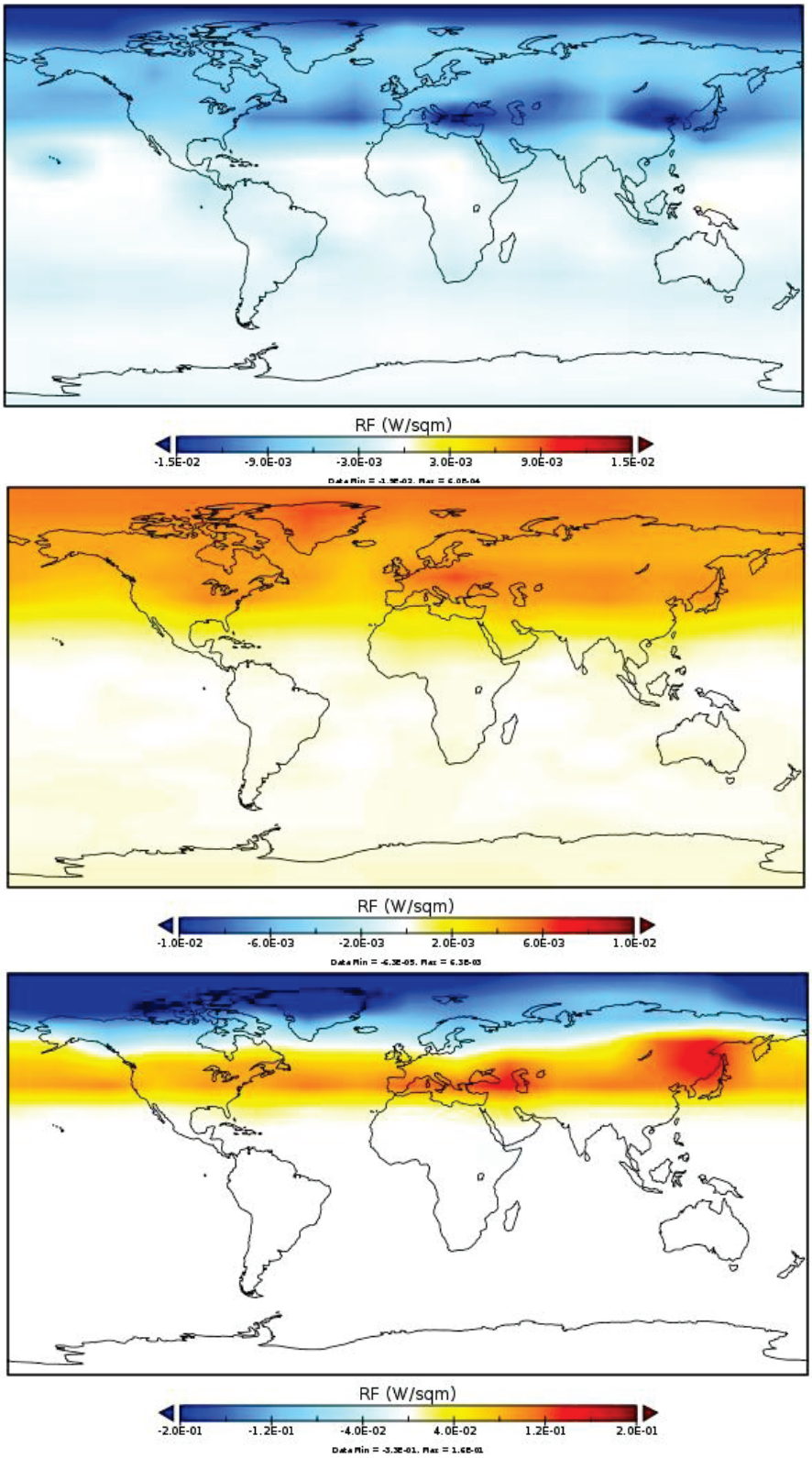

Figure 1: Radiative forcing (RF) for direct (a) sulphate and (b) soot; and (c) soot-cirrus from aviation aerosols in 2006

The RF from the direct and indirect effects of aviation aerosols for base case 2006 are depicted in Figures 1 (a) to (c), which resulted in a global net RF from aerosols of 2.2 mW/m^2. It was found that in contrast to net NO_x effects, the impact from aerosols produced a RF increase when flying lower (9% from the net increase over base case taking into account SO_4, soot and soot-cirrus components, Table 3) and a decrease when flying higher (18%). There are still large uncertainties in the estimation of soot-cirrus, despite the results being consistent with other study (Gettelman and Chen, 2013).

5 IMPACTS FROM CIRRUS CHANGES (CONTRAILS-CIRRUS)

The ECHAM4-CCMod (Burkhardt and Kärcher, 2011) was used to identify and quantify the mitigation possibilities from cirrus-changes (contrail-cirrus) that are caused by spreading contrails. Figure 2 (a) illustrates the spatial distribution of contrail-cirrus RF for base case 2006 and Figures 2 (b) and (c) the difference between the base case RF and the flying higher and lower cases respectively. It can be seen from these maps that the effects from the mitigation options are highly regional, with the largest RF decrease observed over the US and South-East Asia, when the cruise altitudes were shifted downwards.

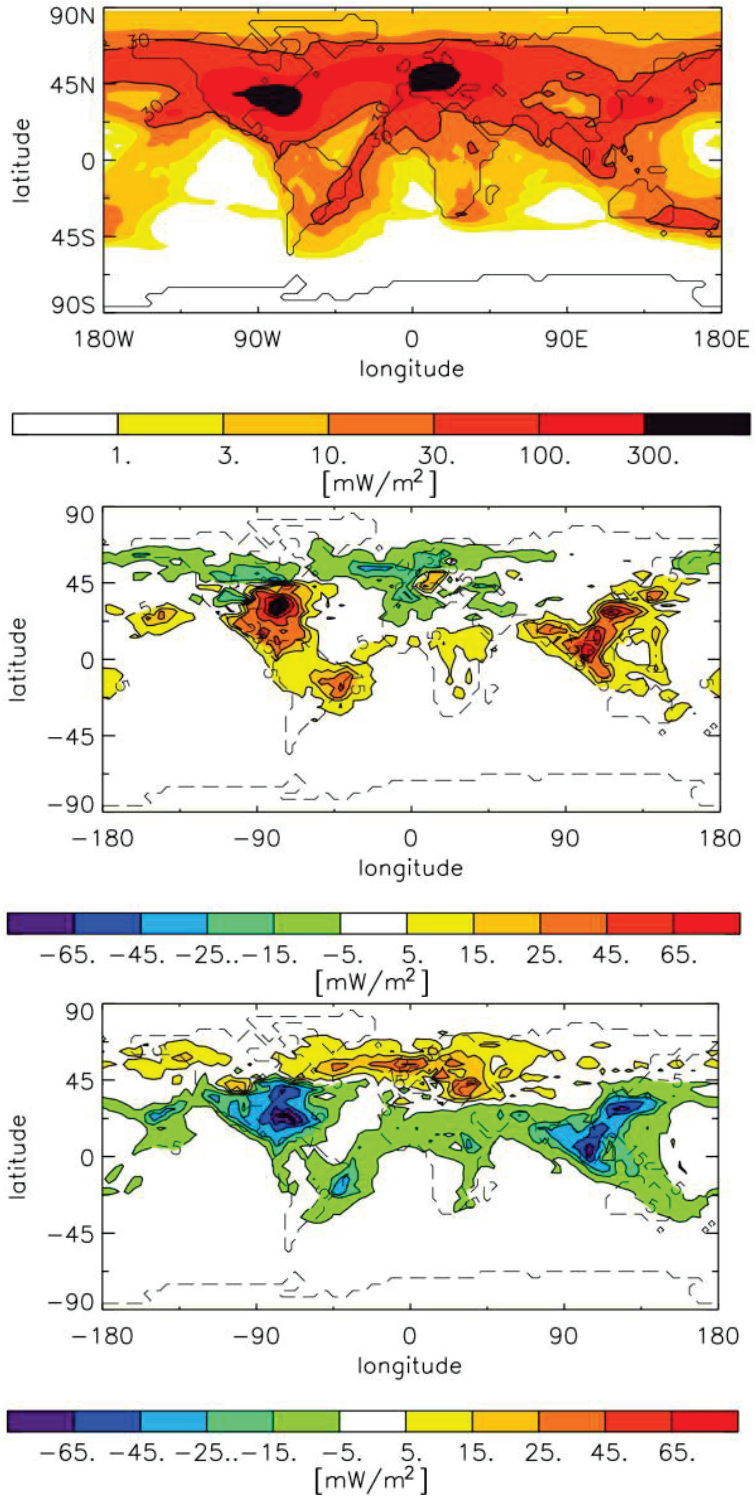

Figure 2: Radiative forcing (RF) for contrail-cirrus in 2006 (a) base case (b) difference between fly higher and base cases and (c) difference between fly lower and base cases

Not accounting for the change in natural cloudiness due to contrail-cirrus, the global RF from contrails-cirrus for 2006 was 45 mW/m^2, with an increase of 3 mW/m^2 when flying higher and decrease of 5 mW/m^2 when flying lower (Table 3). Therefore, globally, on a short-term horizon, it would be beneficial for climate for aircraft to cruise at a lower altitude.

6 SUMMARY

The short-term (non-CO_2) RF impacts from simplified flight pattern are summarised in Table 3. Contrail-cirrus was found to be the largest non-CO_2 effect, at least 4 times larger than the other non-CO_2 effects combined.

Table 3: Global RF in mW/m^2 from the short-term (non-CO_2) impacts

Scenario	Net NO_x	H_2O	SO_4	Soot	Soot-cirrus	Contrail-cirrus	Total non-CO_2
Base case	5.2	1.5	-3.5	0.8	4.9	45	53.9
Lower	3.2	1.1	-3.1	0.8	4.7	40	46.7
Higher	6.8	2.0	-3.9	0.8	4.9	48	58.6

These short-term impacts were also compared with the longer-term CO_2 impacts using other metrics such as GWP and GTP. In general, it was found that contrail-cirrus was the most important RF component on a short-term horizon and CO_2 over the longer-term.

The case for cruising at 'lower' altitudes was found to produce less non-CO_2 effects, largely due to contrails (consequently, contrail-cirrus) that are less likely to form at lower altitudes. However, it should be noted that these mitigation scenarios were idealized and devised to formulate general principles of climate-optimized flight. In reality, the implementation of such simplified measures may not be feasible due to ATM restrictions.

REFERENCES

Burkhardt, U. and B. Kärcher, 2011: Global radiative forcing from contrail cirrus. Nature Climate Change 1, 54-58.

Gettelman, A and C. Chen, 2013: The climate impact of aviation aerosols. Geophys. Res. Lett. 40, 1–5.

Owen, B., D.S. Lee and L.L. Lim, 2010: Flying into the Future: Aviation Emissions Scenarios to 2050. Environ. Sci. Technol. 44, 2255-2260.

Pitari, G., D. Iachetti, G. Di Genova, N. De Luca, O.A. Sovde, Ø. Hodnebrog, D.S. Lee, and L. Lim, 2015: Impact of coupled NO_x/aerosol aircraft emissions on ozone photochemistry and radiative forcing. Atmosphere 6, 751-782; doi:10.3390/atmos6060751.

Søvde, O.A., S. Matthes, A. Skowron, D. Iachetti, L. Lim, Ø. Hodnebrog, G. Di Genova, G. Pitari, D.S. Lee, G. Myhre, and I.S.A. Isaksen, 2014: Aircraft emission mitigation by changing route altitude: A multi-model estimate of aircraft NO_x emission impact on O_3 photochemistry. Atmos. Environ. 95, 468-479, doi: 10.1016/j.atmosenv.2014.06.049.

ACKNOWLEDGEMENTS

This work was supported by the European Commission Seventh Framework Project, 'REACT4C' (contract no. ACP8-GA-2009-233772).

The global impact of weather-dependent climate-optimal trajectories in the North Atlantic

S. Matthes*, S. Dietmüller
DLR-Institut für Physik der Atmosphäre, Oberpfaffenhofen, Germany

O.A. Søvde
Center for International Climate and Environmental Research – Oslo (CICERO), Oslo, Norway

L.L. Lim, A. Skowron
Faculty of Science and Engineering, Manchester Metropolitan University, UK

D. Iachetti, G. Pitari
University of L'Aquila, L'Aquila, Italy

Keywords: Aviation climate impact, mitigation strategies, weather-dependent alternative routing, non-CO_2 impacts

ABSTRACT: The European Project REACT4C, coordinated by the DLR-Institute of Atmospheric Physics, investigated the potential of alternative flight routing concepts for reducing the climate impact of aviation, and accomplished a feasibility study for the North Atlantic. Such climate-optimized flight routing is performed by taking into account prevailing synoptic weather pattern. For winter five distinct patterns were identified, hence accordingly five emission inventories were generated for the NAFC region. Here we present and experiment design and assessment study with a set of chemistry-transport-models in order to evaluate atmospheric and climate impact of nitrogen oxide emissions from optimized routings for a specific winter season. Specifically, two study periods are selected, first, winter 2004/2005 and, second, winter 2006/2007. On a daily basis prevailing weather patterns are analysed as defined in five distinct patterns and the corresponding optimized traffic inventory is integrated in the time series of aviation emissions. Simulations are performed by a set of chemistry-transport models which are OSLO CTM2/3, ULAQ-CTM, EMAC QCTM and MOZART-3, producing a multi-model estimate. Each model simulated two numerical simulations, a reference using economically optimized inventories and, a scenario using climate-optimized inventories. The comparison of atmospheric concentrations between both simulations determines the impact of climate-optimal routing. Results present changes in atmospheric concentrations of reactive species, focusing in particular on nitrogen oxides and ozone, of these weather-dependent climate-optimized inventories. Impact of aviation on atmospheric nitrogen oxide and ozone associated with NOx emissions from climate-optimized trajectories, show an identical pattern with reduced changes in higher altitudes (FL 390) and increased changes in lower altitudes (FL 230) compared to conventionally planned trajectories.

1 INTRODUCTION

The EU FP7 project REACT4C explored the feasibility of operational measures to adopt alternative trajectories such as changes in flight altitude and routes that may lead to reduced climate impact from aviation. When assessing climate impact from aviation emissions it is important to recognize that beside CO_2 also non-CO_2 impacts have to be considered. Here we consider impact of NO_x emissions which shows a strong variation of atmospheric impact with geographic location but also altitude of emission. In order to quantify mitigation gain thru climate-optimization in such a feasibility study, it is required to estimate atmospheric impact of emissions from an alternative routing mitigation-scenario and compare its impact to a conventionally planned inventory, which is economical optimized. Comparing atmospheric impact of both alternative scenarios, determines the impact of mitigation strategy. Several studies used a similar approach to show effects of NO_x emissions from mitigation concepts on tropospheric ozone (e.g. Søvde et al., 2014), with some putting

* *Corresponding author:* Sigrun Matthes, DLR-Institut für Physik der Atmosphäre, Oberpfaffenhofen, D-82205 Wessling, Germany. Email: sigrun.matthes@dlr.de

particular emphasis on the spatial and temporal variation of aviation related impacts (Stevenson and Derwent, 2009; Köhler et al., 2013; Skowron et al., 2015).

In this paper we estimate mitigation gain by climate optimization of aircraft trajectories for a traffic sample between Europe and the USA in the North Atlantic flight corridor, when flying one season (three months in winter) on climate-optimized trajectories. First, we present nitrogen oxide emission inventories for climate-optimal trajectories compared to economically-optimal trajectories. Aircraft emission inventories were generated as part of the REACT4C feasibility study on climate-optimized flight planning. Second, we show results from atmospheric modelling in chemistry-transport models and compare atmospheric impacts of emissions for both optimizations. Here, we present changes in atmospheric concentrations of key species due to nitrogen oxide emissions from climate-optimized trajectories calculated with a set of chemistry-transport models.

2 EMISSIONS OF CLIMATE-OPTIMIZED AIR TRAFFIC BETWEEN EUROPE AND USA

Emission inventories used in this atmospheric modelling study are generated by a bottom-up approach as part of a feasibility study on climate-optimized routing. A reference inventory is produced which corresponds to conventionally planned air traffic between Europe and the USA. An emission scenario represents emissions from weather-dependent climate-optimized air traffic for a traffic sample between Europe and USA in the North Atlantic Flight Corridor.

Aircraft trajectories were optimized for a traffic sample between Europe and USA in the North Atlantic flight corridor (NAFC) with an expanded flight planning tool as developed within the project REACT4C under two optimization criteria: one minimizing climate impact and another one deriving economically-optimized trajectories. These emission inventories were generated as part of a feasibility study which relies on a modelling chain for climate-optimization of aircraft trajectories (Grewe et al., 2014). Each distinct inventory results from a traffic sample of trans-Atlantic air traffic with a total of about 700 flights. Trajectory of each individual flight in this traffic sample is optimized under both optimisation criteria, minimal economic costs and minimal climate impact. Emissions from individual trajectory optimizations are then added up to an overall inventory: one being climate-optimized, the other one economically optimized.

Results for overall optimization for specific daily case studies are provided in Grewe et al. (2014) and Matthes et al. (2016). Expanded flight planning tool allows optimization under both optimization criteria - economic and climate – as it has an additional interface to meteorological data on climate impact, which makes available during trajectory planning additional, spatially and temporarily resolved, meteorological information on climate impact of emitted components. This interface to climate impact information is established via so-called climate cost functions which provide a quantitative measure of how much an emitted component released at a specific position, altitude and time has an impact on radiative balance in the atmosphere and hence climate. Eventually, this allows calculating trajectories for a traffic sample with minimal economic costs but also with minimal climate impact, in order to generate two distinct emissions inventories.

As optimal routes depend on prevailing meteorology (synoptic situation), optimization is performed under distinct meteorological conditions (wind, climate cost functions) and two distinct optimization criteria. Specifically in winter, a set of five archetypical weather situations is considered for economically and environmentally optimal trajectories, respectively. Concept of selecting typical synoptic weather patterns in the North Atlantic follows Irvine et al. (2012) by distinguishing meteorological situations with the help of the North Atlantic Oscillation (NAO) and Artic Oscillation (AO) atmospheric index, and more details are provided in Matthes et al. (2016). Climate cost functions were derived for a typical member of each weather pattern, and traffic sample was then optimized for that specific weather pattern by using associated wind fields and climate cost functions. As a result we receive for winter a set of five weather-dependent climate-optimized scenarios, distinguished by respective weather pattern from 1 to 5 (W1, W2, W3, W4, W5).

3 CHEMISTRY-CLIMATE MODEL SIMULATIONS TO QUANTIFY ATMOSPHERIC IMPACT

Atmospheric impact of two distinct weather-dependent emission inventories, one being climate-optimized and the other one economically-optimized, is calculated by integrating them individually in chemistry-climate models by respecting corresponding prevailing pattern and by analysing changes in chemical key species.

In order to evaluate climate impact of optimized routings for a specific winter season an experiment design was developed, which relies on two separate simulations. One simulation was performed with emissions from conventionally-optimized air traffic (econ) and a second simulation was per-formed with emissions from climate-optimized routing (clim). The difference found in atmospheric concentrations of key species, namely nitrogen oxide and ozone, gives the impact of climate-optimization of aircraft trajectories.

For the case study presented in this paper an episode in winter 2003/2004 was selected, where prevailing meteorological situation is dominated by winter weather pattern W1. During a period of 11 subsequent days and a second period of 6 days W1 is prevailing. For the atmospheric simulation of the selected episode, a time series of weather pattern inventories is generated, which change on a daily basis, considering individual prevailing weather pattern on that specific day. Each model performed two numerical simulations, one using economically optimized inventories and another one using climate-optimized inventories. The temporal distribution of respective weather patterns during study period determines the time series of individual optimized daily emission inventories.

The comparison of atmospheric concentrations between two distinct simulations – one with climate-optimized inventories, the other one with economically optimized inventories determines the impact of climate-optimal routing. Results are shown as changes in atmospheric concentrations of reactive species, focusing in particular on nitrogen oxides and ozone of these weather-dependent climate-optimized inventories.

4 AVIATION EMISSION INVENTORIES: CLIMATE-OPTIMIZED ROUTING FOR NORTH ATLANTIC TRAFFIC SAMPLE

Emission inventories from climate-optimized aircraft trajectories are compared with conventionally planned trajectories. In Figure 1 we show changes in NO_x emissions vertically integrated over all flight levels for five distinct archetypical winter weather patterns, as they are used within the simulation. Specifically, we show how nitrogen oxide emissions from climate-optimized aircraft trajectories compare to economically-optimized trajectories. Such climate-optimized flight routing takes into account prevailing synoptic weather pattern.

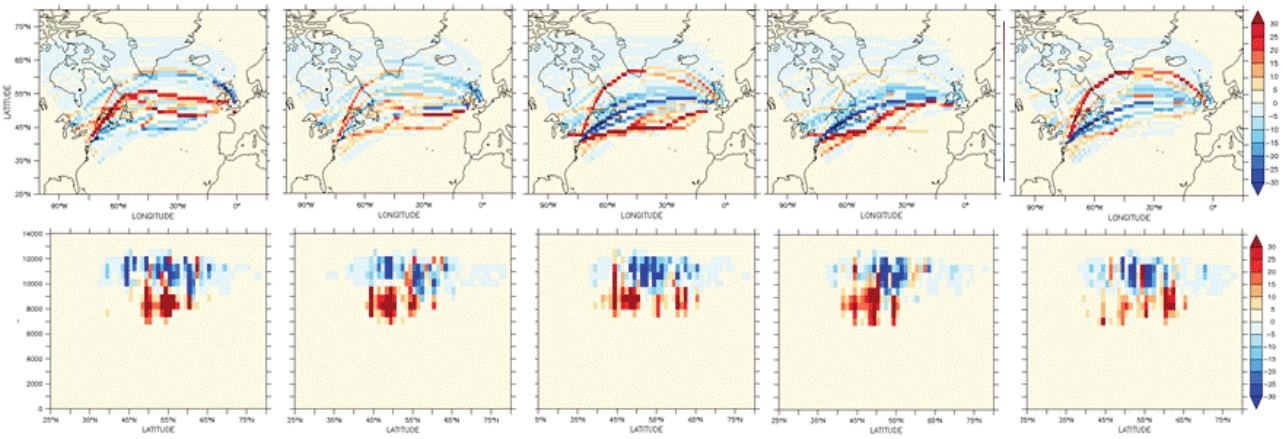

Figure 1: Differences in nitrogen oxide emission (NO_x) between climate-optimal versus economical optimal case are shown in five distinct winter weather patterns (from left to right column): W1 strong jet, W2 tilted strong jet, W3 tilted weak jet, W4 confined strong jet, W5 confined weak jet as geographic distribution (upper row) and zonal average over 30°W-40°W (lower row).

Five distinct patterns for the North Atlantic flight corridor region were identified in winter; hence accordingly five emission inventories were generated. We present changes in spatial distribution of emission inventories when comparing climate-optimized routing with conventionally planned routing (Figure 1). In table 1 emission totals are listed for individual patterns, and compared to the economically optimized trajectories.

Table 1: Nitrogen oxide emissions [Gg NO_2] for economically-optimized (econ) and climate-optimized (clim) trajectories for the North Atlantic Flight Corridor region (120°W-15°E, 15°N-80°N); absolute difference and relative difference between both inventories.

	Econ	Clim	Abs. diff	Rel.diff.
W1	584,2	598,2	14,0	2,40%
W2	585,1	594,6	9,5	1,63%
W3	587,2	603,3	16,1	2,75%
W4	585,7	581,6	-4,1	-0,70%
W5	586,0	588,2	2,2	0,38%

5 ATMOSPHERIC IMPACTS OF AVIATION NO_X EMISSIONS WHEN FLYING CLIMATE-OPTIMIZED TRAJECTORIES

We focus on the study period winter 2004/2005 and we present changes in atmospheric mixing ratios associated with one season (three months) of air traffic with weather-dependent climate-optimized aircraft trajectories compared to conventionally planned trajectories.

Comparing impact of nitrogen emissions from climate optimized aircraft trajectories with impact of conventionally planned trajectories shows that reduced contributions to atmospheric volume mixing ratios of NO_x occur at higher altitudes, while increased contributions appear at lower levels. Decreased atmospheric nitrogen oxide concentrations are found at higher levels north of 30°N around FL 230, with a vertical and geographical mean values (400hPa – 300 hPa, 35°N - 45°N) being up to 15 pmol/mol lower, and a mean decrease of 2 pmol/mol (Figure 2). Calculated impact of one winter season climate-optimized air traffic aviation (changed emissions from December to March) shows peak values in March and tends to disappear in June, with again a slight reduced impact in July, before further diminishing in August. Increased nitrogen oxide volume mixing ratios are found in

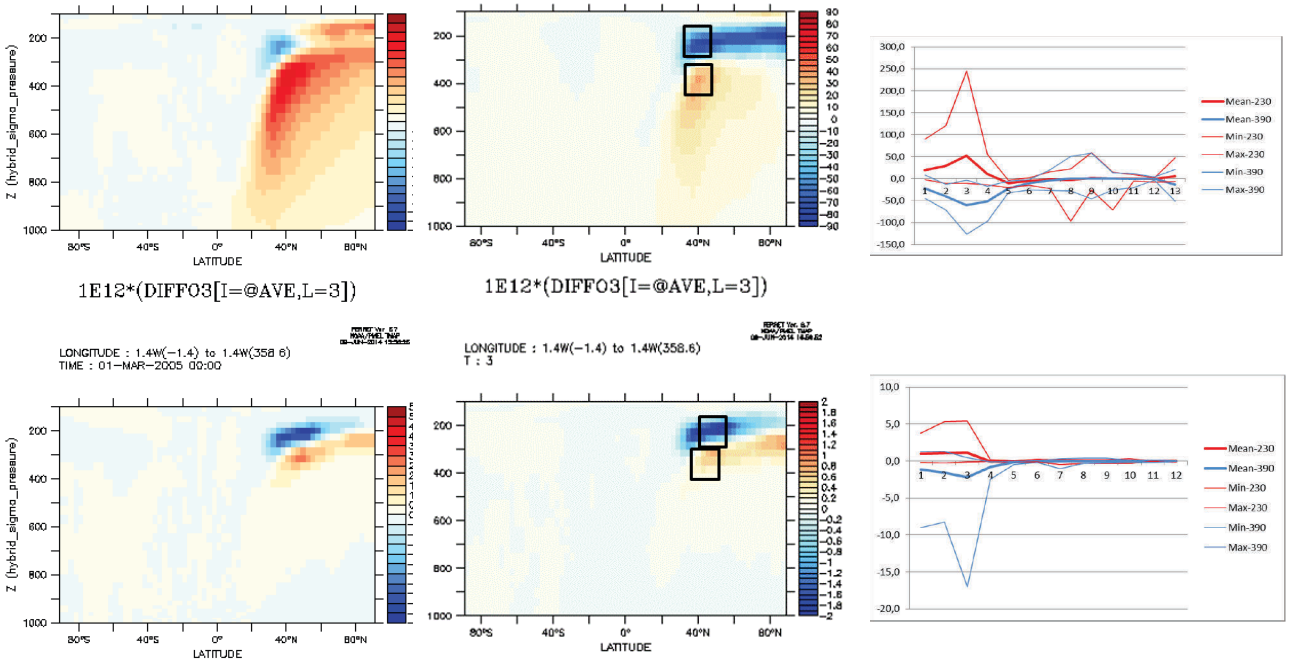

Figure 2: Zonal mean changes in ozone concentration (upper panel) and nitrogen oxides (lower panel) as calculated by atmospheric models in March (after end of perturbation), and temporal evolution of perturbation in FL240 and FL 340 averaged over longitude and region of latitude and altitude. Region 390: 40°N-45°N, 400-300 hPa (around FL390, blue), region 230: 41°N-46°N, 300-200 hPa (around , red).

lower levels at around FL230, with a vertical and regional mean increase of 2 pmol/mol.

Aviation impact on atmospheric volume mixing ratios of ozone shows a similar pattern with an in-creased ratio in lower levels and a decrease in higher levels. For ozone an increase in volume mixing ratios of up to 250 pmol/mol can be found, with a regional mean increase of 50 pmol/mol. Maximum changes are found in March, at the end of the changed emissions period, but changes, also from opposite sign are found from July to October of the same year. However, regional differing values nearly completely equal out and vertical and geographical mean values accordingly tend to zero.

6 DISCUSSION

Changes in atmospheric volume mixing ratios associated with climate-optimized trajectories, show for nitrogen oxide and ozone a similar pattern with lower values in higher altitudes (FL 390) and increased values in lower altitudes (FL 230) compared to conventionally planned trajectories. This is consistent with changes in vertical distribution of direct NO_x emissions due to climate optimization. Under all five weather patterns the emission distributions shows that more trajectories in lower altitudes are preferred and higher flight levels are sometimes avoided.

Comparing changes in latitudinal distribution of individual emission inventories under different prevailing patterns reveals that only in weather pattern W1 higher emissions in central part (around 50-55°N) of NAFC occur, while under W3 two distinct latitudes of increased emissions are found: 45°N and 60°N. In W4 increased emissions occur in the southern part of the flight corridor at around 45°N, and a bit weaker at 55°N. These changes in emission inventories are consistent with shifts of air traffic flows presented in Grewe et al. (2014) und Matthes et al. (2016).

Consistently with changing vertical distribution of aviation emissions for climate-optimized trajectories, changes in nitrogen oxide and ozone show a decreased contribution at higher altitudes, and an increased contribution at lower altitudes. Hence shifting aviation induced ozone to lower altitudes reduces the radiative and climate impact. Analysis shows that perturbation signal of nitrogen oxide and ozone is maximal in March, however, temporal evolution of changes in ozone shows that ozone signal remains perturbed until 7 months after the end of the changing emissions period (scenario), which corresponds to October.

One has to note, that analysing changes in atmospheric volume mixing ratios is crucial for estimating environmental benefit of a mitigation strategy. However, for a full climate impact assessment a subsequent calculation of changes in radiative transfer is required which is currently missing. The intention of this study is furthermore, to present another element for a comprehensive evaluation concept to assess mitigation concepts and their overall climate impact.

7 SUMMARY AND CONCLUDING REMARKS

This study presents a modelling study to calculate impact of weather-dependent climate-optimized routing which considers prevailing synoptic situation. It assesses the potential for improvements of inefficiencies in the air transport system, with regards to climate impact due to non-conventional flight trajectories in a realistic atmosphere, while focusing on non-CO_2 impact via nitrogen oxide emissions. Improved knowledge on the space and time dependence of the impact of aircraft emissions on climate allows formulating specific recommendations on flight planning, aircraft and engine design for future green aircraft.

We present here a model estimate for atmospheric impact of a mitigation strategy for aviation climate impact which is flying flexible, specifically, weather-dependent climate-optimized trajectories. Close cooperation between experts from different fields of expertise is required to assess environmental benefit of climate-optimized flight planning. Such collaborative work has the potential to support implementation of alternative routing strategies, in particular climate-optimized aircraft trajectories, within joint technology initiatives, e.g. within SESAR JU.

REFERENCES

Grewe, V., T. Champougny, S. Matthes, C. Frömming, S. Brinkop, O. A. Søvde, E.A. Irvine, L. Halscheidt, 2014: Reduction of the air traffic's contribution to climate change: A REACT4C case study. Atmospheric Environment 94, 616–625.

Grewe, V., C. Frömming, S. Matthes, S. Brinkop, M. Ponater, S. Dietmüller, P. Jöckel, H. Garny, E. Tsati, K. Dahlmann, O.A. Søvde, J. Fuglestvedt, T.K. Berntsen, K.P. Shine, E.A. Irvine, T. Champougny, and P. Hullah, 2014, Aircraft routing with minimal climate impact: the REACT4C climate cost function modelling approach (V1.0). Geosci. Model Dev., 7, 175-201.

Köhler, M.O., Rädel, G., Shine, K.P., Rogers, H.L., Pyle, J.A., 2013: Latitudinal variation of the effect of aviation NO_X emissions on atmospheric ozone and methane and related climate metrics. Atmos. Environ. 64, 1–9.

Irvine, E. A., Hoskins, B. J., Shine, K. P., Lunnon, R. W., and Frömming C., 2013: Characterizing north Atlantic weather patterns for climate-optimal routing. Meteorol. Appl., 20, 80–93, doi:10.1002/met.1291.

Matthes, S., 2012: Climate-optimised flight planning – REACT4C in Innovation for a Sustainable Aviation in a Global Environment, Proceedings of the Sixth European Aeronautics Days 2011, IOS Press & European Union, ISBN 978-92-79-22968-8.

Matthes, S., U. Schumann, V. Grewe, C. Frömming, K. Dahlmann, A. Koch, and H. Mannstein, 2012: Climate optimized air transport, in Atmospheric Physics, Research Topics in Aerospace, U. Schumann (ed), DOI: 10.1007/978-3-642-30183-4_44, Springer-Verlag, Berlin, Heidelberg, 727-746.

Matthes, S., V. Grewe, C. Frömming, S. Brinkop, T. Champougny, O.A. Sovde, E. Irvine, 2016: Mitigation potential of weather-dependent climate-optimal trajectory planning in the North Atlantic Flight corridor (in preparation).

Skowron, A., Lee, D.S., and De León, R.R., 2015: Variation of radiative forcings and global warming potentials from regional aviation NO_X emissions. Atmos. Environ. 104, 69–78.

Søvde, O.A., Matthes, S., Skowron, A., Iachetti, D., Lim, L., Owen, B., Hodnebrog, Ø., Di Genova, G., Pitari, G., Lee, D.S., Myhre, G., Isaksen, I.S.A., 2014: Aircraft emission mitigation by changing route altitude: A multi-model estimate of aircraft NO_x emission impact on O_3 photochemistry. Atmospheric Environment, doi: 10.1016/j.atmosenv.2014.06.049.

Stevenson, D.S., and Derwent, R.G., 2009: Does the location of aircraft nitrogen oxide emissions affect their climate impact? Geophys. Res. Lett. 36, L17810.

ACKNOWLEDGEMENTS

This work was supported by the European Commission Seventh Framework Projects, ‘REACT4C’ (contract no. ACP8-GA-2009-233772) and Coordination Action ‘Forum-AE’ (contract no. FP7-AAT-2013-RTD-1-605506). We thank Emma Irvine (University of Reading) for providing information on classification of prevailing weather pattern in the North Atlantic. We also thank for financial support from ECATS International Association (IASBL), related to ECATS working group “Climate Impact and Aviation”.

The DLR Transport and the Environment Project – Building competency for a sustainable mobility future

A. Henning
Deutsches Zentrum für Luft- und Raumfahrt (DLR), Institut für Aerodynamik und Strömungstechnik, Göttingen, Germany

M. Plohr
Deutsches Zentrum für Luft- und Raumfahrt (DLR), Institut für Antriebstechnik, Köln, Germany

E. D. Özdemir
Deutsches Zentrum für Luft- und Raumfahrt (DLR), Institut für Fahrzeugkonzepte, Stuttgart, Germany

M. Hepting, H. Keimel
Deutsches Zentrum für Luft- und Raumfahrt (DLR), Institut für Flughafenwesen und Luftverkehr, Köln, Germany

S. Sanok
Deutsches Zentrum für Luft- und Raumfahrt (DLR), Institut für Luft- und Raumfahrtmedizin, Köln, Germany

R. Sausen
Deutsches Zentrum für Luft- und Raumfahrt (DLR), Institut für Physik der Atmosphäre, Oberpfaffenhofen, Germany

T. Pregger
Deutsches Zentrum für Luft- und Raumfahrt (DLR), Institut für Technische Thermodynamik, Stuttgart, Germany

S. Seum*, M. Heinrichs, S. Müller, C. Winkler
Deutsches Zentrum für Luft- und Raumfahrt (DLR), Institut für Verkehrsforschung, Berlin, Germany

T. Neumann
Deutsches Zentrum für Luft- und Raumfahrt (DLR), Institut für Verkehrssystemtechnik, Berlin, Germany

O. Seebach
Deutsches Zentrum für Luft- und Raumfahrt (DLR), Simulations- und Softwaretechnik, Köln, Germany

V. Matthias
Helmholtz-Zentrum Geesthacht, Zentrum für Material- und Küstenforschung, Geesthacht, Germany

B. Vogel
Karlsruhe Institut für Technologie (KIT), Institut für Meteorologie und Klimaforschung (IMK-TRO), Karlsruhe, Germany

Keywords: transport research, transport related climate change, transport and the environment, transport scenario, air quality impact, air quality modeling, climate modeling,

ABSTRACT: This article describes the thematic and organizational approach of the DLR Transport Program's research project "Transport and the Environment" (Verkehrsentwicklung und Umwelt, VEU). It illuminates the research approach, which employs scenario techniques to achieve a common understanding and a framework for the project. Establishing a platform for scientific exchange, VEU clearly facilitates the interdisciplinary integration of research on mobility within the DLR and its partner institutes. A set of transport scenarios for Germany and Europe (time horizon 2040), which are presented in greater detail in this article, is used in this respect and aims to provide answers for pressing societal questions.

* *Corresponding author:* Stefan Seum, DLR Institut für Verkehrsforschung, D-12489 Berlin, Germany. Email: stefan.seum@dlr.de

1 INTRODUCTION

Ensuring mobility while also protecting people, resources and the environment is one of the greatest challenges facing us. The DLR Transport Program's research project "Transport and the Environment" (Verkehrsentwicklung und Umwelt, VEU) has been created to investigate the transport and environmental functional chain . The project integrates fundamental research on new and innovative mobility technologies and concepts with socio-economic analyses of behavior, acceptance and use of these options. It continues its analysis by developing models for future mobility trends and their impacts on people and the environment. The overarching goal of the VEU project is to analyze the effects of possible future transport systems with a focus on mobility developments, noise, air quality, weather patterns and the global climate. Explorative scenarios for the year 2040 are developed and quantified using the VEU model landscape. For this purpose, social developments, political measures and technical innovations are identified that act as catalysts for substantial changes in society and its transport system. The VEU-scenarios generate a joint framework guiding the institutional research and have profited from the interdisciplinary character of the project.

2 PROJECT STRUCTURE

In the VEU sectoral research on specific topics is combined with applied and joint research (Figure 1), developing a set of interconnected models. The VEU project involves ten DLR institutes and two Helmholtz Centers (KIT and HZG) in a unique research network. The VEU project creates platforms for scientific exchange and interdisciplinary research on mobility. It follows the interdisciplinary approach by incorporating social sciences, mathematics, engineering, physics and atmospheric chemistry. Furthermore, it integrates medical research related to traffic noise as well as specific economic analyses. Empirical socio-economic research is linked with several models on different spatial scales. As well as focusing on passenger and freight transport demand in Germany in great detail, and for Europe in lesser detail, the project also covers global air transport. Furthermore, the results of the VEU project are embedded in global climate modeling. The interconnected VEU-models provide a comprehensive and reactive instrument for transport analysis. The instruments to create the joint research platform within VEU are: regular interdisciplinary exchanges, identifying common understanding across disciplines and developing VEU scenarios for possible futures in mobility.

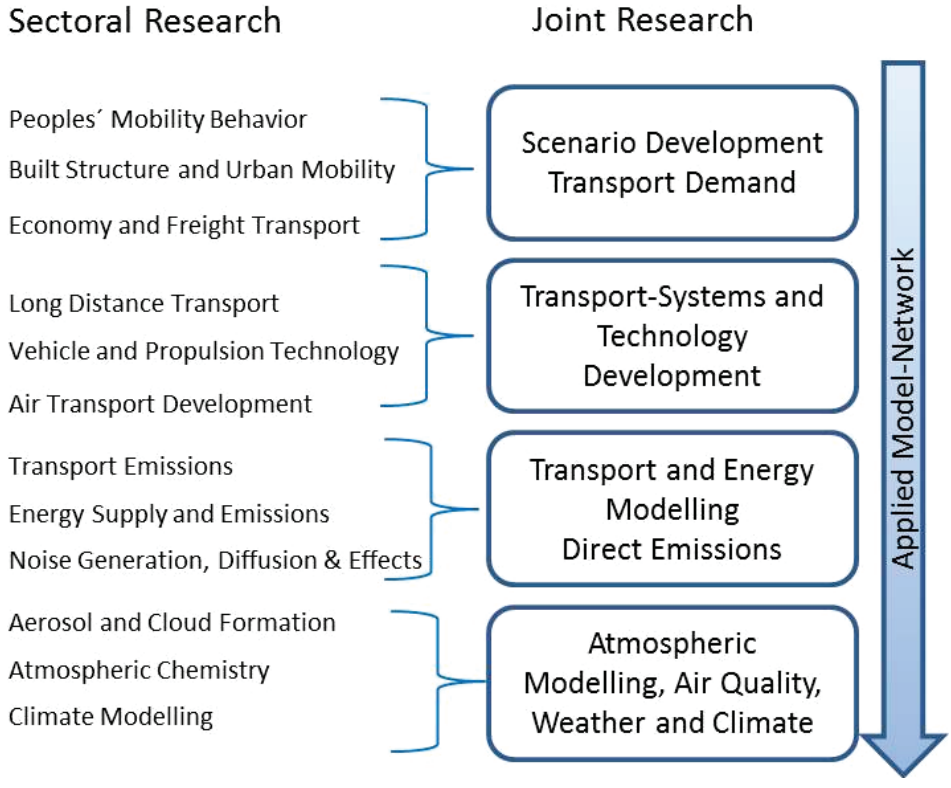

Figure 1: Relationship between sectoral research and joint research topics in VEU

3 THEMATIC ELEMENTS OF THE TRANSPORT AND THE ENVIRONMENT PROJECT

3.1 *Mobility behavior, transport generation and the modeling of future mobility systems*

Transport demand reduction and the shift to healthier and less fuel-consuming modes of transportation are ways to reduce traffic's environmental impact. Re-urbanization and demographic change are a few of the trends in Germany demanding new concepts to ensure mobility and equal societal participation. The densification in metropolitan regions opens new mobility options (e.g. cost-efficient public transport), but also poses continuing challenges including air quality and human health issues.

The socio-economic dynamics of societies, people's behavior and the role these play in the mobility of the future are being comprehensively investigated in the VEU project. For example, issues of modal choice and traffic generation and the interrelationships between mobility and the built environment are likewise at the center of the empirical research. Furthermore, a particular focus lies on long-distance travel by road, rail and air.

The DLR transport research institutes (Institute of Air Transport and Airport Research, Institute of Transportation Systems, Institute of Transport Research) analyze official statistics (e.g. the National Travel Survey "Mobility in Germany", MID) and conduct their own empirical studies on behavior and demand. In addition, the acceptance of new concepts and technologies is also examined, of car sharing, for instance, or the use of information and communication technology, e.g., for management of logistics processes or passenger information on public transport.

The outcomes of the empirical research are integrated into transport demand models, which are developed in the VEU project. The models include discrete-choice and multi-agent approaches that can describe and forecast multifaceted transport processes. Depending on the spatial scale, specific models are deployed. The areas looked at are equally diverse, ranging from the mapping of national transport and energy systems, to small-scale, specific modeling of urban and rural areas. Results of the transport demand models feed into emission models and the chain of modeling for regional air quality and global climate effects.

The economic effects of transport on employment and the certain economic sectors have already been studied in the project's predecessors. This is now being expanded by analyzing the labor market effects of new and innovative technologies.

3.2 *Technologies and energy systems of mobility*

Technological improvements to existing transport technologies and the development of new ones are key aspects in achieving a more environmentally sound transport system. In the areas of rail and road vehicles, there are several possibilities to reduce consumption and conserve resources through technological innovation such as new (and lighter) materials and downsizing, alternative powertrain concepts such as fuel cells and electric motors, and new fuels, such as liquefied natural gas or hydrogen from renewable wind power. New technologies such as lightweight construction or new propulsion and fuel systems can also contribute to greater sustainability in aircraft and their engines.

Several institutes within the VEU project (DLR Institutes of Propulsion Technologies, of Vehicle Concepts and of Engineering Thermodynamics) are examining potential alternative technologies and energy systems. The markets for innovative vehicle technologies are systematically scanned, analyzed and evaluated. Production cost models are developed for essential vehicle components (e.g. for battery, fuel cell etc.) in order to assess the total cost of ownership of different powertrain concepts. Furthermore, life-cycle approaches are used to study the well-to-wheel as well as the production emissions of different propulsion concepts. The agent-based market model developed in the project can then estimate what proportion of vehicles with alternative drive trains is realistic in future vehicle fleets. Other models assess consumption and emission patterns of the commercial civil aviation.

Furthermore, the positive impact of innovative transport systems depends on the way energy is generated – for instance, whether power for electric mobility is conventionally produced or by climate-friendly means. The incorporation of models for future energy systems is thus an integral component of VEU scenario analysis and its well-to-wheel assessment.

3.3 *Transport noise and its effects*

Noise may harm people both physiologically and psychologically. In regions with high transport activities, noise poses an important environmental factor and many people in those areas feel disturbed by transport noise. Better understanding of where noise is created at vehicles, how it diffuses in space and how it affects people is one major task of the sectoral research within the VEU project.

A cluster of three DLR institutes (DLR Institutes of Aerodynamics and Flow Technology, of Aerospace Medicine and of Atmospheric Physics) analyze transport noise with a flexible forecasting procedure. In the VEU project, noise is measured across its whole range, from its generation and transmission to sound propagation and characteristics. Microphone array technique is used in this, combined with video recording when measuring with directional microphones. This allows the causes of noise to be better understood, e.g. what proportion of car noise comes from the engine, tires or road surface, or what role braking, tracks and curves play in train noise.

The research findings are combined in models with further VEU transport development data. This enables precise assessments of future noise pollution. The noise research also incorporates factors such as demographic change, regional classifications and urban structural characteristics.

The effects of noise on people, especially on sleep, are also empirically studied. While air and rail transport has been studied, the gaps in data on road transport are being filled with new field studies. In addition, potential noise-reduction measures are tested, both technical, e.g., silent brakes, new tires and asphalt surfaces etc., and behavioral, e.g., speed limits, economic instruments etc.

3.4 *Effects of transport developments on environment and society*

Transport is responsible for around 24% of greenhouse gas emissions in Europe . Alongside climate-damaging CO_2, transport also releases many other substances which impact local air quality. Already today, thresholds for particulate matter and nitrogen oxides are over-exceeded near many European city streets. Transport emissions such as nitrogen oxides, carbon monoxide and hydrocarbons lead to an increase in ground-level ozone, which is harmful to the environment and to human health. Besides the climate effect of transport CO_2, air emissions from transport also affect our weather and climate indirectly: soot and fine dust, for example, but also gases such as sulfur dioxide, nitrogen oxides and hydrocarbons can form atmospheric aerosol. These aerosol particles reflect and absorb solar radiation, and affect cloud formation (including contrails and contrail cirrus) and eventually weather and climate. Thus, it is crucial to study the emission effects due to changes in mobility patterns and the introduction of new concepts and technologies in order to provide society with solid knowledge for decision making.

The DLR Institute of Atmospheric Physics together with the Karlsruhe Institute of Technology, Institute of for Meteorology and Climate Research and the Institute for Coastal Research at the Helmholtz-Center Geesthacht examine the complex interrelationships between transport and its environmental effects. In the VEU project, passenger and freight transport emissions, embedded in the emissions from other European and global sources, are quantified by using an emission inventory model for Europe and continuously improving it with original data. For example, transport demand results are integrated for more precise effects modeling. The impact of pollutants on air quality, climate and weather are subsequently analyzed with the aid of simulations via numerical models, supplemented by airborne atmospheric measurements. The emissions' effects are both analyzed for the actual current status and forecast for potential future developments. The particular question here is how future mobility systems would affect the environment.

4 SOLVING THE INTERDISCIPLINARY CHALLENGE OF THE RESEARCH PROJECT

The VEU project uses scenario approach, which firstly brings together the sectoral research of the individual aspects. Further, it helps the project to achieve its goal of analyzing the effects of possible future transport systems, focusing on mobility, noise, air quality, weather patterns and the global climate Within the scenarios social developments and political measures are identified that act as catalysts for substantial changes in society and its transport system. The scenarios are exploratively developed for Germany within Europe in the year 2040. The scenarios are then quantified using the

VEU model landscape. In this way, the scenario research fosters the cohesion of the individual research tasks.

4.1 *Creating a common understanding through transport system scenarios*

The aim to work in an interdisciplinary fashion, embracing the entire cause-and-effect chain from microscopic transport demand to global climate modeling is ambitious. Network meetings and a woven fabric of thematic clusters have been used in order to find a common language and to be able to process data throughout the various disciplines. Furthermore, all institutes have been engaged in creating the VEU scenarios, following principle recommendations by the German Environmental Agency (UBA 2011b). The multidisciplinarity of the project participants enabled the VEU scenarios to be created in-house by incorporating experts from engineering, mathematics, physics, planning, social sciences and many more. This approach ensures the recognition of topical research from the various disciplines.

The project has used impact-uncertainty and cross-impact-analysis in developing consistent explorative VEU scenarios. The cross-impact-analysis belongs to the "probabilistic modified trends" scenario methodologies and combines quantitative and qualitative factors for scenario development. Qualitative factors are particularly appropriate for projects with a large scope and long time horizon such as VEU (Amer et al. 2012). We first collected relevant scenario parameters with a collective brainstorming in the STEEP categories (Society, Technology & Energy, Environment, Economy and Politics). Using an impact-uncertainty-analysis, the most critical and suitable parameters for scenario developments were identified. Parameters with a high impact and high uncertainty are those of particular interest (or critical scenario parameter, Wilson 1998) for scenario development. Additionally, some parameters of high impact and a degree of certainty (e.g. population) might be used for scenario development as well. In VEU, out of originally 240 parameters 13 have been filtered as the most relevant ones using the impact-uncertainty-analysis.

In a second step we conducted the cross-impact-analysis, using the Zirius open source software by the University of Stuttgart (Weimer-Jehle 2006). Starting with the depiction of possible development paths for each scenario parameter, the cross-impact-analysis is an advancement of scenario consistency analysis. The cross-impact-analysis provides combinations that are internally consistent, meaning that their interdependencies do not contradict each other. In our case, about 900 scenario parameter combinations were theoretically possible. Applying the Zirius cross-impact-analysis resulted in nine fully consistent scenario parameter combinations. Figure 2 illustrates the VEU scenario process.

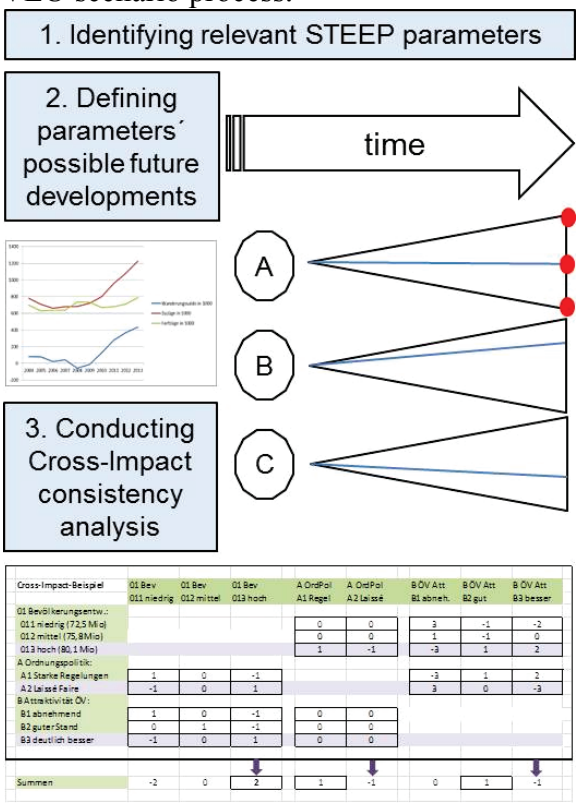

Figure 2: The VEU scenario process

Of the nine fully consistent combinations, the project team chose three to be developed as VEU-scenarios. Besides a reference scenario in which already observable developments and trends are continued into the future, two differing scenarios were created based on specific societal paradigms. One VEU environmental commitment scenario envisions a transport system in 2040 in a society that is thoroughly geared towards environmental protection. Measures aim to reduce the discharge of air emissions, climate-relevant gases and noise. Resource- and energy-efficient production and consumption are core elements of politics and social contracts. A contrasting VEU scenario pictures a transport system in 2040 that is a result of a society under pressure, lacking clear impulses with regard to environmental efficiency and protection. Society's priorities are assumed to foster existing structures and support domestic industry with its focus on the automotive sector and a centralized energy system.

The resulting pictures of the transport system in 2040 are subsequently complemented with concrete measures and trends as well as consistent framework conditions. The VEU scenarios are then analyzed using the VEU model landscape.

4.2 *Developing a research and modeling network*

Figure 3 maps the research areas and models used in the VEU project and how they are connected. The areas and models can be graded spatially (urban/local; national/European; global). They may also be grouped thematically (infrastructure/technology/economy; transport demand; emissions/weather/climate). The mapping of these areas and models allowed us to determine the communication path between them. Results from microscopic demand modeling, for example, inform the national demand modeling. Air and ground transportation join together in the long-distance transport model. Fleet and technology models are linked with the energy model and further contribute to the emission inventory model, which can analyze both local and European level emissions. Findings are processed with the atmospheric and climate models that integrate the influx of atmospheric and emissions data from outside Europe with those generated internally for the German and European transport sector.

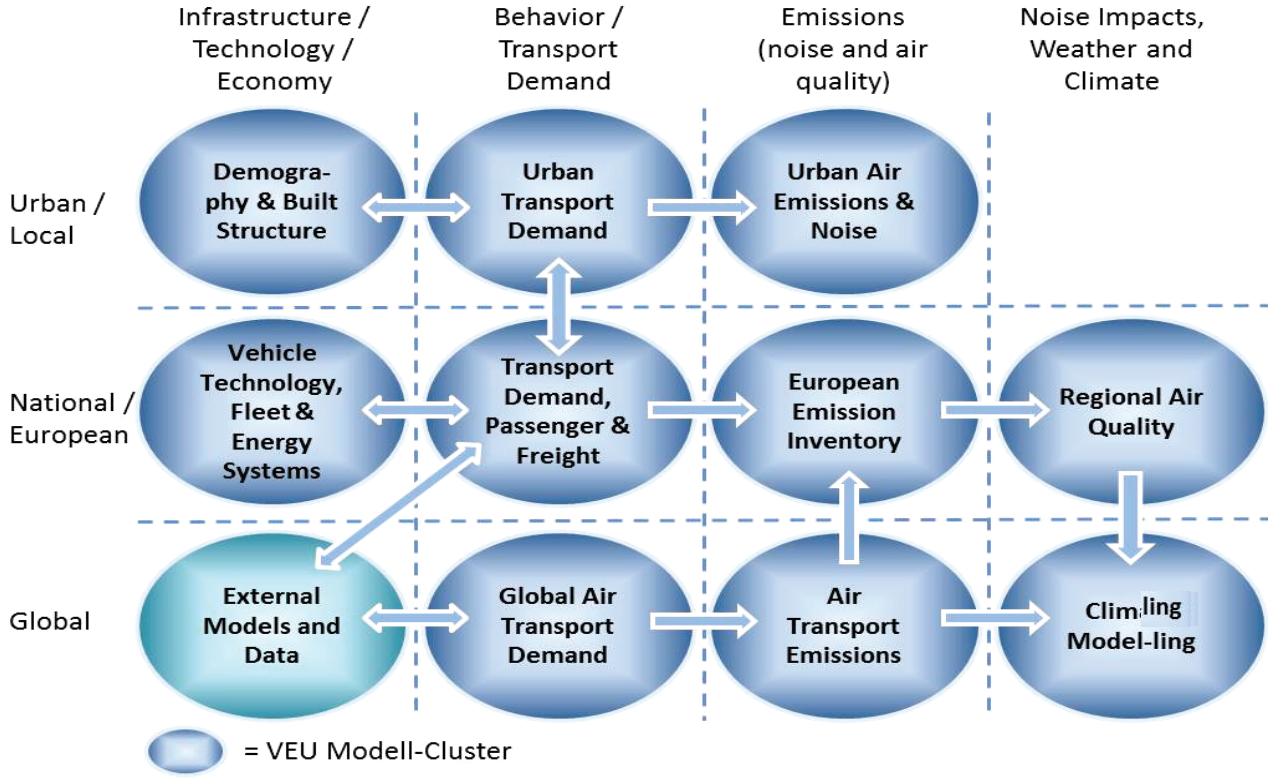

Figure 3: The VEU landscape of models

5 CONCLUSION

The VEU project follows an interdisciplinary scientific approach. Within the VEU project, empirical analyses inform multiple models that are linked together in the VEU model landscape. Possible future developments are analyzed using a set of explorative transport scenarios for Germany and Europe in 2040. The VEU approach acknowledges the interdisciplinary nature of mobility and its environmental effects, providing a comprehensive and reactive instrument for transport analysis.

The VEU research network combines institutional sectoral research under a joint thematic approach, analyzing the entire chain from transport generation to global climate effects. The thematic approach is presented in four topical areas: mobility behavior and demand modeling; technologies and energy developments; noise generation and effects; and the modeling of air quality, weather and the climate impacts of transport. New findings are constantly recognized to better analyze transport and its environmental effects.

The identification of the research areas and models together with linking them to a comprehensive modeling instrument are major milestones achieved so far. Furthermore, the VEU scenario storylines have been established, setting the principle development path for 2040. In the coming months scenarios will be further defined by concrete measures and the models and their interfaces will be tested. We expect modeling results for the scenarios starting in mid-2017.

With our research and our results we aim to strengthen the incorporation of transport in integrated environmental assessments and to open up new insights regarding possible future transport developments. Our results aim to inform supra-national, national and local decision makers so they can better evaluate policy decisions guiding transport developments. The project website may be accessed for further information at www.dlr.de/veu .

Figure 4: QR-code VEU website

REFERENCES

Amer, M.; Daim, T.U., Jetter, A. 2012: A review of scenario planning. Futures 46 (2013) 23-40.

EEA 2014: Transport Emissions of Greenhouse Gases (TERM 002) – Assessment published Dec. 2014.

UBA 2011b: Konsistente Rahmendaten für Modellierungen und Szenariobildung im Umbweltbundesamt. Autoren: Weimer-Jehle, W.; Wassermann, S.; Koscow, H. UBA-Texte 20/2011.

Weimer-Jehle, W. 2006: Cross-impact balances: A system-theoretical approach to cross-impact analysis. In: Technological Forecasting & Social Change 73 (2006) 334-361.

Wilson, I., 1998. Mental Maps of the Future: An Intuitive Logics Approach to Scenarios. In: Fahey, L., Randall, R.M. (Eds.) Learning from the Future: Competitive Foresight. John Wiley & Sons, Inc., New York, US. p. 81-108